Low-frequency distortion in distribution networks

Low-Frequency Distortion in Distribution Networks

PROEFSCHRIFT

ter verkrijging van de graad van doctor aan de
Technische Universiteit Eindhoven, op gezag van de
rector magnificus, prof.dr.ir. C.J. van Duijn, voor een
commissie aangewezen door het College voor
Promoties in het openbaar te verdedigen
op woensdag 2 oktober 2013 om 16.00 uur

door

Vladimir Ćuk

geboren te Pančevo, Servië

Dit proefschrift is goedgekeurd door de promotoren:

prof.ir. W.L. Kling
en
prof.dr.ir. J.F.G. Cobben

This research was supported financially by Agentschap NL, an agency of the Dutch Ministry of Economic Affairs, in the framework of IOP-EMVT (Innovatiegericht OnderzoeksProgramma ElektroMagnetische VermogensTechniek).

Printed by Ipskamp Drukkers, Enschede
Cover design by Nikola Todorović

A catalogue record is available from the Eindhoven University of Technology Library.

ISBN: 978-90-386-3451-7

To my parents and my wife Jovana

Mojim roditeljima i supruzi Jovani

First promotor:
prof.ir. W.L. Kling, Technische Universiteit Eindhoven

Second promotor:
prof.dr.ir J.F.G. Cobben, Technische Universiteit Eindhoven

Core Commitee:
prof.dr.ir.ing. F.B.J. Leferink, Universiteit Twente
Dr.-Ing. J. Meyer, Technische Universität Dresden, Germany
dr.P.F. Ribeiro, Technische Universiteit Eindhoven

Other members:
Univ.-Prof.Dr.-Ing. J.M.A. Myrzik, Technische Universität Dortmund, Germany
Prof.dr.ir. J. Desmet, Universiteit Gent, Belgium
prof.dr.ir. A.C.P.M. Backx (chairman), Technische Universiteit Eindhoven

Summary

The performance of electrical energy users is dependent on the quality of the voltage supplied to them. Production losses, for example, can occur both due to supply voltage interruptions or deviations of the characteristics of the supply voltage (e.g. frequency, voltage level, wave shape, etc.). Already for decades, power delivery is considered as a product, with quality indicators which can be defined and specified in a contract between the supplier (nowadays network operator) and consumers.

One of the aspects which define the quality of the voltage is its wave shape. Already at the terminals of generators, and without any loads connected, the voltage does not have the intended perfectly sinusoidal shape. This phenomenon is called distortion.

Many devices, with a growing trend, act as non-linear loads. This means that their current is distorted even when supplied with a sinusoidal voltage. This causes additional distortion in the network, and is in fact its primary source.

The design of an industrial installation or a distribution network supplying non-linear loads requires also calculation of current and voltage distortion in order to avoid problems. The main goal of this research is to improve the existing methods for distortion evaluation, which can be used in the design stage or for solving arising problems. Another important aspect is the needed quality of the supply voltage, because of its financial impact on network operators, manufacturers and customers. An overview of existing standards and recommendations is made, with an analysis of their shortcomings and possible improvements.

Modelling of distortion propagation can be divided into three parts: modelling the sources, aggregation of these sources, and modelling the frequency dependent impedances.

In the literature, modelling of sources of distortion is handled in several ways, using time-domain, frequency-domain, and hybrid (time and frequency domain) simulations. This research focuses on frequency-domain models. Iterative and non-iterative approaches for frequency domain modelling of harmonic current sources are analysed. Models of different low-voltage equipment are derived from laboratory measurements.

The aggregation of sources is analysed with an empirical approach. Based on field measurements, it is concluded that in most cases the assumptions for existing analytical methods are not satisfied. This makes it difficult to generalize the analytical methodology for aggregation. With an empirical approach, a certain safety margin can be taken to handle the calculation errors which lead to underestimation of distortion levels. Coefficients for empirical aggregation of harmonic currents are analysed based on field measurements, and also the measurement methodology needed to derive these coefficients.

Frequency dependent impedances of different network elements and equivalent system impedances were already analysed in many studies. In this work, attention is

given to the uncertainties of harmonic impedance calculation resulting from different network and load representations, specifically for distribution networks. These aspects are analysed analytically and using computer simulations. Analysed aspects are: lumping loads and feeders, uncertainties of cable lengths, different load compositions, and different models of loads.

The main conclusions from this research are the following:

- Even though global problems are presently prevented by the existing standards and guidelines for controlling the distortion, the rationality for defining the limits is not followed in all cases (e.g. emission limits based on the common design of the device instead on the influence on the network). Defining all limits strictly on the effects would lead to financial savings.
- The existing models of harmonic current sources are compared by their principle and reasons for errors. It was found that none of them has the highest accuracy in all conditions. An improvement is proposed for the harmonic admittance matrix which substitutes the first column of the matrix with a constant current vector. This reduces the errors caused by the fundamental voltage variations.
- Currently proposed summation coefficients lead to underestimation of harmonic currents for most of the results of the field measurements. Some updates for these values are proposed for industrial installations, while a generalisation of the results requires more field measurements.
- From the sensitivity analysis of the harmonic impedance in the low-voltage network, it was found that the highest deviations of the lowest resonant frequency are caused by the different assumption of the input capacitances of loads, which are hard to predict for power electronics (e.g. PV inverters). Lumping of all low-voltage loads causes significant errors only in certain conditions. Differences in assumptions of cable lengths, share of small-power directly coupled motors, and resistive loads results in acceptable deviations.

Samenvatting

Een goede werking van afnemers van elektrische energie is afhankelijk van de spanningskwaliteit. Productieverliezen kunnen bijvoorbeeld worden veroorzaakt door zowel spanningsonderbrekingen als ook door afwijkingen in de karakteristieken van de spanning (bijv. frequentie, spanningsniveau, golfvorm, enz.). Reeds decennia lang wordt energielevering beschouwd als een product, met kwaliteitskenmerken die in een contract tussen leverancier (tegenwoordig netwerkbeheerder) en consument kunnen worden gespecificeerd.

Een van de aspecten die de kwaliteit van de spanning bepalt, is de golfvorm. Zelfs op de klemmen van de generator, zonder aangesloten belasting, heeft de spanning niet de gewenste perfecte sinusvorm. Dit verschijnsel wordt vervorming genoemd.

Steeds meer apparaten gedragen zich als niet-lineaire belastingen. Dit betekent dat hun stroom is vervormd zelfs als ze met een sinusvormige spanning worden gevoed. Dat veroorzaakt verdere spanningsvervorming en vormt in feite de primaire bron van de vervorming in het netwerk.

Om problemen te voorkomen vereist het ontwerp van een industriële installatie of een distributienetwerk die niet-lineaire belastingen voeden, zeker ook de berekening van de stroom- en spanningsvervorming. De belangrijkste doelstelling van dit onderzoek is het verbeteren van de methoden om de “vervuiling” te evalueren die gebruikt worden in de ontwerpfase of voor het oplossen van voorkomende problemen. Een ander belangrijk aspect is de benodigde spanningskwaliteit, vanwege de financiële consequenties voor zowel netwerkbeheerders, fabrikanten als gebruikers. Een overzicht van bestaande normen en een analyse van hun tekortkomingen en aanbevelingen voor mogelijke verbeteringen is gemaakt.

Onderzoek naar de verspreiding van netvervuiling kan in drie onderdelen worden verdeeld: het modelleren van de bronnen, de aggregatie van deze bronnen en het modelleren van de frequentieafhankelijke impedanties.

In de literatuur wordt het modelleren van de bronnen van netvervuiling op verschillende manieren uitgevoerd, gebruikmakend van simulaties in het tijddomein, frequentiedomein en hybridedomein (tijd- en frequentiedomein). Dit onderzoek analyseert voornamelijk modellen in het frequentiedomein. Iteratieve en niet-iteratieve methoden voor de modellering van harmonische stroombronnen zijn geanalyseerd. Modellen van verschillende laagspanningsapparaten zijn gemaakt, gebruikmakend van laboratoriummetingen.

De aggregatie van bronnen is geanalyseerd vanuit een empirische benadering. Op basis van veldmetingen is geconcludeerd dat in de meeste gevallen de aannamen van bestaande analytische methoden niet nauwkeurig zijn. Dit bemoeilijkt een algemene analytische methode voor aggregatie. Echter, met een empirische methode kan een veiligheidsmarge gekozen worden om berekeningsfouten, die leiden tot onderschatting

van vervormingniveaus, te vermijden. Coëfficiënten voor de aggregatie van harmonische stromen zijn geanalyseerd op basis van veldmetingen als ook de meetmethodiek om deze coëfficiënten te verkrijgen.

Frequentieafhankelijke impedanties van verschillende netwerkonderdelen en equivalente systeemimpedanties zijn al in veel studies geanalyseerd. In dit onderzoek is aandacht besteed aan de onzekerheden in de berekening van harmonische impedanties als gevolg van verschillende netwerk- en belastingmodellen, specifiek voor distributienetwerken. Deze aspecten zijn analytisch geanalyseerd met behulp van computersimulaties. Geanalyseerd zijn: aggregatie van belastingen en verbindingen, onzekerheid over de lengte van kabels, verschillende gecombineerde belastingen en verschillende belastingsmodellen.

De belangrijkste conclusies van dit onderzoek zijn:

- Hoewel tot op heden problemen in het algemeen voorkomen worden door de bestaande normen en richtlijnen voor het beheersen van vervormingen, wordt de rationaliteit voor het bepalen van de limieten niet altijd gevolgd (bv. het bepalen van emissielimieten gebaseerd op het algemeen ontwerp van het apparaat in plaats van op zijn invloed op het netwerk). Het bepalen van alle limieten zuiver gebaseerd op hun effect zal tot financiële besparingen leiden.
- De bestaande modellen van harmonische stroombronnen zijn met elkaar vergeleken, zowel principieel alsmede de oorzaak van fouten. Het blijkt dat geen enkel model de grootste nauwkeurigheid geeft voor alle situaties. Een verbetering van de harmonische admittantiematrix is voorgesteld waarbij de eerste kolom van de matrix vervangen is door een constante stroomvector. Dit reduceert de fouten die veroorzaakt worden door de variaties in de grondgolf van de spanning.
- De momenteel aanbevolen aggregatiecoëfficiënten leiden tot onderschatting van harmonische stromen in de meeste resultaten van de veldmetingen. Enkele aanpassingen van deze coëfficiënten worden voor industriële installaties voorgesteld, echter meer veldmetingen zijn noodzakelijk om tot algemeen toepasbare coëfficiënten te komen.
- Uit de gevoeligheidsanalyse van de frequentieafhankelijke impedantie in het laagspanningsnetwerk blijkt dat de grootste afwijkingen van de laagste resonantiefrequentie worden veroorzaakt door verschillen in de aanname voor de ingangscapaciteit van de belasting, welke moeilijk is te bepalen voor vermogenselektronica (bv. PV omvormers). Het aggregeren van alle laagspanningsbelastingen veroorzaakt alleen in bepaalde situaties significante fouten. Verschillen in aannames voor kabellengtes, aandeel van direct gekoppelde motoren met laag vermogen, en voor weerstandsbelastingen resulteren in acceptabele fouten.

Contents

Chapter 1

Introduction

1.1 Electromagnetic Compatibility and Power Quality

The operation of electrical systems has never been completely disturbance-free. During the years, problems which were appearing more frequently have been categorized to make the troubleshooting process easier and to create engineering practices which can avoid problems in the first place.

The most general framework which aims for noninterfering operation in the electromagnetic environment of all devices is called Electromagnetic Compatibility (EMC). It is defined by the International Electrotechnical Commission (IEC) in IEC 61000-1-1 [1] as:

"*The ability of an equipment or system to function satisfactorily in its electromagnetic environment without introducing intolerable electromagnetic disturbances to anything in that environment*".

This definition covers both the emission of disturbances and immunity to them, for devices and systems (e.g. installations and networks). In other words, all devices and systems should satisfy certain emission and immunity requirements to avoid operation interruptions, misoperation and degradation of performance.

In general, disturbances travel in two ways from the source of interference to the receiver (the "victim"), as conducted and/or radiated. Conducted interferences require a galvanic connection between the two points, while the radiated emission couples them via their electromagnetic fields.

Inside a device, both types of coupling can have equally important roles. On the power system level, radiated emission is not mentioned often. The first reason is the relatively large distance between devices. The second reason is the relatively low range of frequencies which can propagate far from the source. However, radiation is sometimes taken into account implicitly, via the electromagnetic coupling of network components, e.g. the mutual inductance between the conductors of a transmission line.

Specific differences between power delivery and communication systems led to the parallel development of a research area called Power Quality (PQ). There is a discussion about the definition of PQ, as reported in [2]. Some authors refer mainly to the quality of the voltage, or voltage quality. This term covers only the supply side of the problem. However, as the quality of the voltage is often dependent on the currents "drawn" by users, most authors stress the importance of the interaction between the supply voltage and the users current. The term current quality, or quality of the current, was introduced as an equivalent to voltage quality, to evaluate the performance of the installation of network users.

Standard IEC 61000-4-30 [3] defines PQ measurement techniques, and also defines Power Quality as:

"*Characteristics of the electricity at a given point on an electrical system, evaluated against a set of reference technical parameters*".

The electricity in this definition refers both to the voltage and current, and reference parameters are defined for both quantities in separate IEC standards.

The Institute of Electric and Electronics Engineers (IEEE) provides recommended practices for supplying sensitive equipment in the standard IEEE 1100 [4], and also defines PQ as:

"*The concept of powering and grounding sensitive equipment in a matter that is suitable to the operation of that equipment*".

The IEEE also describes parameters of both voltage and current which need to be satisfied by the supplier and the users.

Even though there is no formal categorization, PQ could be considered as a part of EMC focused on power delivery systems and with a limited frequency range. The IEC implicitly covers this by placing most of the PQ related standards in the 61000 series of standards within the title EMC.

PQ distinguishes itself by the specific phenomena which it relates to. In the EMC scope, interferences are usually divided into continuous and transient. In PQ, related to the quality of the supply voltage, the following power system specific disturbances are considered:

- Frequency variations,
- Level (RMS) variations,
- Voltage fluctuations and flicker,
- Voltage dips and short supply interruptions,
- Transient overvoltages,
- Unbalance,
- Waveform distortion.

All of these phenomena lead to specific problems encountered in power delivery systems. For example, slow and fast voltage variations have different effects. The frequency of variations labeled as flicker leads to a visual "annoyance" from the lighting exposed to it. Slow magnitude variations cannot cause a visual effect but can cause equipment misoperation, e.g. dielectric breakdown due to the overvoltage or overcurrent due to undervoltage. Also, the sensitivity of equipment is different for flicker and slow voltage variations.

Before the IEC made its own PQ standards, disturbance coordination was based on the "worst case", with a relaxation for abnormal situations. This concept is still in use e.g. in the IEEE 519 standard [5]. The IEC Technical Committee (TC) 77 introduced the concept of compatibility based on confidence levels to PQ. This concept, illustrated in Fig 1.1, is one of the foundations of EMC. The two curves represent probability distributions of the disturbance emission levels in the system and the immunity of devices. Emission and immunity are coordinated in such a way that only on a small number of locations and during very short intervals of time, the emission can exceed the immunity levels.

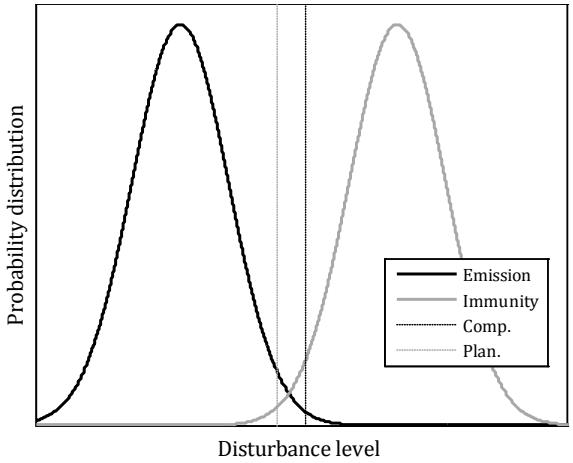

Fig 1.1 Concept of compatibility; Comp. – Compatibility level, Plan. – Planning level

Coordination is achieved via compatibility levels. Compatibility levels are set lower than the immunity of devices, as disturbance levels which should not be exceeded. A certain safety margin should exist between the immunity and compatibility levels.

Based on the compatibility levels, network operators assign planning levels of voltage phenomena, as internal quality objectives. These levels are lower than the compatibility levels and provide a safety margin for the loads added in the future, see Fig 1.1. Planning levels are also used for coordination between different voltage levels.

The generic curves from Fig 1.1 overleap in a small area near the middle of the horizontal axis. This area represents the probability of equipment maloperation or failure due to disturbances. For individual sites this overleap can vary, but for most of them this area is very small. On the system level this area is larger, however, disturbances do not always occur on locations with equipment of lower immunity.

This concept allows problems to occur at very rare occasions, but with considerable savings on the system design. As an example, in some cases equipment malfunction is caused by overvoltages. The problem would not exist if all equipment could tolerate the highest voltage level recorded in the system. As this value occurs extremely rare, the additional cost of mitigation would be greater than the benefit of the measure.

1.2 Waveform distortion

1.2.1 Definitions

Even though AC systems are primarily intended to operate with sinusoidal signals, the wave shapes of voltages and currents deviate from a pure sinusoid already at the terminals of generators. This phenomenon is called waveform distortion. Examples of typical voltage and current distortion are shown in Fig 1.2.

Up to certain levels, distortion of both voltage and current does not cause significant problems. However, major distortion can cause premature aging, misoperation, and even failure of equipment. Therefore, already at the beginning of AC power supply started the interest for the effects and control of distortion in the power delivery system.

A convenient method for analysing distorted waveforms is looking into the spectrum of the signal. Spectrum is a mathematical abstraction of a signal being composed out of

a series of perfectly sinusoidal components, with different frequencies. If the signal is stationary (it repeats itself periodically), it can be decomposed into components of frequencies which are integer multiples of the power system frequency, which is the fundamental frequency of the signal. These components are called harmonics, with the order labelled with *h*, and they are the main focus of this thesis.

If the signal does not maintain its wave shape in all cycles of the fundamental, as in Fig 1.3, spectral components have frequencies which are integer and non-integer multiples of the fundamental. The non-integer multiples are referred to as inter-harmonics.

Signals are never perfectly stationary in practice, which means that certain inter-harmonic components are always present. However, in most situations and most of the time, the levels of inter-harmonics are much lower than of the harmonics. Therefore, inter-harmonics are often neglected in the analysis, but they can be a source of problems in certain situations [6].

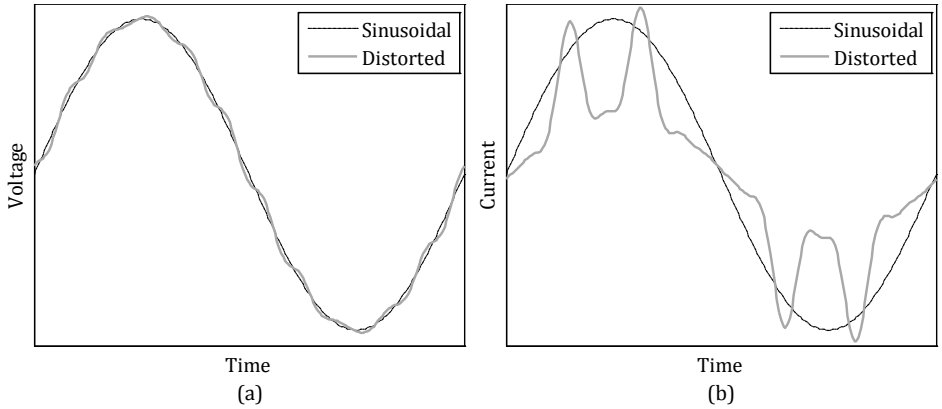

Fig 1.2 Example of a distorted waveform: (a) voltage, (b) current

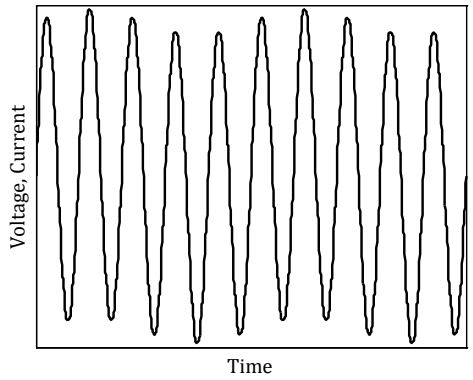

Fig 1.3 Example of a non-stationary signal

Several indices are used to quantify the distortion of a signal. For the overall insight in the deviation from the sinusoid, on the example of voltage (*U*), the Total Harmonic Distortion (THD) is defined as:

$$THD_U = 100\% \cdot \frac{\sqrt{\sum_{h=2}^{\infty} U_h^2}}{U_1} \tag{1.1}$$

where U_1 is the RMS magnitude of the spectral component of the fundamental frequency, and U_h are the RMS magnitudes of components of the h^{th} order. The current THD is defined in the analogue way.

The THD measures the share of harmonic components in the signal. For voltages in the network, typical THD levels are in the range of a few percent. Limits for voltage THD are 5 or 8 % (depending on the country). In extreme conditions values of about 20 % are measured. For currents, values from 10 % to more than 100 % are typically measured.

When the current RMS of a device is very low in comparison with the rated current of the installation or a device, very high levels of current THD may suggest that the disturbance is greater than it actually is. For this reason, the Total Demand Distortion (TDD) is sometimes used for current instead of THD, defined as:

$$TDD = 100\% \cdot \frac{\sqrt{\sum_{h=2}^{\infty} I_h^2}}{I_{1nom}} \tag{1.2}$$

where I_{1nom} is the value of the fundamental of the current in the nominal working conditions, and I_h are the harmonic components in the observed moment in time. This indice takes into account the loading level as well, and gives better information about the impact on the voltage distortion. In normal operating conditions, values of TDD for installations are usually up to 40 %.

The two mentioned indices describe the imperfection of the signal. For quantification of an individual component, a Harmonic Distortion (HD) factor can be defined for the h^{th} harmonic order, on the example of voltage:

$$HD_{U,h} = 100\% \cdot \frac{U_h}{U_1} \tag{1.3}$$

An analogue definition is used for the current. Values of HD are always lower or equal to the THD.

1.2.2 Frequency range and distribution networks

Standards dealing with waveform distortion [3], [5], [7] define the frequency range as up to the 40th or 50th harmonic, which means 2-2.5 kHz for 50 Hz systems and 2.4-3 kHz for 60 Hz systems. This is normally considered as the low-frequency range for power systems, and it is the scope of this thesis. For other applications the upper limit of the low-frequency range is considerably higher (e.g. as up to 300 kHz for radio communications).

Most distortion related problems of high-power loads are still in the low-frequency range, as their AC side converter is normally of a line-commutated type. However, self-commutated converters with multi-level conversion are capable of reducing their low-frequency emission with a drawback of increased higher frequency emission. This leads to higher emissions of these devices in the range from several tens of kHz to MHz. One of the newer developments in the research about waveform distortion is bridging

the “frequency gap”, between 2 kHz and 150 kHz, which currently exists in the 61000 series of the IEC standards.

Current and voltage distortion with frequencies of tens of kHz do not travel far in the network, because capacitive elements act as a low impedance path. Furthermore, cable inductances form a very high impedance in comparison with the “local” capacitances, so current components of high frequencies mostly travel only until the Electromagnetic Interference (EMI) filters of the source device and nearby devices [8]. Due to this, the frequency range above the current scope of PQ standards is not considered in this thesis.

An important difference between transmission and distribution networks is the length of cables and overhead lines used. In transmission systems, lines range between tens of km and about 1000 km, while in distribution networks the lines rarely exceed a few tens of km. This influences the adopted line models. As long as the line length is much shorter than the wavelength of the highest considered frequency component, the line can be modelled with a lumped equivalent. This is mostly the case in distribution networks. When the line length is comparable with the wavelength of considered components, as in transmission systems, a model with distributed parameters is normally needed.

Another property of transmission systems is the higher impedance unbalance at harmonic frequencies, both for untransposed and transposed lines [9], [10]. This exaggerates the unbalance of harmonic voltages, and asks for an unbalanced three-phase analysis. In distribution networks impedance unbalance is not pronounced, and the main source of harmonic voltage unbalance is unbalanced current injection. Therefore, whenever it is not possible to predict the unbalance of current sources, a single-phase analysis is performed.

1.3 Research description

1.3.1 Interest in waveform distortion

The interest in waveform distortion, and PQ and EMC in general, is primarily driven by the annoying effects and financial implications of maloperation. Disturbances can cause direct damage to equipment, or a process interruption, in both cases followed by production losses.

As the power system was becoming more reliable in terms of supply availability, the consciousness about other problems started growing. The analyses of telephone interference, equipment overheating, and high levels of audible noise, were followed by the analyses of accelerated aging of equipment and additional energy losses.

In [11], an overview of reports and publications about the implications of reduced power quality is given. For the period 2003-2004, a survey from 25 European Union (EU) countries accounted 5 % of the estimated 152 billion euros (10^9 €) of PQ related losses to waveform distortion. From this estimation, 90 % is attributed to industrial customers. In the USA, in the year 2000, a PQ related loss between 119 and 188 billion dollars was estimated, without a reference to the share of losses due to distortion. From the total number of reported problems (which is not proportional to the percentage of losses), 22 % of PQ problems in the USA are caused by distortion.

In many countries, the number of PQ related complains showed a growing trend during the last years [11]. A part of it can be attributed to the growing customer awareness of the consumer rights.

1.3.2 Research objectives

The two main goals of this research are:

- *Improve the existing PQ modelling techniques.*

The main idea is preventing PQ problems already during the design stage. Better disturbance evaluation can bring considerable savings during operation, if problems are avoided. For the existing networks and installations, the methodology can be used to determine the root cause and to define the solution.

Issues which need to be considered in this step are the mathematical solver, models of disturbance sources, aggregation of multiple sources, and modelling of the network response.

- *Contribute to the European discussions among the suppliers, manufacturers, network operators, and regulators about the needed quality of the supply voltage.*

The needed quality of the supply voltage is defined by a number of national and international standards. Certain differences in their requirements lead to the conclusion that improvements are still needed. To analyse this, an overview of the existing standards is needed, both for the supply voltage and the connection requirements for installations and individual equipment.

1.3.3 Research approach

The principle for setting the limits in standards is analysed, and the related immunity of equipment. Relations between the limits for harmonic voltages and currents are investigated, and the short-comings in both types of limits.

For better disturbance evaluation, measurement methods for non-stationary signals are analysed, especially for short-term phenomena. Methods are analysed on artificial signals and two case studies with laboratory measurements.

Harmonic analysis is considered in three steps. In the first step, modelling of a single non-linear device is analysed. Behaviour of devices is analysed based on computer simulations. Models of sources are derived for two types of common loads, from laboratory measurements. Existing modelling approaches are compared.

In the second step, aggregation of harmonic sources is investigated. For this purpose, computer simulations, laboratory experiments, and field measurements are used to analyse the process and derive empirical coefficients for the summation of harmonic currents. Also, the methodology for measuring these coefficients is discussed.

In the last step, modelling of harmonic impedances in distribution networks is analysed. Analytical models and computer simulations are used to investigate the uncertainties in impedance estimation caused by different models of components and uncertainties in their parameters.

1.4 The IOP project

This research has been performed within the framework of the project “Power Quality and Electromagnetic Compatibility”. The project is a part of the IOP-EMVT program (Innovation Oriented research Program – Electromagnetic Power Technology), which is funded by Agentschap NL. Agentschap NL is an agency of the Dutch Ministry of Economic Affairs, Agriculture and Innovation (Ministerie van Economische Zaken, Landbouw en Innovatie).

Among other topics, the research program includes projects related to “Intelligent Networks”, which cover network components and structural changes in electrical networks, e.g. the proliferation of generation in distribution networks and introduction of new types of loads. As a part of this program, the Power Quality Laboratory was created at the Eindhoven University of Technology.

The project PQ and EMC is a cooperation of two Ph.D. researchers, one at the Electrical Energy Systems group of Eindhoven University of Technology, and one at the Telecommunication Engineering Group of the University of Twente. Furthermore, industrial partners DNV Kema, Alliander, and Thales are involved.

The goals of the project were:

- Improve the models for analysing low-voltage and medium-voltage networks
- Provide guidance for estimating disturbances in the design stage and solving existing problems
- Analyse the mismatches in standards and make proposals for improvements

1.5 Outline of the thesis

The thesis is organized in the following way:

In Chapter 1, the basic terms are introduced: Electromagnetic Compatibility, Power Quality, waveform distortion, and the basic indices for quantifying distortion. Specifics which apply to low-frequency distortion and distribution systems are explained, followed by the motivation for research in this field. Lastly, the goals of the IOP research project “Power Quality and Electromagnetic Compatibility” are discussed.

In Chapter 2 an overview of the existing standards and recommendations related to harmonic distortion is presented. Shortcomings of the existing standards are analysed and propositions for improvements are discussed.

Measurement methods are discussed in Chapter 3. The conventional Discrete Fourier Transformation is analysed for the case of non-stationary signals. The application of alternative methods for short-term phenomena is discussed, and two of the alternatives are demonstrated by laboratory measurements.

Different models of a single source of distortion are analysed in Chapter 4. The influence of the load power and non-ideal voltage supply on the harmonic currents is discussed. The sources of error are compared for three modelling techniques, and a proposition for modification of the harmonic admittance matrix is presented.

In Chapter 5, the aggregation of harmonic sources is analysed. For the case of variable-speed drives, a computer model was used to investigate the summation of harmonic currents in different operating conditions. For several types of loads, aggregation was analysed based on field measurements from seven industrial locations. Distributions of magnitudes and phase angles of harmonic current are investigated and the dependence between harmonic sources. Propositions for updating the summation coefficients in technical standards are made based on the measured values. Lastly, considerations regarding the measurement of summation coefficients are given.

The influence of harmonic impedances on voltage distortion is analysed in Chapter 6. Uncertainties in the impedance estimation are discussed, based on uncertainties of parameters, and assumptions of load composition. Conclusions of the work and recommendations for future work are presented in Chapter 7.

1.6 References of Chapter 1

[1] IEC/TR 61000-1-1, "Electromagnetic compatibility (EMC) - Part 1: General - Section 1: Application and interpretation of fundamental definitions and terms," 1992.

[2] M. Bollen, "Overview of Power Quality and Power Quality Standards," in *Understanding power quality problems: Voltage sags and interruptions*, 1st ed., Wiley-IEEE Press, 2000, pp. 1–34.

[3] IEC 61000-4-30, "Electromagnetic compatibility (EMC) - Part 4-30: Testing and measurement techniques - Power quliaty measurement methods," 2008

[4] IEEE 1100, "IEEE recommended practice for powering and grounding sensitive electronic equipment," 1992.

[5] IEEE 519, "IEEE Recommended Practices and Requirements for Harmonic Control in Electrical Power Systems," 1992.

[6] P. F. Ribeiro, "Harmonics and interharmonics of adjustable speed drives," in in *Time-Varying Waveform Distortions in Power Systems*, Wiley-IEEE Press, 2010, pp. 253–275.

[7] EN 50160, "Voltage characteristics of electricity supplied by public distribution systems," 2010.

[8] A. Larsson, "On high-frequency distortion in low-voltage power systems," PhD thesis, Lulea University of Technology, Sweden, 2011.

[9] J. Arrillaga, B. C. Smith, N. R. Watson, and A. R. Wood, "Transmission systems," in in *Power system harmonic analysis*, 1997, pp. 33–96.

[10] P. F. Ribeiro, "Investigations of harmonic penetration in transmission systems," PhD thesis, The Victoria University of Manchester, UK, 1985.

[11] S. Bhattacharyya, "Power quality requirements and responsibilities at the point of connection," PhD thesis, Eindhoven Universtity of Technology, 2011.

Chapter 2

Standards and guidelines related to harmonic distortion

2.1 Historical development of standards for limiting harmonics

The presence of harmonic distortion in voltages and currents was noticed already at the start of AC transmission. The early mentioning of problems and analysis related to harmonic distortion were summarized in [1], [2], with records dating back to the 1890s.

As reported in [1], [2], in the early days of AC power delivery the generators had an e.m.f. which was not very close to a sinusoidal wave shape. Their waveforms were close to a square shape, which in combination with higher fundamental frequencies (in some cases 125 or 133 Hz) led to over-voltages arising from transmission line resonances already with relatively short transmission lines. This limited the transmission to 5-10 miles (8 – 16 km). This problem triggered a change in the synchronous generator construction, and already in 1895 a new design was developed with a nearly sinusoidal e.m.f. and a possibility of longer transmission lines.

Other documented problems from this period included telegraph interference form AC transmission lines in 1891 in Switzerland [1], and motor overheating due to harmonic voltages in 1893 in the USA [2]. An early mentioning of mitigation of what was possibly a harmonic resonance problem from 1890 in the USA [2], was on a transmission line which experienced flashovers on an insulator at a specific point. The problem was treated by throwing dirt on the insulator with a shovel whenever a flashover was spotted, and required an employee at this location during the operation hours.

One of the problems of this era of electrification was the availability of measurement equipment which could observe the wave-shape of the voltage and current. Already in the 1890s a wave meter existed which could collect instantaneous values of voltage using a mechanical commutator [2], but they were rare. The values of the samples would then be measured using a bridge method. The time resolution of such sampling was not constant, and due to this the calculation of Fourier coefficients took about one hour per coefficient. The oscillograph, which was the predecessor of the oscilloscope, was introduced at the very end of the 19th century [1]. It was a rare and expensive instrument, so the waveform of the voltage was usually observed only when audible noise from a generator or a transformer was noticed. Due to this, it was not always known if a problem was related to harmonic distortion, and some problems might have been misinterpreted as harmonic.

The first rules for disturbances in the power system appeared in the UK, but in a very vague form. As reported in [3], clause 27 from the Electricity Supply Act from 1899 said: “one customer shall not interfere unduly with the supply to another”. This

covered harmonic distortion as well, but due to the lack of experience it was still not possible to define clear rules for the energy suppliers or for the end users.

The first specific rules for voltage distortion did not cover the whole power system area as well. In [4], which was published in 1913, it can be read: "The standardization rules of the Institute state that the generator e.m.f. waves shall not depart from the sine shape by more than 10 per cent" (the mentioned Institute is AIEE – the American Institute of Electrical Engineers). The referred standard might had the same rules as a document from 1910, mentioned in [2], for which it is also stated that it defined the distortion of the generators e.m.f., as well as the first indices used to characterize the distortion: Distortion factor (DF) and Telephone interference factor (TIF).

This limit of the generator's e.m.f. distortion meant in fact that the voltage THD of the generators had to be limited to 10 %, but it did not limit the distortion in other parts of the system. Already in [4] it was noticed that the voltage THD alone is not a sufficient measure, because the higher order harmonics cause more damage to some equipment than the lower order harmonics of the same magnitude.

The later proliferation of DC powered railway in the 1940s and 1950s introduced a significant share of diode bridge rectifiers in the power systems of some countries, which brought more attention to the harmonic distortion and the need for rules, both for the users and the utilities [3]. In this period, engineering recommendations were written as guidance for the connection of new converters. In 1967 the first harmonic current limits for the connection of new converters were introduced in the UK with the engineering recommendation ER G5/2: "Supplies to converter equipment – Harmonic distortion and permissible pulse number of consumer's rectifiers and inverters". This was an expansion of an existing recommendation, which specified the maximal converter powers at which no analysis is needed, and the maximal allowed harmonic currents of converters. Based on these current limitations, the third edition of this recommendation included the first harmonic voltage limits up to the 19th order in 1976 – ER G5/3: "Limits for harmonics in the United Kingdom electricity supply system". This was the first harmonic standard which covered the whole system, known to the author, and it also introduced the "multiple-stage" procedure for connecting new customers which discriminates cases without a need for further analysis. This approach was kept in all later standards. According to [3] the voltage limits seem to be based only on the voltage distortion expected due to rectifier loads, although they definitively included the existing experiences regarding the thermal impact of harmonic voltages. The limits of harmonic currents were given as absolute (in amperes).

In North America, similar voltage harmonic limits were adopted for the standard IEEE 519 [5], but with limitations for currents dependent on the short-circuit level of the connection point. As noticed in [6], the IEC adopted compatibility levels based on a CIGRE report [7], which includes voltage harmonic levels measured in several countries, described as leading to high probability of problems. The same levels were adopted in the European standard EN 50160 [8], which describes voltage characteristics which can be expected in public networks. Regarding the limitations of harmonic currents, the IEC adopted different documents for individual devices and connection of installations, which are mentioned in the following sub-sections.

2.2 Present limits for voltage distortion

2.2.1 Limits for voltage distortion in public networks

In public networks, responsibilities of the system operator and the customer are assessed at the point of evaluation (POE), which is a metering location on which both parties agree. In most cases this location is either the point of connection (POC) – where the customer is physically connected to the public network, or the point of common coupling (PCC) – the closest location at which other customers can be connected. PCC is usually upstream in the system from the POC.

Presently, many countries use limits based on international standards IEEE 519, IEC 61000-2-2, and IEC 61000-2-12 [5], [9], [10]. European standard EN 50160 [8] is also used as a basis for limits in national grid codes, however, its intended purpose is only to describe the voltage characteristics which users should expect, as quality of a product [6]. The IEC EMC series of standards provides compatibility levels for harmonic voltages [9], [10], which are meant as a basis for limits. The compatibility levels are values for coordinating immunity and emission. Maintaining the disturbance levels lower than the compatibility levels should ensure compatibility for most of the time on most of the locations.

Indicative values of planning levels are given in [11]. Planning levels are internal quality objectives defined by each network operator, equal or less than the compatibility levels. A comparison of the values from mentioned standards is given in Table 2.1 for odd orders and Table 2.2 for even orders, for the low-voltage (LV) and medium-voltage (MV) levels.

Table 2.1 Comparison of limits for harmonic voltages, compatibility levels, and planning levels of odd order harmonics in LV and MV public systems; from [5], [8-11]

Standard	EN 50160	IEEE 519	IEC 61000-2-2 IEC 61000-2-12	IEC 61000-3-6
Purpose	limits	limits	compatibility levels	indicative planning levels
Voltage level	LV and MV	LV and MV	LV and MV	MV
THD_U [%]	8	5	8	3.5
h	Maximal harmonic voltage as a percentage of the fundamental [%]			
3	5	3	5	4
5	6	3	6	5
7	5	3	5	4
9	1.5	3	1.5	1.2
11	3.5	3	3.5	3
13	3	3	3	2.5
15	0.5	3	0.4	0.3
17	2	3	2	1.7
19	1.5	3	1.76	1.5
21	0.5	3	0.3	0.2
23	1.5	3	1.41	1.2
25	1.5	3	1.27	1.09
$25 < h \leq 40$	-	3	$2.27 \cdot (17/h) - 0.27$	$1.9 \cdot (17/h) - 0.2$

In the IEC standards and EN 50160 MV is defined as up to 35 kV, while in the IEEE 519 it is defined as up to 69 kV

The main idea of planning levels is a safety margin, which allows the connection of additional customers without exceeding the compatibility levels. For this reason, the planning levels are lower than the compatibility levels in all cases except for two even

orders (6th and 8th in Table 2.2). For these two orders no safety margin was left, without an obvious reason.

Table 2.2 Comparison of limits for harmonic voltages, compatibility levels, and planning levels of even order harmonics in LV and MV public systems; from [5], [8-11]

Standard	EN 50160	IEEE 519	IEC 61000-2-2 IEC 61000-2-12	IEC 61000-3-6
Purpose	limits	limits	compatibility levels	indicative planning levels
Voltage level	LV and MV	LV and MV	LV and MV	MV
THD_U [%]	8	5	8	3.5
h	Maximal harmonic voltage as a percentage of the fundamental [%]			
2	2	3	2	1.8
4	1	3	1	1
6	0.5	3	0.5	0.5
8	0.5	3	0.5	0.5
10	0.5	3	0.5	0.47
12	0.5	3	0.46	0.43
14	0.5	3	0.43	0.4
16	0.5	3	0.41	0.38
18	0.5	3	0.39	0.36
20	0.5	3	0.38	0.35
22	0.5	3	0.36	0.33
24	0.5	3	0.35	0.32
$25 < h \leq 40$	-	3	$0.25 \cdot (10/h)+0.25$	$0.25 \cdot (10/h)+0.22$

A drawback of the IEEE limits it that they do not allow for any flexibility, as they are defined for the "worst case" in normal operation. In [12] it is explained that the IEC approach of limits for the cumulative probability levels is better, because the long-term effects of harmonics can be covered with limits for 95 % or 99 % probability levels. In this way, some relaxation can be made for short time periods without significant effects on equipment, when it is too expensive to maintain the distortion within the limits.

It is noticeable that the values of EN 50160 are identical to the values of compatibility levels for the lower order harmonics. This is probably due to the common origin, the CIGRE report mentioned earlier. The limits of IEEE 519 probably originate from the British standard G5/3, which also did not have different limits for each individual harmonic order. The G5/3 had one limit for all odd orders and another limit for all even orders. Also, the limit for voltage THD of IEEE 519 for LV and MV matches the LV limit of G5/3, while the limit for individual harmonic voltages of IEEE 519 matches the G5/3 limit for odd orders at 6.6 kV and 11 kV voltage levels.

Even though the immunity of devices was definitively considered when the limits of IEEE 519 and EN 50160 were adopted, there is the impression that immunity is not considered enough. For example, the IEEE 519 has relatively strict limits, except for higher order harmonics, where individual orders have the same limit. For all devices with a considerable input capacitance the higher order harmonics lead to more overheating, which should be taken into account in the limits. On the other hand, the limits from EN 50160 are based on field measurements in which the triple-n harmonics had relatively low values (due to star-delta connection of transformers), so the limits for triple-n harmonics are stricter than the other odd orders, which might not be necessary.

The main reason why these standards are not changing quicker is that there are no global problems with harmonic voltages at the moment. Even with possible shortcomings, satisfying either of the two standards usually leads to problem-free

operation. One might say that it is possible to adopt the less strict requirements of both standards: a voltage THD limit of 8 % and individual harmonic limits of at least 3 % for low order odd orders, and a decrease for higher order harmonics. In section 2.4 we look at the immunity of equipment to harmonic voltages as a part of the answer to this question.

2.2.2 Limits for voltage distortion in non-public networks

As mentioned in the previous section, in public networks, voltage distortion is evaluated at the POE, to assure the responsibility of both parties. Inside industrial and other non-public networks, compatibility levels are defined for any in-plant point of coupling (IPC), which is a location nearest to a particular load at which other loads can be connected.

The purpose of these compatibility levels is the same as in public networks, they are meant for coordinating emission and immunity of loads inside the installation. Only the customer is responsible for the disturbance levels at any IPC, while at the POE responsibility is shared with the system operator.

Depending on the type of installation, these compatibility levels are divided in several standards, e.g. for ships and off-shore installations, aeroplanes, etc. In this work only the compatibility levels for "on-land" industrial networks are considered, given in the standard IEC 61000-2-4 [13].

This standard defines three types of electromagnetic environments:

- Class 1: for very sensitive equipment (e.g. laboratory instruments), with compatibility levels lower than for public networks, commonly connected via an uninterruptible power supply (UPS),
- Class 2: for general PCCs and IPCs, with compatibility levels equal to the levels for public networks,
- Class 3: for harsh environments, with compatibility levels higher than for public networks.

Compatibility levels from [13] are given in Table 2.3.

Table 2.3 Compatibility levels for industrial networks, [13]

Class	1	2	3
THD_U [%]	5	8	10
h	Maximal harmonic voltage as a percentage of the fundamental [%]		
2	2	2	3
3	3	5	6
4	1	1	1.5
5	3	6	8
6	0.5	0.5	1
7	3	5	7
8	0.5	0.5	1
9	1.5	1.5	2.5
10	0.5	0.5	1
11	3	3.5	5
13	3	3	4.5
15	0.3	0.4	2
17	2	2	4
21	0.2	0.3	1.75
triple-n $21 < h \leq 45$	0.2	0.2	1
odd $17 < h \leq 49$	$2.27 \cdot (17/h) - 0.27$	$2.27 \cdot (17/h) - 0.27$	$4.50 \cdot (17/h) - 0.50$
even $10 < h \leq 50$	$0.25 \cdot (10/h) + 0.25$	$0.25 \cdot (10/h) + 0.25$	1

2.2.3 Short-term limits for harmonic voltages

For public networks, IEC defined short-term compatibility levels in [9], as a product of the long-term compatibility levels and a multiplying factor k_{hVS} given by:

$$k_{hVS} = 1.3 + \frac{0.7}{45} \cdot (h - 5) \tag{2.1}$$

The short-term compatibility level for voltage THD is 11 %. The short-term intervals refer to the measurements aggregated on a 150 cycle basis (approximately 3 s). The time aggregation of measurements is explained in Chapter 3.

Expression (2.1) allows the long-term levels to be exceeded by 25 % or more (depending on the harmonic order). The origin of (2.1) is not explained, but it might be formulated with the same approach as the long-term compatibility levels, based on certain cumulative probability levels (e.g. a certain percentage of time and measured locations).

For industrial installations, standard [13] allows 50 % higher short-term values than the long-term values for classes 1 and 3. For class 2, which has levels equal as for public networks, (2.1) is also used for defining short-term limits.

IEEE 519 [5] also defines 50 % higher limits for short periods, during start-ups and unusual conditions, both for individual orders and the THD.

2.3 Present limits for harmonic current emission

The present limits for harmonic current emission are mostly based on the limits for harmonic voltages. As explained in [14], the main logic for setting the harmonic emission limits is related to the emission which would lead to reaching the compatibility levels of harmonic voltages when injected into a set of standard impedances.

The methodology for setting limits is dependent on the size of considered equipment or installation. Small LV equipment (up to 16 A per phase) is considered independent of its connection location, because it should be possible to use such equipment in any installation without causing excess voltage distortion.

For larger equipment, the size of equipment is taken into account. Several sets of limits are defined, and are used dependent on the short-circuit power of the connection point and the rated power of the device.

For installations, limits are not defined explicitly. Recommendations are given as an assessment procedure, used by the system operator during negotiations with customers.

Setting the appropriate emission limits would be simple only if the power system would contain a single nonlinear load. In this case the relation between voltage and current limits could be defined with a single impedance model, such as the one used for compliance testing. Standard IEC 60725 defines the reference impedance for the LV level as 0.24 + j0.15 Ω per phase and 0.16 + j0.10 Ω for the neutral. The reference values of this model were chosen based on survey measurements from several European LV networks. Reference [14] reports on an expanded IEC working group 77A system model and a procedure for deriving permissible harmonic emission taking into account higher voltage levels and multiple sources of emission, using:

$$I_h = \frac{U_h \cdot k_{LV}}{k_C \cdot \left| Re\{\underline{Z}\} + jh \cdot Im\{\underline{Z}\} \right|} \tag{2.2}$$

where U_h is the voltage compatibility level of the h^{th} order, I_h is the permissible emission of the h^{th} order, k_{LV} is the portion of the compatibility level allocated to the LV level, k_C is the compensation coefficient (which takes into account the phase angle diversity, penetration level of nonlinear equipment, etc.), and $\underline{Z}$ is the estimated impedance at the point of connection. A similar formulation is also found in [15]. Coefficient k_C is further analysed in Chapter 5 for industrial installations.

2.3.1 Limits for connecting disturbing installations

IEEE recommends several classes of harmonic current limits for different voltage levels, dependent on the Short-Circuit Ratio (*SCR*), which is the ration between the short-circuit power of the point of connection (S_{SC}) and the installed power of the installation to be connected (S_i) [5], Table 2.3.

$$SCR = {}^{S_{SC}}/_{S_i} \tag{2.3}$$

The limits of Table 2.3 are defined as relative to the maximal load current I_L (fundamental component), and instead of THD they are defined for Total Demand Distortion (TDD), which divides the square sum of harmonics with I_L instead of the "instantaneous" value of the fundamental current. This approach avoids the high relative distortion values when the load current is low, which do not lead to equipment overheating even for THD_I > 100 %.

Table 2.4 Current distortion limits for general distribution systems, voltage levels up to 69 kV [5]

Maximal harmonic current as a percentage of the maximal demand current I_L, individual odd orders [%]						
SCR	h<11	11≤h<17	17≤*h*<23	23≤*h*<35	*h*≥35	*TDD*
<20*	4.0	2.0	1.5	0.6	0.3	5.0
20<SCR<50	7.0	3.5	2.5	1.0	0.5	8.0
50<SCR<100	10	4.5	4.0	1.5	0.7	12
100<SCR<1000	12	5.5	5.0	2.0	1.0	15
>1000	15	7.0	6.0	2.5	1.4	20

* Applicable to power generator equipment regardless of the SCR
Even harmonics are limited to 25 % of these limits

IEC subcommittee 77A did not create a recommendation with harmonic current limits which the system operators can use directly. Instead, it published technical references (guidelines) with a methodology which the operators can use to create their own rules for connecting new potentially disturbing customers. This methodology can include also the present voltage distortion at the connection point in the limit calculation, and allocation of the emission to individual customers which share the connection point [11], [16]. In HV and MV systems for a $SCR \geq 500$, and in LV systems for a *SCR* greater than an internally adopted minimal value, the installation can be connected without further examination. These values of minimal *SCR* take the assumptions that there are no severe resonance effects and that the voltage distortion does not already exceed the planning levels.

In the same criterion, the *SCR* can also be calculated using a "weighted power" of the installation instead of the actual power. For certain types of equipment the power can be multiplied by a factor which takes into account the typical distortion of that type of load. For example, for a 6-pulse rectifier without a series inductance this leads to a *SCR* equal to one half of the actual (stricter approach), while for a 12-pulse rectifier this increases the *SCR* two times (a relaxation due to lower emission).

In case the first *SCR* condition is not met, an approach analogue to the IEEE 519 is used if $SCR \geq 100$ and no Power Factor Correction (PFC) capacitors or filters are used. The indicative maximal values of harmonic currents in this case are given in Table 2.4.

Table 2.5 Indicative IEC current distortion limits for general distribution systems, $SCR \geq 100$, [11], [16]

Maximal harmonic current as a percentage of the maximal demand current I_L, individual odd orders [%]		
h	LV	MV and HV
3	4	-
5	5	5
7	5	5
9	1	-
11	3	3
13	3	3
> 13	$500/h^2$	$500/h^2$

If we look at the recommendations of IEEE and IEC, for the same voltage level and *SCR*, it is interesting that for orders up to the 11th the IEC recommendations are stricter for the currents, while for the voltage limits the IEEE limits are stricter than the compatibility and planning levels of IEC. Except for historical reasons, this can also be explained by the differences of network topologies and load structure in North America and other parts of the world.

Using (2.2) and the IEC 60725 reference impedance mentioned earlier, we can calculate the ratio of the LV allocation coefficient (k_{LV}) and the compensation coefficient (k_C) from the voltage compatibility levels of IEC 61000-2-2 and indicative current limits of IEC 61000-3-6. In the same way we can calculate them from the voltage and current limits of IEEE 519, see Fig 2.1.

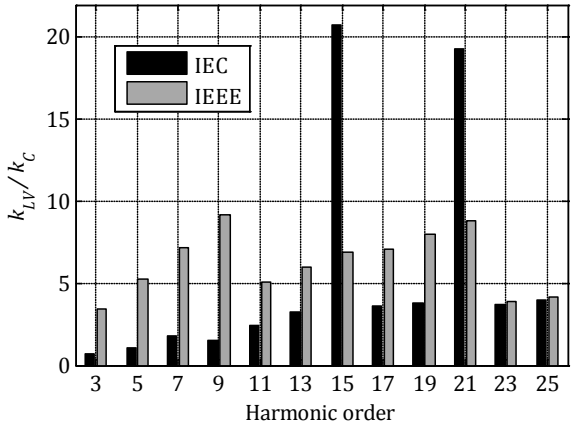

Fig 2.1 Calculated ratios of allocation and compensation constants for different harmonic orders; based on IEC and IEEE standards, and the IEC 60725 reference impedance

Formally speaking, the IEC 60725 should not be used against the IEC 61000-3-6 limits, because the impedance was defined for LV systems and the indicative current limits are defined for MV systems, but we can still see the qualitative change of this ratio for different harmonic orders, which does not principally change for different values of impedance used.

For a predominantly inductive network, the value of k_{LV} is not dependent on h, while the value of k_C is assumed to decrease with the increase of h. This is why the ratios from Fig 2.1 are expected to increase with h, but in both cases they show also some unexpected behaviour. This is specially the case with some of the triple-n harmonics from the IEC standards (15th, 21st), which have very low compatibility levels, due to the low measured levels. This leads to the conclusion that the current emission limits were not purely calculated from the voltage limits using (2.2).

2.3.1.1 Calculation from planning levels

For installations with a SCR < 100, the IEC recommendations give a simplified analysis method which takes into account the existing voltage distortion and the influence of other customers which share the same connection point. On an example of a MV system for a particular harmonic order, it is formulated as in (2.4), where CL_{MV} is the compatibility level for the MV level, $GC_{MV\&LV}$ is the allowed global contribution of the MV and LV levels, GC_{HV} is the global contribution of the HV level, $T_{HV\text{-}MV}$ is the transfer coefficient between HV and MV, and α is the summation coefficient which takes into account the compensation effects of loads.

$$CL_{MV}^{\alpha} = GC_{MV\&LV}^{\alpha} + (T_{HV-MV} \cdot GC_{HV})^{\alpha} \tag{2.4}$$

Once the allowed global contribution level ($GC_{MV\&LV}$) is calculated, the emission limits for the ith installation ($I_{hmax,i}$) can then be determined based on this level, the apparent power of the installation (S_i), the total supply capacity of the system including future expansions (S_t), and the harmonic impedance of the connection point ($Z_{h,i}$) as in (2.5).

$$I_{hmax,i} = \frac{GC_{MV\&LV}}{Z_{h,i}} \sqrt[\alpha]{\frac{S_i}{S_t}} \tag{2.5}$$

For the integration of distributed generation, the approach of hosting capacity is proposed in [17], which calculates the maximal harmonic current of all distributed generators which can be "hosted" in the observed network based on limits or planning levels. From the maximal total current and the emission of individual generators, the capacity of all additional generators is calculated.

The IEEE and IEC methodologies do not offer an analysis method which considers resonance conditions. A method for setting harmonic current limits including resonance conditions in HV networks was given by the German-Austrian-Swiss-Czech EMC working group, and explained in [18]. In this report it is suggested to calculate the harmonic current limit based on approximate value of harmonic impedance Z_h:

$$Z_h = k_h \cdot h \cdot X_{SC} \tag{2.6}$$

where k_h is the resonance factor and X_{SC} is the short-circuit reactance of the connection point. The approximate values of resonance factor are given in Table 2.5. The resonance approximation reduces the maximal emission of the installation k_h times:

$$I_{hmax,i} = \frac{GC_{MV\&LV}}{k_h \cdot h \cdot X_{SC}} \sqrt[\alpha]{\frac{S_i}{S_t}} \tag{2.7}$$

Table 2.6 Approximate values of the resonance factor for impedance calculation in HV networks, [18]

Type of network	$h < h_r - 2$	$h_r - 2 \le h \le h_r + 2$	$h > h_r + 2$
Networks dominated by cables	1	1.5-2.5	~1
Networks dominated by overhead lines		2-3	

h_r - harmonic order closest to the resonant frequency

2.3.2 Limits for individual equipment

For low-voltage equipment of relatively small rated power, which does not require a dedicated transformer (unlike large industrial equipment, for example large variable speed drives), limits for harmonic current emission are set by standard [19] for devices with a rated current up to 16 A, and by [20] for devices with a rated current greater than 16 A and up to 75 A per phase. The main goal of these two standards is to ensure that groups of devices complying to these two standards do not cause exceeding of compatibility levels defined in [10].

Standard [20] has a similar approach as IEEE 519 [5], the limits are dependent on the *SCR* but they do not take into account other devices sharing the same connection. This is justified by the relatively low power of devices covered by this standard.

Standard [19] has only one set of limits for each type of equipment (independent of the *SCR*), expressed in amperes or mA/W. Devices with a rated power up to 16 A usually appear in large numbers, so it would be impractical to investigate the connection of individual devices and *SCR* of each location. The main idea is to limit the distortion of a certain type of equipment, taking into account the numbers of devices used and interaction with other devices, which in turn should limit the total current of a group of devices and the influence on voltage distortion on almost all locations.

The formulas by which the emission limits were calculated were not disclosed in the standards. There is a reason to believe that some of the numbers used as the limits originate from the measurements on existing equipment, with the rational that if there are no global problems with voltage distortion it is sufficient not to allow more emission in the future. The involvement of equipment manufacturers and network operators in the creation of emission standards seems to be unbalanced.

To investigate this assumption, we looked at the example of limits for Class C equipment – lighting equipment, from [19], given in Table 2.6 and Table 2.7.

Table 2.7 Limits for lighting equipment (Class C), $P > 25$ W [19]

h	Maximal harmonic current, as a percentage of the fundamental [%]
2	2
3	$30 \cdot PF$
5	10
7	7
9	5
$11 \le h \le 39$	3

Odd harmonics only, P – active input power, PF – power factor of the device

Lamps with $P \leq 25$ W can comply either with the limits from Table 2.7, or to have the 3rd harmonic current up to 86 % of the fundamental and the 5th harmonic current up to 61 %, if the peak of the waveform is located before 65^0. This "relaxation" stimulates the harmonic phase angle diversity, because the majority of devices have a peak of the waveform around 90^0 (capacitor filtered diode bridge) or between 90^0 and 180^0 (passive power factor correction in rectifiers).

We look now at the maximal permissible total harmonic current for lamps, as a Root Square Sum (*RSS*) of components with $h \geq 2$ and assuming a $PF = 0.6$, and plot it against the measured total harmonic current of six different Compact Fluorescent Lamps (CFLs) with a $PF = 0.57$-0.62, see Fig 2.2.

Table 2.8 Limits for lighting equipment (Class C), $P \leq 25$ W [19]

h	Maximal harmonic current [mA/W]	Maximal harmonic current [A]
3	3.4	2.30
5	1.9	1.14
7	1.0	0.77
9	0.5	0.40
11	0.35	0.33
13	0.30	0.21
$15 \leq h \leq 39$	$3.85/h$	$0.15 \cdot (15/h)$

Odd harmonics only, P – active input power

It is noticeable that the measurements follow the limit almost exactly for each input power. This means that there is a high probability that the limits were based on a particular rectifier topology, rather than on the resulting impact on the harmonic voltages. Also, if we look at the absolute limits calculated for the power range 0-50 W, in Fig 2.3, we can notice that the phase angle based relaxation allows more distortion for very low values of *PF* than for units with $PF = 1$, which cannot be based on the impact on harmonic voltages.

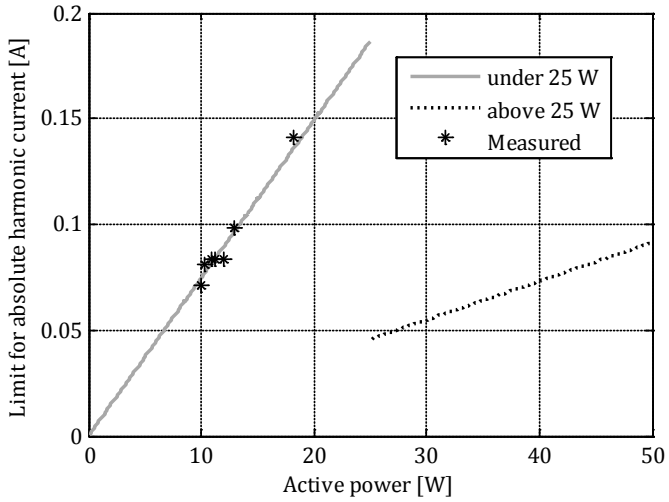

Fig 2.2 Harmonic emission limits for discharge lamps with P ≤ 25 W and PF = 0.6 and measured values

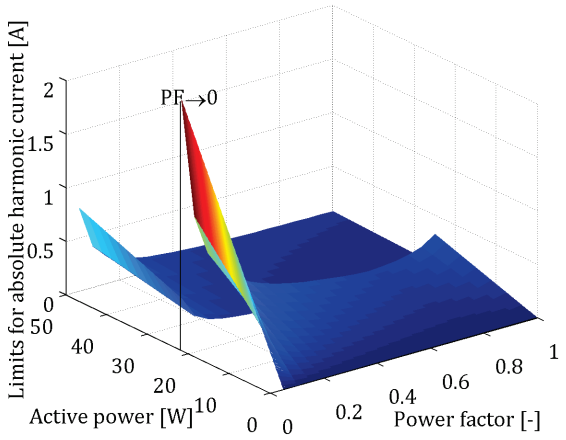

Fig 2.3 Absolute total harmonic current limits for lamps up to 50 W

2.4 Immunity of devices to harmonic distortion

The basic concept of electromagnetic compatibility is to keep the emission levels of disturbances lower than the compatibility levels, and the immunity levels of equipment higher than the compatibility levels. Even though there is a lot of knowledge about the influence of harmonic voltages and currents on electrical equipment, for most equipment the immunity levels are not formally defined. Most of the literature on equipment immunity gives methods to quantitatively determine the additional stress due to harmonic distortion, but not directly the immunity levels which could be used for limits.

When it comes to thermal and insulation stress due to harmonics, the immunity of most devices can be assured by a certain power and/or voltage level derating. The dilemma of assuring compatibility is between mitigating the disturbances (at the sources or centrally) and increasing the immunity of devices (usually by derating). The balance in cost sharing between the equipment manufacturers and network operators is both a technical and a policy question, but the additional costs always reach the end users, either through the price of equipment or tariff for energy.

Finding the balance between the emission and immunity requires good estimates of the costs related to harmonics, and the frequencies of problem occurrences. Examples of such analyses can be found in [21] for the loss of induction motor life due to harmonic voltages in the USA, and in [22] for the frequencies of problem occurrences in Brazil.

2.4.1 Immunity to harmonic currents

Sensitivity of equipment to harmonic currents is mostly connected to the additional losses which cause temperature increase and eventually the breakdown of insulation. Defining the immunity of a device sometimes means unnecessary giving up a part of the rated power. As an example, we look at the derating of power transformers. The calculation of additional power losses due to harmonic currents in transformers is explained in the standard [23] and a number of papers [24], [25]. If a transformer is derated to accommodate the additional losses due to a specific set of harmonic currents, the transformer might be operated at low power levels if the predicted current distortion is not present. This influences its efficiency as well as the initial

costs. For common spectrums of distorted load currents the transformers should be derated 5-25 %, with most cases on the lower end of this range.

In the case of power cables, usually there is less need for derating due to harmonic currents. As shown in [25], even for very distorted waveforms a derating of less than 10 % is needed for phase conductors. One common problem with power cables is the overheating of the neutral conductor when large numbers of single-phase equipment are present, especially if the neutral conductor was initially sized to a cross-section of smaller area than of the phase conductors [24].

The operation of circuit breakers is usually not affected for large short-circuit currents, due to the very large fundamental component [26]. The sensitivity of circuit breakers is usually increased or decreased around the nominal current, leading to false tripping in some cases or no reaction to small overcurrents, due to the wave shape of the current. For example, for circuit breakers with thermal elements the sensitivity is increased 3-5 % due to additional heating [26]. For most types of protection the sensitivity is affected by ±15 % [27], but an inrush current with harmonics can lead to a trip already at 60 % of the defined sensitivity [28]. Similar steady-state results were noticed for residual current protection [29]. Fuses are generally not affected by the presence of harmonics [28].

2.4.2 Immunity to harmonic voltages

Harmonic voltages cause two types of effects in equipment. The first one is the thermal effect, connected to the magnitude of harmonic components, leading to an increase of temperature of the device. The second type is due to the wave shape of the voltage. This includes increased dielectric stress, due to a higher voltage peak, and misoperation of electronic and protective devices.

One of the most common problems related to harmonic voltages is failure of capacitor banks, or blowing up of their fuses. Standard [30] defines the conditions in which capacitors should need to operate, up to: 110 % of the nominal voltage, 120 % of the nominal peak voltage, and 135 % of the rated reactive power. These values could be used to determine their immunity to harmonic voltages, but standards such as EN 50160 allow a voltage level of 110 % of the nominal for 95 % of the time, which already covers the voltage RMS requirement. If we combine the allowed overvoltage with the allowed capacitance tolerance of +10 %, the reactive power requirement (up to 135 % of the rated Q), this allocates only 4 % of the additional reactive power to harmonic voltages [25]. Defining the immunity of capacitors in these conditions would lead to values which are lower than the levels measured in most networks.

Requirements for the maximal current and power try to limit the thermal impact on capacitors, while the voltage RMS and peak value limit the dielectric stress on its insulation. In [31] the influence of harmonic voltages on the partial discharges in HV capacitors was analysed. It was found that if the harmonics lead to the increase in the voltage peak, this leads to a considerable increase of the partial discharge level. However, no immunity or derating levels are proposed. In [32], the electro-chemical reactions caused by dielectric stress in capacitors were analysed. Based on this, the additional loss of life due to harmonic voltages was analysed. In an example calculation it was estimated that a 3rd harmonic voltage with a magnitude equal to 20 % of the fundamental leads to about 60 % reduction of the capacitors lifetime. Most capacitor banks are slightly derated due to this effect (e.g. capacitors for 415 V are capable of operating continuously at a 450 V sinusoidal voltage).

Rotating machines experience additional heating and sometimes pulsating torques as well, when exposed to high levels of voltage harmonics. Unlike capacitors, rotating machines experience more overheating due to lower order harmonics, especially inter-harmonics below the fundamental (the winding impedance increases with frequency). In [33], a weighted total distortion factor is proposed, which takes into account the approximate heating effect in inductive devices (such as AC machines):

$$THD_R = \frac{\sqrt{\sum_{h=1}^{N} \frac{U_h^2}{h^{CR}}}}{U_1} \tag{2.8}$$

where CR is a constant between 1 and 2, dependent on the geometry of the machine, and U_h is the voltage of order h.

Standard [34] proposes derating of squirrel-cage induction motors based on the Harmonic Voltage Factor (*HVF)*, given by:

$$HVF = \sqrt{\sum_{h=1}^{N} \frac{U_h^2}{h}} \tag{2.9}$$

In [35] it is shown that the *HVF* can underestimate the losses in the machine, because (2.9) removes the dependency between the maximal flux and the phase angles of harmonic components.

In [36] a suggestion of 5 % voltage THD limit for induction motors was made, with the possibility that the suggestion originates from experiments with voltage unbalance, which has similar effects on rotating machines. In [21] a formula for estimating induction machine loss of life was suggested, based on the levels of voltage harmonics. From this formula, it was estimated that a motor with a nominal lifetime of 20 years loses approximately 1-2 years when operating with 1 % of voltage unbalance and 3 % voltage THD (of a spectrum measured in a public network). It the voltage THD is increased to 6 %, the loss of life grows to 2-5 years. Due to this, it was suggested that the limit of 5 % voltage THD is kept as a limit by IEEE 519.

Electronic devices, relays, and meters suffered from harmonic voltages relatively often in the past. Newer designs of these devices usually cope well with voltage distortion, as the input stages have better DC voltage stabilization. One problem which can be highlighted is the interaction of single-phase diode bridges with even order harmonics, especially the 2nd [37]. Low levels of even order distortion can cause relatively high values of the DC current emission of the bridge, which can cause damage to power transformers. The amount of DC component depends on the circuit parameters, but for realistic values a 10 % DC current component can be generated due to only 1 % of the 2nd harmonic voltage. Due to this, the authors suggested using a 2nd harmonic limit not greater than 1 % of the fundamental voltage.

The short-term effects of high levels of distortion are an area which needs more exploration. The mentioned short-term limits (section 2.2) are not referring to any specific immunity study. In [38], it is proposed that the short-term distortion is analysed based on the distortion level and duration of bursts. The duration can be observed both as the cumulative duration of all bursts (with levels higher than the

long-term limit) and as the duration of individual bursts. This approach could result in limits for individual bursts, which covers 100 % of the time.

Testing of equipment immunity to harmonic voltages is defined in the standard IEC 61000-4-13 [39], for devices with a rated current up to 16 A per phase. The same standard also recommends test levels, however these levels are not obligatory for any type of equipment. Individual product committees of IEC are responsible for defining immunity requirements for each product type, and so far there are no immunity requirements which are applicable for all devices.

2.5 Conclusions

There are several remarks which can be made about standards covering harmonic distortion. The first is that since there are no global problems with distortion but only local, the standards offer a good solution for most cases. Predictions from the 1970' and 1980' of very high harmonic levels due to proliferation of power electronics never came true, even though in many countries the share or resistive load is reduced considerably. For example, in [40] it was reported that in Australia 69 % of household loads already have a power electronic front end. In [41-43] it was shown that the voltage THD level in the distribution networks in Netherlands remained almost constant between 1998 and 2012. This time period includes load growth, but also the widespread application of PFC in devices, as a result of an EMC directive in the EU. Standards should keep up with the changes of the network, as it is difficult to predict the problems in all cases, and the loads and generation continue to evolve [44].

Some of the voltage limits seem to be based mainly on the measured voltages and some of the current limits are based on the spectrum of a device, rather on the immunity of devices for voltage limits and the influence of harmonic currents on harmonic voltages. Examples for this are EN 50160 for voltage limits, IEC 61000-3-2 for a part of its current limits. The relation between the voltage and current limits within IEEE 519 and between IEC 61000-2-12 and IEC 61000-3-6 shows that (2.2) is not maintained for all harmonic orders. The compensation coefficient (k_C) from this expression is further explored in Chapter 5 for industrial installations.

The immunity of devices and/or additional loss of life should be formally defined for harmonic voltages. For harmonic currents the derating is a practical solution, as it leaves the option of using a device at a higher power when little or no distortion is present. For harmonic voltages a similar approach could be used, where the expected reduction of the lifetime could be estimated based on the expected voltage harmonic levels, and maybe compensated for with a higher voltage and power rating, as it is already done with power capacitors. If the immunity to harmonic voltages would be defined for all (or most) types of devices, it would be relatively easy to coordinate the international limits, and decide if they should be made more relaxed or stricter.

As both the systems using IEEE 519 and EN 50160 normally function well, it might be a fare solution to adopt the less strict rules from both standards. The voltage THD could be limited to 8 % as in EN 50160, and some of the odd harmonic individual limits could be increased to 3 %, as in IEEE 519. The limits for triple-n orders, which are presently very strict, should be revised based on the immunity and additional losses in transformers.

The current limits for installations and individual equipment should correspond with the impact on the voltage distortion for all orders. As the two coefficients used in (2.2) are not available, it is not sure how their ratio changes with the increase of the

harmonic order. The approach of IEC is preferred, as the IEEE 519 does not take into account the background distortion and the same impedance value is used for a range of *SCR* values.

Further research on the short-term effects of harmonic voltages and currents is needed for the improvement of short-term limits, based on short-term DFT or alternative processing methods. Processing of non-stationary signals is discussed in Chapter 3.

2.6 References of Chapter 2

[1] A. Kloss, "The history of harmonics," in Proc. *IEEE ICHPS*, 1986.

[2] E. L. Owen, "A history of harmonics in power systems," *IEEE Industry Applications Magazine*, vol. 4, no. 1, pp. 6–12, Jan. 1998.

[3] R. Dodds, "Experiences from a regional electricity company," in *IEE Colloquium on Sources and Effects of Harmonic Distortion in Power Systems*, 1997, vol. 1997, pp. 6–6.

[4] P. M. Lincoln, "Wave Form Distortions and their Effects on Electrical Apparatus," *Transactions of the American Institute of Electrical Engineers*, vol. 32, no. 1, pp. 765–774, Jan. 1913.

[5] IEEE 519, "IEEE Recommended Practices and Requirements for Harmonic Control in Electrical Power Systems," 1992.

[6] M. Bollen, "Overview of Power Quality and Power Quality Standards," in *Understanding power quality problems: Voltage sags and interruptions*, 1st ed., Wiley-IEEE Press, 2000, pp. 1–34.

[7] CIGRE Working Group 36-05 Report, "Harmonics, characteristic parameters, methods of study, estimates of existing values in the network," 1981.

[8] EN 50160, "Voltage characteristics of electricity supplied by public distribution systems," 2010.

[9] IEC 61000-2-2, "Electromagnetic compatibility (EMC) - Part 2-2: Compatibility levels for low-frequency conducted disturbances and signalling in public low-voltage power supply systems," 2002.

[10] IEC 61000-2-12, "Electromagnetic compatibility (EMC) - Part 2-12: Environment - Compatibility levels for low-frequency conducted disturbances and signalling in public medium-voltage power supply systems," 2002.

[11] IEC 61000-3-6, "Electromagnetic compatibility (EMC) - Part 3-6: Limits - Assesment of emission limits for the connection of distorting installations to MV, HV, and EHV power systems," 2008.

[12] P. F. Ribeiro and G. Carpinelli, "IEEE Std 519 revision: the need for probabilistic limits of harmonics," in Proc. *Power Engineering Society Summer Meeting*, 2001, vol. 2, pp. 809–812.

[13] IEC 61000-2-4, "Electromagnetic compatibility (EMC) - Part 2-4: Compatibility levels in industrial plants for low-frequency conducted disturbances," 2002.

[14] A. Mansoor and J. McKim, "An examination of the rationale for limiting harmonic emissions from low-voltage equipment," in Proc. *IEEE International Symposium on Electromagnetic Compatability*, 1999, vol. 2, pp. 934–939.

[15] VDEW, "EMC guide for public power supply networks - Compatibility levels and permissible emission," 1992.

[16] IEC/TR 61000-3-14, "Electromagnetic compatibility (EMC) - Part 3-14: Assessment of emission limits for the connection of disturbing installations to LV power systems," 2011.

[17] M. H. J. Bollen and F. Hassan, "Power system performance," in in *Integration of distributed generation in the power system*, Wiley-IEEE Press, 2011, pp. 84–101.

[18] J. Meyer and W. Mombauer, "Assessment of emission limits for disturbing installations connected to HV distribution networks in AT, CH, CZ and GE," in Proc. *IEEE ICHQP*, 2012, pp. 262–267.

[19] IEC 61000-3-2, "Electromagnetic compatibility (EMC) - Part 3-2: Limits - Limits for harmonic current emissions (equipment input current <16 A per phase)."

[20] IEC 61000-3-12, "Electromagnetic compatibility (EMC) - Part 3-12: Limits - Limits for harmonic currents produced by equipment connected to public low-voltage systems with input current > 16 A and < 75 A per phase."

[21] J. P. G. de Abreu and A. E. Emanuel, "Induction motor thermal aging caused by voltage distortion and imbalance: loss of useful life and its estimated cost," *IEEE Transactions on Industry Applications*, vol. 38, no. 1, pp. 12–20, 2002.

[22] J. T. Tiznado, S. Yagi, and P. F. Ribeiro, "Operating experience with voltage distortions in the Brazilian network: A survey," in *IEEE ICHPS*, 1990.

[23] IEEE C57.110, IEEE Recommended Practice for Establishing Liquid-Filled and Dry-Type Power and Distribution Transformer Capability When Supplying Nonsinusoidal Load Currents," 2008.

[24] V. E. Wagner, J. C. Balda, D. C. Griffith, A. McEachern, T. M. Barnes, D. P. Hartmann, D. J. Phileggi, A. E. Emannuel, W. F. Horton, W. E. Reid, R. J. Ferraro, and W. T. Jewell, "Effects of harmonics on equipment," *IEEE Transactions on Power Delivery*, vol. 8, no. 2, pp. 672–680, Apr. 1993.

[25] D. E. Rice, "Adjustable Speed Drive and Power Rectifier Harmonics-Their Effect on Power Systems Components," *IEEE Transactions on Industry Applications*, vol. IA-22, no. 1, pp. 161–177, Jan. 1986.

[26] A. Fidigatti and E. H. and Q. of P. Ragaini, "Effect of harmonic pollution on low voltage overcurrent protection," in Proc. *IEEE ICHQP*, pp. 1–4, 2010.

[27] J. F. Fuller, E. F. Fuchs, and D. J. Roesler, "Influence of harmonics on power distribution system protection," *IEEE Transactions on Power Delivery*, vol. 3, no. 2, pp. 549–557, Apr. 1988.

[28] J. Desmet, "Analysis of the behaviour of fusing systems in the presence of nonlinear loads," in Proc. *International Conference on Power Electronics Machines and Drives*, 2002, pp. 616–619.

[29] Y. Xiang, V. Cuk, and J. F. G. Cobben, "Impact of residual harmonic current on operation of residual current devices," in Proc. *10th International Conference on Environment and Electrical Engineering*, 2011, pp. 1–4.

[30] IEEE 18, "IEEE Standard for Shunt Power Capacitors," 2002.

[31] W. Chen and Z. Cheng, "An experimental study of the damaging effects of harmonics in power networks on the capacitor dielectrics," in Proc. *Second International Conference on Properties and Applications of Dielectric Materials*, 1988, pp. 645–648.

[32] L. H. S. Duarte and M. F. Alves, "The degradation of power capacitors under the influence of harmonics," in Proc. *IEEE ICHQP*, 2002, vol. 1, pp. 334–339.

[33] J. Arrillaga and N. R. Watson, "Effects of harmonic distortion," in in *Power system harmonics*, John Wiley & Sons, 2003, pp. 143–190.

[34] IEC TS60034-17, "Rotating electrical machines - Part 17: Cage induction motors whed fed from converters - Application guide," 2002.

[35] C. Debruyne, J. Desmet, S. Derammelaere, and L. Vandevelde, "Derating factors for direct online induction machines when supplied with voltage harmonics: A critical view," in Proc. *IEEE International Electric Machines & Drives Conference (IEMDC)*, 2011, pp. 1048–1052.

[36] T. Meliopoulos, A.P., Chakravathi, K.R., Ortmeyer, "Effects of harmonics on power system equipment and loads," in *IEEE Tutorial 84 EH0221-2-PWR*, 1985, pp. 21–31.

[37] J. A. Orr and A. E. Emanuel, "On the need for strict second harmonic limits," *IEEE Transactions on Power Delivery*, vol. 15, no. 3, pp. 967–971, Jul. 2000.

[38] T. Ortmeyer, W. Xu, and Y. Baghzouz, "Setting limits on time varying harmonics," in Proc. *IEEE Power Engineering Society General Meeting*, 2003, pp. 1172–1175.

[39] IEC 61000-4-13, "Electromagnetic compatibility (EMC) - Part 4-13: Testing and measurement techniques - Harmonics and interharmonics including mains signalling at AC power port, low frequency immunity tests," 2009.

[40] S. T. Elphick, "The modern domestic load and its impact on the electricity distribution network," MSc thesis, University of Wollongong, Australia, 2011.

[41] S. Cobben, "Power quality - Implications at the point of connection," PhD thesis, Eindhoven University of Technology, 2007.

[42] S. Bhattacharyya, "Power quality requirements and responsibilities at the point of connection," PhD thesis, Eindhoven Universtity of Technology, 2011.

[43] Movares report, "Spanningskwaliteit in Nederland, resultaten 2012," RM-ME-130208-01, in Dutch, 2013.

[44] A. de Oliveira, J. C. de Oliveira, A. M. Sharaf, T. H. Ortmeyer, and P. F. Ribeiro, "Harmonic Standards - The Need For An Integrated Perspective," in Proc. *IEEE ICHPS*, 1992, pp. 295–302.

Chapter 3

Measurement methods

3.1 Introduction

The most common approach for describing a signal with its spectral components is by its Fourier series. The well-known expression for this frequency-domain representation of a time-domain signal, adapted from [1], is:

$$f(t) = \sum_{h=-\infty}^{\infty} \underline{c_h} \cdot \mathrm{e}^{jh\omega t} \tag{3.1}$$

where $f(t)$ is the time domain signal, $\underline{c_h}$ is the complex Fourier coefficient of the h^{th} harmonic component, and ω is the angular velocity of the fundamental phasor. The complex representation of the Fourier series contains both components of "positive" and "negative" frequencies, but as the negative frequencies are mirror images of positive ones, it is not necessary to take them into account.

Magnitudes of coefficients $\underline{c_h}$ are $\sqrt{2}$ times greater than the RMS values of spectral components, calculated over the time interval of one data window length. The most common usage of terms "value" and "level" of harmonic components in power systems refers to their RMS value, because the RMS is directly related to the thermal effects of harmonics.

The previous equation is valid only if $f(t)$ satisfies the following conditions: the function must be periodic, it can have only a finite number of finite discontinuities, it must have only a finite number of maximums and minimums, and its integral over one period must converge. The first condition of periodicity is never completely satisfied for a realistic signal, and will be considered in the following sections.

Equation (3.1) cannot be used directly on a sampled (digitally measured) signal, and during the 1950s the Discrete Fourier Transformation (DFT) was developed, which can calculate the Fourier series of one data window of a sampled signal:

$$f[n] = \sum_{k=1}^{N-1} \underline{C_k} \cdot e^{\frac{j2\pi kn}{N}} \tag{3.2}$$

where $f[n]$ is the sampled version of the time domain signal, n is the number of the sample between 1 and N, k is the index of frequency components (integer number representing the frequency), and $\underline{C_k}$ are the complex Fourier coefficients.

The DFT is directly implementable in a computer program, so it became very popular during the last decades, especially its special case where N is a power of two,

which makes the calculation much quicker. Due to this, this version of DFT is known as the Fast Fourier Transformation (FFT).

3.2 DFT of non-stationary signals

All measured signals are time-varying in nature because of load and generation variations, network reconfigurations, impedance variations, etc. Due to this, the first condition of Fourier series (periodicity of the signal) is not satisfied. This introduces errors in the calculation of spectral components, and slightly changes their physical meaning.

To reduce the effects of short-term signal changes and increase the frequency resolution, the DFT is usually not performed over a single period of the power system frequency. Standard IEC 61000-4-30 [2] proposes using a 10/12 period data window for 50/60 Hz systems. This results in a frequency resolution of 5 Hz.

To illustrate one of the difficulties of non-stationary signals, we look at Fig 3.1 (a) in which a signal is shown which has an amplitude reduction of 50 % after 200 ms. The signal contains a fundamental component of 1 p.u. (per unit) and a 3rd harmonic of 0.2 p.u. If the signal changes coincide with data windows, the time changes will not affect the result of individual data windows. Each result is the spectrum with the assumption that the waveform is repeated before and after the data window. The per-unit spectrum of both the first and second time period of 200 ms is shown in Fig 3.1 (b).

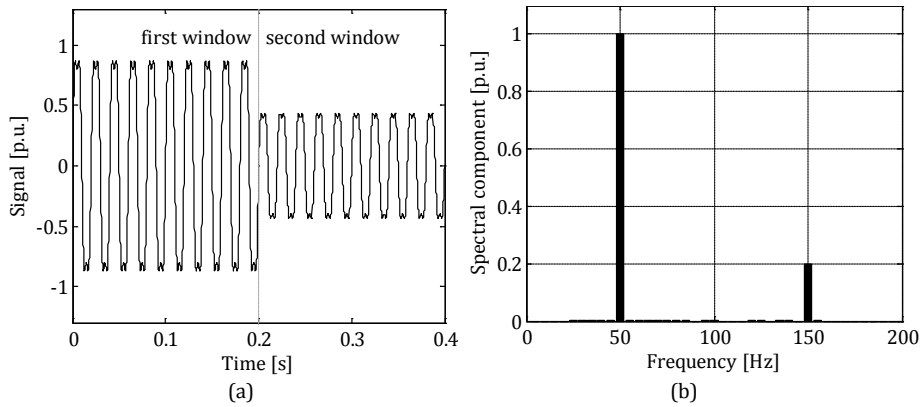

Fig 3.1 Example of a non-stationary signal: (a) fundamental of 1 p.u. and 3rd harmonic of 0.2 p.u. with a magnitude change of 50 % for both components, (b) spectral components for both data windows

It is highly unlikely that the signal changes coincide with data windows, such as shown in Fig 3.1. In Fig 3.2 (a) we look at the same signal with a data window which contains five periods before the amplitude change and 5 periods after the change (again the data window length is 10 periods). The p.u. spectrum of this data window is shown in Fig 3.2 (b). Even though the signal contains only two frequency components in each period, due to frequency spill-over, parts of harmonic components can be found on nearby spectral lines (inter-harmonics), with a reduction of the harmonic components. The reason for this is the frequency resolution. On each window length of the 50 Hz period (DFT resolution of 50 Hz), the signal contains only two frequency components, but on a window length of 10 periods (DFT resolution of 5 Hz), the 50 Hz component is the 10th harmonic. If such a wave shape would repeat itself each 200 ms, these spectral components would continue to exist.

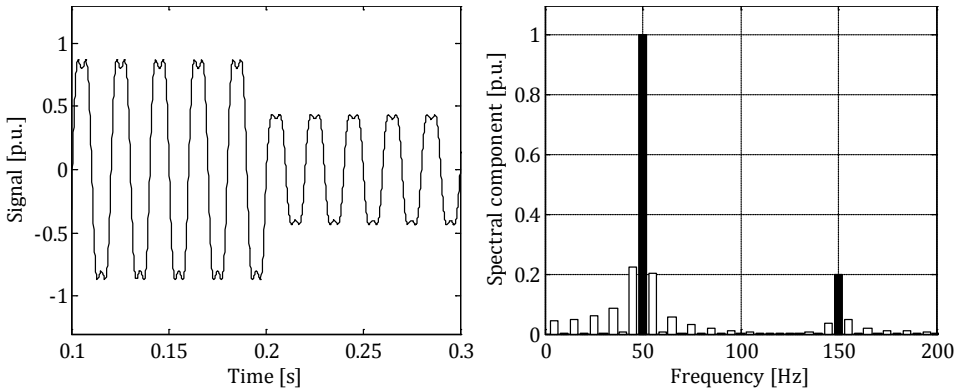

Fig 3.2 Example of a non-stationary signal: (a) data window which includes the signal change, (b) spectral components of this data window

Standard IEC 61000-4-7 [3] addresses the problem of non-stationary signals with spectral grouping. Since a part of the content of a harmonic spills over to nearby inter-harmonics, [3] adopted a concept of harmonic groups and subgroups:

$$G_k^2 = \frac{C_{k-5}^2}{2} + \sum_{i=-4}^{4} C_{k+i}^2 + \frac{C_{k+5}^2}{2} \tag{3.3}$$

$$SG_k^2 = \sum_{i=-1}^{1} C_{k+i}^2 \tag{3.4}$$

where k is the index of the spectral component (groups and subgroups are calculated only for values of k which correspond to harmonics), C_k is the RMS of a spectral component (either harmonic or inter-harmonic), G_k is RMS of a harmonic group, and SG_k represents RMS of a harmonic subgroup.

These approaches summate the power of a narrow frequency band into the power of the associated harmonic component. In this way the non-periodic amplitude variations are partly included in the RMS of the harmonic component, which reduces the errors caused by the non-stationary nature. Harmonic groups include a frequency band broader than subgroups, so they can compensate for larger amplitude variations than harmonic subgroups.

For evaluating harmonic voltages, [2] proposed that harmonic subgroups are used (smaller range around the harmonic), because voltage amplitude variations are usually relatively low in comparison with the nominal value. During voltage dips, values of harmonics are flagged to indicate possible high errors. For evaluating harmonic currents, in the new version of [2] will possibly propose to use harmonic subgroups, while for the purpose of emission testing harmonic groups can be used, because amplitudes of currents can vary much more due to load variations.

The 10/12 cycle RMS is usually not used directly in overall surveys. To reduce the amount of data, 150/180 cycle aggregated values are proposed as short-term values, 10 minute and 2 hour aggregates are proposed as long-term values. Aggregation is done using:

$$AV = \sqrt{\frac{1}{N}\sum_{i=1}^{N} V_i^2} \tag{3.5}$$

where AV is the aggregated value, V_i is the i^{th} 10/12 cycle RMS, and N is the number of values to be aggregated.

3.2.1 Phase angles of DFT components

The complex form of the Fourier series (3.1) can be transformed into a sum of sine or cosine components. In these two forms, each of the harmonics is defined by their magnitudes and phase angles. In this thesis, the sine form is used to characterise the phase angle behaviour of signals, defined by:

$$f(t) = c_0 + \sum_{h=1}^{\infty} c_h \cdot \sin(h\omega t + \varphi_h) \tag{3.6}$$

where c_h are the amplitudes of spectral components and φ_h are their phase angles.

Similarly to calculation of magnitude RMS, measurement of the phase angles of spectral components also suffers from the non-stationary nature of the signal, but in a different way than in the case of magnitudes. If we repeat the experiment from the previous section, with different positions of the data window of the signal from Fig 3.1 for a DFT calculation of phase angles of spectral components, in both cases the phase angles of harmonic components are calculated accurately (equal to 0°). With a data window which includes the magnitude change, only the phase angles of inter-harmonic components change.

Even for a stationary signal with constant inter-harmonic components their phase angles do not have a physical meaning, because their values are time dependent, with a repetition frequency equal to one period of the inter-harmonic.

Now we look at two different scenarios using the same approach. Firstly, we consider a signal with two components, fundamental and 3rd harmonic, with constant magnitudes and a change of the phase angle of the 3rd harmonic. The harmonic changes its phase angle from 0° to 80° at 200 ms, as in Fig 3.3. Note that the change of signal peak is caused entirely by the phase angle change.

If we calculate the DFT of the signal from Fig 3.3 over a data window which includes five periods before the change and five periods after the change, we get phase angles as in Fig 3.4. In this case DFT calculates the average value of phase angles (only for harmonic components) over the entire period. For a change from 0° to 80°, the result is 40°, shown as the red bar in Fig 3.4. If the two periods of different angles do not last equally, the result is close to, but not equal to their average value. In both cases the phase angle of the fundamental component is not affected, as in reality. Phase angles of inter-harmonic components, shown with white bars in Fig 3.4, are affected but they do not contain significant information, because their values are dependent on the observation moment even for a stationary signal.

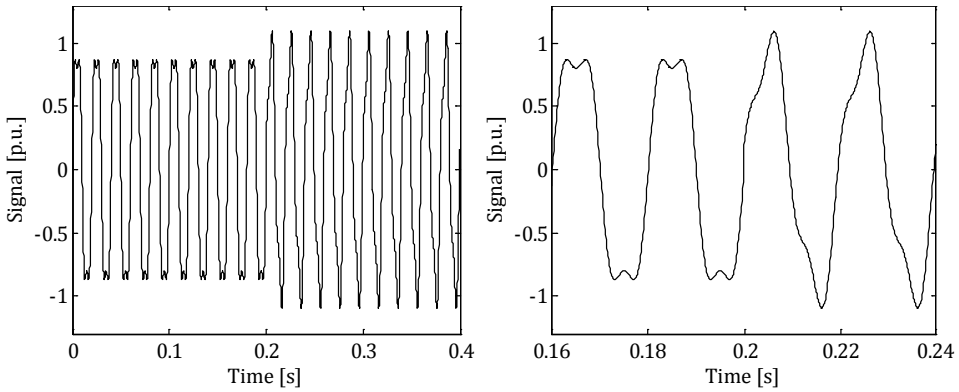

Fig 3.3 Example of a non-stationary signal: (a) fundamental of 1 p.u. and 3rd harmonic of 0.2 p.u. changing its phase angle from 0° to 80°, (b) zoomed in change in the signal

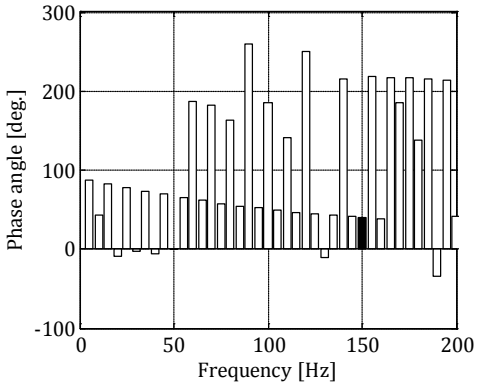

Fig 3.4 Phase angles of spectral components, signal from Fig 3.3

Secondly, we look at the same signal with a change in both the magnitude and phase angle of the third harmonic, as in Fig 3.5. The magnitude is decreased by 50 % and the phase angle is changed from 0° to 80° at 200 ms.

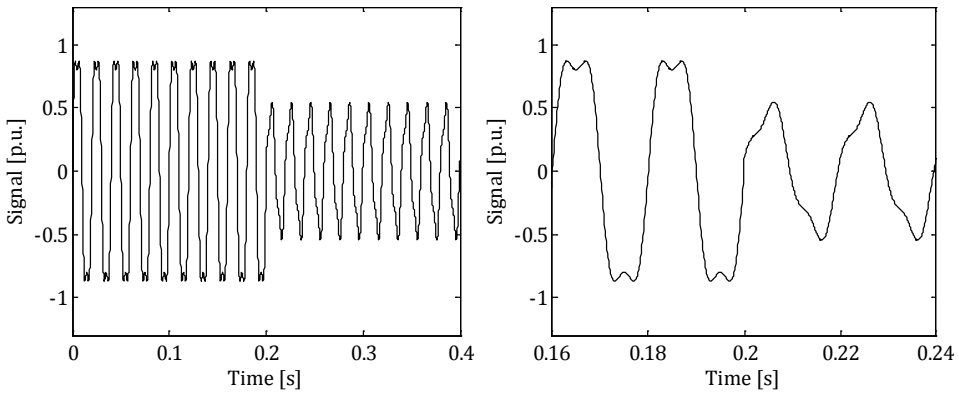

Fig 3.5 Example of a non-stationary signal: (a) fundamental of 1 p.u. and 3rd harmonic of 0.2 p.u. changing both its magnitude and phase angle of the harmonic, (b) zoomed in change in the signal

When both the phase angle and the magnitude change the fundamental phase angle is again not affected, but the angle of the third harmonic is no longer the average over the data window. The calculated value of the phase angle in this case is 24.4° (dark bar in Fig 3.6). This value does not describe well the first or the second half of the data window, it has no physical meaning in this case.

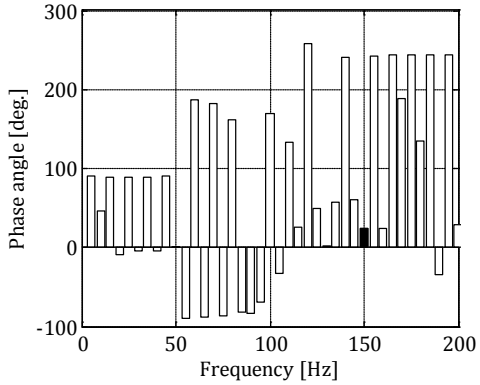

Fig 3.6 Phase angles of spectral components, signal from Fig 3.5

When calculating the magnitude of the signal, the RMS provides a good description even when there is a signal change within the time period of the calculation, because it corresponds to the power. The frequency spill-over is mostly compensated for with the usage of harmonic groups and subgroups. Aggregation of more data windows also does not lead to magnitude information loss. In the case of phase angles, as we could see in the three examples, the situation is different. If the phase angle does not change during the data window, DFT provides accurate phase angle information. If the data window includes phase angle changes, the resulting phase angles do not provide enough information about the signal. Even when the signal changed only in phase angles and the result is exactly or approximately equal to the average value during the data window, the resulting values do not give enough information if the angle changes considerably during the data window. Also, angles of nearby inter-harmonic components do not provide additional information, unlike in the case of magnitude. For these reasons, for phase angle measurements it is important that the angles do not change considerably during data windows. In other words, the data window should be short enough to make the information reliable. This might be a problem with quickly varying loads, such as arc furnaces. Time aggregation to long-term values (e.g. 2 hour values) probably leads to a loss of information in all cases, a range of values during the interval would provide better information.

The measurement method for phase angles of harmonic components is at this moment not defined by the standard IEC 61000-4-7 [3]. The method should be able to deal with time variations of realistic signals from the network, which are probably higher for currents than for voltages. One possibility is expressing the phase angle information as a histogram of all data windows instead of an aggregated value.

3.3 Considerations on short-term indices

The thermal effects of harmonic distortion are normally easy to describe by long-term indices such as ten minute and two hour RMS values. Also, most equipment

operates with relatively slow variations, and does not require data processing with a time resolution better than ten minutes. However, in some cases the variations are too quick to be described with such indices, and this brings the more difficult question of how to describe the effects of high levels of distortion which last relatively short, sometimes referred to as harmonic bursts.

In [4] it was analysed how different effects of harmonics relate to different indices. The thermal time constants of power system equipment create a basis for the ten minute indices, and this covers the effects of harmonic currents in most cases. Regarding the dielectric stress of the insulation, including partial discharges, shorter time intervals are also important for accelerated aging of the equipment. Nuisance tripping of protective devices is another effect of harmonics which requires taking shorter time intervals in account [5].

When a single peak value during a rapid signal variation is of interest it is better to characterize the disturbance as a transient. When an increased voltage peak is sustained for a short period of time (seconds, several minutes) due to harmonic components, or if specific spectral components of a transient lead to misoperation of a device, then it is of interest to characterize the short-term harmonic components. Standard [2] proposes a data window of 150 cycles of the fundamental (180 for 60 Hz systems), which is approximately 3 s, as a short-term indice.

For the effect of harmonic bursts it may not only be important what is the cumulative probability level (value not exceeded for a certain percentage of time in the probability distribution function), but also the duration of individual bursts. In [4] it was proposed to analyse the cumulative distribution of the distortion level as a function of the duration of the individual burst. This approach offers more insight than the cumulative level alone, but it has a problem that the distortion level can vary during a burst. Due to this, it is questionable which distortion level should "represent" an individual burst. For example, if during a harmonic burst with duration of 2 minutes the 150 cycle THD (or HD of a single harmonic) value varies between 8 % and 10 % should we use the maximal, average, RMS, or some probability level of the THD?

The maximal 150 cycle value is not the best solution. One 150 cycle interval contains 15 values based on 10 cycles. If one of the 10 cycle intervals has a level which is much greater than the other 14 intervals this might overestimate the effect of the whole burst. One solution would be to use an approach with cumulative probability values. For example, the 12^{th} greatest value is not exceeded for 80 % of the time, or the 14^{th} greatest value for 93.3 % of the time.

As far as the thresholds for the start and end of a burst, the long-term limits seem as a reasonable solution, since these distortion levels are allowed for 95 % of the measurement time.

The real immunity requirements of equipment would probably require "tailor made" indices for different equipment and effects, but for practical reasons the measurements need to be comparable. Comparable measurements provide information even when the indice is not a perfect fit to the phenomenon (as long as it describes it well enough).

For quantifying the accelerated aging due to dielectric stress on equipment, the Crest Factor (CF) might be a better short-term indice than the THD or HD. CF stresses the peak of the waveform, but the value of the peak is also dependent on the RMS. THD and HD do not describe the peak of the waveform because they do not take the phase angles of harmonic components into account. With the assumption that peaks of harmonic components are in phase the peak value can also be estimated, but for most

of the time it will be overestimated. For dielectric stress, a reasonable solution is also using the peak value of the voltage directly, instead of any of the harmonic indices.

For interference with protective and control devices, the spectral information is more important because iron core magnetization is frequency dependent and for long current loops the interference can even be radiated, as in the case of telephone interference. When the interference is caused by the time derivative of the current or voltage, the problem might better be described as a transient event than as a harmonic burst.

3.3.1 Selection of the data window length for short-term DFT (STDFT)

For a non-stationary signal, decomposition can be performed on a sliding window which is refreshed by a few periods at a time. This is called short-term DFT (STDFT). The calculated RMSs of spectral components depend on the selected data window length. Due to this, the measurement can only be evaluated against the limits which are defined for the measurement technique as discussed before.

If we process the same data with several window lengths, the shortest data window will always have the highest maximal value. For slow variations these differences will not be pronounced, but as the variation speed increases, the difference increases. In Fig 3.7 we look at an inrush current waveform (a), and its 5th harmonic calculated with a sliding widow of 20 ms and 200 ms (b).

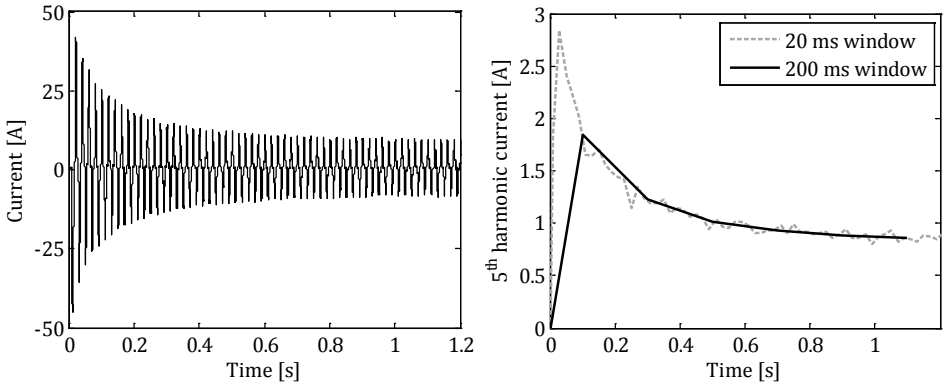

Fig 3.7 Inrush current: (a) waveform, (b) 5th harmonic as a result of two different data windows

Results of the two data windows have different time resolutions. Therefore, the first result of the 20 ms window is located at 10 ms, and of the 200 ms window at 100 ms. Also, there is a significant difference in the highest value. As the waveform reaches the steady state, the difference becomes smaller. For practical reasons, the measurement should not necessarily be “optimized” to calculate the highest levels of distortion during bursts, but it should be able to quantify its physical effects. Using data window lengths, time aggregation intervals, and indices which are not specified in the standards makes sense, but they should be used with caution if they are to serve its purpose. In the following subsection we look at an example of how the data window length influences the robustness of grid impedance measurement based on inter-harmonic injection.

3.3.1.1 Case study – Data window length and interference in impedance measurement

In this case study we look at one version of impedance measurement which is widely used in the anti-islanding protection of PV inverters. Anti-islanding protection techniques are categorized and described with more details in [6]. Globally, they are distinguished as passive, active, and methods which are not resident in the inverter. Passive methods are non-invasive, and use only monitoring of voltage and frequency. Active methods deliberately inject disturbances into the grid, and then monitor its response. Methods not resident in the inverter are implemented in separate measurement devices. Here we look at the impedance measurement method, based on inter-harmonic injection.

This method is suggested by DIN VDE 0126 and EN 50330-1 standards. Requirements for this type of protection is that it detects a change in the network impedance equal or higher than 0.5 Ω, and that it reacts within 5 s. Impedance measurement can be done with power shifting or injection of non-characteristic harmonics or inter-harmonics. Injection of harmonics or inter-harmonics is a widely used variant of this method. It uses a deliberate disturbance which will produce a current at the desired frequency. Simultaneously, voltage and current are measured and their (inter)harmonic components are derived. Impedance is then calculated by dividing the values of voltage and current, and scaled to 50 Hz. To reduce measurement errors, averaging of impedance results is often used.

One of the problems for impedance measurement is inaccurate measurement caused by parallel operation of several devices. False tripping is possible because injection of harmonic currents of several devices will increase the overall harmonic voltage. To reduce the erroneous effect caused by parallel injection, altered injection methods are developed to desynchronize the peaks of inter-harmonic currents [7-9]. This reduces the effects of deliberate disturbances, but the method is not always immune to uncontrolled disturbances, such as inrushes.

We analyse the effect of inrushes on the robustness of impedance measurement by a series of laboratory experiments. The setup of the experiment is schematically shown in Fig 3.8. A commercially available inverter is fed from a photovoltaic simulator, and the AC side of the inverter is connected to a programmable voltage source which is controlled by a Matlab program. Between the network simulator and the inverter, a vacuum cleaner with electronic speed control is connected to produce inrush currents. In front of the point of connection an inductor is placed, labelled with Z_{poc}, to simulate the network impedance. The value of the inductance is varied several times during the experiment.

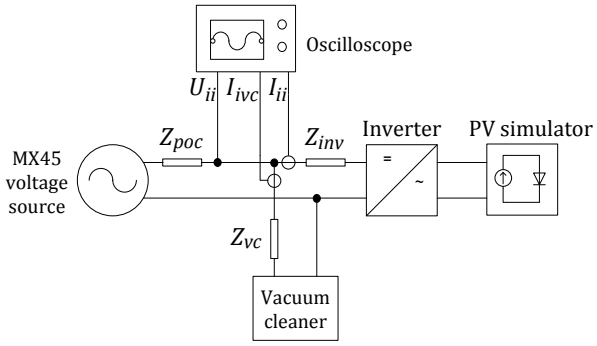

Fig 3.8 Schematic diagram of the experiment

Voltage at the point of connection is measured by a Hioki 8861 oscilloscope. Currents of the inverter and the vacuum cleaner are measured by the same oscilloscope and with Tektronix TCP303 current probes.

Impedance measurement of the inverter during a vacuum cleaner inrush is described by:

$$Z_M = \frac{Z_{poc}(I_{ii} + I_{ivc}) + Z_{inv}I_{ii}}{I_{ii}} \tag{3.7}$$

where Z_M is the equivalent network impedance measured by the inverter, I_{ii} is the inter-harmonic current injected (and measured) by the inverter, Z_{poc} is the actual network impedance at the point of connection, I_{ivc} is the inter-harmonic disturbance of the vacuum cleaner, and Z_{inv} is the impedance of the cable between the inverter and the point of connection.

The measurement error caused by the vacuum cleaner Z_{err} is equal to:

$$Z_{err} = \frac{Z_{poc}I_{ivc}}{I_{ii}} \tag{3.8}$$

To cause a false trip of the anti-islanding protection, the disturbance needs to satisfy:

$$Z_{poc}I_{ivc} \geq 0.5\Omega \cdot I_{ii} \tag{3.9}$$

This condition needs to be met during a time interval needed for one or several measurements. For the inverter analysed, the measurement frequency is 75 Hz, and the injected current is between 1 and 1.2 A.

Vacuum cleaner's and inverter's current waveforms during an inrush and false trip are presented in Fig 3.9 and Fig 3.10. The current spikes visible on the inverter's current waveform are inter-harmonic injections which happen in regular time intervals, for impedance measurement.

Without a trigger, the measurement is done on each two seconds. After a trigger of higher impedance, the impedance is measured each 10 periods. Each inter-harmonic injection lasts two periods of the fundamental, in this way the disturbance level is reduced in comparison with constant injection.

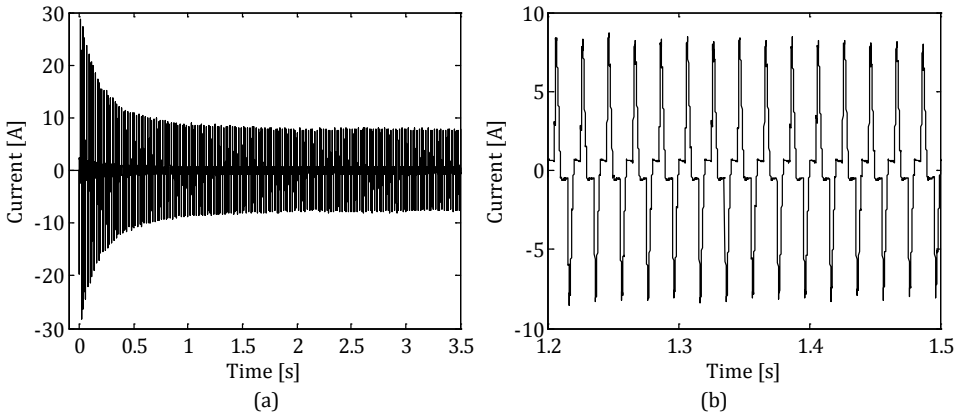

Fig 3.9 Current waveform of the vacuum cleaner: (a) whole inrush, (b) zoom in on the steady state

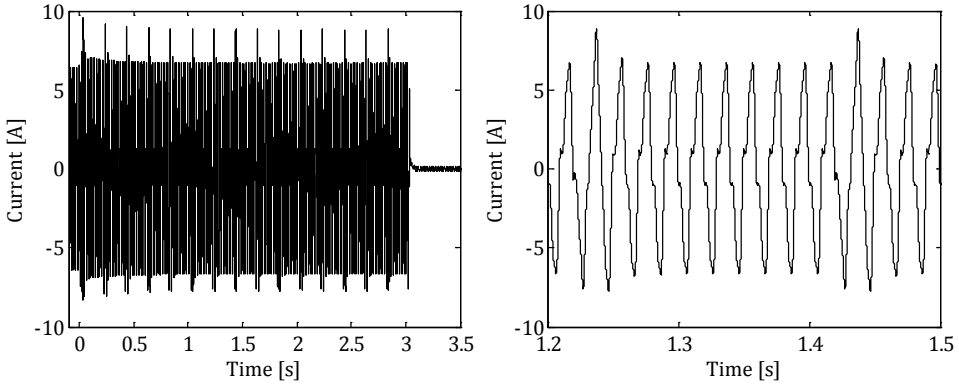

Fig 3.10 Current waveform of the PV inverter: (a) whole time period, (b) zoom in

For the inrush and false trips analysed, 75 Hz components of current and voltage are given in Fig 3.11, calculated with a data window length of two periods and sliding with a step of one period. The last peak from both figures should be disregarded, as it presents the value at the moment when the inverter is being disconnected.

The time change of network impedance at 75 Hz calculated from the measured 75 Hz components of voltage and current is presented in Fig 3.12. Before and after the inrush, the average value of calculated impedance is 0.36 Ω. During the peak of the inrush it reaches a value of 1.67 Ω, which is approximately 1.4 Ω higher than in normal conditions, and it is sufficient to trigger a false trip.

From (3.8) it is clear that the measurement error is dependent on the value of network impedance. Very low impedance values require a very large disturbance level to cause a false trip of the anti-islanding protection. Starting from 200 mΩ, which is a realistic value of LV network impedance, false tripping was possible with the disturbance of the vacuum cleaner.

The inrush of the vacuum cleaner lasts relatively short (around 0.5 s). The length of the data window influences the highest value of the 75 Hz component of the voltage, and the calculated network impedance as well. In Fig 3.13 the 75 Hz component of the vacuum cleaner's current is shown, calculated with three different data window lengths.

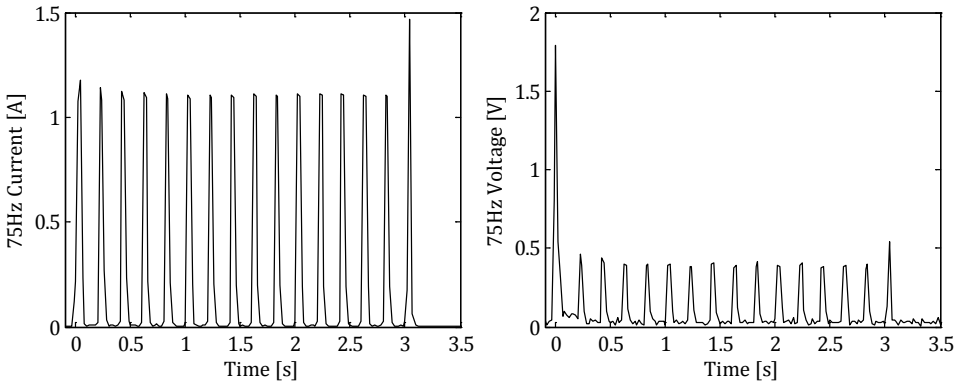

Fig 3.11 The 75 Hz component of the (a) inverters current, (b) voltage

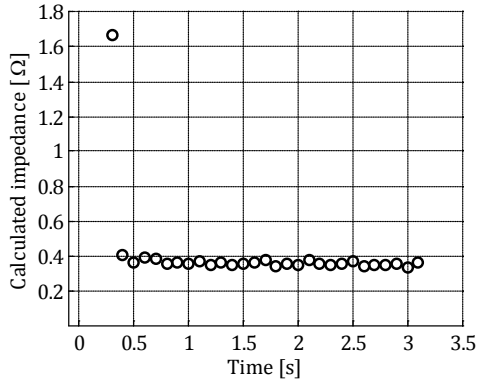

Fig 3.12 Network impedance calculated at 75 Hz

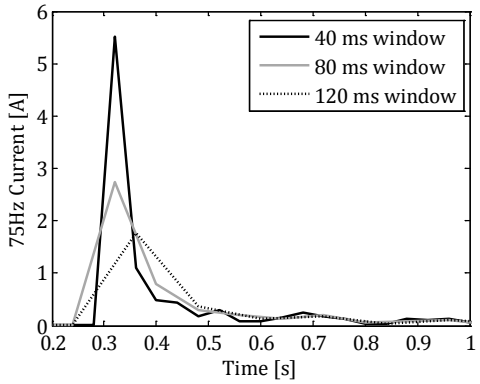

Fig 3.13 Vacuum cleaner's 75 Hz component of the current, calculated with three data windows

The maximal disturbance level decreases two or more times for a longer window length and the maximal error of impedance calculation is directly proportional to this level. Increasing the data window is off course not the only way to increase the robustness of the measurement, but this shows its effect on the measurement.

3.3.2 Decomposition in time-varying harmonic waveforms via DFT

In the previous subsection the STDFT was considered as having a sliding window which is refreshed by a few periods at the time. It is possible to refresh the data window which each new sample, which can result in waveforms of individual components, but this creates a very high computational burden to be done in real time. Usual applications of STDFT have no overlap or very little overlap (for synchronizing aggregated intervals) between the data windows, which results in one result for a time period of one data window.

A recursive DFT method which is capable to decompose a signal in time-varying waveforms of harmonics was presented in [10-12]. The Sliding Window Recursive Discrete Fourier Transformation (SWRDFT) is a version of STDFT which updates the data window for each new measured sample. The Fourier series of the first data window is calculated by the standard DFT approach, with orthogonal coefficients A_k and B_k defined by:

$$f[n] = \sum_{k=1}^{N-1} A_k \cdot \cos\left(\frac{2\pi kn}{N}\right) - B_k \cdot \sin\left(\frac{2\pi kn}{N}\right) \tag{3.10}$$

After the first data window, with each new sample $f[n]$ the oldest sample is discarded and coefficients $A_k[n]$ and $B_k[n]$ are recursively calculated from [11]:

$$A_k[n] = A_k[n-1] + (f[n] - f[n-N]) \cdot \cos\left(\frac{2\pi kn}{N}\right) \tag{3.11}$$

$$B_k[n] = B_k[n-1] - (f[n] - f[n-N]) \cdot \sin\left(\frac{2\pi kn}{N}\right) \tag{3.12}$$

The computational burden of (3.11) and (3.12) is much lower than of (3.10), which makes coefficient calculation possible in real-time, and reconstruction of waveforms for different harmonic components. The resulting harmonic waveforms have the same sampling frequency as the original signal. Based on this approach, a real-time harmonic analyser was proposed in [12].

An example of SWRDFT decomposition of the inrush current waveform from Fig 3.9 (a) is given in Fig 3.14, for the whole time period (a) and zoomed in on the first 200 ms (b).

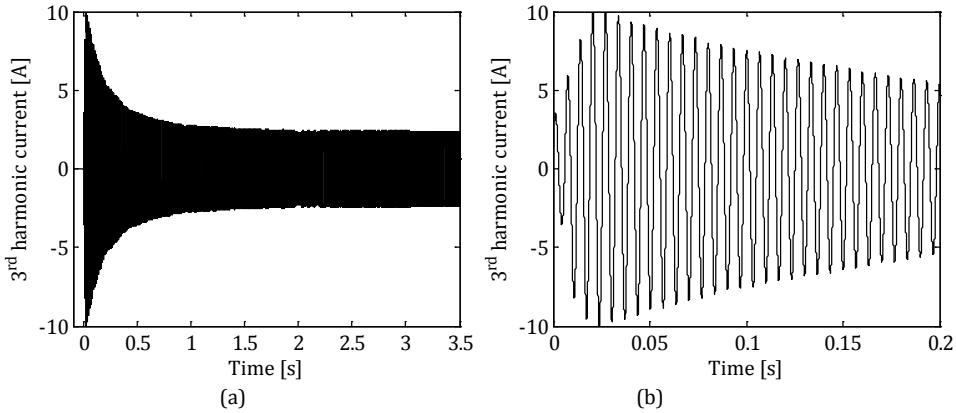

Fig 3.14 The 3rd harmonic current extracted by SWRDFT from the signal from Fig 3.9: (a) whole sequence, (b) zoom in

3.4 Alternatives to the DFT

One of the problems of DFT is that different frequency components vary differently within a data window. Higher frequency components include more cycles within the same time duration, which leads to a higher calculation uncertainty for a non-stationary signal. This problem is addressed better by other signal processing techniques. The most popular alternative to DFT is the Discrete Wavelet Transformation (DWT) [13-17].

In DWT, similarly as in the DFT, the original signal is split into a group of components. The DWT method does not use stationary signals as sine and cosine waves as its basis. It can use any base function, called the wavelet, which satisfies certain conditions (it needs to be oscillatory, to decay to zero, and its average value

needs to be equal to zero). The resulting components are representatives of frequency bandwidths instead of discrete frequency components, so the results are not directly comparable with DFT.

Another difference between the two methods is that the DWT allows for different time resolutions for different frequency components. This is mostly an advantage for calculation of higher frequency components, especially in the case of transients. If we calculate the frequency components with a sliding window, the DFT gives the same number of results for all components, while DWT calculates more results (usually twice more) for each higher frequency bandwidth.

Even though a single frequency component of DFT is not comparable to a bandwidth obtained by DWT, bandwidths are comparable to harmonic groups and subgroups, which are the final results of DFT based measurement instruments. In [18] an application of DWT to the estimation of harmonic groups was presented, with filter bandwidths of 25 Hz. With this approach the DWT can be implemented into a harmonic analyser to calculate the harmonic groups or subgroups directly. The difference between the DFT and DWT approaches for calculating harmonic groups is in the frequency response of "group" band-pass filters. The frequency response of a DFT based group filter has peaks at each multiple of the base frequency (5 Hz), while the DWT based group filter has a "smoother" response. This means that the DWT leads to less error for components of frequencies which are not exact multiples of 5 Hz, for most harmonic groups.

Two alternatives to DFT which have results which are directly comparable to it are filter banks and Hartley transformation. Both analog and digital implementations of band-pass filters can isolate a narrow frequency bandwidth, covering one or several spectral lines. In [19], an application using the multi resolution analysis approach is presented, which uses consecutive high-pass and low-pass filters to separate harmonic components. In this way the computational burden is reduced for calculating waveforms of several harmonic components at the same time.

Hartley transformation is closely related to Fourier transformation, and with results which are directly transformable into Fourier coefficients. Due to a different base function ($\mathrm{cas}(x) = \cos(x) + \sin(x)$ in comparison with $\cos(x) + j\cdot\sin(x)$ of the Fourier transformation) the resulting coefficients are real instead of complex. A harmonic analyser based on this transformation was proposed in [20].

Other methods for frequency decomposition of non-stationary signals include Gabor transform, sliding window Auto Regression (AR), Estimation of Signal Parameters via Rotational Invariance Techniques (ESPRIT), Kalman filters [16], and Welsh transform [17]. The usefulness of all of these methods was demonstrated in the literature. However, due to the early digital implementation and easily understandable results, the DFT remained the first choice as the method for spectral analysis of signals in power systems. Standard [3] allows the possibility of performing harmonic analysis with another method, but describes the measurement procedure only for a DFT based instrument.

3.5 Analog verification of digital time-varying decomposition methods

In this section we verify two digital decomposition methods by a laboratory experiment, to demonstrate their ability to characterize short-term phenomena. One of

the two methods, the SWRDFT, is later used in Chapter 4 to visualise the interaction between devices in an industrial installation.

If the performance of different signal processing techniques is to be compared for a non-stationary signal, the correct output of the processing needs to be defined first. From the previously mentioned methods, two methods can be compared directly – the SWRDFT and digital filter banks. Both methods give the waveforms of harmonic components, and can be compared to the output of an analog filter which can serve as a reference.

In Fig 3.15 we compare the frequency responses of an analog 8-pole Butterworth band-pass filter, digital filter bank, and SWRDFT for the extraction of the 7th harmonic (350 Hz) in an arbitrary signal.

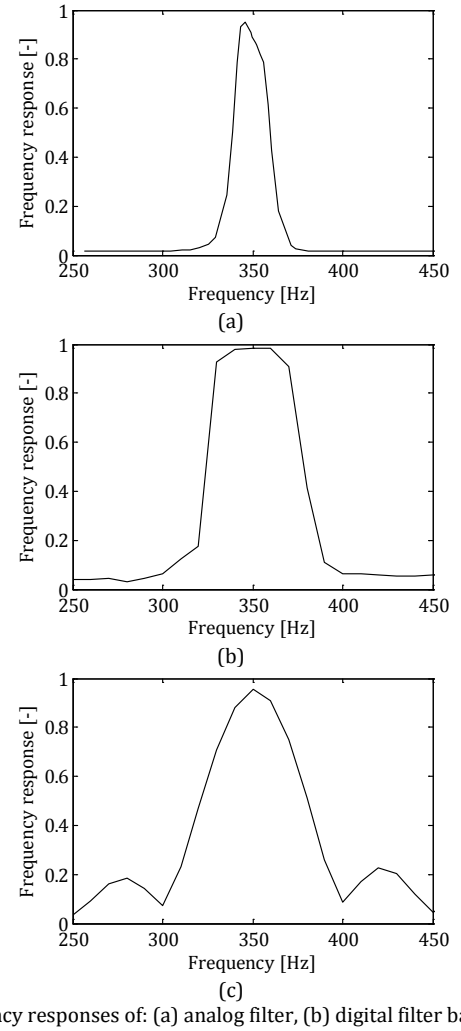

Fig 3.15 Frequency responses of: (a) analog filter, (b) digital filter bank, (c) SWRDFT

The analog filter is made with a frequency bandwidth of approximately 20 Hz, which is slightly narrower than the two digital methods, because it is to be used as the reference decomposition method. The filter bandwidth should be narrow, but should also accommodate the fundamental frequency variations which are multiplied by 7 for

the 7th harmonic. A bandwidth of ±10 Hz for the 7th harmonic covers fundamental frequency changes up to ±1.4 Hz. Regarding the suppression of other harmonic components, the analog filter suppresses them by more than 95 % (-26 dB), while the digital methods suppress them by more than 90 % (-20 dB).

The reference signal (analog filter) has the following features:

• A limited interference of frequencies around 350 Hz (mainly inter-harmonics) is present together with the 7th harmonic. Frequencies which fall inside the bandwidth of the filter normally have very low levels in comparison with the 7th harmonic.

• The dynamic response of the analog filter was not considered, due to the high slew rate (maximum possible rate of change) of the operational amplifiers in the filter, equal to 10 V/μs. This is not considered to cause significant errors.

3.5.1 Measurement setup

The experimental setup of the validation experiment is schematically presented in Fig 3.16. An 11 kW asynchronous machine was operated as a generator with a PWM full-converter connected to a programmable voltage source, with most of its power absorbed in a 5 kW resistor bank connected between the voltage source and the generator. The generator was driven by an 11 kW asynchronous motor with a full converter. The motor drive was connected to a grid decoupled from the programmable voltage source. The measurement was done on the motor's converter which has a six-pulse rectifier as the front end. The variation of the 7th harmonic current was achieved by variations of the torque set-point in the generator's converter. Voltage and current in one phase of the motor's converter were measured with a storage oscilloscope. The current was measured directly and via the analog band-pass filter describe in Fig 3.15 (a).

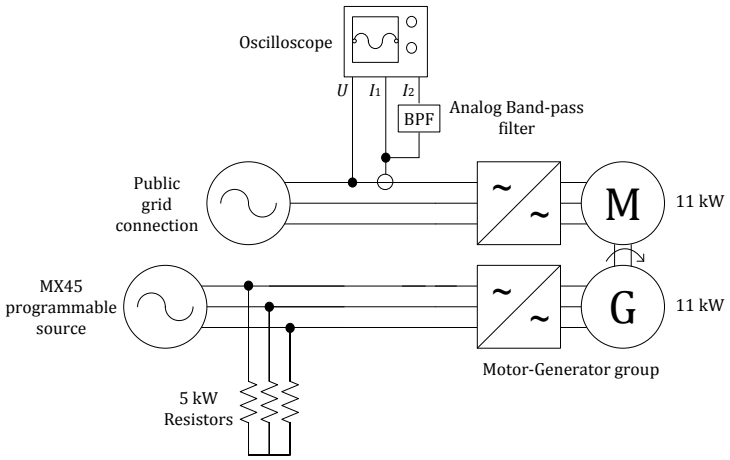

Fig 3.16 Schematic diagram of the experimental setup

3.5.2 Measurement results

In Fig 3.17 the current waveform is shown during a change of the generator's torque reference from 20% to 60%. The waveform shows typical 6-pulse converter harmonics. In Fig 3.18, the 7th harmonic for the whole period of torque transition is shown, for all three methods. Signals of both digital methods have the same wave

shape as of the analog filter, including small variations when the torque is almost constant, which shows the validity of the two digital methods.

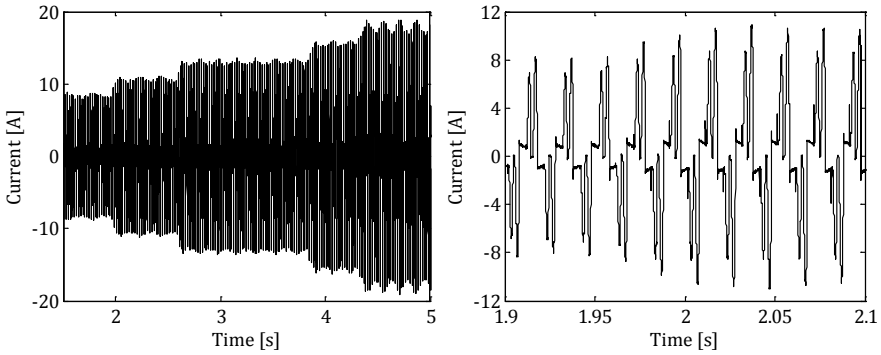

Fig 3.17 Current waveform during a torque change: (a) whole time period (b) zoom in on the first change

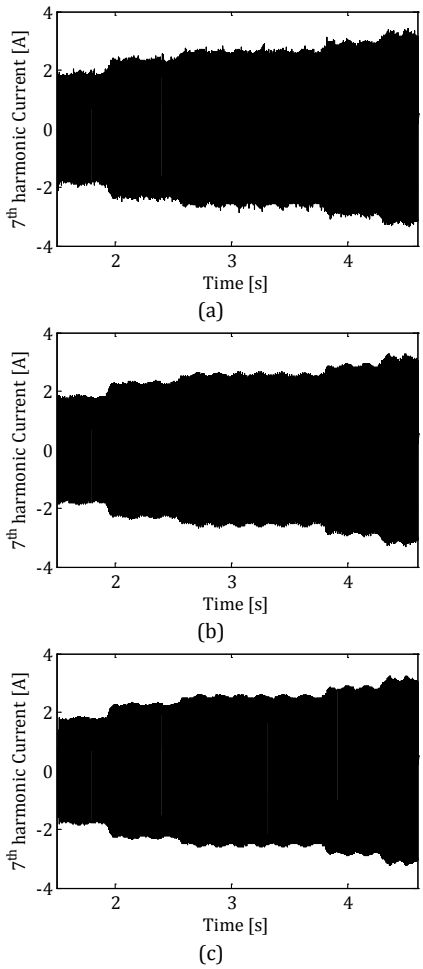

Fig 3.18 The 7th harmonic filtered by: (a) analog filter, (b) digital filter, and (c) SWRDFT during the whole torque variation

The results of the analog filter had noticeable high-frequency noise present, so it was processes also with a digital low-pass filter tuned to 2 kHz. Fig 3.19 shows additionally a zoom-in on the 7th harmonic during one period of the fundamental extracted by the analog filter, digital filter, and SWRDFT.

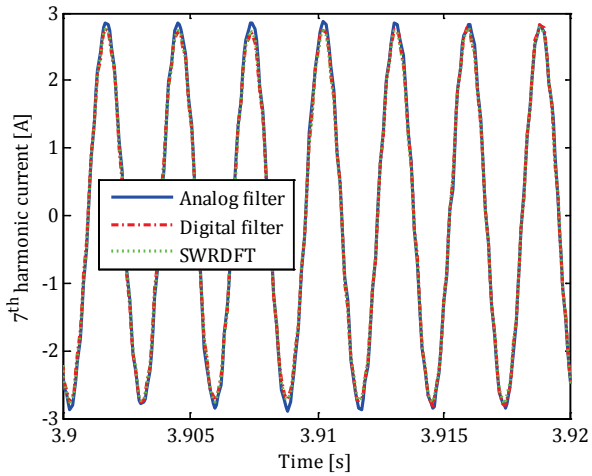

Fig 3.19 Zoom in on the 7th harmonic filtered by the analog filter and both digital methods

3.6 Conclusions

The widely adopted method for describing the spectral components of signals in power systems is the DFT. All measurement techniques, indices, and limits are based on this method as it was proven as a reliable tool.

The Fourier series theoretically applies only to periodic signals, which is a condition which is not met for non-stationary signals. This introduces frequency spill-over between the spectral components. For magnitudes, most of the error can be compensated for with the application of harmonic groups and subgroups.

If the signal is to be characterized by the phase angles of spectral components grouping is not applicable, because it removes the physical meaning from the information. Measurement of phase angles requires that the data window length is short enough in respect to the speed of signal variations, and no time aggregation is advisable for non-stationary signals.

During transients, the distortion levels often exceed the limits defined for ten minute aggregated values. Since the thermal effect of very short-term phenomena is limited this is usually acceptable, but these short harmonic bursts also lead to accelerated aging of electrical insulation and sometimes misoperation of protective and control equipment. The suggested method for characterizing harmonic bursts is using the 150/180 cycle aggregation or treating them as transient events instead of as distortion.

In certain situations it is advisable to use different data window lengths or aggregation intervals, as this can influence the levels measured. This optimization needs to match the effects of harmonic bursts on the observed equipment. As the effects are not the same for all types of equipment, comparability of results is a good compromise for most cases.

Alternative signal processing methods also demonstrated their accuracy on short-term harmonic phenomena, which gives a good foundation for future indices for harmonic bursts.

3.7 References of Chapter 3

[1] J. B. J. Fourier, *Théorie analytique de la chaleur*, Chez Firimin Didot, pére et fils, 1822.

[2] IEC 61000-4-30, "Electromagnetic compatibility (EMC) - Part 4-30: Testing and measurement techniques - Power quliaty measurement methods."

[3] IEC 61000-4-7, "Electromagnetic compatibility (EMC) - Part 4-7: Testing and measurement techniques - General guide on harmonics and interharmonics measurements and instrumentation, for power supply systems and equipment connected thereto."

[4] T. Ortmeyer, W. Xu, and Y. Baghzouz, "Setting limits on time varying harmonics," in Proc. *IEEE Power Engineering Society General Meeting*, 2003, pp. 1172–1175.

[5] M. B. Marz and V. Skendzic, "Negative sequence voltage relay distortion sensitivity and misoperation during cable and transformer energizations," in Proc. *IEEE ICHQP*, 1996.

[6] W. Bower and M. Ropp, "Evaluation of islanding detection methods for photovoltaic utility-interactive power systems," Report IAE PVPS T5-09, March 2002.

[7] F. De Mango, M. Liserre, and A. D. Aquila, "Overview of Anti-Islanding Algorithms for PV Systems. Part II: ActiveMethods," in Proc. *International Power Electronics and Motion Control Conference*, 2006, pp. 1884–1889.

[8] F. Bertling and S. Soter, "A novel converter integrable impedance measuring method for islanding detection in grids with widespread use of decentral generation," in Proc. *International Symposium on Power Electronics, Electrical Drives, Automation and Motion (SPEEDAM)*, 2006., pp. 503–507.

[9] A. V. Timbus, R. Teodorescu, F. Blaabjerg, and U. Borup, "Online Grid Impedance Measurement Suitable for Multiple PV Inverters Running in Parallel," in PRoc. *IEEE Applied Power Electronics Conference and Exposition (APEC)*, 2006, pp. 907–911.

[10] A. Mariscotti, "Fast and scalable spectrum analysis via recursive discrete Fourier transform," in Proc. *IEEE ICHQP*, 1996.

[11] P. M. Silveira, C. Duque, T. Baldwin, and P. F. Ribeiro, "Sliding window recursive DFT with dyadic downsampling — A new strategy for time-varying power harmonic decomposition," in Proc. *IEEE Power & Energy Society General Meeting*, 2009, pp. 1–6.

[12] D. F. Fabri, C. H. N. Martins, L. R. M. Silva, C. A. Duque, P. F. Ribeiro, and A. S. Cerqueira, "Time-varying harmonic analyzer prototype," in Proc. *IEEE ICHQP*, 2010, pp. 1–7.

[13] P. F. Ribeiro, "Wavelet transform: An advanced tool for analyzing non-stationary harmonic distortion in power systems," in Proc. *IEEE ICHPS*, 1994.

[14] A. W. Galli, G. T. Heydt, and P. F. Ribeiro, "Exploring the power of wavelet analysis," *IEEE Computer Applications in Power*, vol. 9, no. 4, pp. 37–41, 1996.

[15] D. C. Robertson, O. I. Camps, J. S. Mayer, and W. B. Gish, "Wavelets and electromagnetic power system transients," *IEEE Transactions on Power Delivery*, vol. 11, no. 2, pp. 1050–1058, Apr. 1996.

[16] M. Bollen and I. Gu, "Processing of Nonstationary Signals," in *Signal processing of power quality disturbances*, 1st ed., Wiley-IEEE Press, 2006, pp. 277–315.

[17] J. Arrillaga and N. R. Watson, "Harmonic analysis," in in *Power system harmonics*, Second edi., John Wiley & Sons, 2003.

[18] J. Barros and R. I. Diego, "Application of the Wavelet-Packet Transform to the Estimation of Harmonic Groups in Current and Voltage Waveforms," *IEEE Transactions on Power Delivery*, vol. 21, no. 1, pp. 533–535, Jan. 2006.

[19] C. Duque, P. M. Silveira, T. Baldwin, and P. F. Ribeiro, "Novel method for tracking time-varying power harmonic distortions without frequency spillover," in Proc. *IEEE Power and Energy Society General Meeting*, 2008, pp. 1–6.

[20] J. Balcells Sendra, "Harmonics analysis based on the fast Hartley transform algorithm," in Proc. *IEEE ICHPS*, 1994.

Chapter 4

Modelling of a single harmonic source

4.1 Introduction

The two main approaches in modelling are in general either physically based or behavioural oriented. Physically based modelling requires detailed representation of devices, and it gives results which can cover different operating regimes. Behavioural models use the "black box" approach. Parameters of the model are obtained from measurements or simulations in certain operating conditions. This reduces the complexity of the model, sometimes with a trade-off of reduced accuracy. Results of such models are completely accurate for the conditions from which the model was derived, but they contain a certain error in other operating conditions.

The choice of the modelling approach is a compromise between the accuracy and complexity. Both approaches are successfully used in practice, depending on the application. When various aspects of device operation are of interest, e.g. influence of voltage unbalance on the non-characteristic harmonics of a converter, the physically based approach gives better results. However, if only the maximal disturbance level is of interest, behavioural models give results which are accurate enough and with reduced complexity.

Commonly used methods for harmonic analysis are covered in Section 4.2. Section 4.3 discusses the frequency domain models which represent sources of distortion, and compares their performance in different conditions. Section 4.4 presents a case study of an industrial installation.

4.2 Methods for harmonic analysis

Several methods of harmonic analysis are described in [1-4]. The methods include time domain, frequency domain, and hybrid (time and frequency domain) calculations. In the following subsections a short overview of these methods is given, including a qualitative comparison of their accuracies and complexities.

4.2.1 Time domain methods

Time domain harmonic analysis is common to transient analysis, but the transient itself is usually not the objective. In this approach the network is represented by a system of differential equations. The quasi-steady state is the solution of the equations after the transient, and the harmonic information is obtained by applying DFT on the resulting waveforms [5].

The system of equations which represents the network is built from the voltage-current relations of all elements, and arranged in a form which is convenient for

solving. Several forms are proposed for the representation, e.g. the state space form [6]. The general state space form of the time domain model is given by:

$$\begin{aligned}[\dot{x}(t)] &= g_1\{t, [x(t)], [u(t)]\} \\ [y(t)] &= g_2\{t, [x(t)], [u(t)]\}\end{aligned} \tag{4.1}$$

where t is the time, $[u(t)]$ is the input vector, $[x(t)]$ is the state vector of the system, $[\dot{x}(t)]$ is the first time derivative of the state vector, $[y(t)]$ is the output vector, and g_1 and g_2 are functions of the system.

For linear systems, (4.1) can be solved analytically, but in most cases the system is non-linear, and it is difficult to solve the system of equations analytically. Due to this, (4.1) is usually solved by numerical integration which is a standard procedure in all Electro-Magnetic Transient Programs (EMTP). A number of methods for efficient numerical solving of time-domain equations is described in [4], e.g. the Fast Periodic Steady-State Solution method, which uses a Newton-type algorithm to reach the steady state without solving the entire transient.

The solution of the time domain approach is accurate in all working conditions in which the equations give a fair representation of the non-linearities. It is very effective for calculating non-characteristic harmonics and takes into account unbalances, saturation of magnetic elements, asymmetries in firing angles, etc. [7].

The biggest drawback of time domain simulation is that it requires a relatively large set of input parameters. For example, the control algorithms of converters are standardly not made available by the manufacturer, which influences the accuracy of their representation greatly.

Another drawback of these methods is the complexity. For example, frequency dependencies of predominantly linear network elements (e.g. change of resistance due to skin effect) increase the model complexity considerably, while some of them can be efficiently implemented in frequency domain methods. Due to this, it is difficult to perform time-domain simulations of very large systems, and they are usually limited to a part of the system close to the disturbing load (e.g. a large converter) [5]. These reasons led to a very high popularity of frequency domain methods for harmonic simulation.

4.2.2 Frequency domain methods

Frequency domain methods represent the system by matrix equations for each frequency of interest, which removes the need for solving a set of differential equations. Equations for different frequencies can in general be linked, but in most cases the system is treated as frequency decoupled, which makes the final solution a linear sum of independent harmonic components.

Another characteristic of the frequency domain is that the non-linearities of network components have a linear representation at each harmonic frequency. For example, the frequency dependence of conductor resistance (due to the skin effect) is modelled by different values of resistance at each frequency. As the system of equations is solved separately for each harmonic, resistance is a linear element in each calculation step.

The solution of frequency domain methods represents a certain time interval, e.g. a single period of the fundamental frequency, which makes the result time invariant during this period – a quasi-steady state. If time changes are to be assessed in the frequency domain, a new solution has to be found for each time interval, using the

previous as the starting point for the calculation. The frequency of variations needs to be lower than the fundamental frequency if the time variations are to be represented accurately.

The frequency domain harmonic analysis can further be subdivided into direct and iterative [1].

4.2.2.1 Direct method

The direct method is the simplest approach for harmonic analysis. It calculates harmonic voltages on all busbars based on a single constant harmonic source, using the nodal method which is a linear matrix equation set:

$$[\underline{U}_h] = [\underline{Z}_h][\underline{I}_h] \tag{4.2}$$

where $[\underline{U}_h]$ is the vector of harmonic voltages of the h^{th} order, $[\underline{Z}_h]$ is a matrix of harmonic impedances which connect all busbars, and $[\underline{I}_h]$ is an input vector of harmonic currents. For a single source, there is a single none-zero element in the vector $[\underline{I}_h]$.

If more harmonic sources are considered, the calculation can be repeated for each of the sources, with the final solution being a linear combination of the particular outcomes [1]. Under unbalance, the method can be applied on sequence components (e.g. the Fortescue symmetrical components), which requires solving three single-phase matrix sets of equations, or directly on phase components, with a single three-phase matrix equation set [3].

The drawback of the direct method is that it is limited in the representation of harmonic sources. The voltage dependence of current sources can be modelled by a non-ideal current or voltage sources, Norton or Thévenin equivalents, which improves the performance, but it does not allow for a detailed representation available to iterative methods. Also, the principle of superposition removes the mutual influence between several harmonic sources [1].

4.2.2.2 Iterative method

The shortages of the direct method can be compensated with an iterative approach. In the direct method, the voltage dependence of a current source (harmonic sources are usually modelled as current sources, but the same holds for voltage sources) can be described with an additional equivalent impedance, which changes the total current in respect to the voltage at its busbar. If the current source of the Norton equivalent needs to be voltage dependent, an iterative approach is needed to match the current of the source to the busbar voltage. At the first iteration, a set of harmonic voltages is assumed at the source busbar (e.g. a clean sinusoidal voltage). The harmonic currents are then calculated based on the voltage, and injected to the system. The new voltage at the busbar is then used to recalculate the source current, and the process is repeated until the difference between two iterations is acceptably small. In this way the problem can be treated with multiple sources as well. Also, the inter-dependency of sources is taken into account, which is not possible in the direct method.

The most common approach for solving the non-linear equation set is the harmonic power flow, which uses a Newton type algorithm for each harmonic frequency. This approach is based on the power flow used for the fundamental frequency, but with a

possibility to link the iterations for different harmonics. Other non-linear solvers can be used as well. Interactions between the fundamental, harmonics, and inter-harmonics are taken into account in the Dynamic Harmonic Domain Method [4].

Except by the approach for solving the equations, iterative methods can be subdivided by the representation of harmonic sources. Proposed models are Norton and Thévenin equivalent, harmonic admittance matrix [8], [9], and harmonic fingerprint [10] which uses a look-up table. More details on these models are considered in section 4.3.

A restriction of the power flow methods is that in certain conditions convergence is not possible, as shown in [11]. This is the case with high input impedance and a high sensitivity of the harmonic currents to the voltage changes ($\delta I_h/\delta U_h$). In the same reference it was shown that the divergence problem can be solved if a part of the system impedance is included in the model of the harmonic source. Without affecting the physical meaning, this reduces the systems input impedance and at the same time reduces the $\delta I_h/\delta U_h$, but only if the moved impedance is inductive.

4.2.3 Hybrid Time-Frequency domain methods

Hybrid methods combine the good characteristics of time and frequency domain methods. The linear parts of the system are represented in the frequency domain, which leads to efficient computation, and the non-linear parts of the system are represented in the time domain, which results in better accuracy [12].

In the first step, voltages at the terminals of non-linear devices are assumed, which gives a starting point for the time domain calculation of their currents. These currents are then used as inputs to the frequency domain calculation, and the resulting voltages are compared to the assumed ones. The process is repeated iteratively until a good match between the two domains is found.

The advantage of this approach is that all non-linear loads can keep a detailed representation, including frequency coupling. At the same time, for the rest of the network, only a matrix equation set needs to be solved, making it possible to model a large network.

4.3 Models of harmonic sources in the frequency domain

This section analyses different models of harmonic sources in the frequency domain. The analysis is focused on rectifier loads, as they are the most common sources of harmonic distortion in distribution networks. Rectifiers are the front end of many devices, which use a DC or variable frequency AC supply for their operation, ranging from lamp drivers of less than 1 W to multi-MW variable speed drives and controllable heaters.

Some specifics about the rectifier harmonics are given first, such as the principle of harmonic generation, influence of the load power and a non-ideal voltage supply. Performance of different models is analysed further, with time-domain simulations and laboratory experiments for validation.

4.3.1 Harmonic currents of rectifier-based devices

In an idealized case, when we consider a line-commutated converter with a constant DC side current of the rectifier and instantaneous commutation, harmonic currents can

be easily expressed as a function of the DC side current. A schematic diagram of an idealized three-phase 6-pulse thyristor rectifier is shown in Fig 4.1. Voltages and current of phase *a* (I_a) are presented in Fig 4.2 (a), and the spectrum of I_a in Fig 4.2 (b). The DC side voltage at the positive terminal (+) is shown in Fig 4.3. The firing (delay) angle of the rectifier is designated with β. Both figures cover the case when rectifier is supplied with a balanced system of purely sinusoidal voltages,

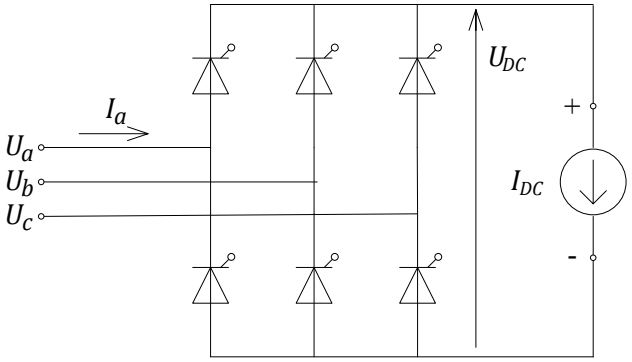

Fig 4.1 Schematic representation of an idealized three-phase thyristor rectifier

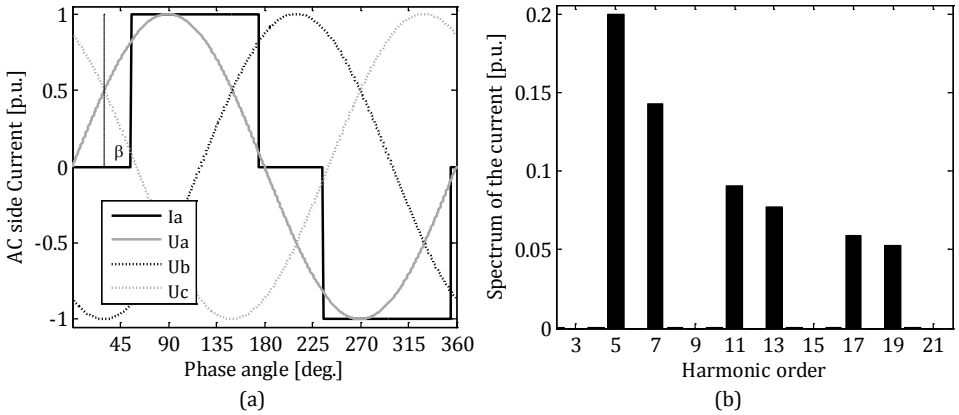

Fig 4.2 (a) AC side voltages and current of phase *a*, (b) Spectrum of I_a

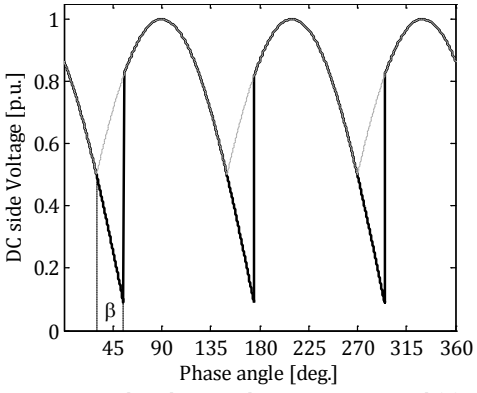

Fig 4.3 DC side voltage at the positive terminal (+)

As derived in [13], under these conditions the AC side current in phase a can be expressed as:

$$I_a(t) = \frac{2\sqrt{3}}{\pi} \cdot I_{DC} \left[\cos(2\pi f t) - \frac{1}{5}\cos(5 \cdot 2\pi f t) + \frac{1}{7}\cos(7 \cdot 2\pi f t) - \frac{1}{11}\cos(11 \cdot 2\pi f t) + \frac{1}{13}\cos(13 \cdot 2\pi f t) - \cdots \right] \tag{4.3}$$

where $I_a(t)$ is the time dependent value of the AC side current in phase a, I_{DC} is the DC side current, f is the fundamental frequency, and t is time.

There are two important details to notice in (4.3). The first is that except for the fundamental component, $I_a(t)$ contains harmonic components only of orders $6 \cdot i \pm 1$, where i is an integer number ($i \geq 1$). For a generalized rectifier of p-pulses, the characteristic harmonic orders are $p \cdot i \pm 1$. The second detail is that even though $I_a(t)$ seems independent of the firing angle, I_{DC} is indirectly a function of β, and the DC side impedance (and possibly the electromotive force). In this idealized example it is a constant value.

The magnitude of harmonic components is inversely proportional to the harmonic order, $I_h = I_1 / h$. Due to this, an increase in the number of converter pulses leads to lower harmonic emission. For relatively low powers (up to several MW in non-isolated systems) it is often sufficient to use six-pulse converters. For higher powers at least twelve-pulse designs are needed to limit the voltage distortion. The threshold is dependent on available short-circuit power and resonant frequencies.

Expression (4.3) does not take into account the commutation process – overlap in the operation of two switches. When commutation is taken into account, harmonic components become dependent both of the commutation angle (and the DC side impedance) and the system impedance, because during the commutation there is an AC side short-circuit formed by the two switches. More details on this influence can be found in [13].

The assumption of constant DC side current is not made strictly for "analytical convenience". Some converters have a relatively high DC side inductance (e.g. DC motor drives) or regulate the DC ripple with inductors (e.g. current source converters), which makes the DC current relatively close to constant. Table 4.1 compares the magnitudes of several characteristic harmonics in the case of constant DC current (infinite DC side inductance) and no DC side inductance (purely resistive load), according to [13]. The influence of the DC side inductance on the harmonic model of the converter is further discussed in section 4.3.4.1.

Table 4.1Comparison of converter harmonics with an infinite DC inductor and with no DC inductance, [13]

h	I_h for constant DC current [% of fundamental]	I_h without DC side inductance [% of fundamental]
5	22.6	20.0
7	11.3	14.3
11	9.1	9.1
13	6.5	7.7
17	5.7	5.9
19	4.5	5.3
23	4.1	4.3
25	3.5	4.0

LV devices of low powers are allowed to be connected to a single-phase supply. In many countries the threshold for this is the nominal current of up to 16 A. In this case

the rectifying stage consists of a diode bridge with the DC voltage filtered by a capacitor in the simplest case, as in Fig 4.4.

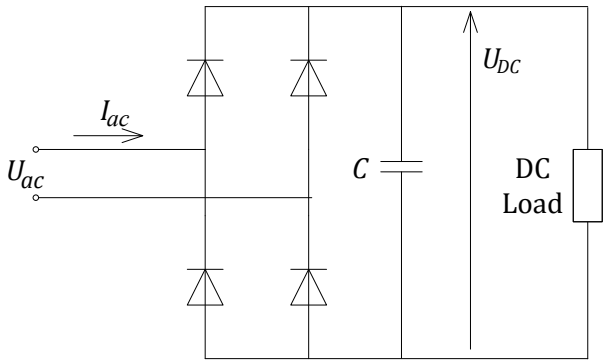

Fig 4.4 Schematic representation of a simple single-phase rectifier

The AC side voltage (phase to neutral) and current of the rectifier from Fig 4.4 when it is supplying a resistive load are shown in Fig 4.5 (a), and the spectrum of the current in Fig 4.5 (b).

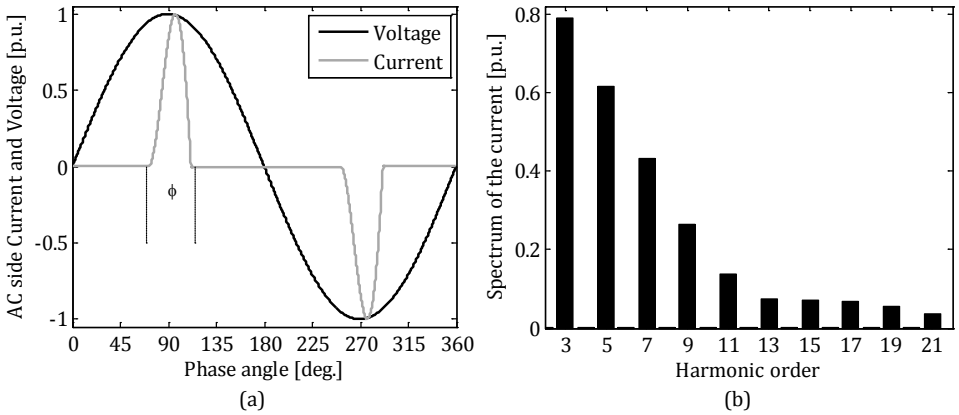

Fig 4.5 Single-phase rectifier from Fig 4.4: (a) AC side voltage and current, (b) spectrum of the current

The "impulse-like" current waveform from Fig 4.5 contains high levels of odd order harmonics, with a THD higher than 100 %. As given in [14], the spectrum of this waveform is approximately equal to:

$$I(t) = \frac{4A\Phi}{\pi^2} \sum_{h=1,3,5,\ldots} \frac{cos\frac{h\Phi}{2}}{1 - \frac{h^2\Phi^2}{4}} \cdot cos\frac{h\Phi}{2} \tag{4.4}$$

where A is the peak of the impulse and Φ is the duration of one impulse (there are two per period) in radians. Expression (4.4) is derived for a waveform with symmetrical impulses, and it is an approximation of the realistic waveform which is slightly "leaned to one side". If the DC side current would be constant, the AC side current would be a square wave without a period of zero value. The spectrum of such a waveform is

similar to (4.3), also with a $1/h$ decay of harmonic components, but including the triple-n orders which do not exist with a three-phase converter.

Most new single-phase rectifiers include a Power Factor Correction (PFC) sub-circuit, which improves the *PF* and efficiency, reduces the voltage stress of components, and reduces the harmonic emission. Depending on the type and power, low-power devices need to comply with emission limits discussed in Chapter 2 so they might be connected to an arbitrary location in the LV network. The PFC can be implemented as a passive or active sub-circuit. A common active PFC topology is shown in Fig 4.6, adapted from [15].

In [16] it is proposed to characterize the harmonic magnitudes of modern home appliances with:

$$I_h = \frac{I_1}{h^{CD}} \tag{4.5}$$

where I_1 is the magnitude of the fundamental component, and *CD* is a constant used to characterize the device type, determined by fitting of the current spectrum.

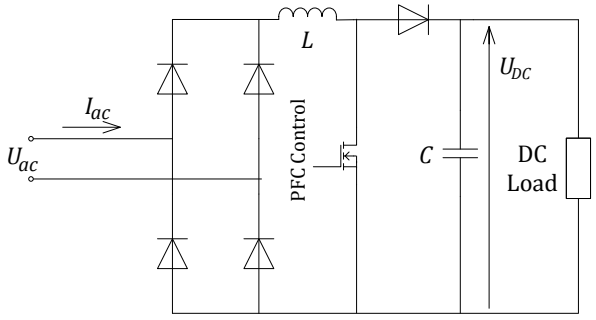

Fig 4.6 Rectifier with active power factor correction, [15]

For a square waveform, the value of *CD* is 1. Measurements from [16] showed values between 0.41 and 2.49 for modern home appliances. All devices with *CD* lower than 1 emit more harmonics than a square waveform.

The current waveform from Fig 4.5 gives much higher levels of harmonics than a square wave. The THD of a square wave is about 45 % while the signal from Fig 4.5 has a THD of more than 100 %. Devices with active PFC have significantly lower harmonic emission, in some cases the THD is about 10 %, which leads to high values of *CD*.

In [17], more than 100 types of compact fluorescent lamps (CFLs) of different powers were compared. Results showed current values of THD between 90 % and 140 %, mostly with a linear increase of low-order harmonics with the input power, which means that their design is very similar for all powers.

4.3.2 Influence of the load power

4.3.2.1 Three-phase rectifiers

Non-linear loads draw different harmonic currents at different loading levels. In practice it is difficult to look at this dependency separately from the influence of the supplied voltage, so we look at a computer simulation of a three-phase rectifier from

Fig 4.1. The voltage is kept ideally balanced and sinusoidal, but the DC side current is no longer an ideal current source, the DC load is modelled as a resistive load fed via a *LC* filter.

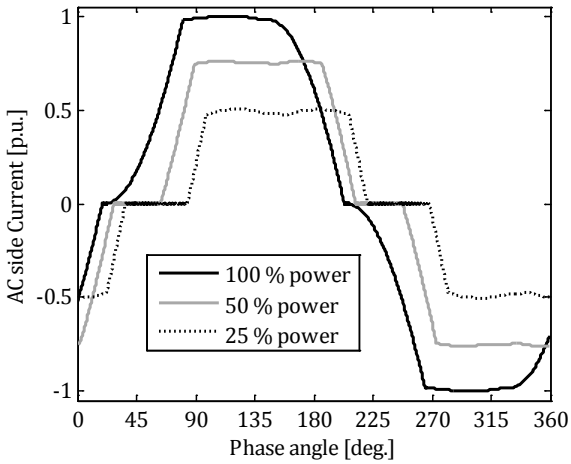

Fig 4.7 Current waveform of the three-phase rectifier for several values of the firing angle

If we keep the load resistance value constant, and change the value of the firing angle, the output power can be varied from zero to the nominal value. The current waveform in phase *a* for several values of the firing angle is shown in Fig 4.7.

The waveform changes its magnitude and the wave shape as well. The dependencies of the first four characteristic harmonics from the output power are shown in Fig 4.8, as relative to their values at nominal power (p.u.) and as *HD* (relative to the fundamental current in percents).

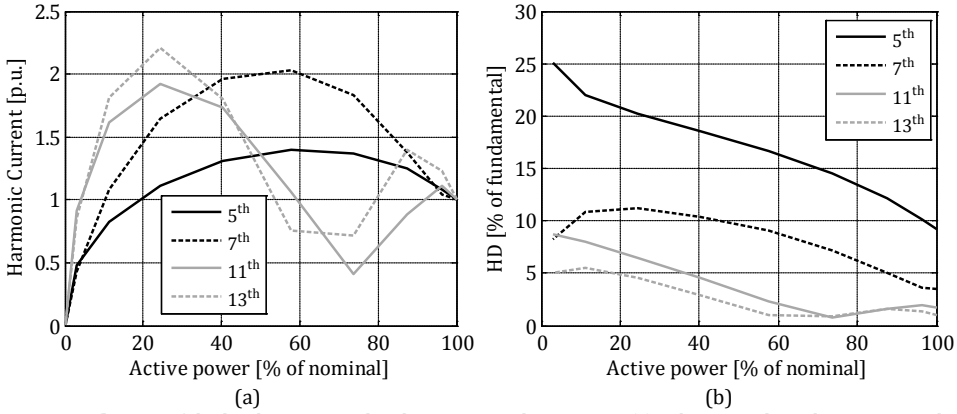

Fig 4.8 Influence of the load power on the characteristic harmonics: (a) relative to the value at nominal power, (b) HD - relative to the fundamental current; three-phase rectifier

At powers lower than the nominal, harmonic currents can be higher both in absolute and relative units. These values are not purely dependent from the value of the firing angle (used to control the power here), they are influenced by the inductance and capacitance as well.

4.3.2.2 Single-phase rectifiers

For the single-phase rectifier from Fig 4.4 the influence of the load power cannot be analysed via the firing angle, because it has a diode bridge. For this reason we analyse the power dependency through the variation of the DC side resistance. The current waveform on the AC side for several values of the resistance is shown in Fig 4.9.

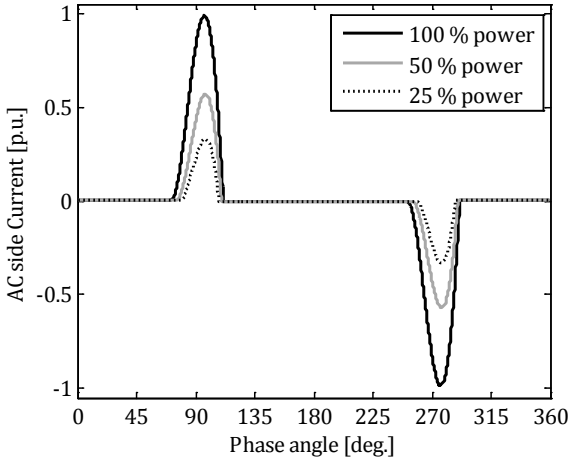

Fig 4.9 Current waveform of the single-phase rectifier for several values of the DC resistance

The dependencies of the first four odd harmonics from the output power are shown in Fig 4.10, also relative to their values at nominal power and as *HD* - relative to the fundamental current.

In this case, the relative values are higher at lower powers, and the absolute values are almost linearly dependent from the output power.

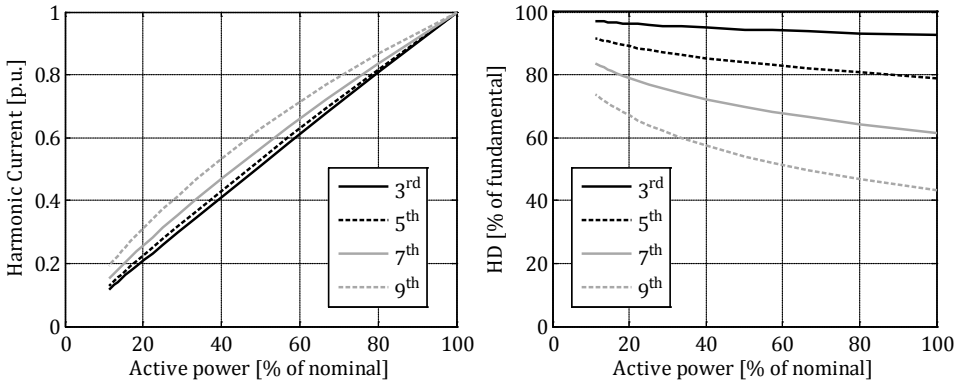

Fig 4.10 Influence of the load power on the odd harmonics: (a) relative to the value at nominal power, (b) HD - relative to the fundamental current; single-phase rectifier

4.3.3 Influence of non-ideal voltage supply

In the simulations from section 4.3.2 the voltage supply was kept ideally sinusoidal, with the nominal magnitude value, and balanced for the three-phase rectifier. Non-

ideal voltage influences the characteristic harmonics of loads, but can also introduce non-characteristic harmonics.

4.3.3.1 Three-phase rectifiers

For three-phase rectifiers, expression (4.3) is valid only for idealized conditions. In reality, spectrums of phase currents are affected by the DC side inductance, but also by the voltages supplied to the rectifier.

In [13] it was shown that triple-n harmonics are absent from the spectrum only as long as the half-cycle of the current waveform is a rectangular pulse of 120˚ width, and any deviation of thyristor pulses introduces these harmonics. Voltage harmonics on the AC side modulate the DC side voltage, which in turn modulates the AC side current. In [14], [18] it is stated that the higher number of converter pulses (e.g. 12 pulses) reduces the characteristic harmonics but it does not provide a solution for the non-characteristic orders. More details on the influence of voltage harmonics on harmonic currents are given in section 4.3.4.

Even order harmonics are usually excluded from the analysis because their levels in the network are normally very low. However, if even harmonics are present in the voltage, they lead to the amplification of the current of the same order and DC current emission on the AC side, as discussed in [19]. If we apply the 2nd harmonic voltage to the thyristor rectifier model with different values of the firing angle β, the resulting 2nd harmonic current is shown in Fig 4.11. In this example the voltage harmonic was balanced in the three phases, the magnitude of the voltage was varied, and the phase angle was kept constant, with 0° in phase *a*.

Voltage unbalance has an effect even with sinusoidal voltages, because it makes the pulses of different phases uneven. As an example, we look at the influence of voltage unbalance on the 3rd harmonic current in phase *a* of the rectifier, see Fig 4.12, again for different values of β.

For this example the unbalance was achieved by lowering the magnitude of the voltage in phase *c*, with the other two phases at the nominal magnitudes, and with all three phase angles balanced. If we would create the unbalance in another way, the results would be slightly different.

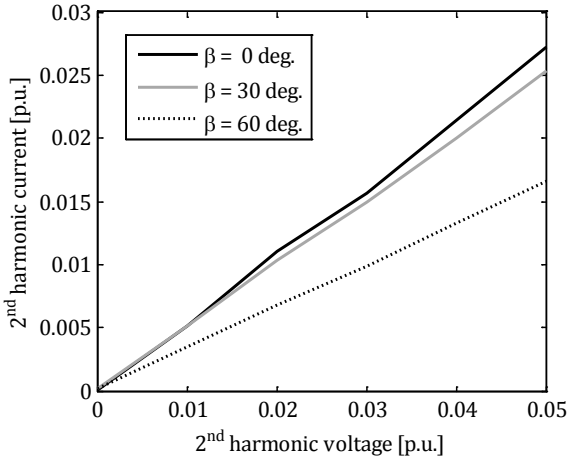

Fig 4.11 Influence of the 2nd harmonic voltage on the 2nd harmonic current of a three-phase rectifier

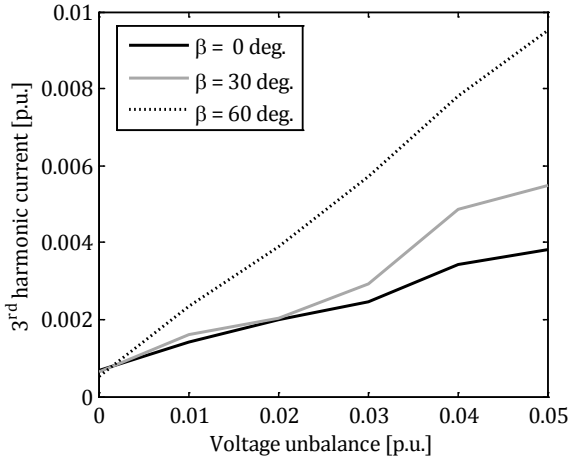

Fig 4.12 Influence of voltage unbalance on the 3rd harmonic current of a three-phase rectifier

4.3.3.2 Single-phase rectifiers

In [20], [21], [22], the behaviour of capacitor filtered single-phase rectifiers (such as in Fig 4.4) was analysed analytically, both due to power and voltage changes. It was found that an increase in voltage distortion, due to the large number of units sharing the point of connection, usually leads to a decrease of harmonic currents, both individual and the total. For this reason the effect was referred to as the Attenuation Factor (*AF*), and it was defined as:

$$AF = \frac{I_h^N}{N \cdot I_h^1} \tag{4.6}$$

where I_h^1 is the h^{th} harmonic current of an individual device, and I_h^N is the aggregated current of N devices of the same type. The attenuation effect of household devices was analysed by laboratory measurements in [16], [20], [21], [23-25].

If devices are not identical, (4.6) in principle includes the effect of phase angle diversity. A discussion about this effect is given in Chapter 5. Even for identical equipment expression (4.6) has a drawback of being dependent on the system impedance, which influences the voltage to which devices are exposed. If we would measure harmonic currents of a same group of devices on different points in the network, or even on the same location at different times, the resulting *AF* would not be the same due to the change of system impedance.

To avoid the influence of system impedance, a Voltage Influence Factor (*VIF*) can be defined similarly as in [16], as:

$$VIF_i = \frac{I_h^{Vi}}{I_h^{Vn}} \tag{4.7}$$

where I_h^{Vi} is the harmonic current influenced by a specific (i^{th}) voltage or system of voltages defined by the magnitude(s), spectrum and unbalance if applicable, and I_h^{Vn} is current influenced by the ideal voltage or system of voltages.

Expression (4.7) removes the influences of system impedance and phase angle diversity. However, it still cannot describe the behaviour of a device with a single coefficient, because it has different values for different voltage characteristics.

In [10], [16] it was shown by laboratory measurements that voltage distortion can lead also to the amplification of harmonic currents. The name attenuation effect originates from the measurements where most of the voltage distortion is caused by the devices under test. This leads to "flattening" of the voltage waveform, which reduces the peak of the current waveform and its odd order harmonics [21].

For CFLs, a reduction of the voltage RMS has a similar effect as the "flattening" of the waveform, as shown in laboratory measurements presented in [26]. A reduced voltage leads to a wider current pulse, which is needed to assure the needed DC power. This leads to a reduction of harmonics in the same way as a "flat-topped" voltage waveform.

4.3.4 Types of models in the frequency domain

In this section, the different types of frequency domain models are analysed and compared. All of the model types are derived from laboratory measurements for a three-phase diode bridge rectifier and a CFL (single-phase).

4.3.4.1 Norton equivalent

The most commonly used frequency domain model is the Norton equivalent. In its simplest form, it is an ideal current source, which means that the harmonic emission is independent of the voltage supplied to the device. For example, the three-phase rectifier is then represented by an ideal current source for each of the characteristic orders (5^{th}, 7^{th}, 11^{th}, 13^{th}, etc.). The magnitudes are equal to $I_h = I_1 / h$, where I_1 is the fundamental current derived from the apparent power of the device. The loading level of the device can be taken into account via the value of the fundamental current.

To include the influence of the voltage, a non-ideal current source can be used, as in Fig 4.13. The impedance part of the model (Z_h) interacts with the voltage at the device terminals (U_h), while the ideal current source (I_h) represents the emission of the device when supplied by an ideal voltage (or system of voltages). The total current of the equivalent (I_{htot}) is a sum of the two parts. If unbalanced conditions are to be accessed, a separate equivalent is needed for each of the phases.

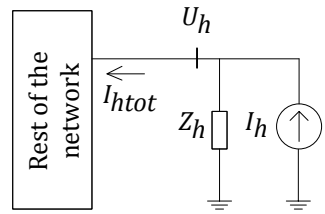

Fig 4.13 Schematic representation of a non-ideal Norton equivalent

The advantage of the Norton equivalent is that it is a relatively simple approach. Not more than two measurements or simulations in different conditions are needed to derive the model, which is much less than for the models of higher complexity. The model can also be derived from a higher number of samples, e.g. with the least square fitting approach.

The drawback of the Norton equivalent is that it decouples the behaviour of the device to individual frequencies, even when the value of I_h is treated as dependent of the load power. Each harmonic current is dependent only on the voltage of the same order via the equivalent impedance of the same order. For example, if we expose the device to the 5th harmonic voltage, the Norton equivalent creates a change only in the 5th harmonic current. This error is acceptable in some situations, but can also be significant, depending on the design of the device. This issue is further discussed at the end of this section.

Approaches for determining the Norton equivalent are given in [16], [27-34]. In [30] it is proposed to use a reactance as Z_h in the case of thyristor bridges for HVDC. The value of the reactance is a function of the commutation reactance, firing angle, and the commutation angle.

In [29], [31], [32], it is proposed to use a capacitance as the equivalent impedance of compensated discharge lamps and PV inverters, based on fitted laboratory measurements. The PFC and/or filters of these devices play a dominant role in their interaction with harmonic voltages, especially for higher order harmonics.

In [28], the values of I_h and Z_h of any load are determined based on at least two field measurements in different conditions. A considerable difference in voltage distortion is required for this approach, e.g. due to capacitor switching. By measuring U_h and I_{htot} in the two conditions, values of I_h and Z_h are determined as a solution of a linear system of equations, for each harmonic order.

In [34], different excitations for determining the Norton equivalent from two measurements and the admittance matrix are compared. It was found that the model performance highly depends on the voltage harmonics used during the comparison.

In [16] it was proposed to use the linear least-squares fitting for obtaining the equivalent elements, from a larger sample of data. In principle, the data samples do not have to include a measurement with a pure sine-wave excitation. This approach was used for model derivation in this chapter, using a set of measurements with different magnitudes and phase angles of voltage harmonics, and including the pure sine-wave excitation.

The Norton equivalent linearizes the voltage-current relation for each harmonic frequency. In the total solution the devices remains non-linear, but at each individual frequency it is completely linear. Here we derive the Norton equivalent model for two types of converters, based on measured data. As examples, a three-phase diode bridge and a CFL are used, because these types of loads are analysed in a case study at the end of Chapter 4 and field measurements in Chapter 5.

4.3.4.2 Norton equivalent of a three-phase diode bridge

The Norton equivalent of a three-phase diode bridge is derived from laboratory measurements conducted in the Flex Power Grid Lab of DNV Kema, based on the schematic in Fig 4.14. The rectifier is feeding a 12 Ω resistor, with a DC side power of approximately 70 kW. The rest of the circuit was configured in six combinations with different values of AC and DC side inductances, as shown in Table 4.2.

The fundamental value of the AC side line to line voltage was 690 V, balanced, and it was superimposed with a single harmonic – 5th, 7th, 11th, 13th, 17th, and 19th, also balanced. Magnitudes were varied from 1 % to 4 % of the fundamental, and the phase-angle step was 60°. The model performance is evaluated in section 4.3.4.5, with voltages distorted with multiple harmonics.

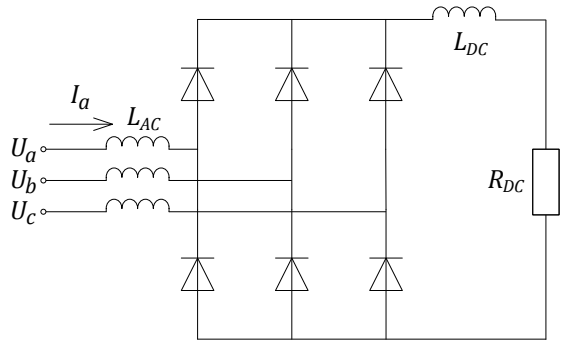

Fig 4.14 Schematic of a three-phase diode rectifier used for laboratory measurements

Table 4.2 Values of rectifier elements used in laboratory measurements

Test number	L_{AC} [mH]	L_{DC} [mH]
1	0.3	0.0
2	0.3	1.0
3	0.3	1.5
4	1.1	0.0
5	1.1	1.0
6	2.1	0.0

If we derive the Norton equivalent of this rectifier for all six inductance configurations, the measured and calculated 5th harmonic current are as in Fig 4.15. Points which correspond to harmonic voltages with a phase angle of 0° are highlighted with a different symbol.

The calculated currents form lines which are shifted by 60°, which was the phase increment of the voltages. Measured currents form a similar shape, but with inconsistent phase-angle differences. At lower inductances the values of phase steps are slightly closer to 60°.

In all six cases the difference between the measured and calculated values is relatively small. The error varies slightly with the magnitudes and phase angles of the applied 5th harmonic voltage. This is not surprising, because the equivalent linearizes the load completely.

The parameters of the Norton equivalent for all six configurations are given in Table 4.3. Magnitudes of I_h vary only slightly for different inductances, between 14.6 A and 16.0 A. The ratio between the fundamental current and I_h is approximately four in all six cases (in the idealized model the ratio is equal to h = 5). The phase angle of I_h is more dependent on the inductance, it varies between -100° and -180°.

The impedance part of the equivalent is predominantly resistive in all cases, with capacitive behaviour for low values of inductances and inductive at higher values. For the highest value of line inductance (2.1 mH at the AC side) it becomes purely resistive. Both I_h and Z_h are more sensitive to the change of L_{AC}.

Table 4.3 Parameters of the 5th order Norton equivalent for the three-phase diode rectifier

Test number	$\underline{I}_h$ [A]	$\underline{Z}_h$ [Ω]
1	-15.57-j0.61	4.12+j0.89
2	-15.50-j1.02	4.25+j0.76
3	-15.41-j1.17	4.35+j0.61
4	-10.61-j12.06	4.02-j0.88
5	-10.28-j11.97	4.16-j1.02
6	-2.08-j14.45	3.86-j2.65

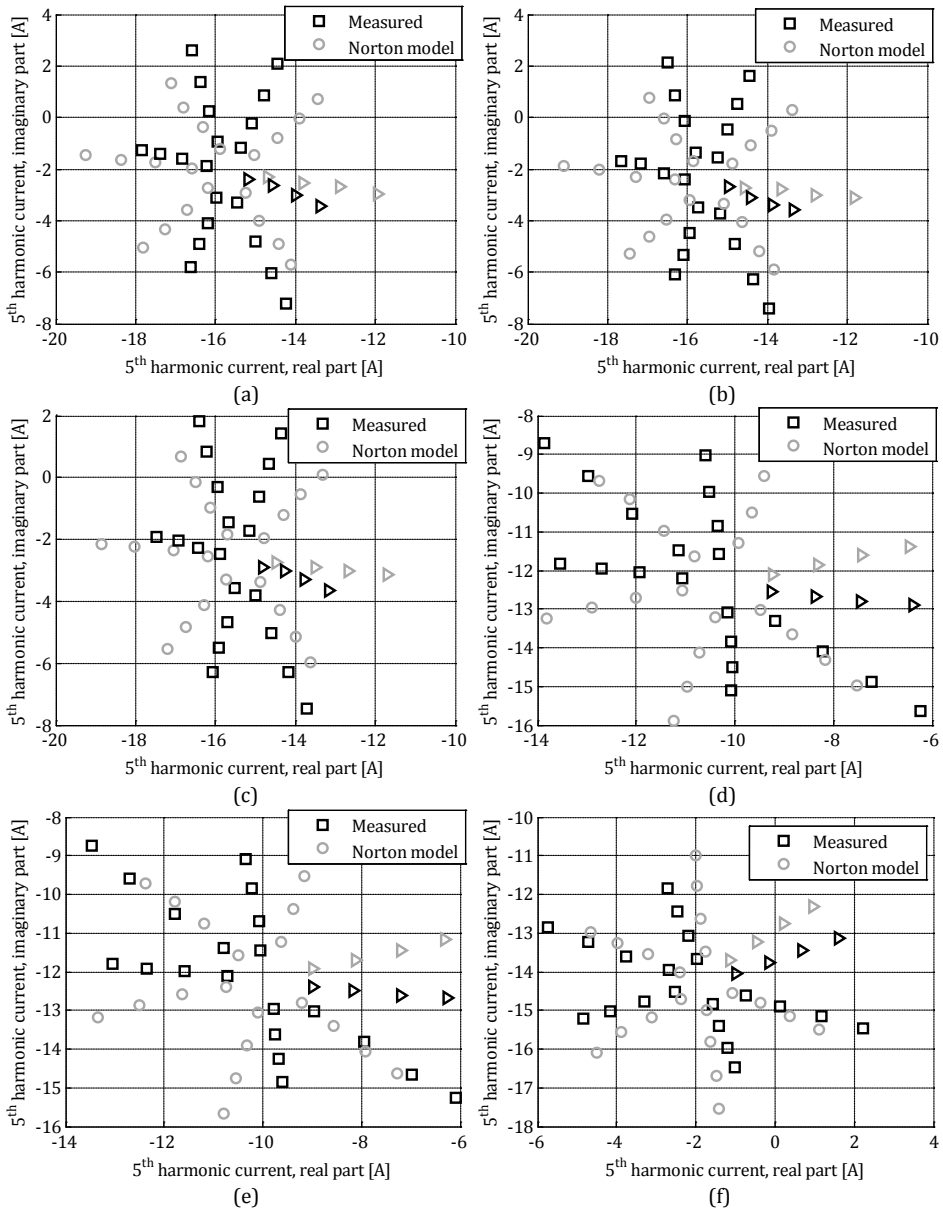

Fig 4.15 Three-phase diode bridge, 5th harmonic current measured and calculated from the Norton equivalent; inductance configurations: (a) 1, (b) 2, (c) 3, (d) 4, (e) 5, and (f) 6

At higher order harmonics the Norton model becomes even more accurate. A comparison of measured and calculated 19th harmonic currents is given in Fig 4.16.

The differences between measured and calculated values are lower than in the case of the 5th harmonic, both for their magnitudes and phase angles. At higher values of L_{AC} the error becomes even lower. Parameters of the Norton equivalent are given in Table 4.4. Magnitudes of I_h vary between 0.7 A and 2.0 A, which is 30 to 80 times lower than the magnitude of the fundamental (for the idealized model the ratio is h = 19). The

phase angle of I_h also covers a wide range, it changes between 70° and -130° for the six configurations.

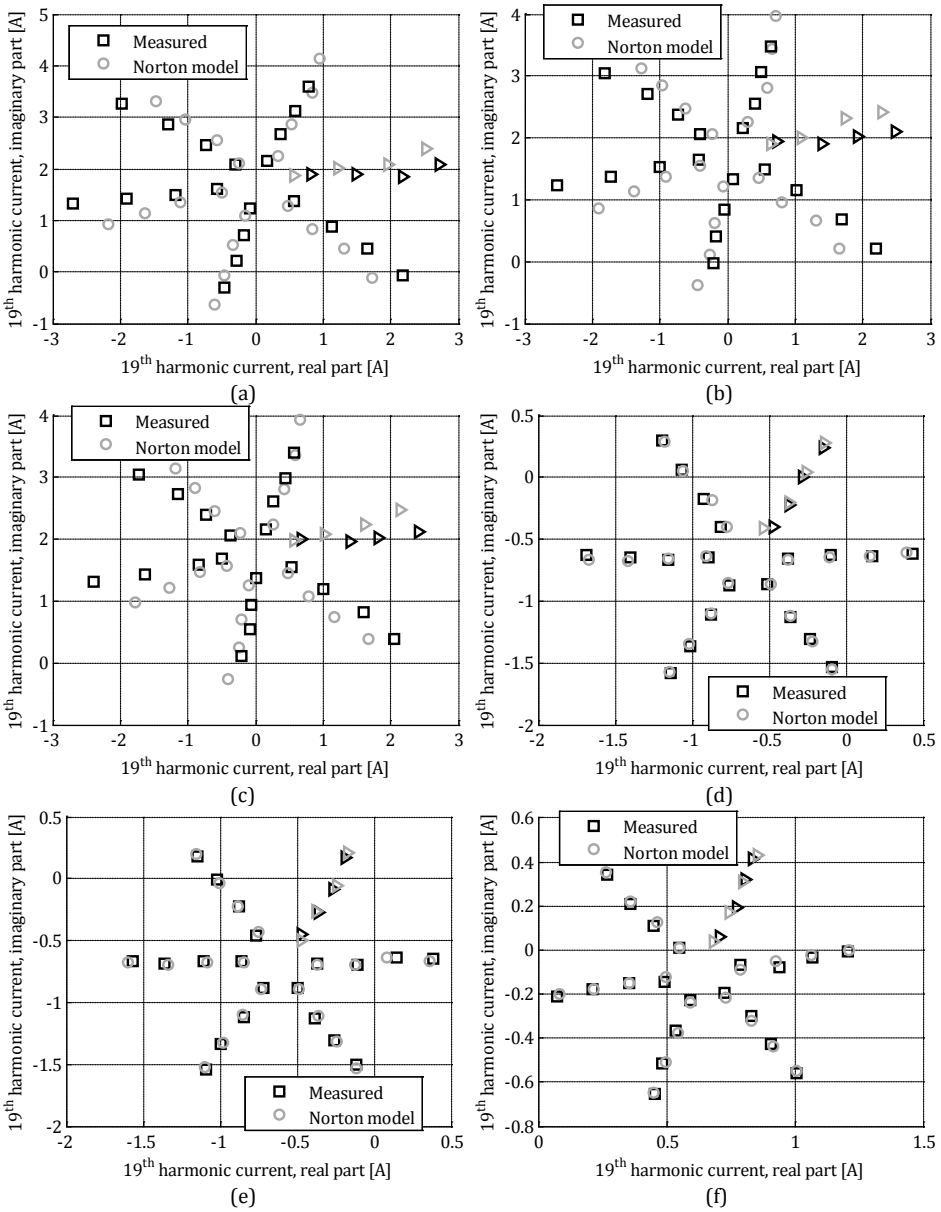

Fig 4.16 Three-phase diode bridge, 19th harmonic current measured and calculated from the Norton equivalent; inductance configurations: (a) 1, (b) 2, (c) 3, (d) 4, (e) 5, and (f) 6

The ratio of the fundamental current to I_h of all tested harmonic orders, is shown in Fig 4.17, for the case of highest value of L_{AC} (lowest value of $|\underline{I}_h|$) and no L_{AC} (highest value of $|\underline{I}_h|$). In both cases the ratio differs from the idealized one (equal to h), especially in the case of high L_{AC}, with a growing difference with the harmonic order. In this graph, the value of 1.1 mH is designated as 5 %, which is an approximate value of

this impedance expressed via the nominal voltage and power of the rectifier (as a percentage of the base impedance).

Impedance Z_h is predominantly resistive for lower values of L_{AC}, with very similar values for all characteristic orders. The resistive part of the impedance (which is dominant) is ranging from 4.1 Ω to 4.8 Ω when L_{AC} < 5 %.

Table 4.4 Parameters of the 19th order Norton equivalent for the three-phase diode rectifier

Test number	$\underline{I_h}$ [A]	$\underline{Z_h}$ [Ω]
1	0.69+j1.72	4.35-j0.17
2	0.67+j1.81	4.62-j0.62
3	0.64+j1.87	4.82-j0.77
4	-0.65-j0.69	5.75-j8.99
5	-0.63-j0.71	6.34-j9.63
6	0.66-j0.11	8.05-j18.3

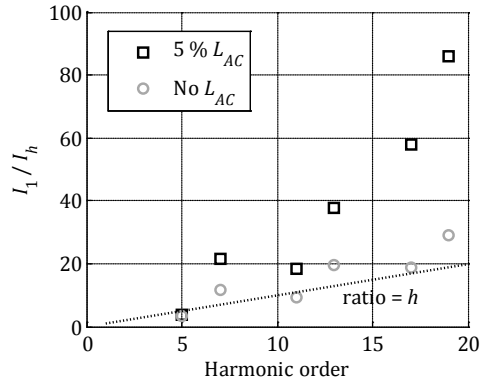

Fig 4.17 Ratio of the fundamental current and I_h with and without L_{AC}

4.3.4.3 Norton equivalent of a compact fluorescent lamp

The majority of CFL lamps on the market use a rectifier with capacitive filtering of the DC voltage (as in Fig 4.4) or a rectifier with a passive PFC, as in Fig 4.18 [33]. The DC load from Fig 4.18 usually contains a DC-DC converter or a high frequency inverter and rectifier which regulates the voltage supplied to the tube.

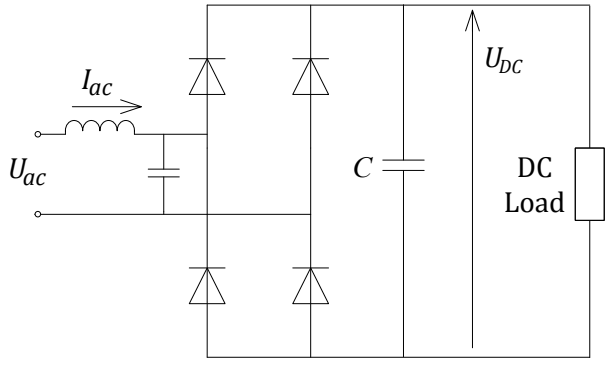

Fig 4.18 Single-phase rectifier with passive PFC

The Norton equivalent of an 11 W CFL was derived based on laboratory measurements, with the same approach as for the three-phase diode bridge, but using the odd harmonic orders up to the 9th, which are the dominant current harmonics of this device. Magnitudes of voltages used were 1 % to 10 % of the fundamental, with a step of 1 %, and phase angle steps were 30°. A comparison of measured and harmonic currents is shown in Fig 4.19. As for the three-phase diode bridge, the calculated currents are based on the harmonic voltages used in the measurement of currents.

In comparison to the diode rectifier with inductive DC side filtering, the CFL shows more non-linear behaviour and more differences between the model and the measurement. This is especially the case with the 3rd harmonic, which shows the highest dependency on the phase angles. The parameters of the Norton equivalent of these four orders are given in Table 4.5.

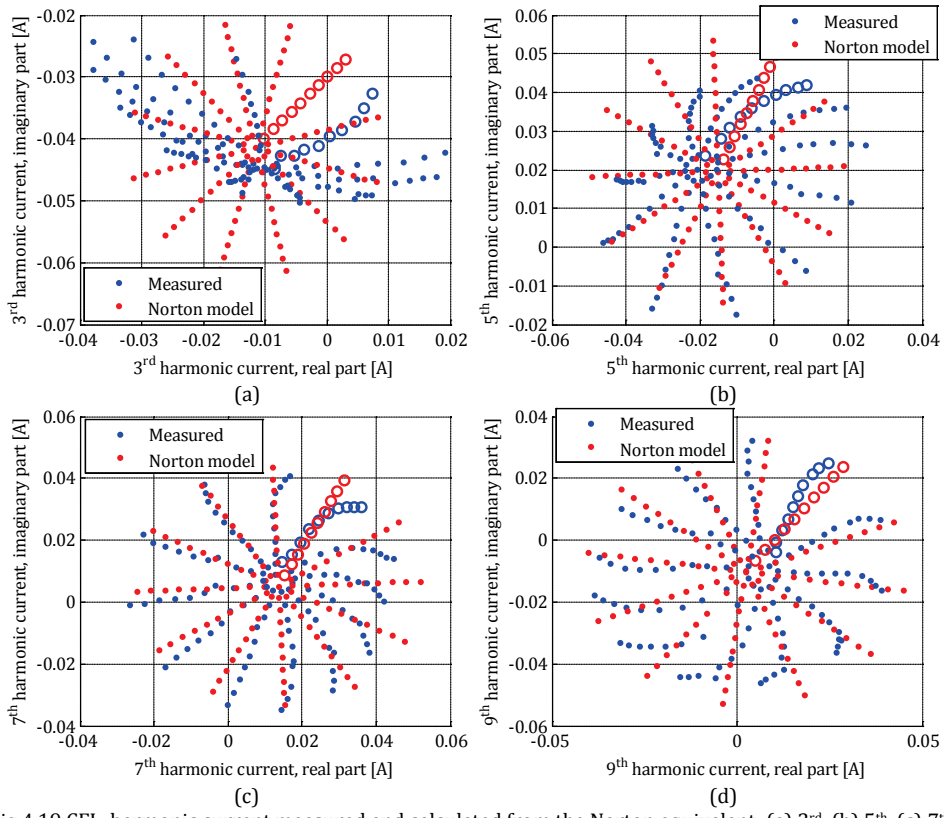

Fig 4.19 CFL, harmonic current measured and calculated from the Norton equivalent: (a) 3rd, (b) 5th, (c) 7th, and (d) 9th harmonic

Table 4.5 Parameters of the Norton equivalent for the 11 W CFL

h	$\underline{I}_h$ [A]	$\underline{Z}_h$ [Ω]	I_1 / I_h
3	-0.01-j0.04	732-j836	1.4
5	-0.01-j0.02	222-j631	2.4
7	-0.01+j0.005	161-j568	4.1
9	0.002-j0.01	207-j485	5.8

The equivalent impedance is predominantly capacitive for all four orders. The ratio between the fundamental and I_h is lower than in the idealized single-phase model (where it is equal to h). The calculated ratios are given in the last column of Table 4.5.

4.3.4.4 Thévenin equivalent

A Norton equivalent of a device or a part of the network can easily be transformed into a Thévenin equivalent – non-ideal voltage source model. The impedances of both equivalents are equal, and the voltage source is equal to the product of the current source and the impedance.

The upstream network (HV or MV) is commonly modelled with a voltage source equivalent because its behaviour is close to an ideal voltage source. If we consider a small load connected to the network, the impedance part of the equivalent does not play a significant role. Therefore, it is intuitively logical to use a Thévenin equivalent for modelling the "background" distortion of the network, even though a Norton equivalent would have the same performance.

For harmonic emitting loads a current source model is preferred because at low voltage distortion levels they usually behave close to an ideal current source. In terms of model performance, the Thévenin equivalent gives the same results.

Synchronous generators produce harmonics of e.m.f. due to geometrical imperfections of the windings and salient poles (for salient pole machines), as described in [14]. This fits the voltage source behaviour better, as with the "background" distortion. A similar behaviour can be found in induction motors, induced in the stator winding from the rotors field, mostly at inter-harmonic frequencies. Due to the relatively low magnitudes, it is often disregarded for both types of machines.

In [35], [36] it is argued that capacitor filtered diode bridges, such as the CLF example from 4.3.4.1, behave as voltage sources, because their current waveform is strongly dependent on the system impedance. In principle, this characteristic only makes them "less ideal" current sources.

The two devices used as examples for the Norton equivalent are not threated here, as the derivation of the Thévenin from Norton equivalent is trivial. The comparison of the measurements with the results of the model would yield the same results as found in 4.3.4.1.

4.3.4.5 Harmonic admittance matrix

The equivalents discussed before linearize the behaviour of a device and remove cross-influence of different harmonic frequencies (e.g. the influence of the 5th harmonic on the 7th, and vice versa). The harmonic admittance matrix is a more complex form of linearization, which maintains all cross-frequency influences but still requires linear dependencies between harmonic currents and voltages.

The matrix formulation of the admittance matrix model is given in [8]:

$$\begin{bmatrix} \underline{I_1} \\ \underline{I_2} \\ \vdots \\ \underline{I_N} \end{bmatrix} = \begin{bmatrix} \underline{Y_{11}} & \underline{Y_{12}} & \cdots & \underline{Y_{1N}} \\ \underline{Y_{21}} & \underline{Y_{22}} & \cdots & \underline{Y_{2N}} \\ \vdots & \vdots & \ddots & \vdots \\ \underline{Y_{N1}} & \underline{Y_{N2}} & \cdots & \underline{Y_{NN}} \end{bmatrix} \cdot \begin{bmatrix} \underline{U_1} \\ \underline{U_2} \\ \vdots \\ \underline{U_N} \end{bmatrix} \tag{4.8}$$

where $\underline{Y}_{ik}$ are the complex admittances which relate the i^{th} harmonic current and the k^{th} harmonic voltage. This type of a model was used in [8], [9], [37], [38], [39], [40], with the elements derived analytically or from simulated or measured results.

In a special case, when the $[\underline{Y}]$ matrix has only its first column and the main diagonal ($\underline{Y}_{ik} = 0$ if $j \neq k$ or $j \neq 1$), (4.8) becomes comparable to the Norton equivalent. The first column then represents the current source part, and the main diagonal represents the impedance part of the non-ideal current source. The difference from the Norton equivalent is that the admittance matrix provides the current source indirectly, as a product of the voltage matrix and the corresponding admittances. Due to this, the current source part of the equivalent is voltage dependent.

A drawback of applying (4.8) to measured data is that the values of admittances use only the proportional part of the linearly fitted dependency. This is illustrated in Fig 4.20 with an example set of data, which is fitted using only the proportional parameter and also when using both the proportional and a constant parameter.

Another drawback of the admittance matrix approach is that all cross-frequency dependencies need to be linear. In reality, the elements of the admittance matrix show some dependency from the input voltage.

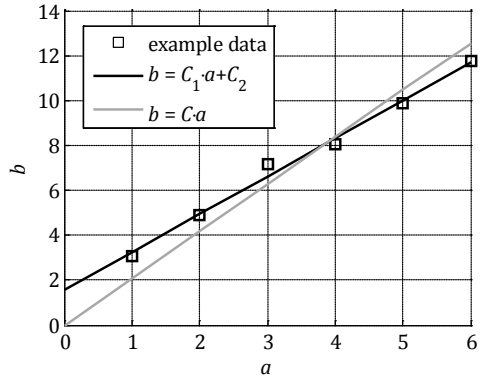

Fig 4.20 Linear fitting using only the proportional parameter and both parameters, example data

From the arbitrary example data (Fig 4.20), the slope different for the two cases, and if $C_2 \neq 0$ there is also an offset. For the non-linear behaviour of converters this error adds up to the error of linearized dependency.

These two errors are highest in the dependency from the fundamental voltage, due to the highest magnitude of this voltage. To reduce this error, we introduce a modification of (4.8), which removes the linear dependency from the fundamental voltage:

$$\begin{bmatrix} \underline{I}_1 \\ \underline{I}_2 \\ \vdots \\ \underline{I}_N \end{bmatrix} = \begin{bmatrix} \underline{I}_1^0 \\ \underline{I}_2^0 \\ \vdots \\ \underline{I}_N^0 \end{bmatrix} + \begin{bmatrix} \underline{0} & \underline{Y}_{12} & \cdots & \underline{Y}_{1N} \\ \underline{0} & \underline{Y}_{22} & \cdots & \underline{Y}_{2N} \\ \vdots & \vdots & \ddots & \vdots \\ \underline{0} & \underline{Y}_{N2} & \cdots & \underline{Y}_{NN} \end{bmatrix} \cdot \begin{bmatrix} \underline{0} \\ \underline{U}_2 \\ \vdots \\ \underline{U}_N \end{bmatrix} \tag{4.9}$$

In (4.9), $[I_h^0]$ is a constant matrix, representing the emission of the device without voltage distortion as an ideal current source. If we apply (4.9) to sinusoidal voltages of different magnitudes, calculated harmonic currents remain constant (which is not the case in reality).

A comparison of results of (4.8) and (4.9) based on the laboratory measurements on the three-phase diode rectifier in Test 1 (according to Table 4.2), are given in Fig 4.21. Points which correspond to harmonic voltages with a phase angle of 0° are highlighted with a different symbol. In this example (4.9) performs better.

Another approach for reducing the shortcomings of (4.8) was proposed in [41], based on the analytical model of a thyristor rectifier. The extended expression from [41] is given as:

$$\begin{bmatrix} \underline{I_1} \\ \underline{I_2} \\ \vdots \\ \underline{I_N} \end{bmatrix} = \begin{bmatrix} \underline{Y_{11}^+} & \underline{Y_{12}^+} & \cdots & \underline{Y_{1N}^+} \\ \underline{Y_{21}^+} & \underline{Y_{22}^+} & \cdots & \underline{Y_{2N}^+} \\ \vdots & \vdots & \ddots & \vdots \\ \underline{Y_{N1}^+} & \underline{Y_{N2}^+} & \cdots & \underline{Y_{NN}^+} \end{bmatrix} \cdot \begin{bmatrix} \underline{U_1} \\ \underline{U_2} \\ \vdots \\ \underline{U_N} \end{bmatrix} + \begin{bmatrix} \underline{Y_{11}^-} & \underline{Y_{12}^-} & \cdots & \underline{Y_{1N}^-} \\ \underline{Y_{21}^-} & \underline{Y_{22}^-} & \cdots & \underline{Y_{2N}^-} \\ \vdots & \vdots & \ddots & \vdots \\ \underline{Y_{N1}^-} & \underline{Y_{N2}^-} & \cdots & \underline{Y_{NN}^-} \end{bmatrix} \cdot \begin{bmatrix} \underline{U_1^*} \\ \underline{U_2^*} \\ \vdots \\ \underline{U_N^*} \end{bmatrix} \tag{4.10}$$

where $[Y_{jk}^+]$ and $[Y_{jk}^-]$ are admittance matrixes that represent the dependency from the matrix of harmonic voltages $[U_h]$ and the matrix of conjugated harmonic voltages $[U_h^*]$, respectively. Due to the higher number of parameters, this model can represent the non-linearity of the device more accurately. When derived from measurement results, (4.10) has a problem of having multiple solutions due to the second input variable (the conjugated voltage matrix).

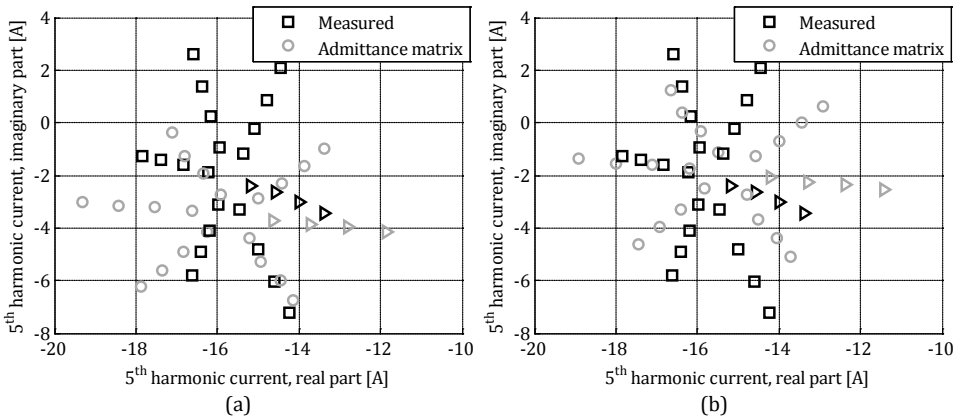

Fig 4.21 Three-phase diode bridge, 5th harmonic current measured and calculated from the Norton equivalent; inductance configurations: (a) according to (4.8), (b) according to (4.9)

4.3.4.6 Harmonic admittance matrix of a three-phase diode rectifier

The harmonic admittance matrix of the three-phase diode bridge was derived based on the laboratory measurements described in 4.3.4.1 (used also for the Norton equivalent), based on expression (4.9). The measured and calculated 5th harmonic current for all six inductor configurations is given in Fig 4.22. A comparison of the 19th harmonic is shown in Fig 4.23. Similarly as with the Norton equivalent, the admittance matrix provides better accuracy for the 19th order, due to the more linear response to harmonic voltages.

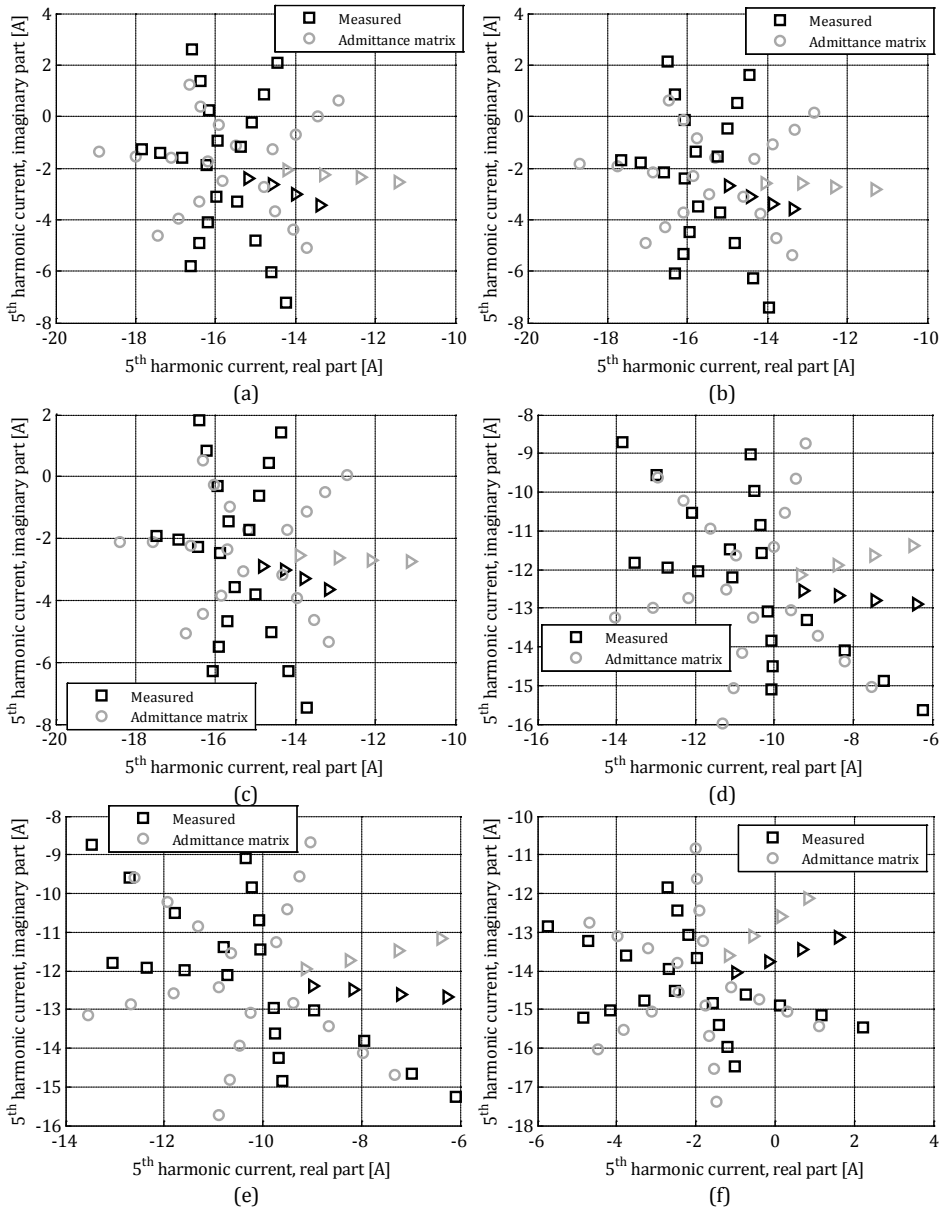

Fig 4.22 Three-phase diode bridge, 5th harmonic current measured and calculated from the admittance matrix; inductance configurations: (a) 1, (b) 2, (c) 3, (d) 4, (e) 5, and (f) 6

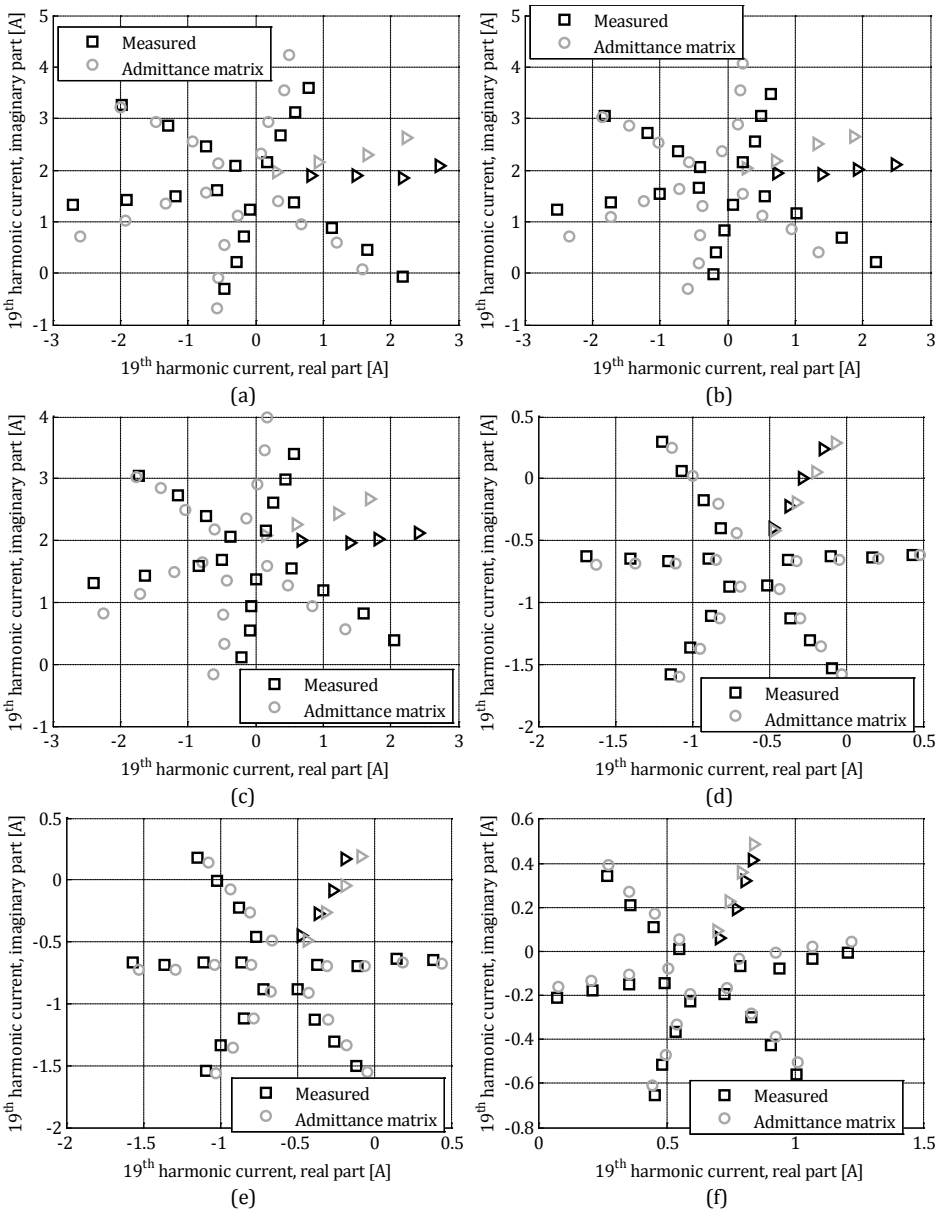

Fig 4.23 Three-phase diode bridge, 19th harmonic current measured and calculated from the admittance matrix; inductance configurations: (a) 1, (b) 2, (c) 3, (d) 4, (e) 5, and (f) 6

4.3.4.7 Harmonic admittance matrix of a CFL

The harmonic admittance matrix of a 11 W CFL was derived based on the laboratory measurement shown in 4.3.4.1, also using expression (4.9). A comparison of measured and calculated harmonic currents of the first four odd orders is shown in Fig 4.24.

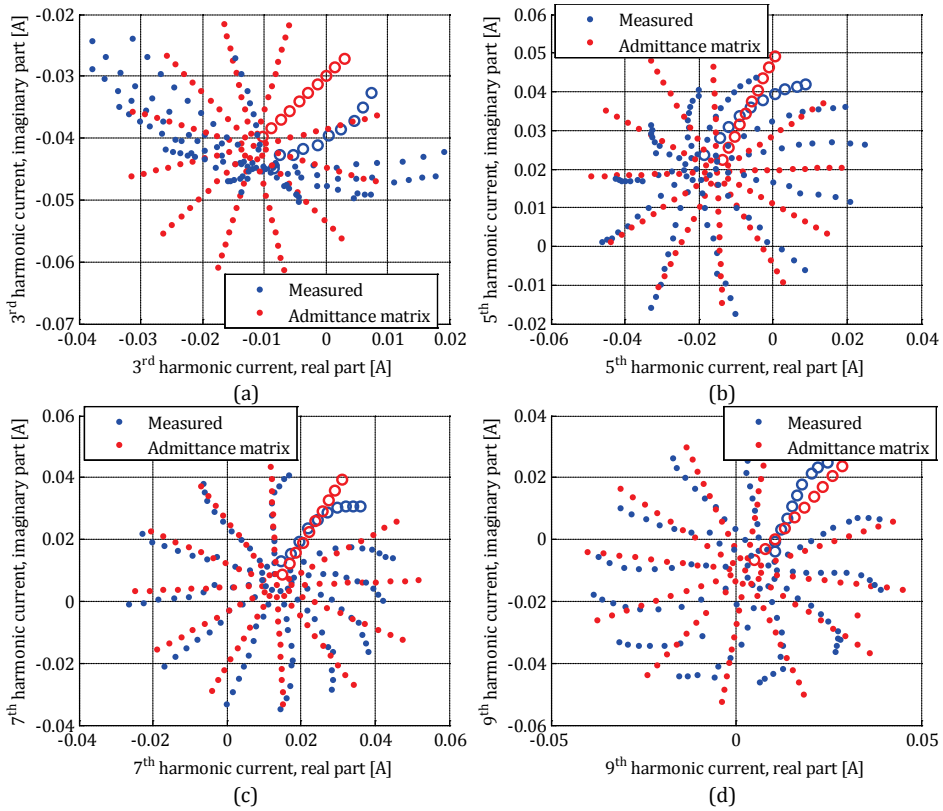

Fig 4.24 CFL, harmonic current measured and calculated from the harmonic admittance matrix: (a) 3rd, (b) 5th, (c) 7th, and (d) 9th harmonic

The result of the admittance matrix is similar as of the Norton equivalent, because both methods linearize the dependency from the harmonic voltages and the results are obtained from a single voltage harmonic. In the last part of this section we compare the methods when several voltage harmonics are applied at the same time.

4.3.4.8 Harmonic fingerprint

Harmonic fingerprint is a method which uses a piecewise linearization of the voltage-current dependencies for each harmonic order. Based on measured or simulated data, a look-up table is made which represents the voltage dependent current sources for all considered frequencies, as presented in [10], [42].

For the creation of the fingerprint look-up table, emission of the device under test is measured with an undistorted voltage, and with a series of distorted voltages which contain an additional harmonic component varied in amplitude and phase angle. The

process is repeated for each harmonic order of interest. An incomplete table of the 3rd harmonic fingerprint of a CLF is given as an example in Table 4.6.

For harmonic voltages at which the current is measured the fingerprint gives the exact solution, as long as only one harmonic voltage is present. For voltages with magnitudes and/or phase angles between the measurement points a piecewise linearization needs to be performed, taking an average value between the closest measurements.

Table 4.6 An example look-up fingerprint table, 3rd harmonic current of a 11 W CFL

3rd harmonic current [% of fundamental]	3rd harmonic voltage magnitude [% of the fundamental]			
3rd harmonic voltage phase angle [°]	1	2	…	10
0	-14.2-j75.7	-13.2-j75.4	…	13.3-j59.3
30	-17.1-j74.8	-19.2-j73.5	…	-26.6-j49.0
…	…	…	…	…
330	-14.6-j77.1	-8.8-j77.4	…	39.3-j70.9

The piecewise linearization introduces less error than linearizing the dependency for each harmonic order, which is done in previously presented methods. The two main sources of error in this method are the influence of fundamental voltage variations and the cross-frequency influence.

Similarly to the ideal current source part of the Norton equivalent and the modified admittance matrix, the fingerprint is derived for one value of the fundamental voltage. If the spectrum of the device is dependent on the magnitude of the fundamental voltage (e.g. devices that behave as a constant power load), this effect cannot be taken into account.

The cross-frequency influence can be taken into account, since all harmonic orders are measured with each harmonic voltage, however, it leads to a very complex model. The resulting current is then a sum of currents caused by each of the present voltage harmonics. This linearizes the cross-frequency influence, similarly to the other methods, and does not necessarily improve the accuracy of the model.

A comparison of measured and calculated harmonic currents with a single harmonic voltage which was presented for the Norton equivalent and harmonic admittance matrix is not shown here, because in this case the fingerprint results match the measurements exactly (the look-up table consists of these measurements). A comparison of measured and calculated values when multiple harmonic voltages are present is shown in the next subsection, for all three methods.

4.3.4.9 Error comparison for different models

Now we compare the three methods presented before qualitatively, in terms of accuracy. The three-phase diode bridge and CFL examples are used again, but with voltage distortions which contain multiple orders simultaneously. A comparison of measured and calculated currents for the diode bridge, in inductor configuration 1, for three measurement points with multiple voltage harmonics is shown in Fig 4.25. A comparison with the same approach in the case of the CFL is shown in Fig 4.26. In these two figures colours represent different methods, and numbers represent observed measurement points. In Fig 4.25 (b), the three points of the harmonic fingerprint are identical, due to the resolution of the fingerprint table and small variations of the 19th harmonic voltage in the presented measurements.

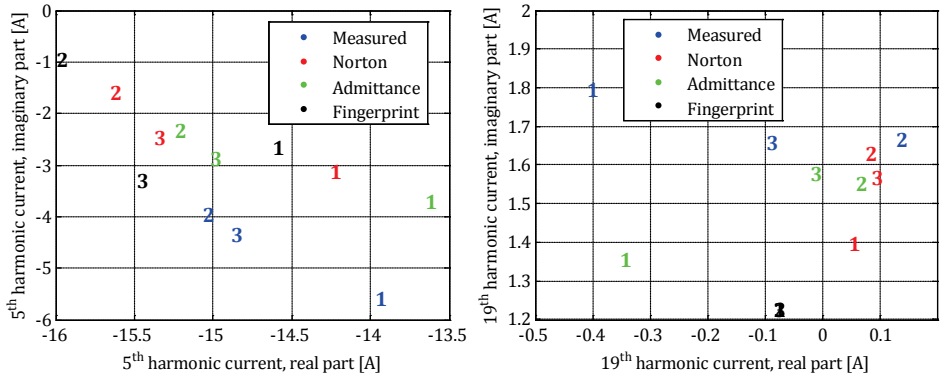

Fig 4.25 Comparison of measured and calculated currents when multiple voltage harmonics are applied; Diode bridge: (a) 5th harmonic current, (b) 19th harmonic current

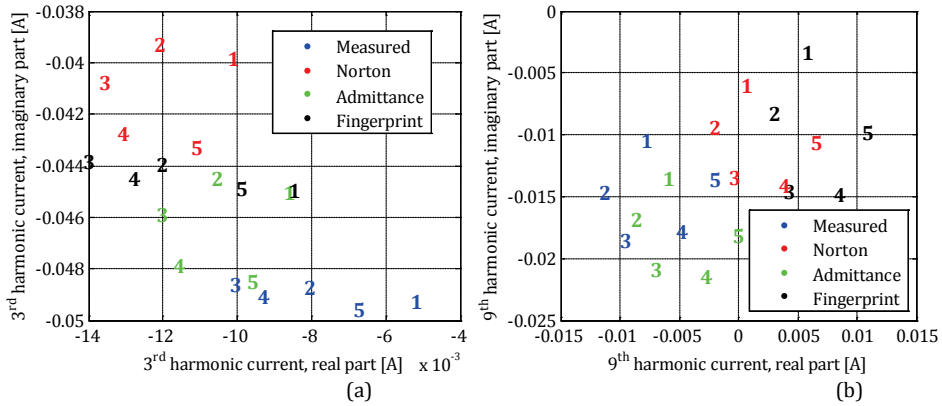

Fig 4.26 Comparison of measured and calculated currents when multiple voltage harmonics are applied, CFL: (a) 3rd harmonic current, (b) 9th harmonic current

One of the sources of errors in measurement based methods is the voltage reproduction during the model derivation. For example, if we derive the dependency of harmonic currents from a specific harmonic voltage, harmonic voltages of other orders introduce an error in the parameters. Analytical derivation of parameters can avoid this problem.

Another significant source of errors is the dependency from the fundamental voltage level. If this dependency is not linear, the admittance representation does not perform well. The constant current source representation reduces the sensitivity to fundamental voltage changes, but it introduces an error of its own. The harmonic fingerprint could take it into account with repeated measurements at different voltage levels, but requires a very large number of measurements and results in an impractically large model of the device.

In [16] it is concluded that the Norton equivalent has lower average errors than the harmonic admittance error, but this is not a general conclusion, as was shown in the two examples presented here.

When only one harmonic voltage is present, the harmonic fingerprint has the lowest modelling error, because it linearizes the dependency only between two points, rather than for each harmonic order. However, since more harmonic voltages are always present in practice, none of the presented methods has the highest precision in

general. As it is assumed that the harmonic current is a linear sum of influences, this introduces a magnitude and phase dependent error in all methods, which is different in each of them.

A numerical comparison of these results is difficult because differences of complex numbers cannot be compared directly (it would be mathematically incorrect to say which complex number is greater). As an illustration, we compare the magnitudes and phase angles of differences between measured and simulated values, as the mean square error (MSE). Results from Fig 4.25 and Fig 4.26 are presented in Table 4.7 and Table 4.8, respectively.

Based on the MSE values of presented results, it is noticeable that the harmonic admittance method had the lowest magnitude errors, while the phase-angle errors are lowest either for the harmonic fingerprint or admittance matrix, depending on the observed point. These results cannot be generalised, because the errors are dependent both on the set of voltages which are used to determine the models and the observed harmonic voltages.

Table 4.7 Comparison of different models, diode bridge rectifier; mag. – magnitude, ph. – phase angle, diff. – difference, Nort. – Norton equivalent, Adm. – Admittance matrix, Fing. – Harmonic fingerprint

	$h = 5$			$h = 19$		
Method	Nort.	Adm.	Fing.	Nort.	Adm.	Fing.
MSE amplitude [A^2]	15.6	8.3	18.1	0.25	0.16	0.82
MSE ph. [deg.^{2}]	$1.8 \cdot 10^4$	$2.4 \cdot 10^4$	$1.5 \cdot 10^4$	$3.5 \cdot 10^4$	$2.8 \cdot 10^4$	$2.5 \cdot 10^4$

Table 4.8 Comparison of different models, CFL; mag. – magnitude, ph. – phase angle, diff. – difference, Nort. – Norton equivalent, Adm. – Admittance matrix, Fing. – Harmonic fingerprint

	$h = 5$			$h = 19$		
Method	Nort.	Adm.	Fing.	Nort.	Adm.	Fing.
MSE amplitude [A^2]	$6.6 \cdot 10^{-4}$	$1.2 \cdot 10^{-4}$	$2.8 \cdot 10^{-4}$	$8.1 \cdot 10^{-4}$	$1.3 \cdot 10^{-4}$	$17 \cdot 10^{-4}$
MSE ph. [deg.^{2}]	$3.2 \cdot 10^4$	$1.5 \cdot 10^4$	$2.3 \cdot 10^4$	$2.0 \cdot 10^5$	$1.3 \cdot 10^5$	$2.1 \cdot 10^5$

4.4 Case study of an industrial installation

This section presents a case study in which the interaction of devices in an industrial installation is described. A group of devices is then modelled based on field and laboratory measurements, using the Norton equivalent.

4.4.1 Field measurement description

The topology of the industrial site is schematically presented in Fig 4.27. One 1600 kVA MV/LV transformer is feeding two LV cabinets, with a short-circuit impedance of 6 %. In one of the cabinets, a 453 kW DC motor is connected, fed by a six-pulse thyristor rectifier with line inductors of L = 0.0225 mH per phase (approximately 2 % of the base impedance Z_B, defined as Un^2/Sn). The other cabinet is supplying the lighting system in the factory hall, 54 kW in total, composed of gas discharge lamps with electromagnetic ballasts and parallel compensation.

The reason why this installation was chosen is that the protection equipment of the lighting system experienced problems, with the occurrence being related to the drives operation. The initial measurement showed that the current of lamps and the voltage distortion increase significantly in some modes of the drives operation, with noticeable notches in the voltage waveform.

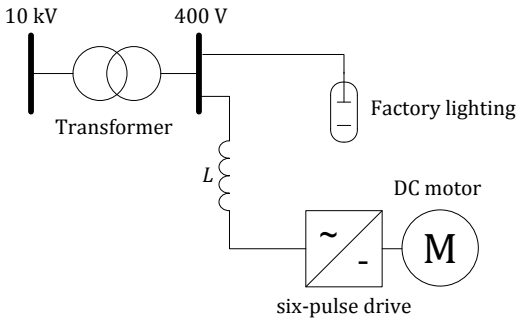

Fig 4.27 Schematic diagram of the measurement site

The measurement was done with a power quality analyser and a storage oscilloscope. The analyser was measuring at the converters connection to the supply, while the storage oscilloscope was measuring on six channels (three voltages and three currents) at the terminals of the lighting system. The sampling frequency of the oscilloscope was 20 kHz, and two recordings were made with duration of approximately two minutes each.

Three specific regimes were aimed for in the measurements. In the first regime the DC drive is lightly loaded, with RMS current values up to 200 A. In the second regime the drive has a constant high loading, with currents of approximately 600 A. In the third regime the drive is suddenly changing its loading with short-term currents reaching 1000 A.

4.4.2 Results of the field measurement

The current waveforms of lamps in phase *a* during one 95 s time interval is shown in Fig 4.28. The number of lamps switched on was not changing during this measurement interval, the changes in the current are only caused by the changes in the current of the six-pulse converter. As indicated, three working regimes can be distinguished on the figure. The lowest value of the current corresponds to low loading of the DC drive – designated with "A". Higher values without peaks correspond to constant high loading of the drive – period "B". Current transients occur during sudden changes of the drives load – labelled with "C".

In the time interval A, peak values of the current are approximately 125 A. In the time interval B, peak values are around 140 A. During high-peaks (regime C), peak values are between 250 and 300 A. Different load changes correspond to different peak current values in this regime, and the duration was changing from 1 to 1.5 s.

One period of the lighting current for all three working regimes is shown in Fig 4.29. The current in regime A is "lightly" distorted. The current in regime B has more distortion, with six distinctive oscillations per period – every time when a voltage notch happens. The current in regime C behaves in the same way, but with significantly higher oscillations.

The voltage waveform of one phase in all three regimes, during one half-cycle, is shown in Fig 4.30. Regime A does not cause visible notches, only slight deviations of the waveform are visible at switching moments since the drives current is relatively low. In regimes B and C voltage notches are noticeable. Sudden load changes cause very large notches, since the peak currents can be almost twice as large as during the constant high loading.

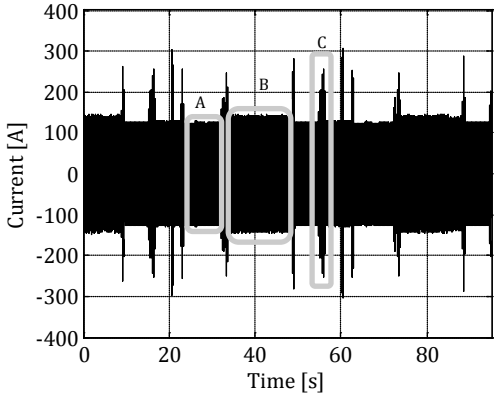

Fig 4.28 Current waveform of the factory lighting during one 95 s time interval

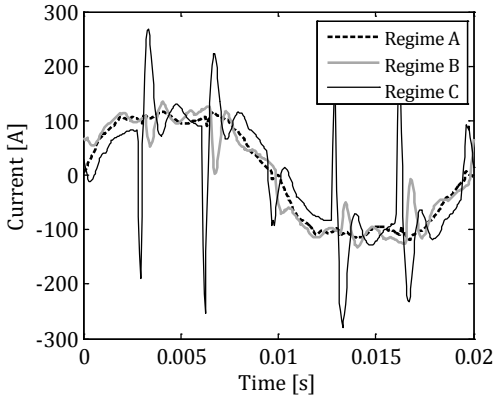

Fig 4.29 Current waveform of the factory lighting during one period in all three working regimes

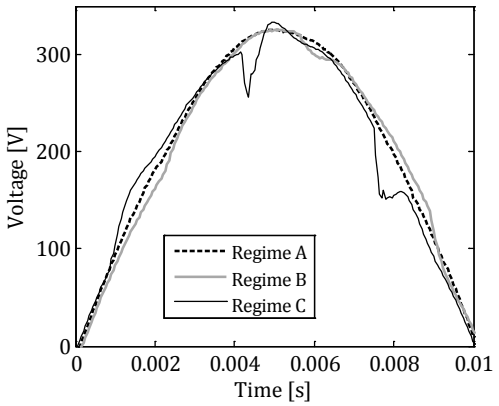

Fig 4.30 Voltage waveform in phase *a* during one half-period, in all three working regimes

4.4.3 Processing of the field measurement results

To illustrate the nature of the current transients, a 4 s period of time was chosen, containing short time intervals of all three working regimes. The changes of lamp's voltage and current THD during this time period are shown in Fig 4.31, calculated with a data window length of one cycle of the fundamental. Working regimes are labelled on

the figure, and it is noticeable that the shape of the current THD resembles the shape of the voltage THD.

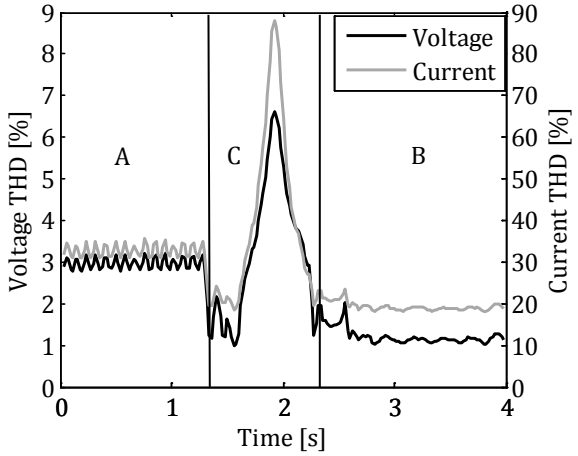

Fig 4.31 Changes in time of the voltage and current THD in all three working regimes

As mentioned, during transients, the current peak is increased up to three times. However, the fundamental current of lamps is slightly decreased during these periods, due to a higher voltage drop. At the same time harmonic orders characteristic for a six-pulse converter are increased, due to high levels of harmonic voltages. To visualise this, we use the SWRDFT method to derive the waveforms of harmonic components, as discussed in Chapter 3. The fundamental current and the 17th harmonic are shown in Fig 4.32, for the same time interval as in Fig 4.31.

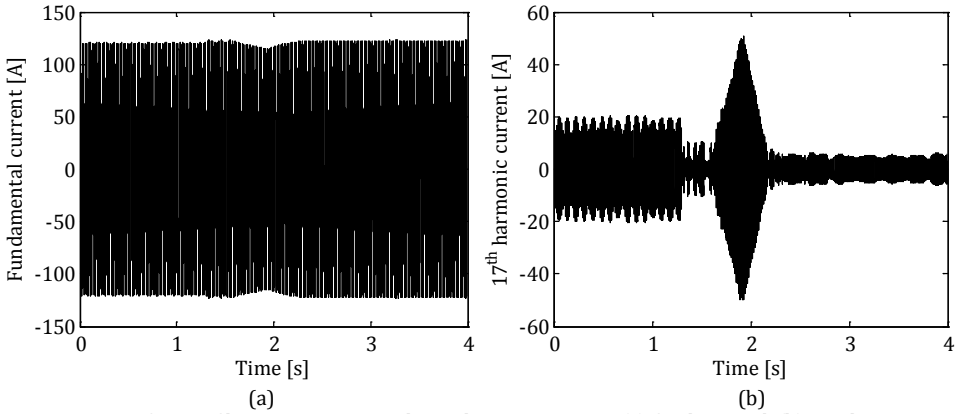

Fig 4.32 Waveforms of harmonic currents derived using SWRDFT: (a) fundamental, (b) 17th harmonic

The current spectrum of the lamps contains harmonic orders characteristic of a six-pulse converter. The 3rd and 9th harmonics are also present, because all lamps are single-phase units. The spectrums of the current and voltage during all working regimes are presented in Fig 4.33. In regime A, the 3rd current harmonic is dominant, when the influence of the DC drive is low. This regime is the closest to working with an undistorted voltage supply. In regime B voltage distortion is higher, with almost no changes in the 3rd harmonic, but with a considerable increase of the characteristic

harmonic voltages. In this regime the level of the 11th current harmonic of lamps is almost the same as the 3rd. In regime C the 3rd harmonic is again almost unaffected, while characteristic harmonics are increased even more, both for the voltage and current.

Significant increase of the voltage distortion suggests that a parallel resonance might be excited during the transition periods. However, a number of voltage harmonics are increased in the same way, instead of only a small bend of frequencies. This is suggesting that no parallel resonance is being excited, and that transients are a reaction of lamps to the short-term voltage distortion.

The maximal value of the voltage THD calculated over a data window of 20 ms was around 7 % at almost all peaks. At rare occasions, the short-term harmonic levels were higher than the limit defined for the 10-minute aggregated values (this is allowed by the LV compatibility levels).

From the previous figures it is obvious that the current transients of the factory lighting are a reaction to the increases in the voltage distortion caused by the drive. From the time changes of voltage and current harmonics it was possible to calculate the impedance of lamps at different frequencies. Impedances were calculated at characteristic harmonic orders of the DC drive (5th, 7th, 11th, etc.), which had relatively high levels in regime C, and the voltage was not influenced significantly by the lamps at these frequencies.

The load impedance at certain frequencies can be calculated from harmonic currents caused by the applied harmonic voltages. Harmonic currents of the load when no harmonic voltage is present create an error in the impedance calculation. In the laboratory it is possible to measure this error, but there is no such possibility in a field measurement. Also, harmonic voltages on most frequencies have relatively low values, which further reduce the accuracy of impedance calculation.

To avoid these errors as much as possible, impedance was calculated only for the orders equal to $6 \cdot k \pm 1$, where harmonic voltages are sufficiently high during transients, and harmonic currents are greatly increased when compared to moments without transients.

The impedance-frequency dependency of the factory lighting is shown in Fig 4.34. High current values can be expected especially if a high content of higher order voltage harmonics is present, because of a decreasing value of load impedance at higher frequencies, as Fig 4.34 is showing.

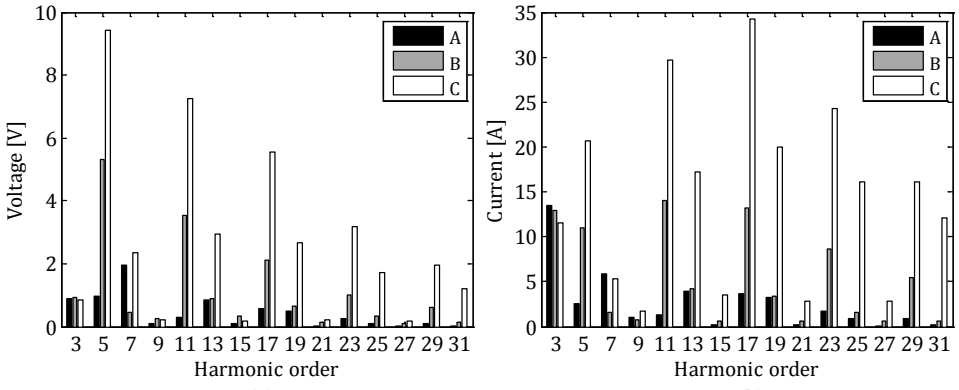

(a) (b)

Fig 4.33 (a) Spectrum of the voltage, (b) spectrum of the current of lamps

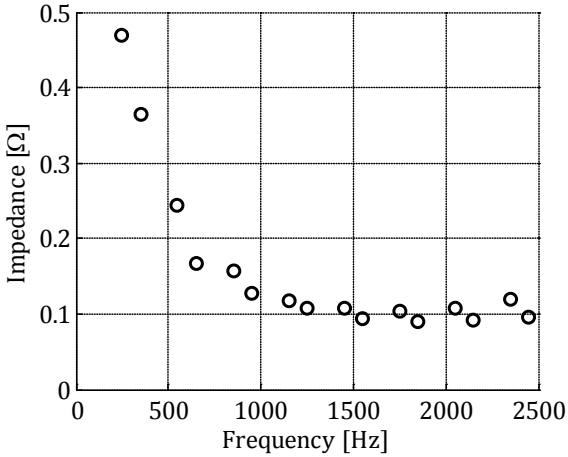

Fig 4.34 Calculated impedance of the factory lighting, as a function of frequency

4.4.4 Laboratory measurements and the Norton model of the lamps

To create a more accurate harmonic model of the used industrial lamps (further referred to as lamps), a set of experiments was conducted on a single lamp in the laboratory, with a programmable voltage source which minimizes the influence of the lamps current. A harmonic fingerprint of the lamp was created, but the impedance characteristic from Fig 4.34 implied that a simple Norton model can represent the lamp accurately, with a capacitor as the equivalent impedance.

The fingerprint of the 3rd harmonic current of the lamp is shown in Fig 4.35. The shape of the measured currents in the polar plane corresponds to the shape of voltage measurements very well, also for other harmonic orders. This confirms that it is possible to create an accurate Norton equivalent of the lamp.

From the fitted measurements, the parameters of the Norton model are derived and given in Table 4.9 (the first four odd orders for the current source part), with currents expressed as a percentage of the fundamental current. The calculated capacitance value is 47.7 μF, which is in good agreement with the size of the PFC capacitor of the lamps ballast, which has a nameplate value of 45 μF ± 10 %.

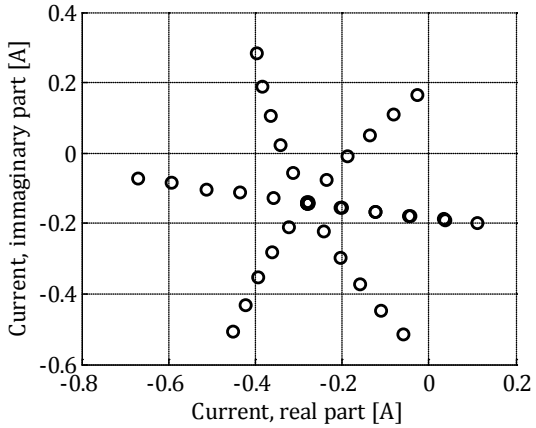

Fig 4.35 Harmonic fingerprint of the 3rd harmonic current, single lamp

Table 4.9 Parameters of the Norton equivalent of the lamp, derived from laboratory measurements

C [µF]	I_3 [A]	I_5 [A]	I_7 [A]	I_9 [A]
47.7	-0.28-j0.14	0.03+j0.08	0.04-j0.04	-0.02+j0.00

4.5 Conclusions

An overview of harmonic modelling techniques is given in this chapter, followed by an analysis of the frequency domain models of individual harmonic sources. The Norton and Thévenin equivalent, harmonic admittance matrix, and harmonic fingerprint are compared by the principle of operation, and specific errors of each type of models are analysed and illustrated with examples.

For the harmonic admittance matrix, a modification is proposed, given with expression (4.9), which reduces the errors caused by the inaccurate dependency from the fundamental voltage level.

A comparison of errors for the three methods is given, where it was shown that none of the presented methods has the highest accuracy in general, because their errors are dependent on the magnitudes and phase angles of applied voltage harmonics.

Lastly, a case study about harmonic interaction in an industrial installation is presented. The influence of a DC motor drive on the current transients of the factory lighting was analysed by a field measurement, and the behaviour of the used lamps was further analysed by laboratory measurements. Due to the topology of the lamp, a simple and accurate Norton model could be derived, presented in Table 4.9.

4.6 References of Chapter 4

[1] J. Arrillaga, B. C. Smith, N. R. Watson, and A. R. Wood, "Introduction," in *Power system harmonic analysis*, John Wiley & Sons, 1997.

[2] A. Medina, "Harmonic simulation techniques (methods & algorithms)," in Proc. *IEEE Power Engineering Society General Meeting,* 2004., vol. 2, pp. 762–765.

[3] A. Medina, N. R. Watson, P. F. Ribeiro, and C. J. Hatziadoniu, "Harmonic analysis in frequency and time domains." IEEE PES tutorial on harmonics modeling and simulation, Chapter 5, 2007.

[4] A. Medina, J. Segundo-Ramirez, P. F. Ribeiro, W. Xu, K. L. Lian, G. W. Chang, V. Dinavahi, and N. R. Watson, "Harmonic analysis in frequency and time domain," *IEEE Transactions on Power Delivery*, vol. to be publ.

[5] C. J. Hatziadoniu, W. Xu, and G. Chang, "Procedure of time-domain harmonics modeling and simulation." IEEE PES tutorial on harmonics modeling and simulation, Chapter 8, 2007.

[6] R. H. Kitchin, "New method for digital-computer evaluation of convertor harmonics in power systems using state-variable analysis," in Proc. *IEE* C, vol. 128, 1981.

[7] P. Ribeiro, "Probabilistic Modeling of Single High-Power Loads," in *Time-Varying Waveform Distortions in Power Systems*, 1st ed., Wiley-IEEE Press, 2010, pp. 73–92.

[8] M. Fauri and P. F. Ribeiro, "A novel approach to non-linear load modelling," in Proc. *IEEE ICHPS*, 1994, pp. 201–205.

[9] A. R. Wood and J. Arrillaga, "The frequency dependent impedance of an HVDC converter," in Proc. *IEEE ICHPS*, 1994, pp. 75–81.

[10] S. Cobben, W. L. Kling, and J. Myrzik, "The making and purpose of harmonic fingerprints," in PRoc. *CIRED*, 2007.

[11] C. D. Callaghan and J. Arrillaga, "Convergence criteria for iterative harmonoic analysis and its application to static convertors," in Proc. *IEEE ICHPS*, 1990, pp. 38–43.

[12] A. Semlyen and A. Medina, "Computation of the periodic steady state in systems with nonlinear components using a hybrid time and frequency domain methodology," *IEEE Transactions on Power Systems*, vol. 10, no. 3, pp. 1498–1504, 1995.

[13] Kimbark E.W., "Harmonics and filters," in *Direct current transmission*, John Wiley & Sons, 1971, pp. 295–390.

[14] J. Arrillaga and N. R. Watson, "Harmonic sources," in *Power system harmonics*, John Wiley & Sons, 2003, pp. 61–142.

[15] ON Semiconductor, "Power factor correction handbook." p. HBD853/D, 2011.

[16] A. B. Nassif, "Modeling, measurement and mitigation of power system harmonics," PhD thesis, University of Alberta, Canada, 2009.

[17] P. Blanco, A.M.; Gasch, E.; Meyer, Jan; Schegner, "Web-based platform for exchanging harmonic emission measurements of electronic equipment," in Proc. *IEEE ICHQP*, 2012.

[18] J. Arrillaga, Y. H. Liu, and N. R. Watson, "Line-commutated HVDC conversion," in *Flexible power transmission - The HVDC options*, John Wiley & Sons, 2007, pp. 57–96.

[19] J. A. Orr and A. E. Emanuel, "On the need for strict second harmonic limits," *IEEE Transactions on Power Delivery*, vol. 15, no. 3, pp. 967–971, Jul. 2000.

[20] A. Mansoor, W. M. Grady, A. H. Chowdhury, and M. J. Samotyi, "An investigation of harmonics attenuation and diversity among distributed single-phase power electronic loads," *IEEE Transactions on Power Delivery*, vol. 10, no. 1, pp. 467–473, 1995.

[21] A. Mansoor, W. M. Grady, R. S. Thallam, M. T. Doyle, S. D. Krein, and M. J. Samotyj, "Effect of supply voltage harmonics on the input current of single-phase diode bridge rectifier loads," *IEEE Transactions on Power Delivery*, vol. 10, no. 3, pp. 1416–1422, Jul. 1995.

[22] D.-G. Kim, T. Nakajima, and E. Masada, "Harmonic analysis of a capacitor-filtered rectifier in low voltage distribution network," in Proc. *IEEE ICHPS*, 1988, pp. 161–165.

[23] A. B. Nassif, "Characterizing the Harmonic Attenuation Effect of Compact Fluorescent Lamps," *IEEE Transactions on Power Delivery*, vol. 24, no. 3, pp. 1748–1749, Jul. 2009.

[24] A. B. Nassif and J. Acharya, "An investigation on the harmonic attenuation effect of modern compact fluorescent lamps," in Proc. *IEEE ICHQP*, 2008, pp. 1–6.

[25] E. E. Ahmed, W. Xu, and G. Zhang, "Analyzing Systems With Distributed Harmonic Sources Including the Attenuation and Diversity Effects," *IEEE Transactions on Power Delivery*, vol. 20, no. 4, pp. 2602–2612, Oct. 2005.

[26] J. Cunill-Sola and M. Salichs, "Study and Characterization of Waveforms From Low-Watt (<25 W) Compact Fluorescent Lamps With Electronic Ballasts," *IEEE Transactions on Power Delivery*, vol. 22, no. 4, pp. 2305–2311, Oct. 2007.

[27] W. Xu, H. W. Dommel, M. B. Hughes, G. W. K. Chang, and L. Tan, "Modelling of adjustable speed drives for power system harmonic analysis," *IEEE Transactions on Power Delivery*, vol. 14, no. 2, pp. 595–601, Apr. 1999.

[28] E. Thunberg and L. Soder, "A Norton approach to distribution network modeling for harmonic studies," *IEEE Transactions on Power Delivery*, vol. 14, no. 1, pp. 272–277, 1999.

[29] E. Bompard, E. Carpaneto, G. Chicco, P. Ribaldone, and C. Vercellino, "The impact of public lighting on voltage distortion in low voltage distribution systems," *IEEE Transactions on Power Delivery*, vol. 16, no. 4, pp. 752–757, 2001.

[30] J. E. Drakos, Y. Mansour, and A. Chang, "A three-phase converter model for harmonic analysis of HVDC systems," *IEEE Transactions on Power Delivery*, vol. 9, no. 3, pp. 1724–1731, Jul. 1994.

[31] J. H. R. Enslin and P. J. M. Heskes, "Harmonic Interaction Between a Large Number of Distributed Power Inverters and the Distribution Network," *IEEE Transactions on Power Electronics*, vol. 19, no. 6, pp. 1586–1593, Nov. 2004.

[32] A. C. Ernauli, "Modeling of photovoltaic inverters for power quality studies," M.Sc. Thesis, Eindhoven University of Technology, 2012.

[33] Z. Wei, N. R. Watson, and L. P. Frater, "Modelling of compact fluorescent lamps," in Proc. *IEEE ICHQP*, 2008, pp. 1–6.

[34] A. S. Koch, J. M. A. Myrzik, T. Wiesner, and L. Jendernalik, "Evaluation and validation of Norton approaches for nonlinear harmonic models," in Proc. *PowerTech*, 2013.

[35] F. Z. Peng, "Application issues of active power filters," *IEEE Industry Applications Magazine*, vol. 4, no. 5, pp. 21–30, 1998.

[36] F. Z. Peng, "Harmonic sources and filtering approaches," *IEEE Industry Applications Magazine*, vol. 7, no. 4, pp. 18–25, 2001.

[37] M. Fauri, "Harmonic modelling of non-linear load by means of crossed frequency admittance matrix," *IEEE Transactions on Power Systems*, vol. 12, no. 4, pp. 1632–1638, 1997.

[38] D. J. Hume, A. R. Wood, B. C. Smith, and J. Arrillaga, "Linearised direct harmonic solution method for a back-to-back HVDC link," in Proc. *IEEE ICHQP*, 1998, pp. 727–733.

[39] Y. Sun, G. Zhang, W. Xu, and J. G. Mayordomo, "A Harmonically Coupled Admittance Matrix Model for AC/DC Converters," *IEEE Transactions on Power Systems*, vol. 22, no. 4, pp. 1574–1582, Nov. 2007.

[40] J. G. Mayordomo, Á. Carbonero, L. F. Beites, and W. Xu, "Decoupled Newton Algorithms in the Harmonic Domain for the Harmonic Interaction of Line Commutated Converters With AC Systems," *IEEE Transactions on Power Delivery*, vol. 25, no. 3, pp. 1721–1733, Jul. 2010.

[41] J. G. Mayordomo, L. F. Beites, R. Asensi, F. Orzaez, M. Izzeddine, and L. Zabala, "A contribution for modeling controlled and uncontrolled AC/DC converters in harmonic power flows," *IEEE Transactions on Power Delivery*, vol. 13, no. 4, pp. 1501–1508, 1998.

[42] J. van Casteren and S. Cobben, “Harmonics: Harmonizing a shared responsibility,” in Proc. *CIRED*, 2007.

Chapter 5

Summation of harmonic currents

5.1 Introduction

Due to the diversity and variability of non-linear loads and network changes, the sum of multiple harmonic currents is usually lower than the arithmetical sum of their magnitudes. In a general case, as in Fig 5.1, harmonic currents and voltages can be either attenuated or amplified at a point located further from the sources, with the latter happening due to resonance effects. Due to distributed impedance effects, current I'_1 does not have to be equal to the current of the source, I_1. If we look at a particular node (e.g. a transformer busbar), at low frequencies the first Kirchhoff's law is satisfied and the complex total current is equal to the vectorial sum of individual components. This leads to a total magnitude lower than the arithmetical sum of magnitudes, if the individual components do not have exactly the same phase angle.

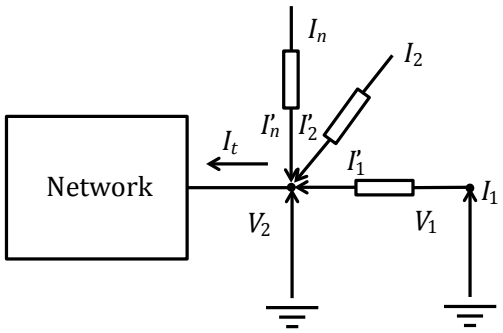

Fig 5.1 Summation of harmonic currents, a generalized example; I_t: total current of multiple sources; $I_1 - I_n$: currents at the sources; $I'_1 - I'_n$: currents after the connection impedances

The question of aggregating harmonic sources can be traced back to 1972, and it is periodically returning as the non-linear loads are evolving. During the 1970s the uncontrolled rectifier (diode bridge) was a very common load. Later advancements in the solid state switching technology, and partly the regulations about the maximal harmonic current emission and the minimal power factor of devices, led to changes of the device front-end and their behaviour as well.

In contrast to about 40 years ago, most small power electronic loads nowadays act as a constant power load, which changes the way in which they interact with harmonic voltages. Regarding the large power electronic loads, one major change was the transition from DC to AC motor drives. Another significant change which we are facing is the increasing share of inverter-interfaced generators in the network, which also evolved during the last few decades from line-commutated to self-commutated, leading

to an increase in the switching frequencies, and continuously updated new control algorithms which can satisfy the newest connection requirements.

This chapter addresses summation of harmonic sources, using laboratory experiments, computer simulations, and field measurements. In section 5.2 we analyse the aggregation of harmonic currents for a quasi-steady state, and in section 5.3 we look at the summation including the time variations of harmonic currents and the empirical coefficients which can be used as a guideline for simplified summation of harmonic sources.

5.2 Quasi steady state analysis – Diversity Factors

As already mentioned, several harmonic phasors usually have a sum lower than the arithmetical sum. According to [1], this effect was first studied in several technical reports from the 1970s, and to quantify it, a diversity factor was defined as:

$$DF_h = \frac{\sum_{i=1}^{N} \underline{I_{h,i}}}{\sum_{i=1}^{N} \left| \underline{I_{h,i}} \right|} \tag{5.1}$$

where DF_h is the diversity factor for the h^{th} harmonic order, $\underline{I_{h,i}}$ are individual complex phasors of harmonic current, and N is the total number of sources. It was not defined which current values should be used (instantaneous or cumulative probability levels). The reported results of measurements and simulations are given in Table 5.1, without a separation by harmonic orders or a clarification of the conditions which they describe.

In [2], indicative values of diversity factors for converters were given as in Table 5.2. Values were estimated dependent on the harmonic order and Short-Circuit Ratio (*SCR*). Table 5.2 does not apply for uncontrolled rectifiers with capacitive smoothing, for which $DF = 1$ is suggested.

Table 5.1 Measured and simulated diversity factors, as reported in [1]

Apparatus	*DF*
Rectifiers - uncontrolled	0.9
Rectifiers – controlled, correlated operation	0.75
Rectifiers – controlled, operation not correlated	0.5 – 0.6
Television receivers	0.7
Light dimmers	0.3
Washing machines	0.5
Fluorescent lights	0.7

Table 5.2 Indicative values of *DF* given in [2] for converters

SCR	*h*						
	3	5	7	11	13	17	19
≤ 0.01	0.3	0.1	0.1	0.1	0.1	-	-
0.02	0.4	0.3	0.2	0.1	0.1	0.1	-
0.05	0.6	0.5	0.3	0.2	0.2	0.1	0.1
0.1	0.7	0.7	0.5	0.4	0.4	0.3	0.1
0.2	0.9	0.8	0.7	0.6	0.6	0.5	0.5
≥ 0.5	1.0	1.0	1.0	1.0	1.0	1.0	1.0

This effect was further studied on different devices both with laboratory measurements and computer simulations in [3-8]. In [6], the influence of load power on the harmonic currents of a diode rectifier was analysed analytically, and *DF* was calculated for different numbers of loads, using a Monte Carlo simulation. Results for a small number of loads ($N < 10$) are given in Table 5.3. Field measurements on semiconductor producing machines were presented in [8], with values of *DF* mainly ranging between 0.3 and 0.7 for $h > 3$.

Table 5.3 Diversity factors of diode rectifiers, as reported in [6]

h	*DF*
< 7	~ 1
7 < *h* < 13	0.8 – 0.85
> 13	~ 0.6

In [9], a normalized compatibility index was proposed, which is a diversity factor of harmonic currents with normalized magnitudes. This factor does not show the actual compensation effect of two or more devices, it shows the phase-angle difference instead. In this thesis we refer to this indice as the normalized diversity factor (*NDF*), defined by:

$$NDF_h = \frac{1}{N} \cdot mag\{\sum_{i=1}^{N} \frac{\underline{I}_{h,i}}{|\underline{I}_{h,i}|}\} \tag{5.2}$$

where NDF_h is the normalized diversity factor for the h^{th} order, and $\underline{I}_{h,i}$ are the complex phasors of individual harmonic currents.

As an expansion, an aggregated compatibility index was proposed in [9] as a weighted Root Sum of Squares (RSS) of compatibility indexes of all harmonic orders, which expresses the overall compatibility of two or more devices in one factor. The weights in the RSS emphasize the harmonic orders with the highest magnitudes, they are based on a typical CFL, and decreasing with the increase of *h*. Using one indice for all orders is practical, but it removes the physical meaning from the index since it gives a measure of all harmonic orders at the same time but removes the information about individual harmonic orders.

Further, a phase-angle "compatibility" categorization was proposed in [9], which shows if two devices have harmonic currents in phase, based on the *DF* and the phase-angle difference, as shown in Table 5.4.

Table 5.4 Categorization of phase-angle "compatibility" based on phase-angle diversity, [9]

high	*DF* > 0.71	angle difference < 90°
medium	0.5 < *DF* < 0.71	90° < angle difference < 120°
low	*DF* < 0.5	angle difference > 120°

Insight into the origin of harmonic diversity among the same type of devices was given in [10], where the influence of tolerances of rectifier inductors and capacitors and the loading level on the harmonic phase angles were analysed by simulation. On an example of rectifiers with passive PFC, typical values of elements were varied within the tolerance limits and it was shown that for example the phase angle of the 3rd harmonic faces very limited influence, while the phase angle of the 11th harmonic can change as much as 60° from each of the factors examined. This is in agreement with the

laboratory measurements, where the *DF* always had lower values for higher order harmonics.

In [11], aggregation of a large number of personal computer loads was analysed. A formula for estimating the current THD dependent on *N* (number of devices or loads) was proposed based on the fitted measurement results with different numbers of active loads.

Measurement surveys with presently available household appliances and their potential diversity related compensation are presented in [12-17]. In [14] it was reported that comparing to the previous generation of household devices, the harmonic emission is decreasing, together with their active power. In [12] it was also concluded that the diversity factors of devices of the same type increased, which means that even though the individual emission is decreasing on an average, the total emission of several devices does not have to be lower in general.

5.2.1 Household equipment

Household devices, due to their large numbers, are expected to have a strong cancellation effect. This is in general a good assumption, because harmonic problems are only local in distribution systems, but in specific cases it may lead to high harmonic voltages.

Based on this assumption, the harmonic emission limits for household equipment allow a relatively high current THD for individual units. Such emission of a single load of large power fed via a dedicated transformer would almost always require a highly de-rated transformer and cable, or filtering of harmonics.

An additional relaxation in the emission limits was discussed in Chapter 2 for discharge lamps with an active power lower than 25 W, which allows them to have an even more distorted current waveform as long as the last peak of the waveform appears before or at 65^0, which leads to high compensation effect in combination with devices with passive PFC (which normally have a peak after 90^0).

Examples of polar plots of harmonic currents of several household devices are given in Fig 5.2, including two CLFs, a TV, a desktop PC, and a Vacuum Cleaner (VC) with the lowest speed setting. During the experiment, devices were supplied with a sinusoidal voltage.

Due to the low magnitudes, currents of CFLs are not visible well in Fig 5.2. In Fig 5.3 only the currents of CFLs are shown, for all four harmonic orders. Both lamps are of the same rated power, but have different manufacturers. Due to a very similar rectifier topology their 3rd harmonic currents are almost in phase, with only 5^0 difference. As the frequency increases, the tolerances of their circuit elements make the difference greater, leading to higher differences of their phase angles. For the 9th harmonic, the difference is almost 30^0.

If we connect these devices together, the resulting *DF* and *NDF* will have values as shown in Table 5.5, with and without the vacuum cleaner.

Table 5.5 Diversity factors of household devices from Fig 5.2, with and without the vacuum cleaner

h	without the vacuum cleaner		with the vacuum cleaner	
	DF	*NDF*	*DF*	*NDF*
3	0.93	0.65	0.49	0.46
5	0.86	0.37	0.29	0.41
7	0.87	0.18	0.47	0.04
9	0.90	0.47	0.75	0.36

The vacuum cleaner has the greatest harmonic currents, and also the greatest influence on the *DF*, causing strong harmonic cancelation. During most of the time the vacuum cleaner is not operating, which makes the cancellation effect relatively low for this group of devices.

These results cannot be generalised for all household devices and manufacturers. The cancelation effect is dependent on the types of devices in operation. In most studies about the *DF,* the values decrease with the increase of the harmonic order [4], [6], [7], [9].

In practice we can never assume an equal number of devices of the same type, so the total *DF* is dependent also on the numbers of individual types of devices in operation as well. In a simplified scenario, if we consider a single TV operating together with a variable number of lamps of type CFL1 from the previous example, the *DF* will depend on the number of CFLs connected. Table 5.6 shows this dependency, with an assumption that all lamps are completely identical.

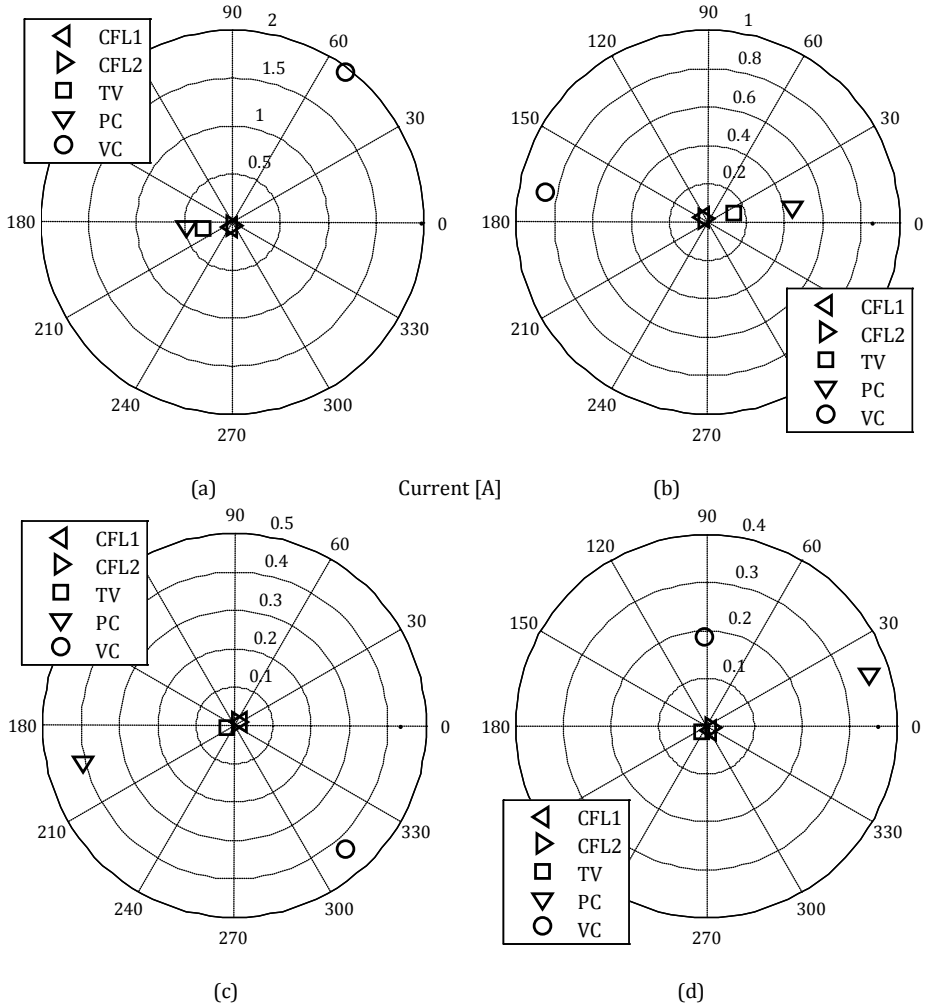

Fig 5.2 Harmonic currents of several household devices in the polar plain: (a) 3rd harmonic, (b) 5th harmonic, (c) 7th harmonic, (d) 9th harmonic

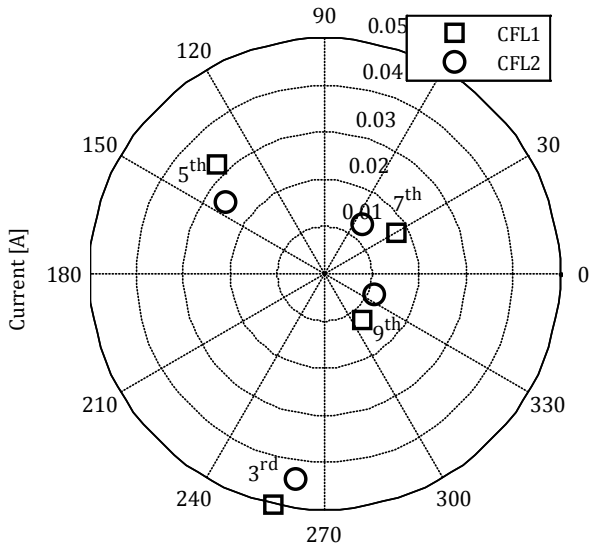

Fig 5.3 Harmonic currents of the two CFLs: 3rd, 5th, 7th, and 9th order

Table 5.6 *DF* of a TV operating together with a variable number of CFLs

	N=	*1*	3	*5*	*10*	*20*
NDF	***h***	*DF*	*DF*	*DF*	*DF*	*DF*
0.34	**3**	0.93	0.86	0.85	0.85	0.89
0.21	**5**	0.75	0.55	0.53	0.63	0.76
0.05	**7**	0.16	0.42	0.61	0.78	0.88
0.29	**9**	0.73	0.78	0.84	0.90	0.95

The *DF* shows some differences for different numbers of devices (3rd, 5th, and 9th harmonic), but when their *NDF* is very low the *DF* is highly dependent on their numbers, as for the 7th harmonic. Depending on the number of devices per house the total *DF* of a house can vary significantly, in the example of the 7th harmonic it changes almost four times for N = 3 or 5 lamps working together with one TV set. When N becomes large the *DF* value approaches 1 for all orders, because at a certain point the current of the TV becomes insignificant.

In Fig 5.4, polar plots of harmonic currents of four types of PV inverters are presented and labelled as PV1 through PV4, supplied with a sinusoidal voltage and operated at rated power. The rated powers of the analysed inverters are: 8000 W, 850 W, 1500 W, and 1800 W, respectively. Only inverter PV1 is a three-phase unit, with approximately 2700 W per phase (for easier comparison with the single-phase units).

It is noticeable that inverters PV1 and PV2 have significantly lower harmonic currents, especially of the 3rd order. These inverters are of a newer generation, and are obliged to comply with stricter rules for harmonic emission. In many countries PV inverters are now obliged to have a current THD up to 5 %, while the older generations of inverters (including inverters PV3 and PV4) have a current THD in the range 10-20 %. Other differences in the emission are due to the inverter controls, rated power, and design (e.g. inverter PV3 includes a high-frequency transformer while other inverters are transformerless).

Values of *DF* and *NDF* from this example are given in Table 5.7, at rated power output and half of the rated power. For the 3rd harmonic order all inverters are almost in phase, leading to a *DF* almost equal to one. Phase angles of inverters PV2 and PV4

are very close for all four harmonic orders, with up to 20^0 differences (both at rated power and half of rated power), however, there is more cancelation effect with inverters PV1 and PV3 leading to lower values of *DF* at the 5th, 7th, and 9th order.

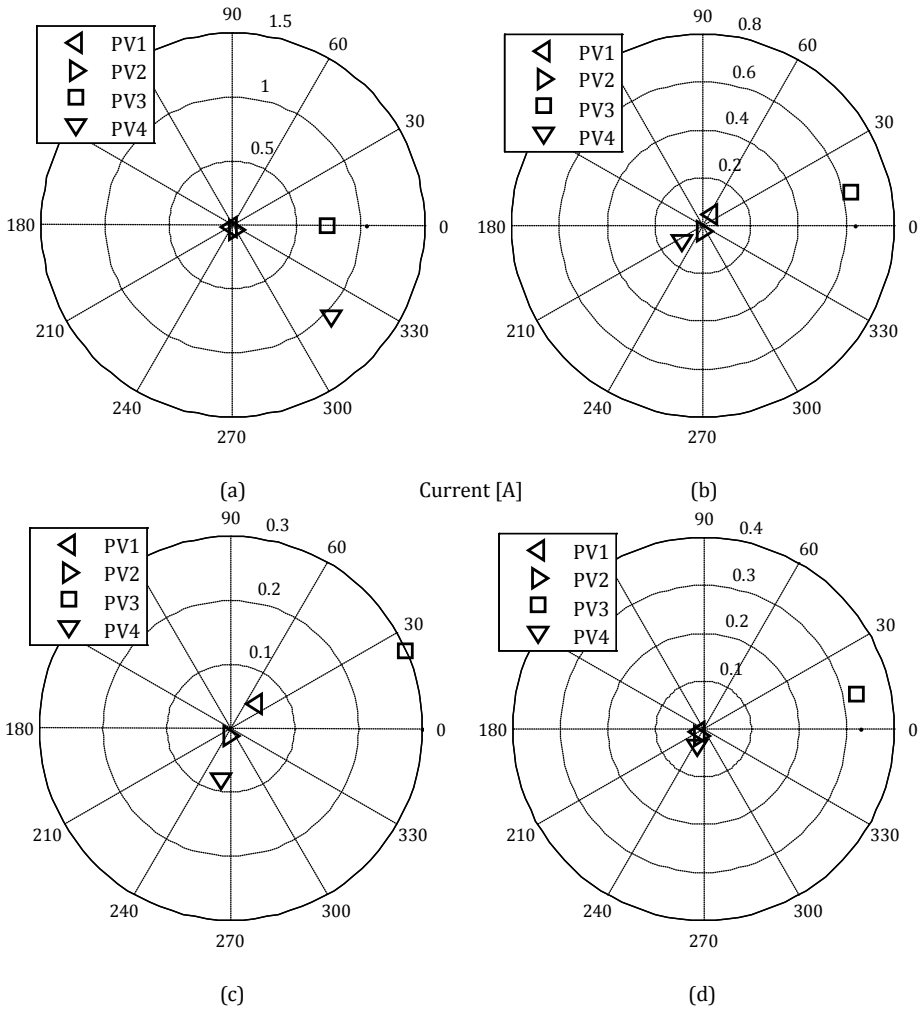

Fig 5.4 Harmonic currents of four types of household PV inverters in the polar plain: (a) 3rd harmonic, (b) 5th harmonic, (c) 7th harmonic, (d) 9th harmonic

Table 5.7 Diversity factors for the PV inverters from Fig 5.4, at rated power and half of rated power

h	Rated inverter power		Half of rated power	
	DF	*NDF*	*DF*	*NDF*
3	0.91	0.53	0.83	0.65
5	0.69	0.19	0.71	0.20
7	0.68	0.31	0.39	0.27
9	0.74	0.44	0.76	0.54

5.2.2 Variable speed induction motor drives

In this subsection we analyse the influence of the device power output on the phase angles of its harmonic currents, specifically for three-phase induction motor VSDs,

which take a large share of the power among the non-linear industrial loads.

First, we look at a very simplified representation of a variable speed drive, as being a six-pulse thyristor rectifier feeding a constant current DC load, and second we look at a more detailed model of a VSD. In some cases, constant DC side current is a fair representation, but in case there is no DC link inductor (or a very small inductor) this is not a fair assumption.

In case of a constant DC link current, with instantaneous commutation, and under sinusoidal network voltages, the phase voltages and the current in one phase are as shown in Fig 4.2 (Chapter 4). As discussed in [18], in this case the phase angles of all current harmonics can be represented as:

$$\varphi_h = -h \cdot \beta + \frac{\pi}{2} \cdot (1 - (-1)^i) \tag{5.3}$$

where φ_h is the phase angle of the h^{th} harmonic current, β is the firing angle of the thyristor bridge, and i is an the integer number which defines the characteristic harmonic orders of a six-pulse rectifier with $h = 6 \cdot i \pm 1$ ($i = 1$ for $h = \{5$ and $7\}$, $i = 2$ for $h = \{11$ and $13\}$, etc.).

In the special case when $\beta = 0^0$ (which is equal to a three-phase diode bridge), the phase angle of all harmonic currents are independent of the load current. That means that two diode bridge rectifiers operate with $DF = 1$ under these assumptions.

On the full operating range $\beta = 0$ - 180^0, φ_h can have values between 0^0 and 360^0. This means that two thyristor bridge converters can theoretically have a normalized *DF* between 0 and 1 for any harmonic order, but not for all of them at the same time. If we look at a case of two identical converters where one is operating with a fixed firing angle and the other one is varying the firing angle from 0^0 to 180^0, their *NDFs* for several harmonic orders are shown in Fig 5.5. In Fig 5.5 (a), the first converter has a firing angle of 0^0, while in Fig 5.5 (b) it is fixed at 45^0.

For each h the *NDF* covers the range from 0 to1 h times, and has $(h+1)/2$ minimums and maximums, so a very favourable case for the 5^{th} harmonic can be very unfavourable for the 11^{th} harmonic, for example. In Fig 5.5 (a), all orders are aligned only for $\beta = 0^0$ and $\beta = 180^0$. In terms of harmonic compensation, the ideal case would be $\beta = 180^0$, because the $NDF = 0$ for all harmonic orders (opposite phase angles, magnitudes are not necessarily equal), but in this case the DC side voltage is negative, which is not common for variable speed drives. In Fig 5.5 (b), all orders are aligned only for $\beta = 45^0$, which is an unfavourable case because $NDF = 1$ for all orders. In this case there is no β of the second converter for which all orders have $NDF = 0$.

This idealized model of a converter does not describe its behaviour accurately in all conditions, but it illustrates the differences between the lower order and higher order harmonics. Since φ_h is a linear function of $h \cdot \beta$, for higher order harmonic even a small change of the firing angle leads to large changes of φ_h, but all harmonic orders (with $h >$ 2) can cover the full 0-360^0 range.

If we look at a small range of firing angles, low orders will have a lower diversity of phase angles. For example, if we look at the first 20^0 in Fig 5.5 (a), the 5^{th} harmonic current covers about 100^0, while the 13^{th} harmonic covers about 260^0. However, if we randomly pick an array of firing angles, higher order harmonics are not more probable to have a lower *NDF* on the average. Even if we look at small variations of β around a steady state value, depending of the chosen steady state value, a higher harmonic order does not necessarily lead to higher compensation potential (lower *NDF*). This is off course only valid for orders with φ_h dependent on β.

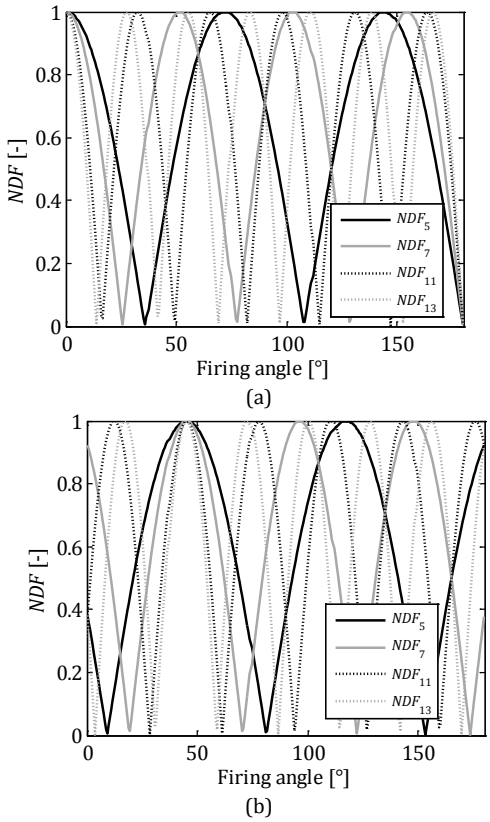

Fig 5.5 Dependency between the *NDF* and the firing angle for several harmonic orders: (a) one rectifier with a fixed $\beta = 0^0$; (b) one rectifier with a fixed $\beta = 45^0$

Now we look at a more detailed Simulink model of a VSD with a voltage source inverter on the motor side, and an induction motor, as shown in Fig 5.6. The behaviour of this model cannot be generalized to all types of induction motor variable speed drives due to different design and control principles, but it allows us to see the behaviour of φ_h under non-idealized conditions, which means that the DC link current is not constant and the commutation is not instantaneous. Also, we look at the changes caused by different ratings of line inductors, and different mechanical loading levels and speed references.

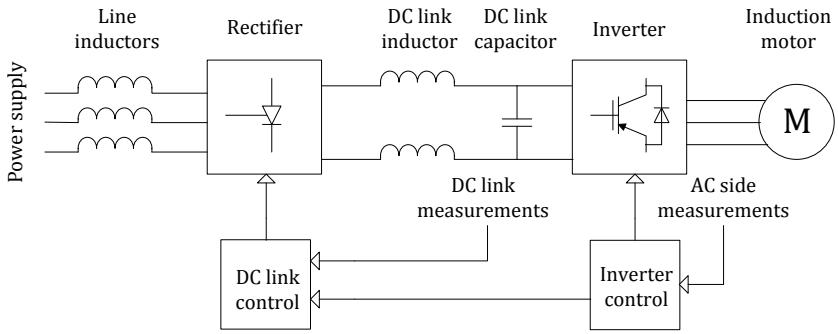

Fig 5.6 Simulink model of a Voltage Source Inverter based VSD

5.2.2.1 Variation of the rotor speed

If we keep the DC link inductance fixed at 1 % and the mechanical torque loading at its nominal value, and then vary the values of the line inductances from 1 % to 3 % and the speed reference from 10 % to 100 % of the nominal speed, the steady state values of the firing angle are given in Fig 5.7.

It is important to notice that the firing angle covers only a limited range of values in the steady state (in this case around 70^0) unlike the case of a DC motor drive where 0-180^0 range is needed. Rectifiers of inverter-based VSDs mainly control the DC side voltage on a constant value, while the AC side voltage control is managed mainly by the inverter.

If we consider two drives, where one has a constant speed reference and nominal mechanical load, and the other drive changes its speed reference from 10 % to 100 %, their steady state *DFs* with different ratings of line inductors are given in Fig 5.8 and Fig 5.9.

In this example the system impedance is low, so the influence of the harmonic voltages on the drives currents is minimal. If we average the *DF* for all values of the reference speed, we can notice that it does not monotonously decrease with the increase of the harmonic order.

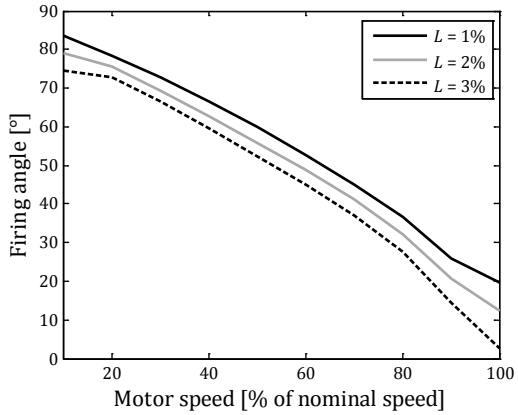

Fig 5.7 Connection between the firing angle and the motors speed (at nominal torque); *L* – size of the line inductors

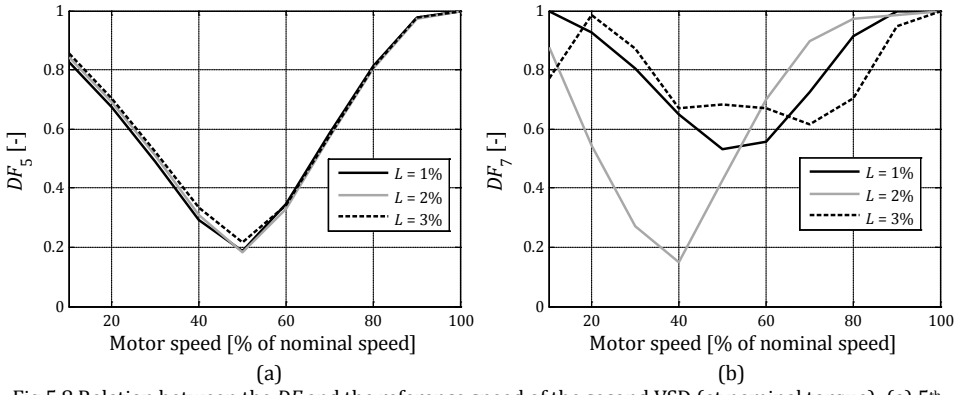

(a) (b)

Fig 5.8 Relation between the *DF* and the reference speed of the second VSD (at nominal torque): (a) 5th harmonic, (b) 7th harmonic; *L* – size of the line inductors

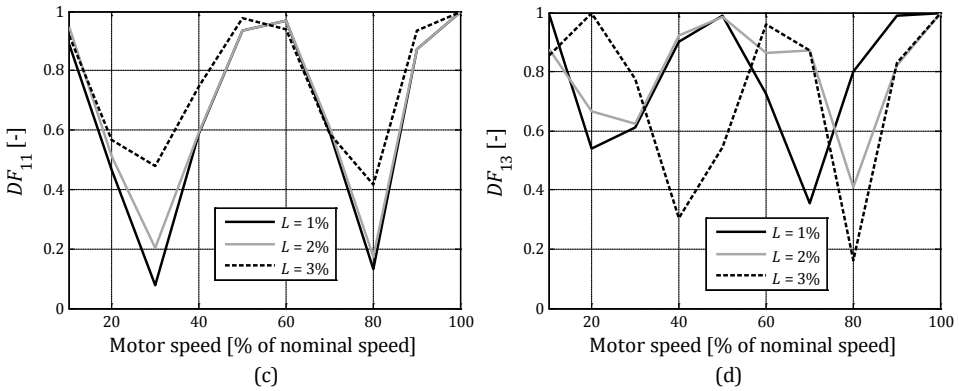

Fig 5.9 Relation between the *DF* and the reference speed of the second VSD (at nominal torque): (a) 11th harmonic, (b) 13th harmonic; *L* – size of the line inductors

This means that the higher order harmonics do not necessarily have a higher diversity effect than the lower order harmonics for any range of operating speeds. The values of *DF* for different harmonic orders depend greatly on the operating conditions of the drive. At the end of this chapter we will compare these results to field measurements with VSDs.

The *DF* describes how much the loads "compensate" each other, but it gives no measure of the total current magnitude. Relative total magnitudes from the previous example are presented in Fig 5.10 and Fig 5.11. The relative total magnitude is defined as the ratio between the sum of harmonic currents and the sum of the harmonic currents when both VSDs are operating under nominal conditions (nominal speed and nominal mechanical load), indicated with a solid line.

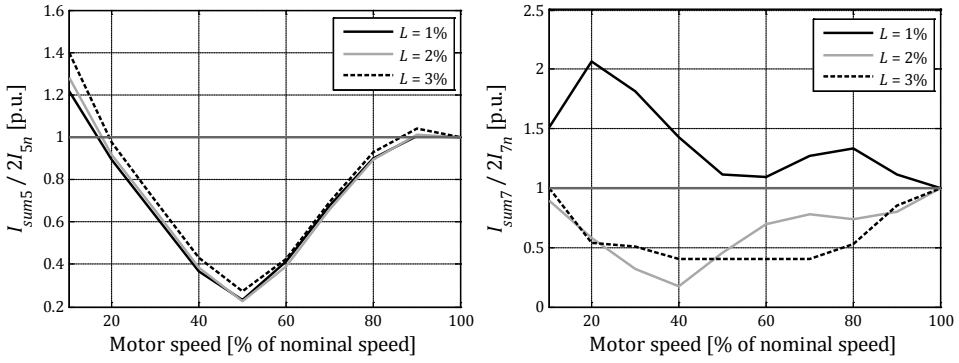

Fig 5.10 Relation between the relative total magnitude and the reference speed of the second VSD (at nominal torque): (a) 5th harmonic, (b) 7th harmonic; L – size of the line inductors

Curves from Fig 5.10 and Fig 5.11 do not follow exactly the curves from Fig 5.8 and Fig 5.9, due to different magnitudes at different operating speeds. In some cases the relative value is higher than one, because the absolute value of the harmonic current can be lower at the nominal speed than at a speed lower than nominal.

In most cases a higher value of the line inductance leads to a lower total current magnitude of the harmonics. In some cases (especially the 11th harmonic) the result is opposite (in absolute units, a higher value of inductance always leads to a lower harmonic current). The reason for this is mostly the higher value of the *DF* in these

situations (Fig 5.9). Even if the individual magnitudes are lower, the sum can still have a higher value due to the lower compensation effect.

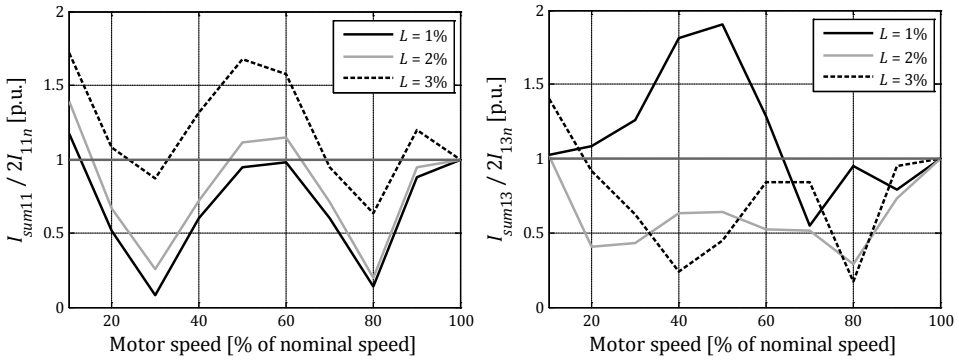

Fig 5.11 Relation between the relative total magnitude and the reference speed of the second VSD (at nominal torque) : (a) 11th harmonic, (b) 13th harmonic; L – size of the line inductors

5.2.2.2 Variation of the mechanical torque

If we repeat the simulations from the previous subsection with the rotor speed fixed at the nominal value, and we vary the mechanical torque from 10 % to 100 % of the nominal, the results are considerably different. In this case the firing angle takes an even smaller range of values, see Fig 5.12.

Due to the small range of the firing angles, the *DFs* also vary less due to torque variations. The dependence between the *DF* and the mechanical torque of the load is presented in Fig 5.13 and Fig 5.14, for several harmonic orders.

The *DF* of the 5th harmonic has very little change, much less than in the idealized case from Fig 5.5. For higher harmonic orders the variations are larger, as expected, but still lower than in the case of variable rotor speed.

The relation between the relative total magnitudes (defined in the same way as in the case of speed variations) and the mechanical torque are presented in Fig 5.15 and Fig 5.16, for the same harmonic orders.

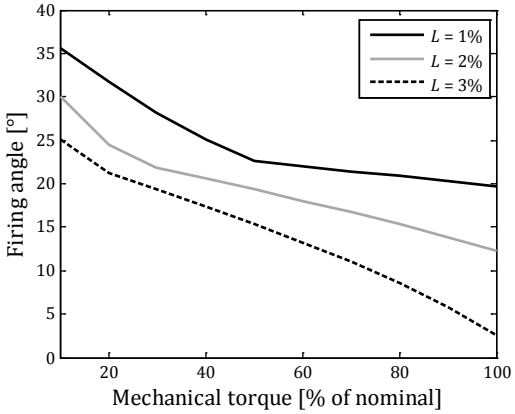

Fig 5.12 Connection between the firing angle and the mechanical load (at nominal speed); *L* – size of the line inductors

In this situation a higher value of line inductance usually leads to a higher total current, mostly due to higher values of *DF*. Also, it is noticeable that the mechanical torque variations lead to less variations than the speed, both for magnitudes and phase angles.

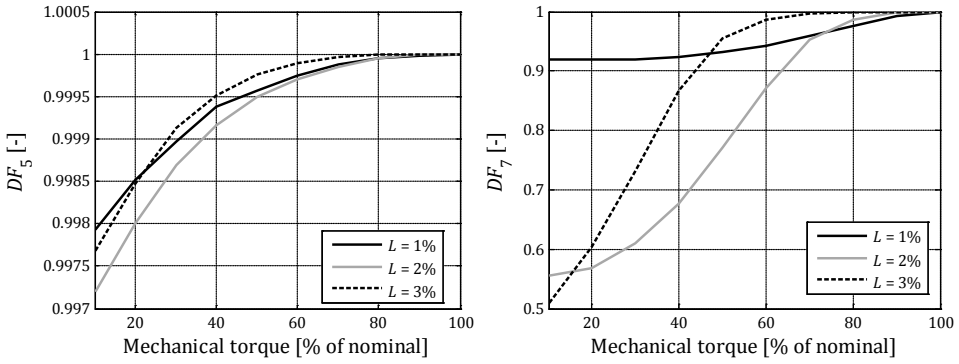

Fig 5.13 Relation between the *DF* and the mechanical load of the second VSD (at nominal speed): (a) 5th harmonic, (b) 7th harmonic; *L* – size of the line inductors

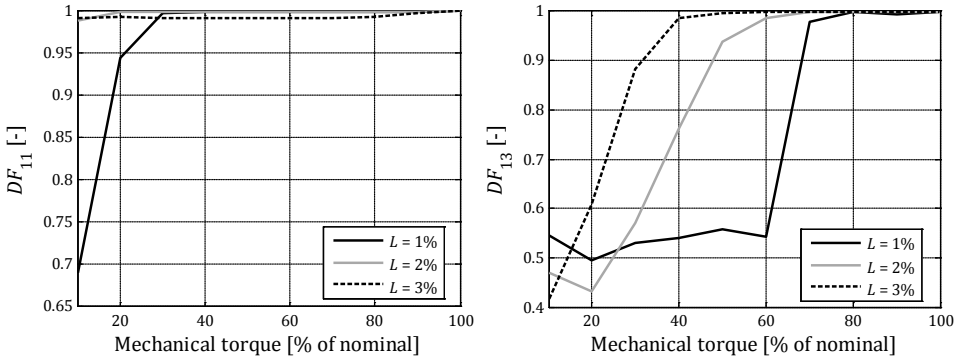

Fig 5.14 Relation between the *DF* and the mechanical load of the second VSD (at nominal speed): (a) 11th harmonic, (b) 13th harmonic; *L* – size of the line inductors

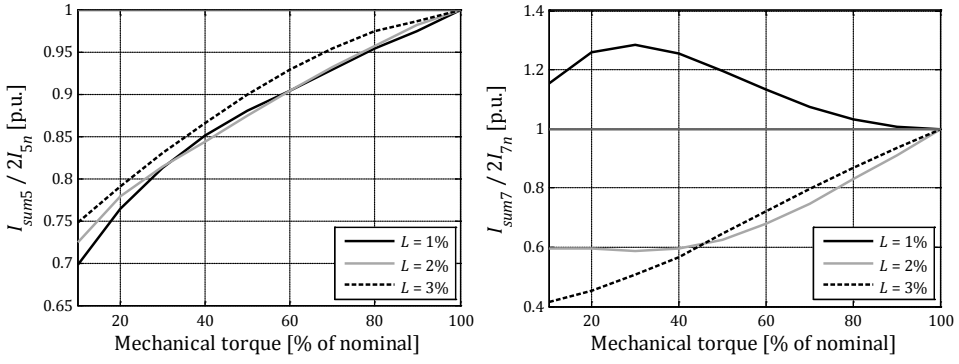

Fig 5.15 Relation between the relative total magnitude and the mechanical load of the second VSD (at nominal speed) : (a) 5th harmonic, (b) 7th harmonic; *L* – size of the line inductors

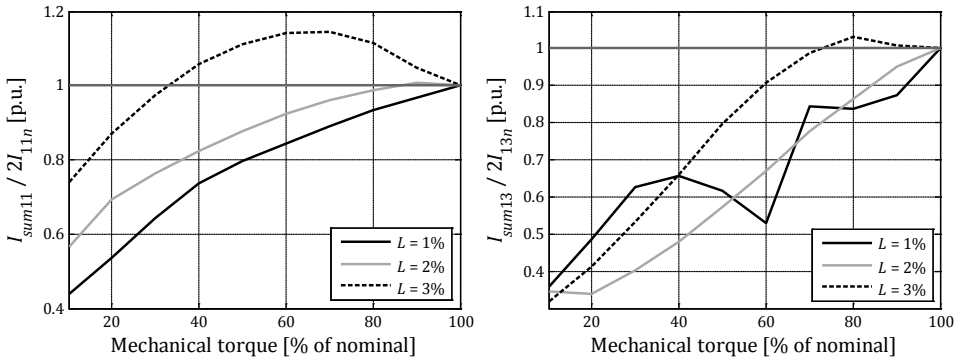

Fig 5.16 Relation between the relative total magnitude and the mechanical load of the second VSD (at nominal speed) : (a) 11th harmonic, (b) 13th harmonic; *L* – size of the line inductors

5.3 Time-varying analysis

In the previous section the summation of harmonic currents for a single moment in time was analysed. The problem becomes more complicated when the time changes of each of the harmonic sources are considered. The solution for any of those moments cannot characterize a long time interval, which brings the need to include the time variations into the problem.

Harmonic sources produce different harmonic currents at different loading levels, and changes of the harmonic voltages at the point of connection cause different changes in the current. This process is time-varying in nature, so it is very hard to predict the exact magnitudes and phase angles of harmonic currents in any particular moment of time.

In this section, the problem is analysed in the following steps. An overview of the existing literature is given first, followed by the description of a measurement campaign done in industrial installations. The results of the field measurements are analysed further, including the calculated summation indices of these locations. Lastly, some considerations for the technical standards and the measurement approach are given.

5.3.1 Overview of the existing literature

Summation of phasors with time varying phase angles, and in some cases magnitudes, were analysed statistically in [18-32]. In [19] it was assumed that the phase angles have a uniform distribution over the full range (0-360°), and that all phasors are statistically independent. With these conditions it was shown that if the number of sources is at least 8, and there are no dominant vectors which make 55% or more of the total sum, the RSS gives a result which is highly unlikely to be exceeded.

In [21], a statistical analysis of the probability distribution function (pdf) of the sum of vectors with arbitrary pdfs is given. The analytical result was compared with a Monte Carlo simulation, again assuming a uniform distribution of phase angles. The resulting summated current was found to have a normally distributed magnitude values if the number of devices is greater than three.

In [18], [22], [23], Monte Carlo simulations were performed for a number of identical devices connected to the same bus. In these cases the speed of drives [18], [22] and

battery states of charge [23] were varied randomly, and the magnitudes and phase angles of individual harmonics were calculated from them. Real and imaginary components of harmonic current of rectifiers were expressed as functions of the firing angle in [18]. It was assumed that the firing angles of several rectifiers vary uniformly distributed between two pre-assigned values from the range 0-90° and the distribution of the two components of the total current was determined analytically and via a Monte Carlo simulation. It was shown that these assumptions lead to the normal distribution of the total current, and that the real and imaginary part of the current can be linearly correlated even when the number of rectifiers is large. An important conclusion was that the magnitude and phase angle of the total current are not statistically independent even for a large number of devices.

In [24],[32] it was proposed to separate the distribution of harmonic currents into a deterministic part (known load changes) and a random part with a known pdf. In [24] it was proposed that the nonlinear loads should be categorized by their statistical behaviour, which would allow for using certain pdf as statistical models of devices by type. Knowing this data, it is possible to calculate the pdf of the summated current by using the convolution integral for the random part of the current phasors, and adding it up to the deterministic part.

In [25], a supply system with multiple harmonic current sources was simulated, and the effect of phase-angle differences and network line lengths on the harmonic voltages of several busbars was analysed. The results of vectorial summation were compared with simplified approaches: RSS, arithmetic sum, sum of vectors with random phase angles, and sum of vectors with both the magnitudes and phase angles being random. The results showed that in some situations each of these methods gives a good estimate of the harmonic voltages, but overall all of them can overestimate or underestimate the voltages depending on the system conditions. The topology of the system supplying the loads showed a significant influence on the resulting harmonic voltages and currents generated by loads.

5.3.1.1 Previous field measurement results

The variations of harmonic currents including the phase angles were measured in the industry, and presented for the first time in [26]. The load was a thyristor based locomotive, measured in two time intervals of 30-40 min with 1 s data windows. Measurement results showed that lower order harmonics cover only a limited range of phase angles, and it cannot be assumed that they are uniformly distributed on 0-360°. The higher order harmonics were scattered on a larger range of angles, making them closer to this assumption.

Further measurement of amplitudes and phase angles in traction systems were presented in [27]. In this case the loads were 12-pulse rectifiers which supply a DC voltage to trains. In addition to the pdf of the current harmonics, correlations of different orders were analysed. It was found that the characteristic orders (in this case 11^{th}, 13^{th}, etc.) have a strong correlation with the fundamental. Other orders (2^{nd}, 5^{th}, 7^{th}, etc.) have weak or very weak correlation to the fundamental, so they can hardly be correlated with the firing angle of the rectifier.

An interesting field experiment with phase-angle variations is presented in [30]. Using a tap changer, the voltage RMS in a substation was varied in the range +5/-10 %, and the effect on the phase angles of harmonic currents was observed. A change of -6/-16° change for the 3^{rd} harmonic current was reported. Without such an experiment it is

hard to determine the influence of voltage RMS on the phase angles of current harmonics, because they are influenced by load changes as well.

In [31], Gaussian models of three current sources were derived from a field measurement with a time resolution of 30 s and a duration of 40 min. For two measurements the distribution could be fitted well, while in the third case the data was not suitable for a Gaussian model. A time interval of 40 min might not have a large enough number of samples to bring out the random nature of the process, and perhaps it does not include all possible working conditions.

5.3.1.2 Summation coefficients

When a network is being planned, the pdfs of harmonic currents are normally not available. For this reason international reference documents offer simplified approaches for calculating the total harmonic current generated by multiple feeders. Standard [33] mentions that the arithmetic summation of harmonic currents is unlikely, but proposes it as a simple approach. Technical reports [34], [35] propose using a summation law expressed as:

$$I_{h,sum}^{\alpha} = \sum_{i} I_{h,i}^{\alpha} \tag{5.4}$$

where $I_{h,sum}$ is the magnitude of the summated current of the h^{th} order, $I_{h,i}$ is the magnitude of the i^{th} component in the sum, and α is the summation coefficient with different proposed values for different harmonic orders, given in Table 5.8. For small LV installations, a set of lower values is proposed for low odd orders in the annex of [35], given in Table 5.9.

Table 5.8 Summation exponent for harmonics [34], [35]

Harmonic order h	α
$h < 5$	1
$5 \le h \le 10$	1.4
$h > 10$	2

Table 5.9 Summation exponent for small LV installations [35]

Harmonic order h	α
$h = 3$	1
$h = 5, 7, 9$	1.2
$h = 11, 13$	1.3

Currents $I_{h,sum}$ and $I_{h,i}$ are values not exceeded for 95 % of the time (95 % cumulative probability values) based on the 10-minute measurements. The same approach is proposed also for 99 % probability levels based on 3-s values. An analogue equation is also proposed for the summation of harmonic voltages. In this work only the application to harmonic currents is analysed.

When α is equal to 1, (5.4) represents arithmetic summation. If α = 2, the equation becomes root sum of squares (RSS). For α smaller than 1, the total current is greater than the arithmetic sum, this amplification can happen in case of a resonance.

If $I_{h,sum}$ is lower than the lowest of the component currents ($I_{h,sum} < min\{ I_{h,i}\}$), α has a negative value. If $I_{h,sum}$ satisfies the condition: $min\{ I_{h,i}\} < I_{h,sum} < max\{ I_{h,i}\}$, than it is not

possible to define α which satisfies (5.4).

Considerations on the principle and errors of summation using summation coefficients are given in [14], [36-41]. In [36], summation coefficients were calculated using measurements from four sites with multiple arc furnaces, up to the 7th order. These calculations used 95 % probability and 99 % probability values (values not exceeded for 99 % of the time), and two different data windows for measurements – 200 ms and 10 min. Using 10 min aggregated values and 95 % probability values, the results showed α ranging from 1.1 to 1.7 for the 3rd and 5th order, and between 1.2 and 1.4 for the 7th order. Also, calculation using the 99 % probability values usually resulted in a higher value of α. As far as the measurement approach, the 200 ms data windows led to slightly higher values of α.

Summation coefficients for harmonic voltages caused by railway rectifiers are calculated using measured harmonic currents in [37]. It was proposed that values in the range 1.8-2.0 can be used for α in case of railway rectifiers, up to the 20th order.

References [38], [39] analysed the summation coefficients for wind farms using computer simulations. It was shown that summation coefficients from Table 5.8 can lead both to an overestimation or underestimation of the total current. The results were dependent on the design of the wind farm, as well as the assumptions regarding the distributions of magnitudes and phase angles.

In [14] the cancelation effect of household equipment was analysed, especially for the 5th harmonic current. For this type of equipment, it was found that the proposed value of 1.4 for the 5th harmonic is slightly too high. Also, it was noticed that newer equipment with active power factor correction emit less 5th harmonic currents, but also with a lower potential for harmonic cancelation.

5.3.2 Measurement campaign in industrial installations

Measurements at seven industrial sites were performed using a 15 channel measurement system, with three channels for voltages and 12 channels for currents. The system is composed out of a NI cDAQ acquisition chassis with one NI 9225 module for voltage measurement, three NI 9234 low-voltage measurement modules and current transducers for current measurement, and a Labview program running on a portable computer. Some considerations about the accuracy of the measurement system are given in Appendix 1.

The total current of one phase of the low-voltage busbar was measured simultaneously with the currents of all devices or feeders connected to the busbar, as in Fig 5.17. In this way it was possible to analyse the vectorial summation of harmonic currents in each time interval, and the time changes of all magnitudes and phase angles. For locations with a significant share of single-phase loads it would be of value to measure the current in all three phases, but due to technical restrictions the current was measured in a single-phase on all locations.

Measurement locations included the following load types:

- Locations VSD1 and VSD2: induction-motor variable speed drives with six-pulse rectifiers as the front-end. On location VSD1 mechanical loads are hydraulic pumps. On location VSD2 mechanical loads are machines for cutting and shaping metal parts.
- Location VSD3: same as location VSD1, with twelve-pulse rectifiers as the front-end.
- Location TH: triac controlled heaters; phase to phase connected groups connected

as balanced three-phase loads.
- Location PV: Photovoltaic inverters, five three-phase inverters connected to a single connection point.
- Location ML1: mixed single-phase and three-phase drives, tools, lighting, and office equipment, connected in five feeders. Most of the loads are operated only during
- Location ML2: mixed loads as in location ML1, connected in three feeders.

On locations with a single type of load, installations have the same topology. Loads are connected less than 20 m away from the busbar, with approximately the same cable lengths, as in Fig 5.17 (a). Locations with mixed loads have a different topology, their LV cables have different lengths as in Fig 5.17 (b), 50 to 100 m long.

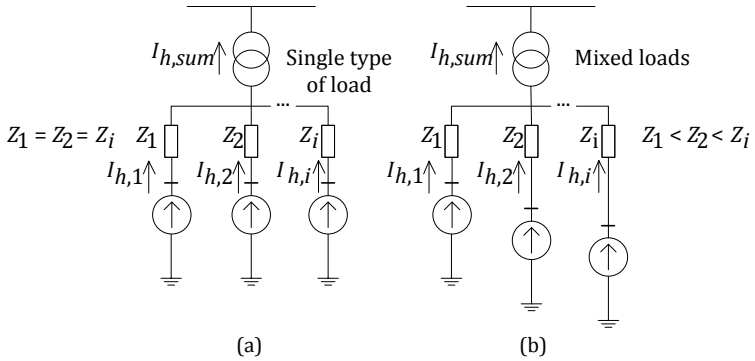

Fig 5.17 Topologies of measured locations: (a) Topology of locations with VSDs, TH, and PV; (b) Topology of locations ML1 and ML2.

Voltage and current harmonics are calculated until the 50th order, both their magnitudes and phase angles. In the analysis of the results, harmonic orders with magnitudes lower than 100 mA are ignored for the reason of accuracy. In all cases it means disregarding the even order harmonics and orders higher than 21, except for locations with variable speed drives, where orders higher than 31 are excluded.

The duration of each measurement was approximately one week, with a time resolution of 1 s. Due to a relatively steady daily loading pattern, one week duration is considered sufficiently long for the analysed loads. If the load shows large seasonal variations, which is applicable for household loads and some commercial and industrial loads, a longer measurement interval would be needed. The results were later aggregated also to 1 min, 10 min, and 1 h values. In this way it could be checked which time resolution is appropriate both in terms of accuracy and amount of data.

5.3.3 Analysis of the measurement results

A part of the measurement results is shown in Fig 5.18 through Fig 5.25 in the polar plain (a), and the pdfs of magnitudes (b) and phase angles (c). Currents of individual devices or feeders and the total current are displayed together for the 5th harmonic order of all locations until Fig 5.24. In Fig 5.25 the 3rd harmonic of location TH is shown because it shows a special case where the phase to phase groups of heaters form a balanced three-phase load, resulting in strong triple-n harmonic cancellation. More measurement results can be found in Appendix 2.

Different load types show different behaviour for the same harmonic order. On location TH for example, phase to phase connected triac heaters were configured to

achieve a balanced total load, resulting in strong cancelation of triple-n harmonics (Fig 5.21 a) between different groups connected to one phase. This is a rare situation, other harmonic orders of this location, and other locations do not display such behaviour.

On location ML1 all harmonic orders show a strong cancellation effect, due to the phase-angle behaviour of one of the load groups (Feeder 1).

On location VSD3, the 5th harmonic currents are significantly lower than on other two locations with VSDs. The reasons for this are the 12-pulse converters of this location, for which the 5th harmonic does not belong to characteristic orders.

5.3.3.1 Distributions of magnitudes and phase angles

Although it is convenient to assume that magnitudes have a normal distribution and phase angles have a uniform distribution over the range 0-360°, in reality these distributions can be quite different. Examples of probability distribution functions of magnitudes and phase angles are presented in Fig 5.18 (b) and (c) through Fig 5.25 (b) and (c). On location TH, both the magnitudes and phase angles have distributions which resemble the normal distribution. On all other locations both distributions have multiple peaks, due to a larger number of steady state operating points.

Depending on the industrial process, the magnitudes can indeed have a distribution which is very close to the normal distributions, as on location TH where all loads have only slight load variations. On the remaining locations the pdfs of magnitudes had multiple peaks, even at locations ML1 and ML2 where the number of devices is large, due to higher variations of the loads. On location PV the differences between individual inverters are very small, because all five units are of the same type and their currents depend on the same irradiance level. Due to this, there was very little compensation effect.In general, normal distribution is a good assumption only if it is known that the loads operate around a steady set-point, in all other cases it is important to determine the deterministic elements of the process. Even with a large number of loads certain loading patterns can lead to multiple peaks of the pdf curve, both for lower and higher order harmonics.

Phase angles of harmonics up to the 13th order mostly had an operating range up to 90° wide, while on higher orders this range was between 90° and 180° wide. In some situations there were measurement points to be found on a full range of 360°, but only for a small fraction of the time did the angles leave the 180° wide range. Regarding the pdfs of phase angles, a similar comment can be made as for the magnitudes. On location TH the distributions were also close to the Gaussian, for the same reason as for magnitudes, while on all other locations they had two or more peaks within a 90° or 180° wide range. None of them resembled the uniform distribution.

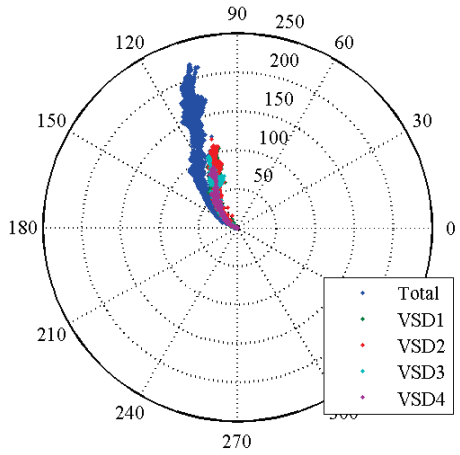

(a)

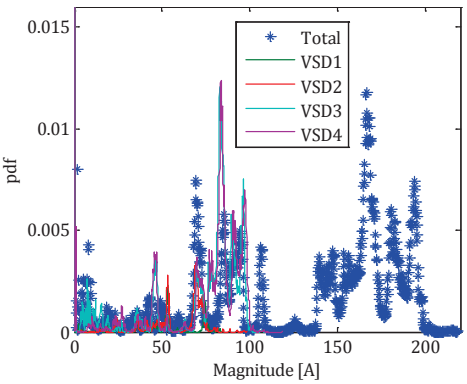

(b)

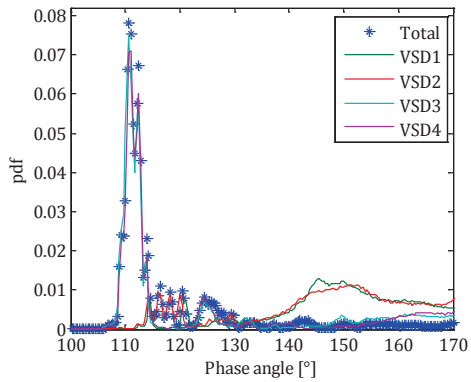

(c)

Fig 5.18 Location VSD1: (a) polar plot of currents, (b) pdf of magnitudes, (c) pdf of phase angles, 5th harmonic order

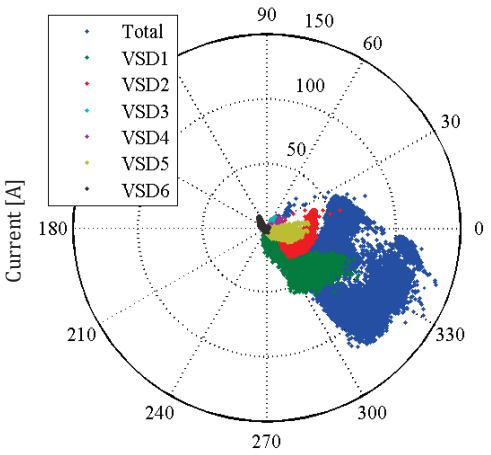

(a)

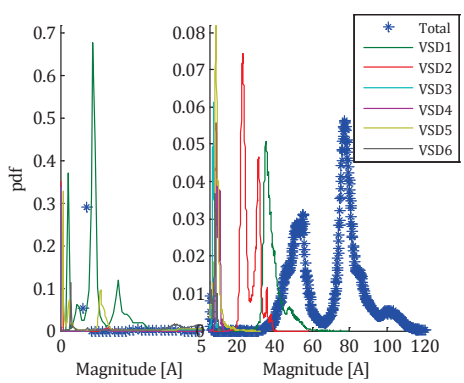

(b)

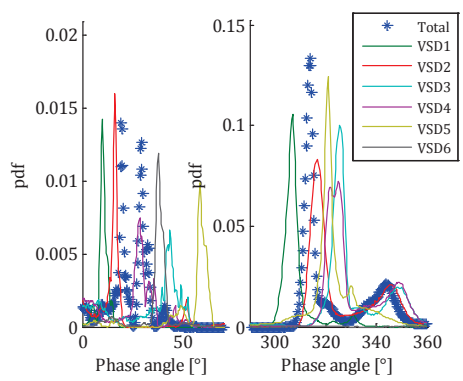

(c)

Fig 5.19 Location VSD2: (a) polar plot of currents, (b) pdf of magnitudes, (c) pdf of phase angles, 5th harmonic order

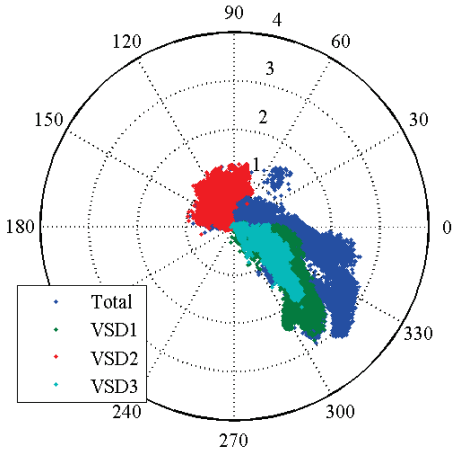

(a)

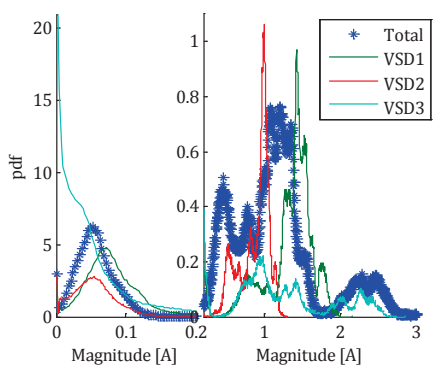

(b)

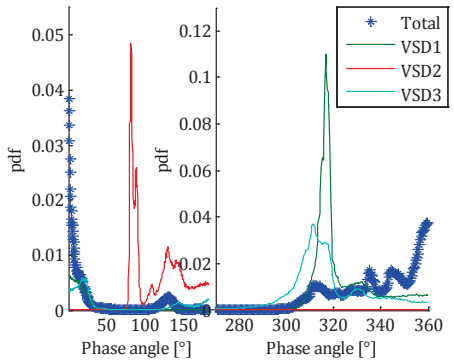

(c)

Fig 5.20 Location VSD3: (a) polar plot of currents, (b) pdf of magnitudes, (c) pdf of phase angles, 5th harmonic order

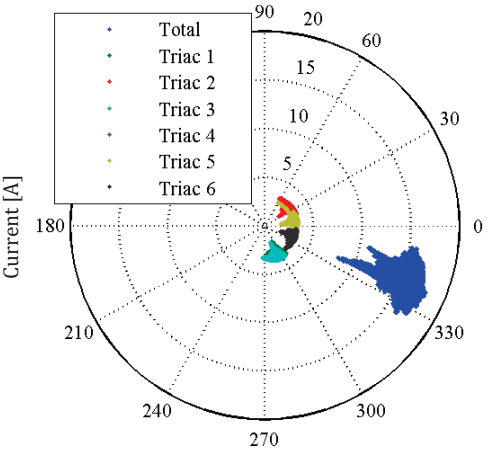

(a)

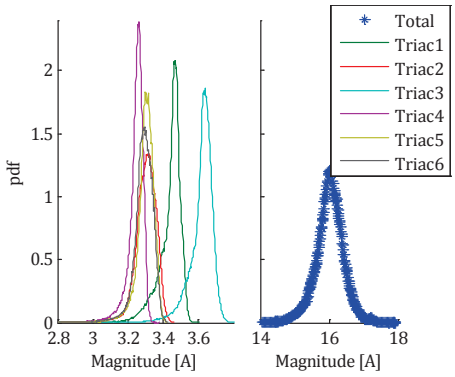

(b)

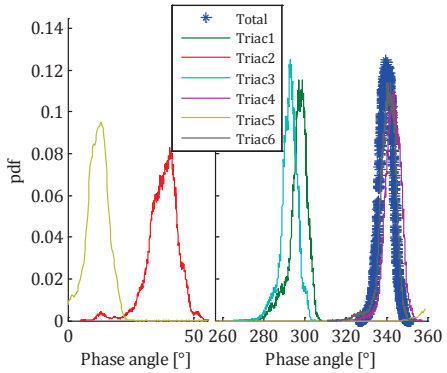

(c)

Fig 5.21 Location TH: (a) polar plot of currents, (b) pdf of magnitudes, (c) pdf of phase angles, 5th harmonic order

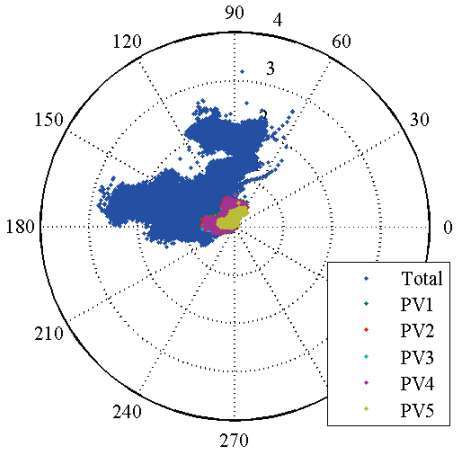

(a)

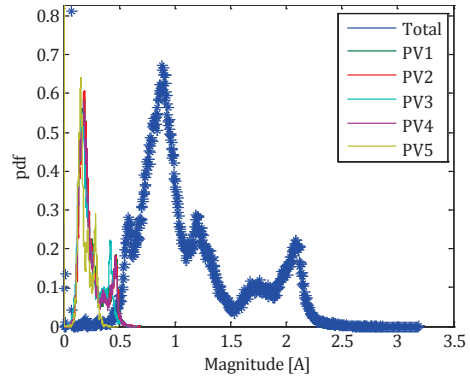

(b)

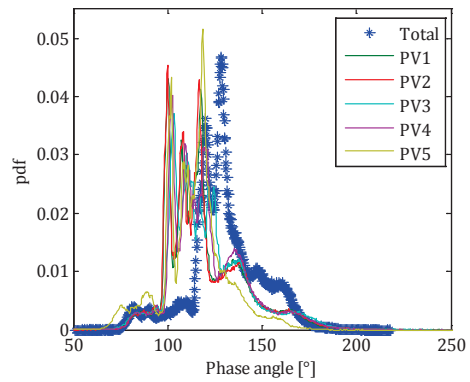

(c)

Fig 5.22 Location PV: (a) polar plot of currents, (b) pdf of magnitudes, (c) pdf of phase angles, 5th harmonic order

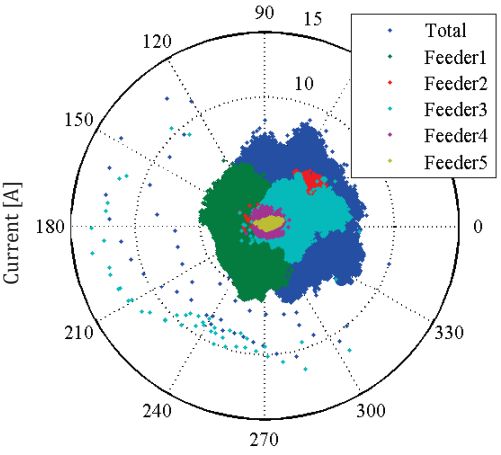

(a)

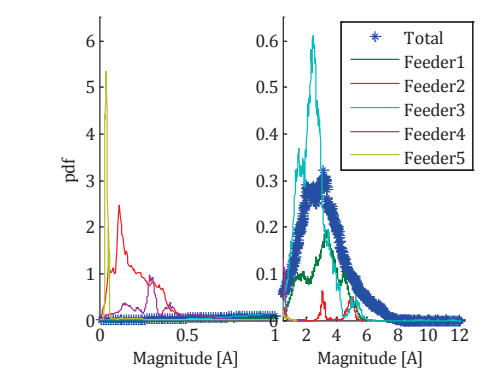

(b)

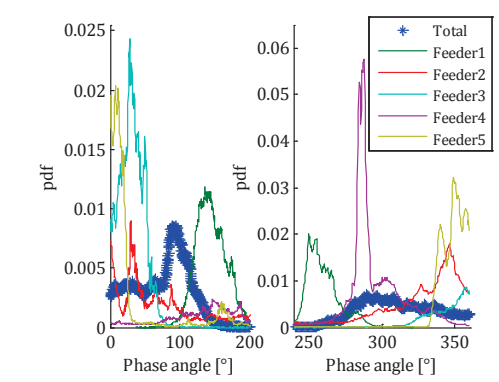

(c)

Fig 5.23 Location ML1: (a) polar plot of currents, (b) pdf of magnitudes, (c) pdf of phase angles, 5th harmonic order

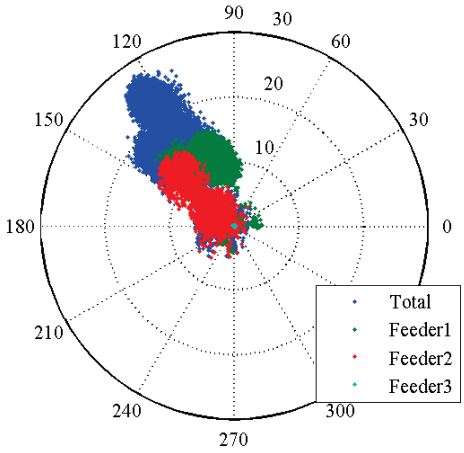

(a)

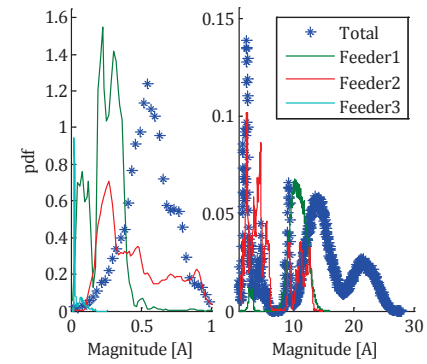

(b)

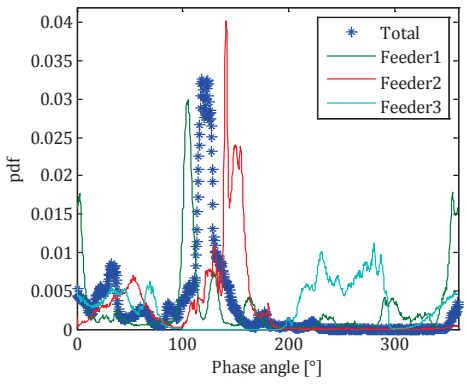

(c)

Fig 5.24 Location ML2: (a) polar plot of currents, (b) pdf of magnitudes, (c) pdf of phase angles, 5th harmonic order

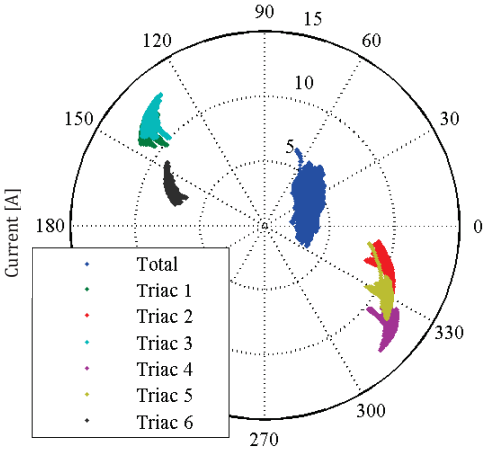

(a)

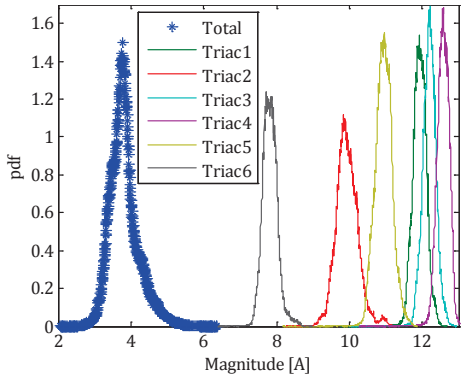

(b)

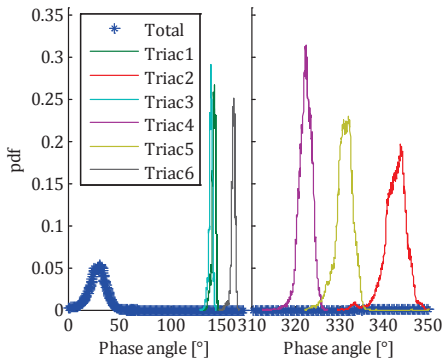

(c)

Fig 5.25 Location TH: (a) polar plot of currents, (b) pdf of magnitudes, (c) pdf of phase angles, 3rd harmonic order

5.3.3.2 Correlations between current sources

One common assumption in probabilistic harmonic studies is that current sources are statistically independent vectors. Proving that two vectors are uncorrelated does not prove in general that they are also independent, but a strong correlation between two vectors proves that they are dependent.

In this work, vectors of individual currents were correlated using a vectorial correlation method proposed in [42], which is a version of the scalar product-moment correlation. More details on this method are given in Appendix 3. Averages of individual correlation coefficients for each harmonic order are given in Table 5.10 and Table 5.11, together with their uncertainty intervals. The uncertainty intervals show the difference of each average correlation coefficient to the maximal and minimal coefficient between all loads of that location, for the same harmonic order.

Table 5.10 Average correlation coefficient for locations with variable speed drives, together with uncertainty intervals

	VSD1		*VSD2*		*VSD3*	
h	ρ_{AV}	*Ui*	ρ_{AV}	*Ui*	ρ_{AV}	*Ui*
3	0.17	+0.14 -0.09	0.65	+0.14 -0.17	0.29	+0.41 -0.23
5	0.33	+0.60 -0.24	0.65	+0.31 -0.29	0.35	+0.54 -0.28
7	0.31	+0.57 -0.22	0.68	+0.30 -0.35	0.38	+0.43 -0.24
9	0.32	+0.50 -0.24	0.50	+0.43 -0.41	0.27	+0.46 -0.24
11	0.30	+0.65 -0.27	0.37	+0.59 -0.22	0.33	+0.50 -0.28
13	0.28	+0.60 -0.24	0.73	+0.26 -0.39	0.32	+0.53 -0.27
15	0.34	+0.42 -0.20	0.80	+0.20 -0.26	0.20	+0.34 -0.19
17	0.30	+0.65 -0.26	0.64	+0.36 -0.33	0.27	+0.18 -0.12
19	0.28	+0.62 -0.24	0.55	+0.43 -0.52	0.24	+0.29 -0.16
21	0.27	+0.42 -0.22	0.60	+0.36 -0.28	0.25	+0.31 -0.19

ρ_{AV} – Average of individual correlation coefficient, *Ui* – Uncertainty interval, *VSD* – Variable speed drive

Locations ML1, VSD1 and VSD3 had the lowest correlation coefficients. On other four locations the coefficients are mostly higher than 0.5, which could be described as a relatively strong correlation. For PV inverters the correlations were strongest (up to 0.96).

One of the sources of the correlation is the fact that the phase angles of similar devices cover a similar range of phase angles. Also, their operating times are similar or the same, which correlates them via the fundamental current. Lastly, the same harmonic voltages are affecting the currents of all devices. This connection via the voltage is complex, because the total current is causing a part of the harmonic voltages and is affected by it at the same time.

In some cases, the correlation coefficient between the total harmonic current and the harmonic voltage of the same harmonic order was higher than 0.95, while individual current components have a weaker correlation with the voltage. Harmonic voltages are

affected by the "background" distortion and by the topology of the installation, which has a significant influence on the resulting currents via the voltage. If loads are connected via different impedances, they are affected by different harmonic voltages. This can lead to a reduction or amplification of the harmonic currents, and in most cases to a shift in the phase angles.

Table 5.11 Average correlation coefficient for remaining locations, together with uncertainty intervals

	TH		*PV*		*ML1*		*ML2*	
h	ρ_{AV}	*Ui*	ρ_{AV}	*Ui*	ρ_{AV}	*Ui*	ρ_{AV}	*Ui*
3	0.54	+0.10 -0.08	0.63	+0.15 -0.27	0.18	+0.18 -0.09	0.72	+0.16 -0.15
5	0.48	+0.14 -0.09	0.96	+0.03 -0.04	0.15	+0.17 -0.10	0.59	+0.06 -0.03
7	0.53	+0.13 -0.08	0.96	+0.03 -0.04	0.25	+0.29 -0.20	0.30	+0.12 -0.08
9	0.54	+0.10 -0.08	0.91	+0.04 -0.06	0.39	+0.44 -0.36	0.82	+0.07 -0.05
11	0.54	+0.11 -0.08	0.94	+0.03 -0.05	0.24	+0.46 -0.21	0.46	+0.08 -0.08
13	0.52	+0.13 -0.11	0.87	+0.10 -0.16	0.26	+0.25 -0.19	0.43	+0.21 -0.18
15	0.56	+0.13 -0.12	0.62	+0.14 -0.20	0.25	+0.42 -0.19	0.53	+0.36 -0.19
17	0.55	+0.13 -0.08	0.90	+0.05 -0.07	0.32	+0.33 -0.23	0.52	+0.32 -0.17
19	0.56	+0.16 -0.09	0.71	+0.10 -0.13	0.24	+0.37 -0.19	0.33	+0.13 -0.19
21	0.59	+0.13 -0.09	0.42	+0.23 -0.32	0.35	+0.43 -0.29	0.53	+0.10 -0.13

ρ_{AV} – Average of individual correlation coefficient, *Ui* – Uncertainty interval, *TH* – triac heaters, *PV* – photovoltaic inverters, *ML* – mixed single-phase and three-phase loads

In general, industrial processes create a certain level of dependence between currents of nearby devices, and the level of dependence is different for each application. Correlation coefficients on location VSD2 are two to three times higher than on location VSD1, even though it is the same type of load. This shows that in general it is not correct to treat harmonic phasors as independent variables, and for PV inverters it is a definitive conclusion because their currents are dependent on nearly the same irradiance level. On three out of seven locations correlations were relatively weak (0.15 – 0.38), which brings them closer to the assumption of independence, although low correlation is not the only condition of independence.

5.3.4 Calculated summation coefficients and diversity factors

From the measured data, diversity factors and summation coefficients were calculated. Diversity factors can be calculated directly using (5.1). Summation coefficients can be calculated from (5.4), which is a nonlinear equation. In this work the Newton method was used, as suggested in [38].

In the literature, diversity factors were mainly used to characterize the summation of a single steady state. Here we use them with the 95 % probability levels, in the same manner as the summation coefficients. The advantage of diversity factors is that they directly show by which percentage the vectorial sum is lower than the arithmetic.

Resulting summation coefficients are presented in Fig 5.26 for VSDs and Fig 5.27 for the remaining locations. In most cases the total current is higher than the highest

component current and lower than the arithmetic sum. This leads to α > 1. In a few cases α was higher than two, which means that the sum was even lower than the RSS. Fig 5.26 (a) and Fig 5.27 (a) zoom in on the coefficients which have values between one and two, and compare them to the values recommended by IEC.

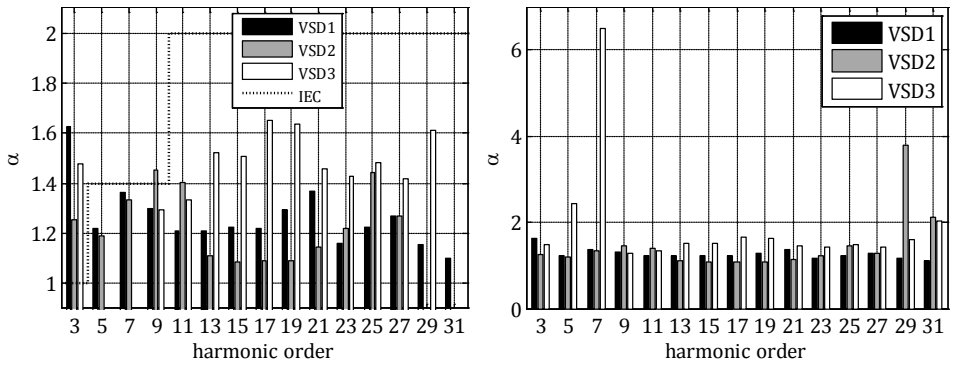

Fig 5.26 Calculated summation coefficients for VSDs: (a) zoomed in values between 1 and 2, (b) all values

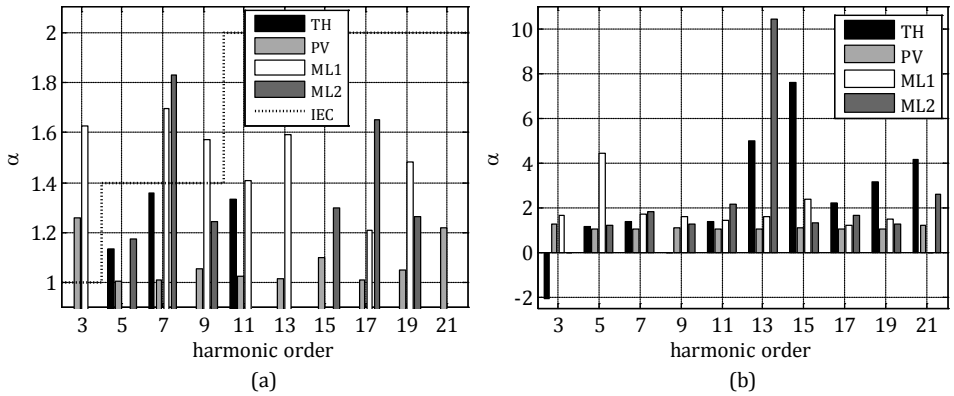

Fig 5.27 Calculated summation coefficients for remaining locations: (a) zoomed in values between 1 and 2, (b) all values

In three situations out of 85, it was impossible to calculate α which satisfies (5.4). This is a special case when the total current is higher than the lowest of the component currents, but lower than the highest of them ($min\{I_{h,i}\} < I_{h,sum} < max\{I_{h,i}\}$).

In one case, 3rd harmonic on location TH, the total current was even lower than the lowest of the components. If this condition is met, α has a negative value (as can be seen in Fig 5.27). This is a rare situation, other loads in general do not show such behaviour.

Summation coefficients were in good agreement with Table 5.8 only for triac heaters. For other loads Table 5.8 is too optimistic, with a few values of α exceeding 2, but not for all higher order harmonics. Variable speed drives showed lower compensation effects, with values of α varying between 1.1 and 1.6, with a majority of values up to 1.4. Feeders with mixes loads had α starting at 1.2, and usually larger than 1.4 for $h > 9$. Photovoltaic inverters showed very limited compensation effects, with α > 1.2 only for two harmonic orders.

A common characteristic is that α starts at 1.1 for all devices except for PV inverters,

so this value could be used as a conservative approach for all other loads instead of the arithmetic summation, while even 1.2 could be used when analysing mixed types of loads. The values did not show a monotonous increase with the harmonic order, but a value of 1.4 for $h > 9$ covers most loads quite well, with the exception of PV inverters.

Calculated diversity factors are shown in Fig 5.28. In most cases *DF* had values between 0.6 and 0.9. With triac heaters these values were lower, especially for triple-n harmonics. As with summation coefficients, there was no monotonous trend with the increase of the harmonic order. For triac heaters, we could use $DF = 0.6$ for $h \leq 11$ and $DF = 0.4$ for $h > 11$. For variable speed drives we could use a value of between 0.6 and 0.85 for all orders.

In general, for all loads except PV inverters, 10 % of the generated harmonic current did not reach the transformer. This means that as a conservative approach we can use $DF = 0.9$ instead of the arithmetic summation.

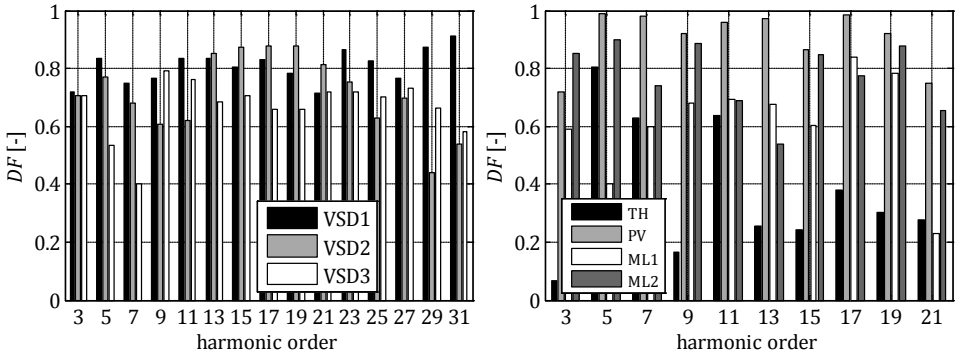

Fig 5.28 Calculated diversity factors for all locations: (a) VSDs, (b) remaining loads

A disadvantage of diversity factors is that they do not take into account the effect of a dominant current source. For example, if we would use a $DF = 0.8$ when summating two currents where one is 10 times greater than the other, we would estimate a total current lower than physically possible. This underestimation is unwanted in practical assessments.

To analyse this effect, we introduce the ratio $RC = max\{I_{h,i}\} / \sum I_{h,i}$, which represents the share of the maximal current source in the arithmetic sum. In Fig 5.29 the dependency between *DF* and *RC* is given.

It can be seen that in the majority of cases (75 out of 85):

$$RC \leq DF \leq 0.9 \tag{5.5}$$

Even though the relation between *DF* and *RC* cannot be generalized and formulated into an analytical expression, *RC* can be used as a simple check of the validity of *DF* in a particular case based on the sizes of loads. Ratio *RC* is equal to the most optimistic value of *DF*, while 0.9 is the most pessimistic value. Almost all exceptions to (5.5) come from PV inverters (with most of the *DF* values higher than 0.9).

A summary of estimated values of α and *DF* for the measured load types is given in Table 5.12. For diversity factors (5.5) should be taken into account as a limitation.

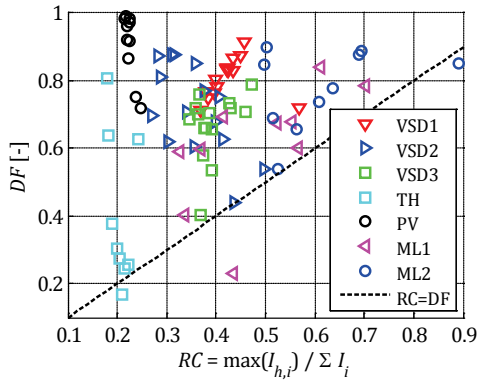

Fig 5.29 Dependency between the diversity factor and the share of the maximal current in the arithmetic sum

Table 5.12 Indicative values of α and *DF* for the measured load types

h	Variable Speed Drives	PV inverters	Triac heaters	Mixed loads
		α		
≤ 9	1.1 – 1.4	1.0	1.4	1.2
> 9	1.1 – 1.4	1.0	1.6	1.4
		DF		
≤ 9	0.6 – 0.9	1.0	0.6	0.7
> 9	0.6 – 0.9	1.0	0.4	0.6

5.3.5 Summation indices for short time intervals

Results of the previous sub-section show indices which represent the relation between 95 % cumulative probability levels, which means that they are in general not valid for any specific moment in time. Only by incident could these indices exactly match the summation of a chosen steady state. If we calculate the *DF* and α for each measurement point, using short-term values of currents instead of cumulative levels, the results will be time-varying as well.

Time changes of summation indices calculated for 10-minute intervals are shown in Fig 5.30, for the 5th harmonic current of location VSD2. To illustrate the influence of the sizes of individual loads, normalized indices are presented as well, in Fig 5.30 (b) for *NDF* and Fig 5.30 (d) for α normalized in an analogue way: for each time interval the total current is calculated from normalized individual complex currents (with magnitudes equal to 1) and then the normalized value of α is calculated for that time interval.

Looking at the *DF* variations, we see that it is mostly varying in a relatively narrow range, with some higher changes at the end of the measurement. The average value over the whole measurement period is 0.81, which is very close to the value calculated with the 95 % cumulative probability levels which is equal to 0.77. During most of the time the *DF* based on the 95 % probability level was more optimistic than the short-term value, but for most of the time with very slight differences.

In the case of α, the 95 % probability value was also slightly more optimistic than the short-term values during most of the time, with a 95 % probability value of 1.15 in comparison with 1.19 as the average short-term value. During most of the time, both cumulative indices describe the summation with acceptable accuracy.

The normalized indices show the influence of the sizes of loads on the total sum of currents. If all loads had the same magnitude, the summation would be influenced only

by the phase angles of harmonic currents, *DF* would be equal to *NDF*, and α would be equal to normalized α.

Due to some loads being smaller than the others, their current phase angles have less influence on the total current, and *NDF* is always lower or equal to *DF*, and normalized α is always higher or equal to α when α is greater than 1. At certain time intervals (in the second half of the measurement) the normalized indices showed very optimistic values, but this has little to no influence on the total current.

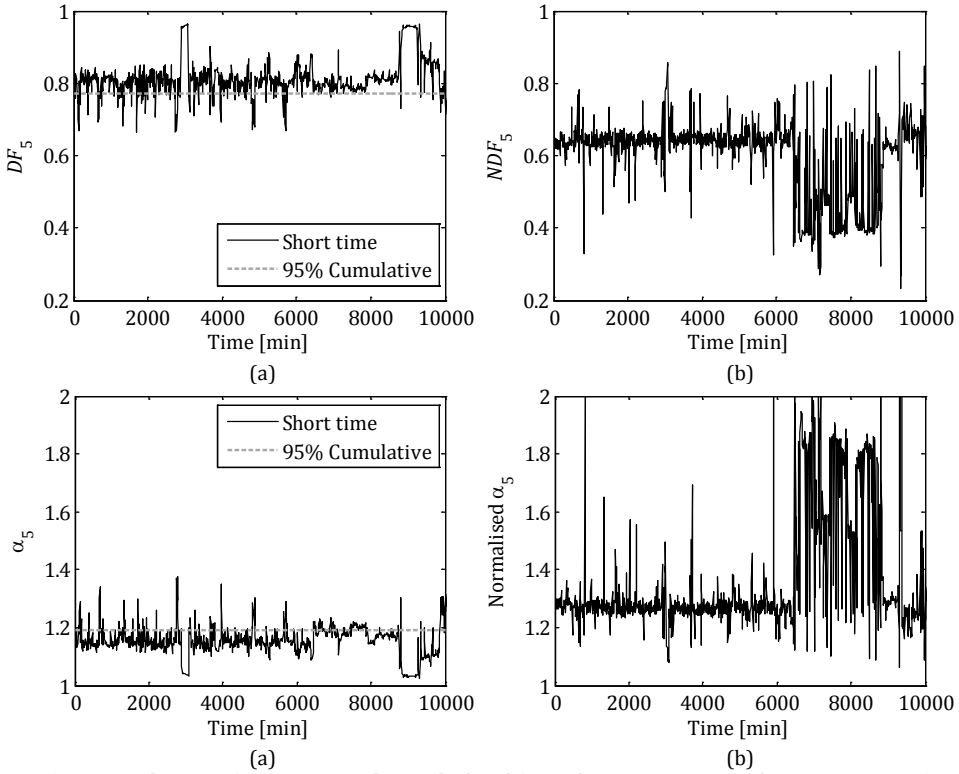

Fig 5.30 Time changes of summation indices calculated for each 10-minute interval, Location VSD2, 5th harmonic current: (a) *DF*, (b) *NDF*, (c) α, and (d) normalized α

Differences between Fig 5.30 (a) and (b), as well as between Fig 5.30 (c) and (d), point out that caution is needed for applying diversity factors and summation coefficients. When loads are of equal sizes, a higher compensation effect can be expected than from an average measurement. In contrast, when one load is dominant, the compensation effect becomes very limited, as can be seen also in Fig 5.29 on the relation between the *DF* and *RC*.

5.3.6 Differences between using 95 % and 99 % probability values

Technical references [34], [35] define the summation law (5.4) as a method to calculate the 95 % probability values of the total current. The emission coordination uses the 95 % probability values based on 10-minute measurements, but as a very short-term indice the 99 % probability values based on 3 s measurements can be used as well. References which incorporate diversity factors mainly used a single steady

state value of the current to calculate this factor. In this work both the diversity factors and the summation coefficients are compared when calculated with 95 % and 99 % probability values of harmonic currents.

Comparisons for variable speed drives and the remaining locations are shown in Table 5.13 and Table 5.14, respectively. Depending on the cumulative distributions of current magnitudes, using 99 % probability values can lead to calculating higher values of diversity factors and lower values of summation coefficients (e.g. location TH in Table 5.14), or the other way around (e.g. location VSD2 in Table 5.13).

Table 5.13 Comparison between *DF* and *α* based on 95 % and 99 % probability values, variable speed drives

h	VSD1				VSD2				VSD3			
	DF95	*DF99*	*α95*	*α99*	*DF95*	*DF99*	*α95*	*α99*	*DF95*	*DF99*	*α95*	*α99*
3	0.72	0.49	1.63	2.27	0.71	0.69	1.25	1.27	0.70	0.66	1.48	1.61
5	0.83	0.61	1.22	1.58	0.77	0.74	1.19	1.22	0.53	0.48	2.44	*N.D.*
7	0.75	0.49	1.37	2.12	0.68	0.64	1.33	1.43	0.40	0.43	6.50	7.72
9	0.76	0.51	1.90	1.92	0.61	0.58	1.45	1.51	0.79	0.75	1.29	1.37
11	0.84	0.66	1.21	1.47	0.62	0.54	1.40	1.58	0.76	0.65	1.34	1.67
13	0.84	0.52	1.21	1.92	0.85	0.79	1.11	1.17	0.69	0.64	1.52	1.67
15	0.80	0.52	1.22	1.87	0.87	0.85	1.09	1.11	0.71	0.66	1.51	1.62
17	0.83	0.61	1.22	1.58	0.88	0.83	1.09	1.13	0.66	0.59	1.65	1.97
19	0.78	0.58	1.29	1.67	0.88	0.82	1.09	1.13	0.66	0.63	1.63	1.81
21	0.71	0.57	1.37	1.71	0.81	0.79	1.14	1.16	0.72	0.67	1.46	1.58
23	0.87	0.53	1.16	1.52	0.75	0.69	1.22	1.29	0.72	0.64	1.43	1.68
25	0.83	0.61	1.23	1.60	0.63	0.55	1.44	1.57	0.70	0.58	1.48	2.09
27	0.77	0.50	1.27	2.06	0.70	0.68	1.27	1.29	0.73	0.68	1.42	1.56
29	0.87	0.57	1.15	1.69	0.44	0.50	3.78	1.96	0.66	0.57	1.61	2.07
31	0.91	0.64	1.10	1.51	0.54	0.50	2.12	2.19	0.58	0.53	2.02	2.52

DF95 – diversity factor based on 95 % probability values, *DF99* – diversity factor based on 99 % probability values, *α95* – summation coefficient based on 95 % probability values, *α99* – summation coefficient based on 99 % probability values, *N.D.* – not defined

For VSDs, the differences are significant only on location VSD1, for all orders. On locations VSD2 and VSD3 the differences are up to 10 % for most cases where the cancelation effect was not pronounced, i.e. $1 < \alpha < 2$ and $DF > 0.5$.

The main reason why values are so much different on location VSD1 is the relatively low number of operating hours of the drives. This leads to significant differences between the 95 % and 99 % probability levels. Cumulative distribution functions of locations VSD1 and VSD3 are compared in Fig 5.31.

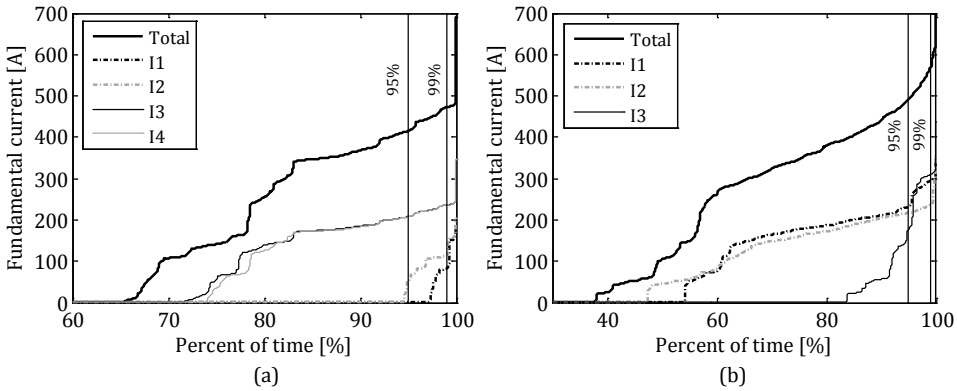

Fig 5.31 Cumulative distribution functions of locations (a) VSD1, (b) VSD3

Table 5.14 Comparison between *DF* and *α* based on 95 % and 99 % probability values, remaining locations

h	TH				PV				ML1				ML2			
	DF95	*DF99*	α*95*	α*99*	*DF95*	*DF99*	α*95*	α*99*	*DF95*	*DF99*	α*95*	α*99*	*DF95*	*DF99*	α*95*	α*99*
3	0.07	0.07	-2.09	-2.30	0.75	0.73	1.21	1.24	0.59	0.54	1.62	*N.D.*	0.85	0.86	*N.D.*	*N.D.*
5	0.81	0.81	1.13	1.12	1.00	0.98	1.00	1.01	0.40	0.40	4.44	4.06	0.90	0.92	1.17	1.13
7	0.63	0.63	1.36	1.35	0.99	0.97	1.01	1.02	0.60	0.54	1.69	1.97	0.74	0.63	1.83	4.77
9	0.17	0.19	*N.D.*	*N.D.*	0.91	0.93	1.06	1.04	0.68	0.65	1.57	1.61	0.89	0.88	1.24	1.28
11	0.64	0.66	1.33	1.29	0.97	0.99	1.02	1.00	0.69	0.63	1.41	1.54	0.69	0.70	2.12	2.03
13	0.26	0.28	4.96	3.53	0.97	0.94	1.02	1.04	0.67	0.67	1.59	1.57	0.54	0.55	10.4	7.14
15	0.24	0.28	7.58	3.92	0.84	0.86	1.13	1.11	0.60	0.60	2.34	2.13	0.85	0.83	1.30	1.36
17	0.38	0.36	2.22	1.94	0.97	0.95	1.02	1.03	0.84	0.78	1.21	1.33	0.78	0.78	1.65	1.61
19	0.30	0.36	3.15	2.32	0.90	0.85	1.07	1.12	0.78	0.72	1.48	1.70	0.88	0.88	1.26	1.24
21	0.27	0.32	4.14	2.85	0.72	0.67	1.26	1.34	0.23	0.24	*N.D.*	*N.D.*	0.65	0.66	2.57	2.39

DF95 – diversity factor based on 95 % probability values, *DF99* – diversity factor based on 99 % probability values, α*95* – summation coefficient based on 95 % probability values, α*99* – summation coefficient based on 99 % probability values, *N.D.* – not defined

In Fig 5.31 (a), one of the drives does not operate for more than 95 % of the time, so its 95 % probability level is 0 A. In Fig 5.31 (b) which displays location VSD3, the differences between the two probability levels are similar for all drives. Therefore, summation indices did not differ significantly for 95 % and 99 % cumulative levels on this location.

For all other types of loads, the differences between the two probability levels are mainly up to 10 %, also with the exception of $\alpha > 2$. This means that the diversity factors and summation coefficients calculated for 95 % probability values can be used for 99 % probability values for six out of seven measured locations.

5.3.7 Influence of measurement time resolution

As diversity factors and summation coefficients are not defined in terms of the time resolution of their measurement, it is interesting to look into the effect of different time resolutions on their values. The coefficients from the previous parts of this section were calculated using data with a time resolution of 1 s. In Table 5.15 and Table 5.16 we compare them with results obtained from aggregated data, with time resolutions of 1 min, 10 min, and 1 h, for locations VSD1 and ML1. Values from these two tables are calculated using the 95 % probability levels for all time resolutions.

Table 5.15 Influence of time resolution on diversity factors and summation coefficients, location VSD1

h	*DF1s*	*DF1m*	*DF10m*	*DF1h*	*α1s*	*α1m*	*α10m*	*α1h*
3	0.72	0.69	0.68	0.68	1.63	1.68	1.69	1.73
5	0.83	0.83	0.83	0.81	1.22	1.22	1.22	1.26
7	0.75	0.75	0.76	0.73	1.37	1.37	1.35	1.41
9	0.76	0.76	0.76	0.71	1.30	1.30	1.29	1.39
11	0.84	0.84	0.85	0.84	1.21	1.21	1.19	1.20
13	0.84	0.84	0.83	0.78	1.21	1.21	1.22	1.30
15	0.80	0.79	0.74	0.76	1.22	1.25	1.32	1.27
17	0.83	0.83	0.81	0.80	1.22	1.22	1.25	1.27
19	0.78	0.79	0.79	0.78	1.29	1.29	1.28	1.30
21	0.71	0.71	0.69	0.65	1.37	1.36	1.40	1.48
23	0.87	0.86	0.85	0.82	1.16	1.16	1.18	1.23
25	0.83	0.80	0.80	0.77	1.23	1.24	1.27	1.31
27	0.77	0.76	0.83	0.71	1.27	1.28	1.33	1.26
29	0.87	0.85	0.83	0.77	1.15	1.18	1.21	1.31
31	0.91	0.90	0.85	0.81	1.10	1.12	1.18	1.24

DF1s, α1s – diversity factor and summation coefficient based on 1 s time resolution, *DF1m*, *α1m* – diversity factor and summation coefficient based on 1-minute time resolution, *DF10m*, *α10m* – diversity factor and summation coefficient based on 10-minute time resolution, *DF1h*, *α1h* – diversity factor and summation coefficient based on 1-hour time resolution.

Table 5.16 Influence of time resolution on diversity factors and summation coefficients, location ML1

h	*DF1s*	*DF1m*	*DF10m*	*DF1h*	*α1s*	*α1m*	*α10m*	*α1h*
3	0.59	0.59	0.59	0.60	1.63	1.63	1.61	1.58
5	0.40	0.40	0.40	0.44	4.44	4.52	4.34	3.15
7	0.60	0.60	0.60	0.62	1.69	1.69	1.66	1.60
9	0.68	0.68	0.67	0.68	1.57	1.57	1.58	1.55
11	0.69	0.69	0.69	0.69	1.41	1.40	1.40	1.39
13	0.67	0.67	0.67	0.70	1.59	1.60	1.58	1.46
15	0.60	0.60	0.60	0.60	2.35	2.33	2.29	2.35
17	0.84	0.81	0.80	0.82	1.21	1.27	1.29	1.24
19	0.78	0.77	0.77	0.79	1.48	1.61	1.52	1.43
21	0.23	0.22	0.21	0.21	*N.D.*	*N.D.*	*N.D.*	*N.D.*

Diversity factors did not show significant differences, among the compared time resolutions. In the case of summation coefficients, differences were significant only when α had values greater than 2. When α was ranging between 1 and 2, different time resolutions showed very similar results. None of the locations was an exception to this. Comparisons for the remaining five locations are given in Appendix 4.

This leads to a conclusion that measuring at a 1 s or 1 minute resolution does not show a significant advantage over measuring at 10 minute or 1 hour resolution, except if summation coefficients with values higher than 2 are to be used. This is in good agreement with the conclusions of [43], where the influence of aggregation interval on the results of continuous disturbances was analysed.

5.4 Conclusions

The summation of harmonic currents is usually characterized with two indices: the diversity factors (DF_h) which are commonly used to described a quasi-steady state as in (5.1) (but can be used also for cumulative probability levels), and the summation coefficients α_h which are normally used with 95 % and 99 % cumulative probability levels as in (5.4).

For household devices which appear in large numbers, the cancelation effect is usually strong enough to achieve a relatively low total harmonic current even with relatively high values of individual current THDs. The *DF* generally decreases with the increase of *h*, at the 3rd harmonic order the cancelation effect is not pronounced, but at higher orders it has a significant influence. When a mixture of devices is assessed, the numbers of different types of devices change the *DF* of the total mixture significantly, unless the devices are nearly in phase.

For variable speed induction motor drives the *DF* highly depends on the operating conditions, mainly the reference speed of the drive. Based on simulations, it was found that the *DF* does not have to have a lower value for higher order harmonics then the lower order harmonics. Field measurements confirmed this conclusion, the values of *DF* and α based on cumulative levels do not change monotonously as *h* increases.

Regarding the assumptions for probabilistic studies, from the field measurements we can conclude that distributions of magnitudes and phase angles of harmonic currents mostly differ from the usually assumed normal distribution for magnitudes and uniform distribution for phase angles. Both magnitudes and phase angles had multimodal distributions, except in the case of triac heaters where all orders had a nearly normal distribution. Phase angles also had multimodal distributions, and nearly normal distributions for triac heaters. Until the 13th order, phase angles were mostly covering a 90° range, and above the 13th order between 90° and 180°.

Correlations coefficients between harmonic currents of examined industrial loads showed that when similar loads are summated it would not be correct to assume that their currents are statistically independent. This assumption might be suitable when a very large number of different loads are present. This is one of the reasons why the total current usually does not have a normal distribution.

Regarding the summation coefficients, it can be concluded that a good conservative approach is using α = 1.1, and for mixed types of loads even 1.2 could be used. Arithmetic summation does not have to be used even for the 3rd harmonic order. For orders higher than the 9th, a value of 1.4 could be used. PV inverters are an exception to this, because they showed very limited cancellation effects. Values of α between 1 and 1.1 could be used for all orders for PV inverters.

Diversity factors based on cumulative values were ranging between 0.9 and 0.6, with no general trend with the increase of the harmonic order. Their dependency from the share of the largest component is described by (5.5), where $DF = RC$ represents the optimistic approach and $DF = 0.9$ is the conservative approach. A summary of the measured values is given in Table 5.12. As with summation coefficients, PV inverters were an exception, values between 0.9 and 1

Comparison between coefficients calculated using 95 % and 99 % probability levels showed good agreement on six out of seven locations. Significant differences occurred only on the location with a low number of operating hours, resulting in a 95 % level of 0 A for one of the VSDs.

Regarding the time resolution of their measurement, for all analysed loads 10 minute and 1 hour aggregated values were equally suitable as 1 s or 1 minute values. For quickly varying loads (e.g. as arc furnaces), this should be applied with caution, as shown in [36] where time resolution and probability levels showed larger differences.

5.5 References of Chapter 5

[1] J. M. Crucq and A. Robert, "Statistical approach for harmonics measurements and calculations," in Proc. *CIRED*, 1989, pp. 91–96.

[2] VDEW, "EMC guide for public power supply networks - Compatibility levels and permissible emission," 1992.

[3] W. M. Grady, A. Mansoor, E. F. Fuchs, P. Verde, and M. Doyle, "Estimating the net harmonic currents produced by selected distributed single-phase loads: computers, televisions, and incandescent light dimmers," in Proc. *IEEE Power Engineering Society Winter Meeting. Conference Proceedings*, 2002, vol. 2, pp. 1090–1094.

[4] S. Hansen, P. Nielsen, and F. Blaabjerg, "Harmonic cancellation by mixing nonlinear single-phase and three-phase loads," *IEEE Transactions on Industry Applications*, vol. 36, no. 1, pp. 152–159, 2000.

[5] A. Mansoor, W. M. Grady, P. T. Staats, R. S. Thallam, M. T. Doyle, and M. J. Samotyj, "Predicting the net harmonic currents produced by large numbers of distributed single-phase computer loads," *IEEE Transactions on Power Delivery*, vol. 10, no. 4, pp. 2001–2006, 1995.

[6] A. Mansoor, W. M. Grady, A. H. Chowdhury, and M. J. Samotyi, "An investigation of harmonics attenuation and diversity among distributed single-phase power electronic loads," *IEEE Transactions on Power Delivery*, vol. 10, no. 1, pp. 467–473, 1995.

[7] A. Mansoor and W. M. Grady, "Analysis of compensation factors influencing the net harmonic current produced by single-phase nonlinear loads," in Proc. *IEEE ICHQP*, 1998, vol. 2, pp. 883–889.

[8] W. M. Eisenmann, F.G., Parsons, A.C., Grady, "A study of harmonic current cancellation in a semiconductor fabrication plant," in Proc. *IEEE ICHQP*, 1996, pp. 534–541.

[9] A. B. Nassif, "Modeling, measurement and mitigation of power system harmonics," PhD thesis, University of Alberta, Canada, 2009.

[10] A. J. Collin, C. E. Cresswell, and S. Z. Djokic, "Harmonic cancellation of modern switch-mode power supply load," in Proc. *IEEE ICHQP*, 2010, pp. 1–9.

[11] S. Mujović, V. A. Katić, and J. Radović, "Improved analytical expression for calculating total harmonic distortion of PC clusters," *Electric Power Systems Research*, vol. 81, no. 7, pp. 1317–1324, Jul. 2011.

[12] S. Hardie and N. Watson, "The effect of new residential appliances on Power Quality." in Proc. *IEEE AUPEC,* pp. 1–6, 2010.

[13] M. Domagk, J. Meyer, and P. Schegner, "Identification of consumer topologies in low voltage grids by time series analysis of harmonic currents," in Proc. *International Conference on Electrical Power Quality and Utilisation*, 2011, pp. 1–6.

[14] J. Meyer, P. Schegner, and K. Heidenreich, "Harmonic summation effects of modern lamp technologies and small electronic household equipment," in Proc. *CIRED 2011*, 2011, pp. 1–4.

[15] V. Cuk, J. F. G. Cobben, W. L. Kling, and R. B. Timens, "An analysis of diversity factors applied to harmonic emission limits for energy saving lamps," in Proc. *IEEE ICHQP*, 2010, pp. 1–6.

[16] R. B. Timens, F. J. K. Buesink, V. Cuk, J. F. G. Cobben, and F. B. J. Leferink, "Diversity and summation of large number of energy saving lighting," in Proc. *Asia-Pacific Symposium on Electromagnetic Compatibility*, 2012, pp. 229–232.

[17] R. B. Timens, F. J. K. Buesink, V. Cuk, J. F. G. Cobben, W. L. Kling, and F. B. J. Leferink, "High harmonic distortion in a new building due to a multitude of electronic equipment," in Proc. *IEEE International Symposium on Electromagnetic Compatibility*, 2011, pp. 393–398.

[18] Y. J. Wang, L. Pierrat, and L. Wang, "Summation of harmonic currents produced by AC/DC static power converters with randomly fluctuating loads," *IEEE Transactions on Power Delivery*, vol. 9, no. 2, pp. 1129–1135, Apr. 1994.

[19] W. G. Sherman, "Summation of harmonics with random phase angles," In Proc. IEE, vol. 119, no. 11, p. 1643, 1972.

[20] D. B. Corbyn, "This business of harmonics," *Electronics and Power*, vol. 18, no. 6, p. 219, 1972.

[21] E. W. Kazibwe, T. H. Ortmeyer, and M. S. A. A. Hammam, "Summation of probabilistic harmonic vectors (power systems)," *IEEE Transactions on Power Delivery*, vol. 4, no. 1, pp. 621–628, 1989.

[22] A. E. Emanuel and S. R. Kaprielian, "Contribution to the Theory of Stochastically Periodic Harmonics in Power Systems," *IEEE Transactions on Power Delivery*, vol. 1, no. 3, pp. 285–293, 1986.

[23] J. A. Orr, A. E. Emanuel, and K. W. Oberg, "Current Harmonics Generated by a Cluster of Electric Vehicle Battery Chargers," *IEEE Transactions on Power Apparatus and Systems*, vol. PAS-101, no. 3, pp. 691–700, Mar. 1982.

[24] Y. Baghzouz and O. T. Tan, "Probabilistic Modeling of Power System Harmonics," *IEEE Transactions on Industry Applications*, vol. IA-23, no. 1, pp. 173–180, Jan. 1987.

[25] P. F. Ribeiro, "Investigations of harmonic penetration in transmission systems," PhD thesis, The Victoria University of Manchester, UK, 1985.

[26] R. E. Morrison and A. D. Clark, "Probabilistic representation of harmonic currents in AC traction systems," in Proc. IEE, vol. 131, no. 5. pp. 181–189, 1984.

[27] M. Fracchia, A. Mariscotti, R. E. Morrison, and L. Pierrat, "Statistical Analysis of the Measured Harmonic Disturbances on the Ac Side of a Metrorail Supply System," in Proc. *IEEE ICHQP*, 1998, vol. 2, pp. 1229–1234.

[28] D. O'Kelly, "Probability characteristics of fundamental and harmonic sequence components of randomly varying loads," in Proc. *IEE C,* vol. 129, 1982.

[29] Y. Baghzouz, R. F. Burch, A. Capasso, A. Cavallini, A. E. Emanuel, M. Halpin, R. Langella, G. Montanari, K. J. Olejniczak, P. Ribeiro, S. Rios-Marcuello, F. Ruggiero, R. Thallam, A. Testa, and P. Verde, "Time-varying harmonics. II. Harmonic summation and propagation," *IEEE Transactions on Power Delivery*, vol. 17, no. 1, pp. 279–285, 2002.

[30] EPRI report EL-6754, "Photovoltaic generation effects on distribution feeders," 1991.

[31] A. Cavallini, R. Langella, A. Testa, and F. Ruggiero, "Gaussian modeling of harmonic vectors in power systems," in Proc. *IEEE ICHQP*, 1998, vol. 2, pp. 1010–1017.

[32] A. Cavallini and G. C. Montanari, "A deterministic/stochastic framework for power system harmonics modeling," *IEEE Transactions on Power Systems*, vol. 12, no. 1, pp. 407–415, 1997.

[33] IEEE 519, "IEEE Recommended Practices and Requirements for Harmonic Control in Electrical Power Systems," 1992.

[34] IEC 61000-3-6, "Electromagnetic compatibility (EMC) - Part 3-6: Limits - Assesment of emission limits for the connection of distorting installations to MV, HV, and EHV power systems," 2008.

[35] IEC/TR 61000-3-14, "Electromagnetic compatibility (EMC) - Part 3-14: Assessment of emission limits for the connection of disturbing installations to LV power systems," 2011.

[36] J. Wikston, "Harmonic summation for multiple arc furnaces," in Proc. *IEEE Power Engineering Society Winter Meeting*, 2002, vol. 2, pp. 1072–1075.

[37] X. Shaofeng, L. Qunzhan, Z. Liping, and X. Yinglei, "Study on summation exponents of harmonic of electrified railway," in Proc. *International Conference on Power Electronics and Drive Systems,* 2003, vol. 1, pp. 816–820.

[38] F. Medeiros, D. C. Brasil, P. F. Ribeiro, C. A. G. Marques, and C. A. Duque, "A new approach for harmonic summation using the methodology of IEC 61400-21," in Proc. *IEEE ICHQP*, 2010, pp. 1–7.

[39] D. Medeiros, D. C. Brasil, C. A. G. Marques, C. A. Duque, and P. F. Ribeiro, "Considerations on the aggregation of harmonics produced by large wind farms," in *ICHQP 2012*, 2012, pp. 1–6.

[40] Y. Xiao and X. Yang, "Harmonic Summation and Assessment Based on Probability Distribution," *IEEE Transactions on Power Delivery*, vol. 27, no. 2, pp. 1030–1032, Apr. 2012.

[41] Y. Xiao and X. Yang, "Harmonic summation and assessment based on probability distribution of phase angle," in Proc. *IEEE ICHQP*, 2012, pp. 1–4.

[42] H. B., K. K., M. K., R. S.M., and W. C.J., "Vector correlation: review, exposition, and geographic application," *Annals of the Accociation of American Geographers*, vol. 82, no. 1, pp. 103–116, 1992.

[43] M. Dogmark, J. Meyer, P. Schenger, G. Eberl, and T. Darda, "Influence of aggregation intervals on power quality assessment according to EN50160," in Proc. *CIRED*, 2013.

Chapter 6

Modelling of harmonic impedances

6.1 Introduction

Chapter 4 and Chapter 5 described the modelling of a single source of distortion and aggregation of multiple sources, respectively. To determine the influence of the analysed source(s), it is needed to represent the rest of the network as well, with or without additional sources of distortion. This chapter focuses on the impedance of the network "seen" by an individual source or a group of sources, in the frequency domain.

The time-domain method represents each component as $u(t) = g(i(t))$, where function g is in general non-linear and may contain differentiation and/or integration. In the case of a time-invariant resistance, $g = R$, and requires only a multiplication. In all other cases function g requires differentiation or integration as well.

The frequency-domain method, which is analysed here, uses a linear relation for all components, except for the analysed sources of distortion. The relation is defined separately for each harmonic order (h), adapted from [1]:

$$\left[\underline{U_h}\right] = \left[\underline{Z_h}\right] \cdot \left[\underline{I_h}\right] \tag{6.1}$$

where $[\underline{U_h}]$ is the matrix of busbar voltages, $[\underline{Z_h}]$ is the impedance matrix, and $[\underline{I_h}]$ is the matrix of injected harmonic currents. Expression (6.1) represents the direct method for calculating harmonic voltages and currents in the network, and also a single iteration in iterative methods (section 4.2.2.1).

Elements of the impedance matrix are labelled as $Z_{i,k}$, and each of them represents the relation between the voltage of the i^{th} busbar and the current injection in the k^{th} busbar. If only one source is present, the voltage is defined by:

$$\underline{U_i}(h) = \underline{Z_{i,k}}(h) \cdot \underline{I_k}(h) \tag{6.2}$$

For $i = k$, element $\underline{Z_{i,i}}$ is the self-impedance of busbar i, and it is commonly referred to as the "system impedance" of busbar i.

If we determine $\underline{Z_{j,i}}$ or $\underline{Z_{i,k}}$ for all frequencies of interest, the process is called a "frequency scan", and the result is the impedance-frequency characteristic of a busbar or between two busbars. A frequency scan reveals resonances of the system, and if significant emission is present at one of the resonant frequencies a potential harmonic problem is diagnosed. In the rest of this chapter only the self-impedance is analysed on examples. Analysis of mutual-impedances between busbars is analogue.

To illustrate the frequency scan of the system impedance with an example, we look at the network from Fig 6.1 and analyse the system impedance seen by the converter.

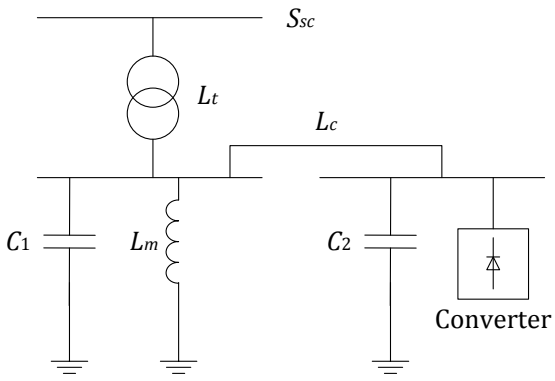

Fig 6.1 Single-line diagram of an example distribution system

There are two usual ways to represent the impedance characteristic. The first consists of the magnitude-frequency and phase angle-frequency dependencies, as in Fig 6.2. The other approach is a polar plot of the complex impedance characteristic, also known as the locus [1], see Fig 6.3. For both approaches the 5th, 7th, 11th, and 13th harmonic are highlighted, because they are the characteristic orders for a six-pulse rectifier. In Fig 6.3 (b), the loop of the second parallel resonance is zoomed in, together with the start and end points of the frequency scan – 0 Hz and 3 kHz.

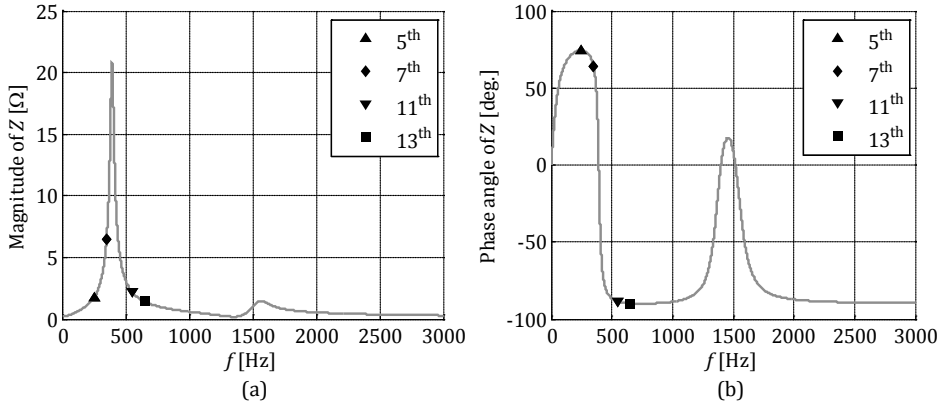

Fig 6.2 Frequency scan results for the example network: (a) magnitude of the impedance, (b) phase angle

The first parallel resonance of the system is located close to the 7th harmonic, visible as the first magnitude peak in Fig 6.2 (a). A small variation of the system impedance (e.g. due to network reconfigurations) can lead to the converter exciting this resonance, and a high level of the 7th harmonic voltage.

Series resonances are the minima of the magnitude characteristic. The example network has the first series resonance close to the 28th harmonic. Both types of resonances represent zero-crossings of the phase angle characteristic, Fig 6.2 (b).

On the locus, resonances are visible as the points where the impedance curve crosses the real-axis, i.e. $Re\{\underline{Z}\} = 0$. Parallel resonances correspond to local maxima of $|\underline{Z}|$ and series resonances correspond to the local minima on the horizontal axis.

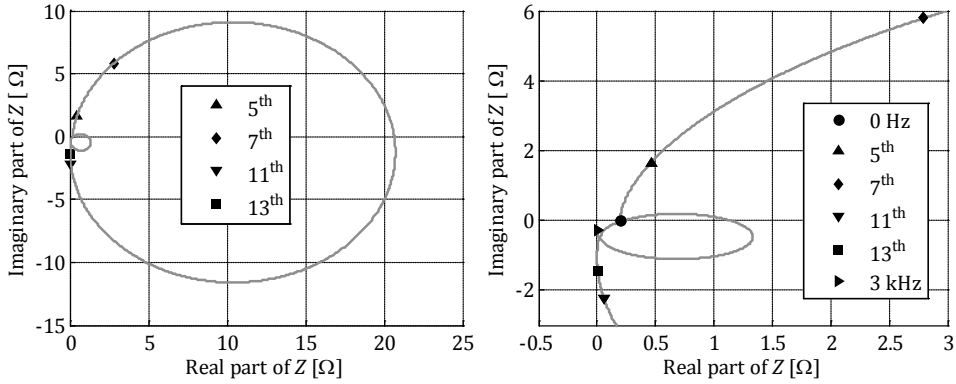

Fig 6.3 Frequency scan results for the example network: (a) locus – impedance in the polar plane, (b) zoom in around the second parallel resonance

The system impedance is influenced by many components. Knowing the exact composition of loads, both in the LV network and upstream networks, is usually difficult and also time-varying. Network reconfigurations also add to the time varying nature of the impedance, so each calculation can serve only for a particular moment in time. For this reason it is usual to calculate the impedance-frequency characteristic for all predicted major topology and load changes.

Calculations and analysis of harmonic impedances in transmission systems can be found in [2-6].Different models of system components are described in [2-12]. Examples of distribution system impedance modelling are given in [9], [13-16]. Sensitivity of transmission system impedance estimations are discussed in [3], [5], [17-19].

Uncertainties of impedance modelling in distribution networks and errors caused by simplifications and parameter errors were not analysed in previous works. The aim of this chapter is to analyse these effects, and to estimate possible errors in harmonic impedance calculations due to different model and parameter changes.

6.2 Models of power system components

Each element of the impedance matrix is calculated based on a number of physical components. For this calculation, components need to be represented by their own frequency dependent impedances. This subsection briefly discusses the models of generators, transformers, distribution lines (cables and overhead lines), PFC and passive filters, and loads which are not taken into account as harmonic sources.

6.2.1 Generators

At frequencies higher than the fundamental, generator impedance Z_{gh} is usually modelled as a series *R*-*L* branch [7]:

$$\underline{Z_{g,h}} = R_g\sqrt{h} + jh \cdot X_g \tag{6.3}$$

where R_g is the resistance representing the machine losses and X_g is the equivalent reactance of the generator. In the resistive part the skin effect is taken into account

with the square root of h. A frequency dependent coefficient can be used for the reactance as well.

Several values for the reactance are suggested in the literature, as discussed in [5], [20]. The sub-transient reactance X_d", and ½(X_d" + X_2) are the common representations for the steady-state reactance, where X_2 is the negative sequence reactance of the generator.

6.2.2 Distribution transformers

The frequency response of transformers is dominated by the inductance at the low frequency range. A transformer model for frequencies up to the first resonance is shown in Fig 6.4.

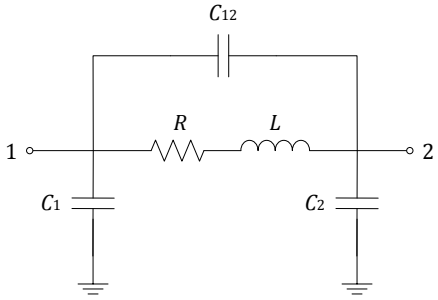

Fig 6.4 Transformer model for frequencies up to the first parallel resonance [20]

The capacitances of the transformer are usually neglected, because their influence becomes significant at frequencies higher than 7 kHz [20]. Also, in cable systems, the phase to ground capacitance of transformers is normally negligible in comparison to the capacitance of the cables connected to the transformer (~pF in comparison with ~μF).

This leaves a model identical to (6.3), with the values of resistance and inductance determined for the fundamental frequency. In [5] alternative models are also listed, as the parallel *R*-*L* circuit and a resistance in series with a parallel *R*-*L* branch.

6.2.3 Distribution lines

Distribution lines, both cables and overhead lines, are usually represented by their π equivalent [5], [7]. For relatively short lines, a lumped impedance model is used – the nominal π, as in Fig 6.5. Generally, a conductance element can be added to the two shunt capacitances. Parameters *R*, *L*, and *C* are determined from the line length and per unit values which depend on the geometry and type of material. Capacitance effect of lines has a significant influence on the impedance, especially in cable networks due to a higher per unit capacitance of cables.

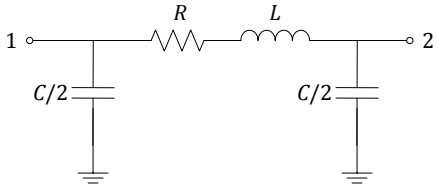

Fig 6.5 The nominal π (lumped equivalent) of a distribution line

For transmission and long distribution lines, a model with distributed parameters is normally needed, or an equivalent π model with hyperbolic corrections [21]. However, if the length of the distribution line is short enough, and the highest frequency of interest is low enough, the nominal π model is sufficient. If the length of the line is a considerable part of the wavelength of the highest frequency of interest (e.g. more than a quarter of the wavelength), the accuracy of the nominal π decreases considerably [7]. To give an example of the limitations of the lumped model, for the 50^{th} harmonic this gives approximately 30 km. For the 20^{th} harmonic it is approximately 75 km.

The resistance and inductance can be corrected for skin and proximity effects. In [5] the following coefficients were proposed:

$$R = R_{DC} \cdot \left(1 + \frac{0.646h^2}{192 + 0.518h^2}\right) \tag{6.4}$$

for overhead lines, and:

$$R = R_{DC} \cdot \left(0.187 + 0.532\sqrt{h}\right) \tag{6.5}$$

for cables, where R_{DC} is the resistance of the line measured with a DC voltage.

Measurements from [22] showed that the resistance of cables changes "faster" for a larger cross-section, due to the more pronounced skin effect. The inductance of cables decreases with increased frequency, without a high influence of the cross-section.

6.2.4 Power factor correction units and passive filters

PFC units and passive filters have a very significant influence on the system impedance at higher frequencies. Most loads primarily influence the low-frequency resonances in terms of impedance amplitude, but capacitive equipment such as PFC and filters influence the resonant frequencies itself. Therefore, it is very important to include all of these devices in the model, with all of their physical components. Two topologies of passive filters are shown in Fig 6.6. The model should include all parts of the filter, and not only the capacitance. With PFC capacitors, several switching states are possible commonly. It is important to determine which of the switching states creates the "worst case" scenario.

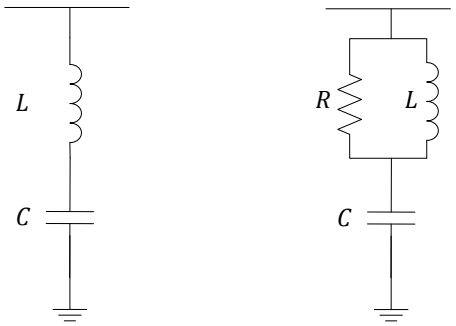

Fig 6.6 Examples of passive filter topologies: (a) single-tuned, (b) band-pass filter (absorbs high frequencies)

6.2.5 Loads

Loads provide a "damping" effects in the network, decreasing the resonant magnitudes with their resistance, but they also influence the resonant frequencies with their inductance and capacitance. This subsection discusses the models of some common types of loads.

6.2.5.1 Induction motors

Similarly to the fundamental frequency model, induction motors can be represented by a *R*-*L* circuit, as in Fig 6.7 (a) [5], [7]. Subscripts 1 and 2 of the resistance and inductance correspond to the stator and rotor. Inductance L_m represents the magnetising inductance of the machine. The rotor slip $s(h)$ is dependent on the observed harmonic order and given as:

$$s(h) = \frac{\pm h \cdot \omega_1 - \omega_{rot}}{\pm h \cdot \omega_1} \tag{6.6}$$

where ω_1 is the synchronous angular speed of the machine and ω_{rot} is the angular speed of the rotor. Signs + and – in (6.6) correspond to positive and negative sequence harmonic orders, respectively.

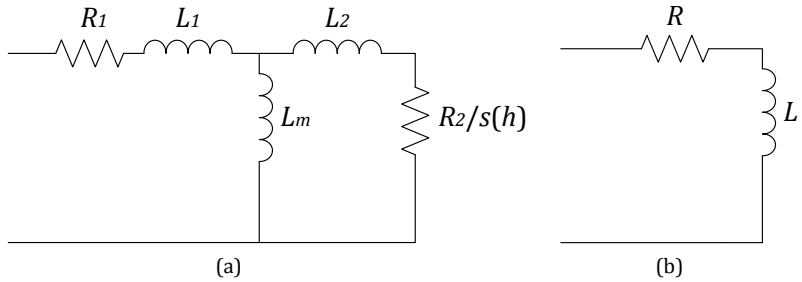

Fig 6.7 Equivalent model for an induction motor: (a) detailed, (b) simplified

At higher frequencies the rotating speed of the electro-magnetic field becomes much greater than the speed of the rotor, the motor slip becomes very close to 1. Due to this, the rotor resistance is very close to the locked-rotor resistance of the machine (R), and can be considered independent of the machine speed. Since the magnetising inductance is much higher than the leakage inductances, the model can be simplified to an a single *R*-*L* branch, as in Fig 6.7 (b). As in the fundamental frequency studies, the resistance is also sometimes disregarded if the R/X ratio is very low.

6.2.5.2 Aggregated linear loads

Some industrial and household devices, e.g. heaters, can be represented with a shunt resistance. Even though their model is simple it is hard to determine the total power of resistive loads present in the network, or per busbar.

One approach for representing mixed loads is using the measured powers, if they are available. Measured active and reactive powers should not be used directly to determine values of linear elements, as discussed in [5], [7]. Active power of power

electronic and motor loads should not be included in the value of the resistance. Measured reactive power does not reveal the mixture of inductive and capacitive loads, and locked-rotor inductance of motors is lower than the one calculated from measured reactive power (which represents the motors only at the fundamental frequency). Finally, the measured reactive power usually contains the distortion power, which does not correspond to physical inductances or capacitances. Due to these reasons, the measured active and reactive powers might be misleading. A practical way for dealing with this problem is assuming several load compositions and performing the frequency scan for each of the scenarios.

A generalised load model is proposed by the CIGRE working group 36-05 in [23], which is based on field measurements in MV networks made using a ripple-control generator. The model approximates the impedance of loads between the 5th and 20th harmonic, as shown in Fig 6.8.

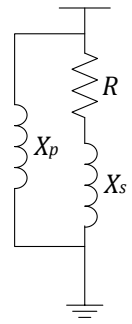

Fig 6.8 CIGRE model for grouped loads between the 5th and 20th harmonic order

It is proposed that the values of elements from Fig 6.8 are calculated as:

$$R = \frac{U^2}{P_1} \tag{6.7}$$

$$X_s = 0.073 \cdot h \cdot R \tag{6.8}$$

$$X_p = \frac{h \cdot R}{6.7 \cdot \frac{Q_1}{P_1} - 0.74} \tag{6.9}$$

where U is the supply voltage level, and P_1 and Q_1 are the estimated active and reactive power of loads at the fundamental frequency. Constants from (6.8) and (6.9) were derived from a set of measurements in one country. It is difficult to estimate how well do they correspond to the load mixtures in other countries.

Reactance X_p is an aggregated equivalent for directly coupled induction machines, while the series R-L branch represent predominantly resistive loads. Similar models are discussed in [5], with a reduced or increased number of parameters (e.g. including the equivalent resistance of a group of induction motors).

6.2.5.3 Power electronic devices

Power electronic loads, when not considered as sources, are difficult to include in the impedance representation. The impedance equivalent, e.g. the admittance matrix

model (section 4.3.4.3), is developed to represent the device as a source, and its voltage dependent error makes it unreliable for the purpose of locating resonant frequencies. At high values of harmonic voltages, which are present in the case of an excited resonance, the response can deviate more from a linear characteristic, as can be seen in Fig 4.18 on the example of a CFL.

However, when the input circuit of the device contains linear components (e.g. line filters), these values can be used as their impedance representation, as shown in [15]. If these values are not known, they can be determined by a laboratory measurement. When these values are not easy to assume, power electronic devices are commonly represented by an open circuit in the frequency scan [7].

6.3 Case study of a distribution network

The aim of this section is to analyse the uncertainties of impedance modelling in distribution networks on an example. Model changes were analysed analytically, and on an example of a real low-voltage cable network, in which a parallel resonance was observed. The aim is to analyse the effects of models simplifications and parameter uncertainties.

This analysis is intended as a guideline in the modelling process. It emphasizes which components of the network have a significant impact on the resulting harmonic impedance, and which components have a minor influence.

6.3.1 Example network and used models of components

The adopted test network is a residential area LV network analysed from the LV busbar of the transformer. This network contains a high share of PV inverters and it was chosen because the capacitance of PV inverters shifts the first parallel resonance in the low frequency range, as reported in [24].

A schematic diagram of the low-voltage part of the example network is shown in Fig 6.9. The medium-voltage part of the network is presented in Fig 6.10. The LV network is connected to busbar 12 of the MV network. All four feeders are numbered in the LV network, while in the MV network only four busbars are numbered (2, 9, 12, and 13), since changes of parameters were applied only to these busbars.

In the case study, cables were modelled with their π equivalents. Both the LV and the MV parts are cable networks. Skin effect was not taken into account.

Transformers were modelled as series *R*-*L* circuits. Their capacitances were not taken into account as the maximal frequency of interest was 3 kHz. Even at higher frequencies the transformer capacitances are probably insignificant in comparison with the capacitances of cables connected to them.

Power factor correction units were modelled only as a capacitance without losses.

Household loads were modelled as parallel *R*-*L*-*C* circuits (in several scenarios). The capacitance represents the input capacitance of all power electronic devices, mainly their input filters. In [15], a range of (0.6 – 6) μF per house is proposed. In this case study 0.6 μF per house is used. Induction motors were modelled as their locked-rotor inductance. The total adopted power of linear loads in this LV network part was 500 W per house, and induction motors were accounted as (0 – 30) % of this load, in several steps. Other linear loads, e.g. heaters of washing machines, are represented with shunt resistances. Depending on the amount of induction motors, resistance was changed to get the same total power of linear loads

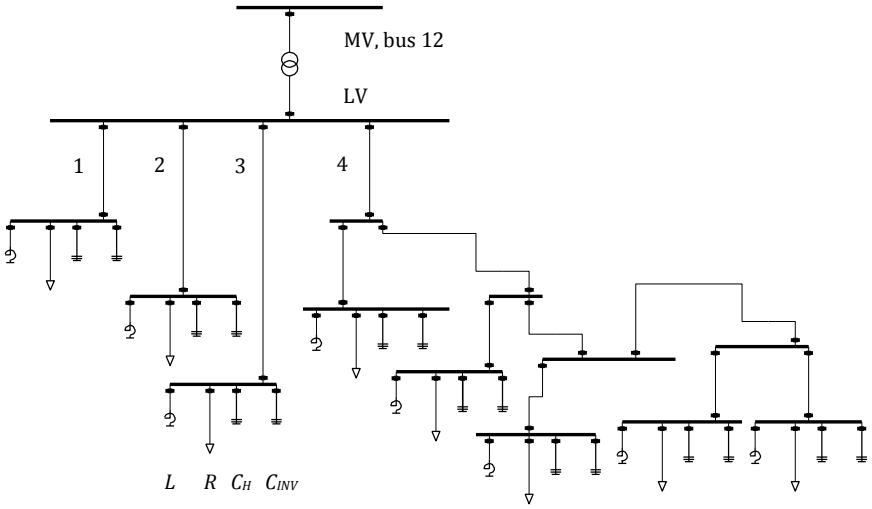

Fig 6.9 Single-line diagram of the LV part of the example network; L – locked-rotor inductance of motors, R – resistance of other linear loads, C_H – capacitance of household loads, C_{INV} – capacitance of inverters

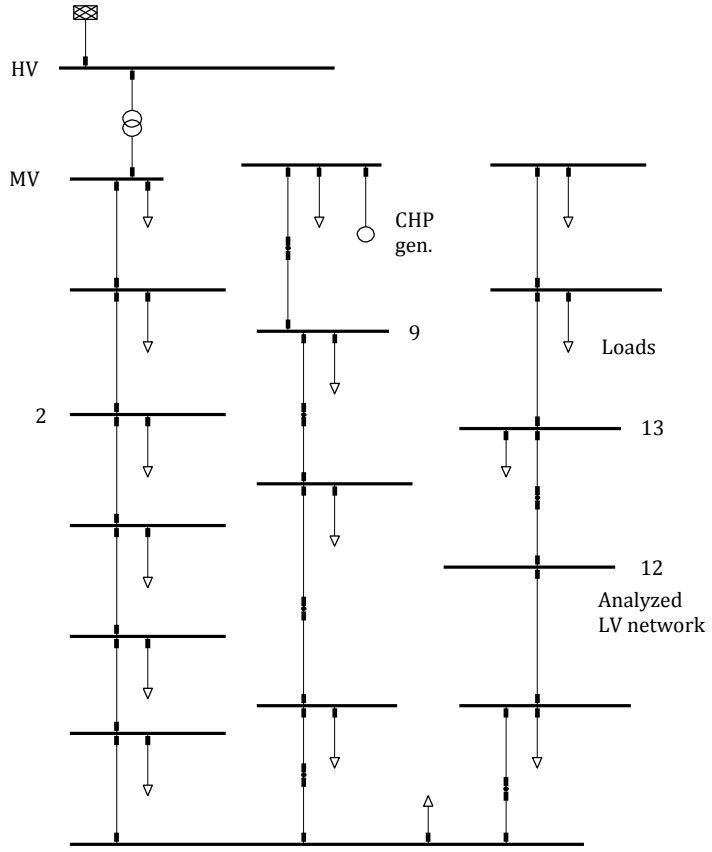

Fig 6.10 Single-line diagram of the MV part of the example network; CHP gen. – CHP generator

Photovoltaic inverters were modelled as their input capacitance. Reference [15] proposes using values of (0.5 – 10) μF for a (1 – 3) kW inverter, based on measurements. Several values from that range are used here, to show the effect if this value is not known. The total installed power of PV inverters in the LV network part is 300 kW, mostly composed of 2 kW units, while the peak load of all loads together is approximately 150 kVA.

The effect of lumping loads was examined in three steps. In the first step, all loads were connected directly at the LV busbar. In the second step, feeders were separated in the LV network, with lumped loads on feeders and feeder branches. In the last step, all houses and inverters were modelled separately.

The MV network was modelled in two ways. The simple version of the model is a series *R*-*L* circuit, representing the short-circuit power of the network and the *R* to *X* ratio. A more detailed model was also used, representing all MV feeders until the HV/MV substation, one 1.4 MW Combined Heat and Power (CHP) generator in the MV network, and several configurations of PFC in the MV network. The HV network was represented with the short-circuit impedance.

The analysis of the harmonic impedance is divided into several parts. The effect of lumping loads, load models, cable lengths, and MV network models are investigated separately. Mechanisms of parameter changes are examined analytically (on simplified examples), and on a DIgSILENT Power Factory model of the network. In all cases the impedance was calculated on the low-voltage side of the MV/LV transformer.

6.3.2 The effect of lumping loads

The number of loads in a LV network is usually too large to allow for modelling each load separately. For this reason, loads are commonly lumped into equivalent loads with some feeders and load parameters neglected. This leads to uncertainty of the outcome.

To illustrate the effect of lumping analytically, we can look at a simplified network model with two parallel feeders, as in Fig 6.11, and derive its equivalent impedance. In this figure, L represents the upstream system inductance, L_1 and L_2 represent feeder inductances, and C_1 and C_2 represent capacitances of loads connected to these two feeders.

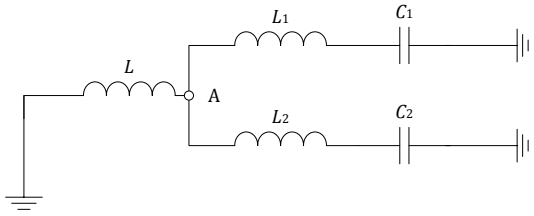

Fig 6.11 Simplified example for lumping feeders

If we lump the two capacitances together (as $C_1 + C_2$), and neglect the inductances L_1 and L_2, the impedance Z_A at point A is given by:

$$Z_A = j\omega L/(1 - \omega^2 L \cdot (C_1 + C_2)) \tag{6.10}$$

If we do not lump the two feeders and take inductances L_1 and L_2 into consideration, the impedance is given by:

$$Z_A = \frac{j\omega L(1-\omega^2 L_1 C_1)(1-\omega^2 L_2 C_2)}{1+\omega^4 L_1 L_2 C_1 C_2 - \omega^2(L(C_1+C_2)+L_1 C_1 + L_2 C_2)} \tag{6.11}$$

If the inductance L is much greater then L_1 and L_2, and the lowest parallel resonance frequency f_{r1} is in the low frequency range, (6.11) will give a solution for f_{r1} which is close to the solution of (6.10). Besides the difference in calculated f_{r1}, L_1 and L_2 also introduce two series resonances and an additional parallel resonance with a higher resonant frequency. The frequency of the second parallel resonance increases as L_1 and L_2 decrease. If cable lengths are not very long, the resonant frequency of the second parallel resonance and both series resonances are usually too high to be of interest for distribution systems.

To illustrate the difference between (6.10) and (6.11), we assume $C_1 = C_2$ and $L_1 = L_2$ and vary the ratio between L and L_1 from 10 to 0.4. The difference in the lowest parallel resonant frequency calculated by (6.10) and (6.11) is shown in Fig 6.12 (a). An equivalent example with four parallel feeders is shown in Fig 6.12 (b).

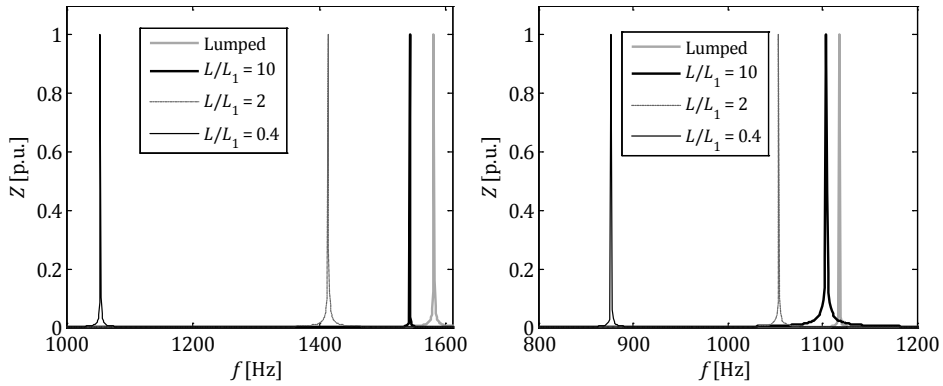

Fig 6.12 The first parallel resonance calculated with lumped feeders and without lumping for different values of L/L_1: (a) two feeders, (b) four feeders

The uncertainty is dependent on the number of feeders and their lengths. If the feeder inductance is much lower than the upstream system inductance, lumping will not lead to significant errors in the resonant frequency. For realistic values of L/L_1 in LV networks, ranging between 0.4 and 10, the uncertainty is very high for two feeders if all of the capacitance is located at the ends of feeders. However, if the capacitance is distributed along the cable, and if there are more than two feeders, the uncertainty becomes considerably lower.

In this example for a ratio of 10, the difference is about 50 Hz for two feeders and less than 20 Hz for four feeders. However, for longer feeder lengths, this error is much higher. For a ratio of 0.4, in this example, the difference is about 500 Hz for two feeders and about 200 Hz for four feeders.

In a realistic case the topology is much more complex than in Fig 6.11. To illustrate the effect of lumping on a realistic LV network (with four feeders), we compare the harmonic impedance versus frequency at the LV busbar of the example network from Fig 6.9 in three cases. In the first case we look at the whole LV network as a single parallel *R-L-C* load connected directly at the transformer busbar, designated as "all lumped". In the second step, we lump the loads of the four feeders as shown in Fig 6.9, designated as "lumped feeders". In this case the feeders and feeder branches are

lumped as parallel *R-L-C* loads at cable ends. In the third step, we distribute the loads to even more branches, with short feeders divided in five sections and longer feeders in 10 sections, designated as "no lumping". The resulting frequency scans of the impedance are presented in Fig 6.13.

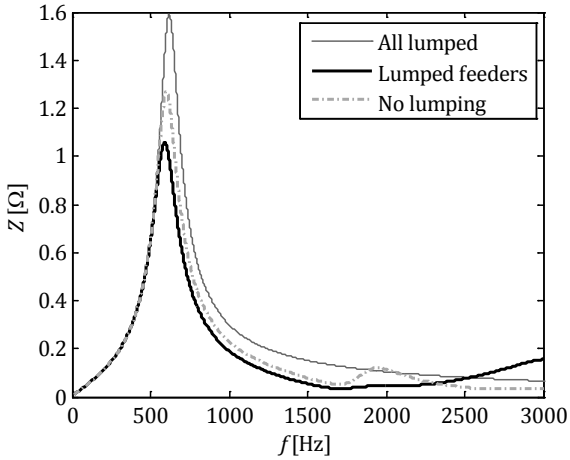

Fig 6.13 Impedance at the LV busbar, effects of lumping loads

The solution of the "most realistic" case (the "no lumping" case) falls within the two other cases. In comparison with the case with everything lumped at the busbar, lumping complete feeders will add extra inductance in the circuit, resulting with a lower resonant frequency, in this case almost 30 Hz. In the case where nothing is lumped, most capacitances are connected via a lower inductance, resulting in a lower frequency change, less than 20 Hz. It is important to notice that the sensitivity to model changes is highest around the resonant frequency. The same is visible also in the following sections.

In conclusion, lumping all loads leads to an increase of the resonant frequency, but with acceptable errors when feeder lengths are short and/or capacitances are distributed along the feeders. A greater number of cables leads to less error. Also some resonances are not noticed in this way. Lumping separate feeders leads to a decrease in the resonant frequency, with less error. It reveals additional resonances but the uncertainty is larger at higher frequencies. To avoid high model complexity, in the following subsections the model with lumped four feeders is used for analysing other effects.

6.3.3 The effect of different load models

Determining appropriate load models is very important and difficult at the same time. Loads provide dumping in the network, but can also change the resonant conditions, especially at higher frequencies. Load demand and composition change in time, making it necessary to assess several scenarios.

To analyse the impact of motor loads, we start with a simplified model from Fig 6.14. In this figure, L is the inductance of the upstream system, C is the capacitance of loads, and L_m is the locked-rotor inductance of motor loads.

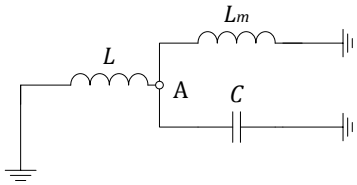

Fig 6.14 Simplified example for the influence of motor loads on the frequency scan

In this case, the impedance at point A is given by:

$$Z_A = j\omega L_{par}/\left(1 - \omega^2 L_{par} C\right) \tag{6.12}$$

where L_{par} is an inductance equal to the value of L in parallel with L_m. Its value is lower than the lower of the two inductances, and if L_m is much higher than L (motor of low power), it will be almost identical to L. As we decrease L_m (increase the power of the motor) the resonant frequency will become higher. If the power of the motor is very large, the resonant frequency is affected significantly by the motor inductance.

In a realistic network this dependency becomes more complicated. To illustrate it on the example network, we look at the impedance at the LV busbar for different motor load shares in the network, in Fig 6.15.

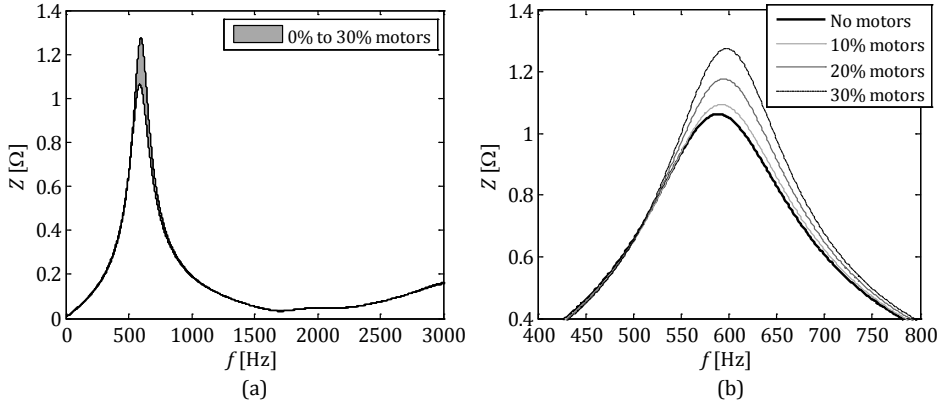

Fig 6.15 Impedance at the LV busbar, the effect of the share of motor loads: (a) area representing the change between 0 % and 30 % motor share, (b) impedance around the resonance

In the first step, no motors were present in the network. In the next steps the motor share was increased up to 30 % of the active power consumption. These changes result in the changes of the resonant peak (mostly due to the change of resistance), but the resonant frequency is shifted up for only 5 Hz. If the short-circuit power would be lower, the upstream network would have a larger inductance leading to larger differences. This leads to the conclusion that if the amount of small motors is not known in the network, it should not lead to significant errors when determining the lowest resonant frequency. However, neglecting large motors would lead to larger differences.

To analyse the impact of capacitive loads, we can look at expression (6.12) again. The capacitance changes the resonant frequency directly, a relative increase of $\Delta C/C$

reduces the resonant frequency by $1/\sqrt{\Delta C/C}$ (a decrease of capacitance increases f_r in the same way).

In the example network there are no PFC units in the LV network, the capacitances are mostly located in input filters of PV inverters. If the value of the inverter capacitance is not known, this leads to a large range of possible solutions. The impedance characteristic for four capacitance assumptions is shown in Fig 6.16. Initially, 8 µF is assumed for each 2 kW inverter; then a ± 20 % capacitance uncertainty is taken into account (typical tolerances for capacitors are ± 10 %); in the end, it was assumed that is the input capacitance of each 2 kW inverter is 2 µF.

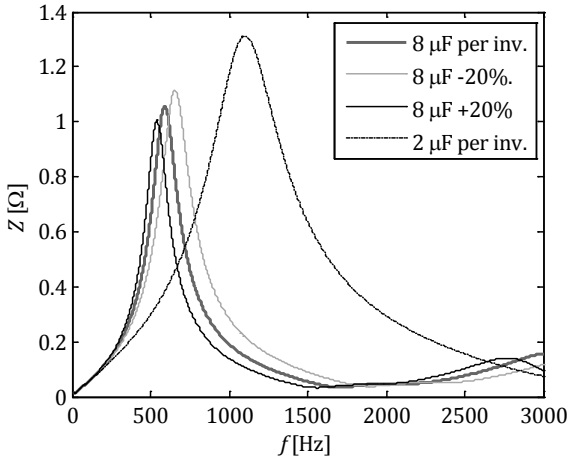

Fig 6.16 Impedance at the LV busbar, the effect of inverter capacitance

If the capacitance is not known initially, the difference between assuming 2 and 8 µF per inverter in this case leads to a 500 Hz difference in the resonant frequency. If the capacitance is known, and the uncertainty is taken into account as ± 20 %, differences of 60 Hz are noticed. If PFC is present, the uncertainty of total capacitance is close to the tolerance of PFC capacitors, because input capacitances of other devices are much lower.

The frequency of the lowest parallel resonance is usually not influenced significantly by the value of resistive loads used. However, resistive loads provide damping in the system, so they are also responsible for the peak values of impedance. If we neglect resistive loads, it may happen that we overestimate harmonic voltages due to unrealistic values of impedance. In contrast, if we overestimate the power of resistive loads, we may underestimate the impedance and harmonic voltages.

The influence of variable load resistance on the impedance in the example network is shown in Fig 6.17. The initial resistive load was changed by ± 20 %, without changes in other parameters.

The value of the resonant peak changed by about 20 % in both directions, while the resonant frequency changed by only 1 Hz. This is a convenient property of resistance modelling: changing its value will not affect the resonant frequency significantly. The critical case is always the lowest power of resistive loads (highest resistance). While other parameters need to be analysed in several conditions, for the resistance it is usually sufficient to observe the case with the lowest resistive loading. As mentioned earlier, the power on which the resistance value is based should exclude power

electronic devices and electrical motors. Also, if higher frequencies are of interest, resistances have a more complicated impact.

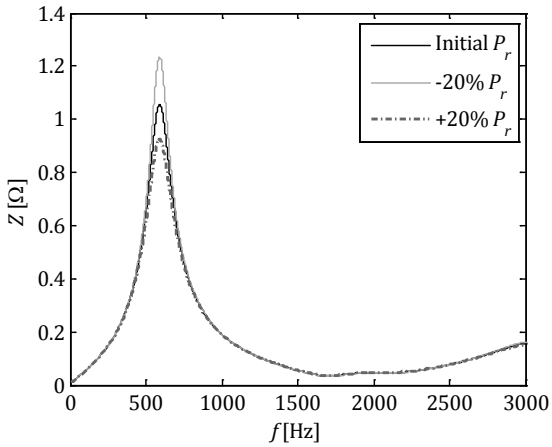

Fig 6.17 Impedance at the LV busbar, the effect of resistive loads

6.3.4 The effect of cable lengths

The effect of cable lengths was already mentioned in the analysis of lumping loads. It was noticed that complete load lumping (with LV feeders neglected) introduces errors in the resonance analysis, both for the frequency and peak amplitude. In this subsection we analyse the effect of cable length uncertainty on a model with loads lumped on feeders.

Equation (6.11) can be used to explain this effect. Inductances L_1 and L_2 contain the uncertainty of cable lengths in this expression. If these inductances are comparable with L, which is often the case, the final result can be influenced significantly. If they are much lower than L, or if the capacitance is distributed along the cable, the effect is not significant.

Using the model from Fig 6.11, we look at the effect of cable lengths analytically, again with $L_1 = L_2$ and $C_1 = C_2$. Lower cable lengths lead to a higher resonant frequency, and vice versa. Ratio L/L_1 determines if the influence of cable lengths is significant. Resulting resonances for several values of L/L_1 are shown in Fig 6.18, for two and four cables in parallel.

If the ratio is high (e.g. 10), the influence of cable length is low. If the ratio is low (e.g. 0.4), the influence is significant. Values which correspond to ±20 % changes are shown with dotted lines (+20 % are the dotted lines on the left and -20% are the dotted lines on the right).

A greater number of cables reduces the effect of cable length uncertainty, as seen in Fig 6.18 (b). Frequency resolutions of Fig 6.18 (a) and (b) are different, the differences with two cables are approximately two times larger than with four cables.

The effect of ± 20 % cable length changes in the LV part of the example network is shown in Fig 6.19. In this example, a 20 % change leads to a 5 Hz change in the resonant frequency. This is close to the changes for four cables in Fig 6.18 (b), with $L/L_1 = 2$. On the example network we cannot determine this ratio because capacitive loads are distributed along the cables, and cables have different lengths.

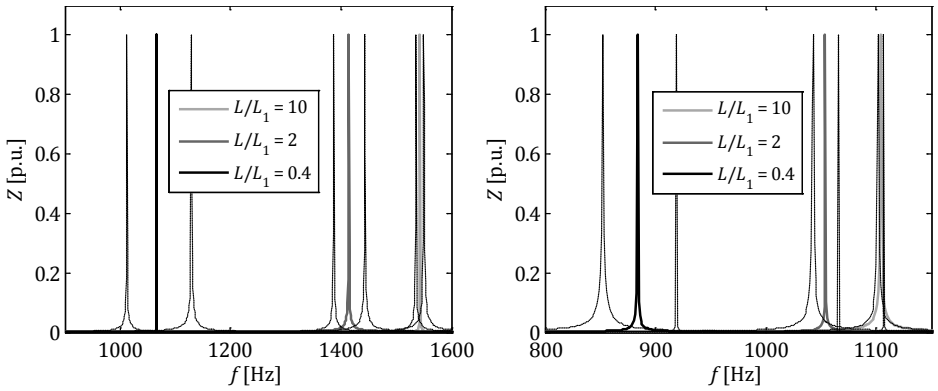

Fig 6.18 Influence of ±20 % cable length on the frequency of the first parallel resonance: (a) two cables, (b) four cables

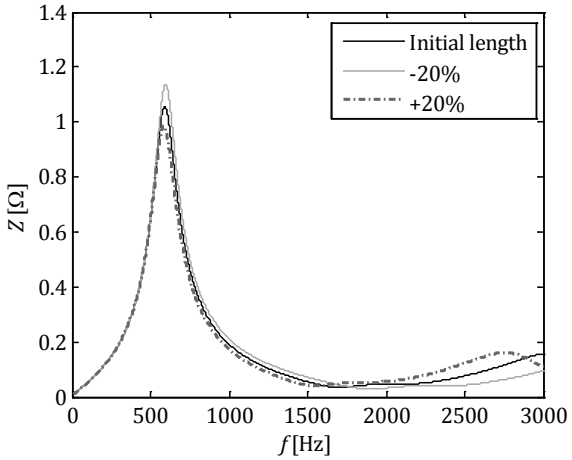

Fig 6.19 Impedance at the LV busbar, the effect of LV cable lengths

6.3.5 The effect of MV network representation

In the first approximation, the MV network is usually considered as a short-circuit impedance. However, some components of the MV network may be very important for impedance estimation, especially PFC units and generators. Since the impedance of MV equipment can be transposed to the LV level, approximations in the MV network have similar effects as the ones for the LV feeders.

To illustrate the effect of different MV network representations, several variations of the MV topology were introduced to the network from Fig 6.10. In Fig 6.20 the single impedance representation of the MV network is compared with the model which includes the MV feeders and loads, with and without the CHP generator connected.

In these three cases the first parallel resonance is shifted by 20 Hz. Also, the peak amplitude is changing by 15 %, and additional resonances with small peaks are visible with the more complex model.

In Fig 6.21 the effect of PFC in the MV network is considered, without and with the CHP generator connected. On busbars 2 and 9, PFC units of 0.5 Mvar are connected.

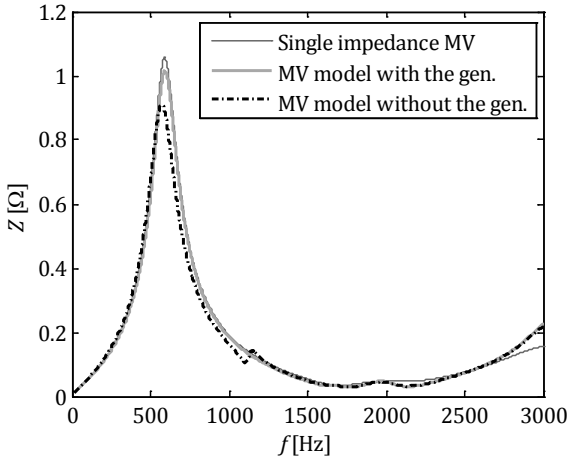

Fig 6.20 Impedance at the LV busbar, the effect of MV network representation, without PFC

This caused only minor effects if the generator is connected, with the resonant frequency reduced by 5 Hz and a higher discrepancy at higher frequencies, see Fig 6.21 (b). However, if the generator is disconnected, the effect is much higher, with additional series resonances in the lower frequency range, see Fig 6.21 (a).

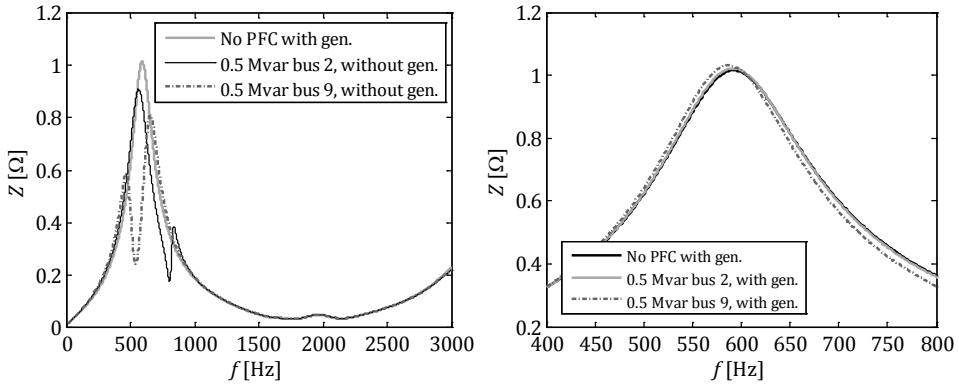

Fig 6.21 Impedance at the LV busbar, the effect of PFC on busbars 2 and 9 in the MV network: (a) with 0.5 Mvar on buses 2 and 9, without the CHP generator, (b) with 0.5 Mvar on buses 2 and 9, with the CHP generator

In Fig 6.22 the effect of PFC on busbar 13, which is located closer to the observed LV network, is considered. A PFC unit of 1 Mvar was connected to busbar 13, both on its MV and LV side when the CHP generator is in operation. Also, the effect of 0.5 Mvar on the MV side of busbar 13 was analysed, with and without the CHP generator.

It is visible that the effect is more significant if the PFC is closer to the analysed busbar. Also, similarly as with long MV feeders, PFC on the LV side of busbar 13 has only a minor effect due to the additional impedance of the MV/LV transformer. Generators in the MV network make this interaction even more complex, because they create additional series resonances.

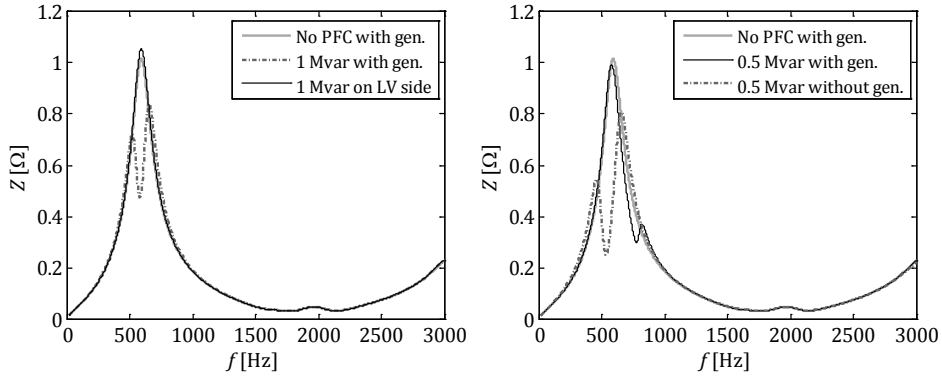

Fig 6.22 Impedance at the LV busbar, the effect of PFC on the MV and LV side of busbar 13: (a) 1 Mvar on the MV and LV side of busbar 13 with the CHP generator, (b) 0.5 Mvar on the MV side of busbar 13, with and without the generator

6.4 Conclusions

Considerations on harmonic impedance estimation in distribution networks are presented in this chapter. Effects of different model abstractions, load compositions, and parameter changes were analysed analytically and illustrated on an example of a LV network.

The results of the analysis can be summarized as follows:

- Lumping of LV loads in some cases introduces large differences in the network impedance. However, the influence is low if the feeders are short, if the capacitance of loads is distributed along the feeder, and if the number of feeders is large.
- The uncertainty of capacitance of loads and PFC in the analysed network has the most significant impact. If this value has to be assumed, large errors might be expected.
- Resistive loads have a minor impact on the frequency of the first parallel resonance. Due to the damping effect, resistances are important for the magnitude of the resonant peak, but the frequency can be determined with the first approximation.
- The share of small directly coupled motor loads does not have a significant impact on the first resonant frequency. However, large motors should be included in the model. The amplitude of the impedance-frequency characteristic is affected more by the share of motor loads.
- It is confirmed that values of load resistances, inductances, and capacitances should not be derived directly from measurements of active and reactive powers. Resistances should be derived from the active power without power electronics and motor loads. Motors should be represented by their locked-rotor equivalents. Capacitances should account only for physical capacitances in the network (it should exclude the capacitive reactive power of converters).
- Cable length assumptions can have a significant impact, depending on the ratio between the inductance of the upstream system and cable inductances. If cable inductances are higher, the error is significant. A greater number of cables in parallel reduces the uncertainty. Also, it capacitances are distributed along the cables, instead of concentrated at the end, the effect becomes lower.

- MV network representations and reconfigurations are very important if power factor correction units are connected directly on the MV level, and/or if generators are present.

This analysis can be used as a guideline for harmonic analysis in distributive and industrial networks. Choosing the appropriate load models and network representations is a vital step for determining harmonic impedances to which a non-linear load is connected. Assessment of the harmonic impedance can indicate if filtering is needed in the network. On the other hand, it can also show if compensation of a disturbing load with a passive filter is unnecessary or leads to additional problems (e.g. creation of an additional series resonance), which is equally important for the costs involved.

6.5 References of Chapter 6

[1] J. Arrillaga, B. C. Smith, N. R. Watson, and A. R. Wood, "Direct harmonic solutions," in *Power system harmonic analysis*, 1997, pp. 97–132.

[2] N. G. Hingorani and M. F. Burbery, "Simulation of AC system impedance in HVDC system studies," *IEEE Transactions on Power Apparatus and Systems*, vol. PAS-89, no. 5, pp. 820 – 828, 1970.

[3] G. D. Breuer, J. H. Chow, T. J. Gentile, C. B. Lindh, G. Addis, R. H. Lasseter, and J. J. Vithayathil, "HVDC-AC harmonic interaction Part II: AC system harmonic model with comparison of calculated and measured data," *IEEE Transactions on Power Apparatus and Systems*, vol. PAS-101, no. 3, pp. 709–718, 1982.

[4] T. J. Densem, P. S. Bodger, and J. Arrillaga, "Three phase transmission system modelling for harmonic penetration studies," *IEEE Transactions on Power Apparatus and Systems*, vol. PAS-103, no. 2, pp. 310–317, 1984.

[5] P. F. Ribeiro, "Investigations of harmonic penetration in transmission systems," PhD thesis, The Victoria University of Manchester, UK, 1985.

[6] A. A. Girgis, W. H. Quaintance, J. Qiu, and E. B. Makram, "A time-domain three-phase power system impedance modeling approach for harmonic filter analysis," *IEEE Transactions on Power Delivery*, vol. 8, no. 2, pp. 504–510, 1993.

[7] J. Arrillaga and N. R. Watson, "Computation of harmonic flows," in *Power system harmonics*, John Wiley & Sons, 2003, pp. 261–350.

[8] R. Langella, L. Nunges, F. Pilo, G. Pisano, G. Petretto, S. Scalari, and A. Testa, "Preliminary analysis of MV cable line models for high frequency harmonic penetration studies," in Proc. *IEEE Power and Energy Society General Meeting*, 2011, pp. 1–8.

[9] M. F. McGranaghan, R. C. Dugan, and W. L. Sponsler, "Digital simulation of distribution system frequency-response characteristics," *IEEE Transactions on Power Apparatus and Systems*, vol. PAS-100, no. 3, pp. 1362–1369, 1981.

[10] A. S. Morched and P. Kundur, "Identification and modelling of load characteristics at high frequencies," *IEEE Transactions on Power Systems*, vol. 2, no. 1, pp. 153–159, 1987.

[11] IEEE Task Force On Harmonic Modeling And Simulation, "Modeling and simulation of the propagation of harmonics in electric power networks, Part I: Concepts, models, and simulation techniques," *IEEE Transactions on Power Delivery*, vol. 11, no. 1, pp. 452–465, 1996.

[12] IEEE Task Force On Harmonic Modeling And Simulation, "Modeling and simulation of the propagation of harmonics in electric power networks, Part II: Sample systems and examples," *1996*, vol. 1, no. 466–474, 11AD.

[13] T. Hiyama, M. S. A. A. Hammam, and T. H. Ortmeyer, "Distribution system modeling with distributed harmonic sources," *IEEE Transactions on Power Delivery*, vol. 4, no. 2, pp. 1297–1304, 1989.

[14] P. F. Ribeiro, "Guidelines On Distribution System And Load Representation For Harmonic Studies," in Proc. *IEEE ICHPS*, 1992, pp. 272–280.

[15] J. H. R. Enslin and P. J. M. Heskes, "Harmonic Interaction Between a Large Number of Distributed Power Inverters and the Distribution Network," *IEEE Transactions on Power Electronics*, vol. 19, no. 6, pp. 1586–1593, Nov. 2004.

[16] F. Wang, J. L. Duarte, and M. A. M. Hendrix, "Analysis of harmonic interactions between DG inverters and polluted grids," in Proc. *IEEE International Energy Conference*, 2010, pp. 194–199.

[17] A. De Lorenzi, P. Bettini, and L. Zanotto, "Harmonic impedance measurements and calculation in the EHV transmission network," in Proc. *IEEE ICHQP*, 2002, pp. 162–168.

[18] V. Sharma, R. J. Fleming, and L. Niekamp, "An iterative approach for analysis of harmonic penetration in the power transmission networks," *IEEE Transactions on Power Delivery*, vol. 6, no. 4, pp. 1698–1706, 1991.

[19] A. Testa, D. Castaldo, and R. Langella, "Probabilistic aspects of harmonic impedances," in Proc. *IEEE Power Engineering Society Winter Meeting*, 2002, pp. 1076–1081.

[20] A. Mahmoud and R. Shultz, "A Method for Analyzing Harmonic Distribution in A.C. Power Systems," *IEEE Transactions on Power Apparatus and Systems*, vol. PAS-101, no. 6, pp. 1815–1824, Jun. 1982.

[21] J. Arrillaga, B. C. Smith, N. R. Watson, and A. R. Wood, "Transmission systems," in *Power system harmonic analysis*, 1997, pp. 33–96.

[22] S. Cobben, "Power quality - Implications at the point of connection," PhD thesis, Eindhoven University of Technology, 2007.

[23] CIGRE Working Group 36-05 Report, "Harmonics, characteristic parameters, methods of study, estimates of existing values in the network," 1981.

[24] J. Lava, J. F. G. Cobben, W. L. Kling, and F. Overbeeke, "Addressing LV network power quality issues through the implementation of a microgrid," in Proc. *International Conference on Renewables and Power Quality*, 2010.

Chapter 7

Conclusions and recommendations

7.1 Conclusions

Previous chapters covered the research topics in detail. This chapter gives an overview of the conclusions. A number of ideas appeared during the research, which opened new questions. At the end of this chapter they are formulated as recommendations for future research.

7.1.1 Standards related to harmonic distortion

Even though at the moment there are no global problems with harmonic distortion in the networks, there is room for improving the limits for harmonic voltages and currents. This could help prevent the problems which appear on the local level, which are sometimes difficult to predict, and make relaxations for limits which are too strict.

Voltage limits of EN 50160 and compatibility levels of IEC 61000-2-2 and IEC 61000-2-12 are based on measurements in networks. This led to very strict limits of some harmonic orders, e.g. triple-n orders, since their levels are usually very low in practice. This does not reflect the immunity of equipment at these specific frequencies.

IEEE 519 adopted a stricter voltage THD limit, possibly for avoiding the reducing of lifetime of directly coupled motors. The individual limits are equal for all harmonic orders. This does not correspond to their effects on some devices, e.g. capacitor banks which are often damaged due to higher order harmonics.

Limits for harmonic currents are difficult to define, because the influence on harmonic voltages depends on the system impedance at the point of connection and nearby loads as well. Limits for disturbing installations of IEC (61000-3-6, 61000-3-14) are based on compatibility levels for voltages, a reference impedance value, and two coefficients which account for the compensating effects between loads and the margin assigned for that voltage level. From the existing limits and expected values of the two coefficients, it seems that the current limits do not match the voltage limits completely. The same can be said for the current and voltage limits of IEEE 519.

Current limits for individual equipment have the same logic as for installations. However, from the example of limits for lighting equipment (IEC 61000-3-2, class C), it seems that they are based on the currents of the commonly used converter topology instead of the influence on the voltage.

For easier coordination of limits it is important to formally define the immunity of equipment to harmonic voltages, the derating of the installation and/or the reduction of lifetime. The concept of transformer derating due to harmonic currents is a good solution, and a similar approach is already in use for derating capacitor banks, even though it is not defined for harmonic voltages.

7.1.2 Measurement methods

The frequency spill-over which appears in DFT due to the non-stationary nature of signals is compensated well for magnitudes through the usage of harmonic groups and subgroups. The RMS of a narrow frequency bandwidth around the harmonic corresponds well to both the thermal effect and the dielectric stress (for current and voltage, respectively), and leads to acceptable errors.

For the phase angles this approach is not applicable. It was shown that for a time-varying signal the DFT makes an average if the signal is changing only in its phase angle, or it makes a more complex solution if the signal changes its magnitude as well. In both cases the physical information is lost from the phase angle. To get a good phase-angle characterization of the signal, it is important to use a data window during which the signal does not change considerably. Aggregation of phase angles over longer time periods, e.g. ten minutes, is not applicable.

The phase angles of harmonic components are not used often, but they provide valuable information about the compensation effects within a group of harmonic sources. This is especially difficult for loads which quickly change their loading level.

For very short-term phenomena, different data windows and aggregation intervals can be used to fit the problem, as they influence the measured levels. Alternative signal processing techniques offer a good solution for quickly varying signal. The result of the SWRDFT and digital filter banks are validated with a laboratory measurement.

7.1.3 Modelling of harmonic sources

Frequency domain modelling of harmonic sources has several alternatives. Performance of the Norton equivalent, harmonic admittance matrix, and harmonic fingerprint are analysed. For the admittance matrix, a modification was proposed, which substitutes one column on the matrix with a constant current vector. This combination of the matrix and the Norton model reduces the errors for constant power loads, caused by the sensitivity to fundamental voltage changes.

An indirect comparison of errors for the three methods was done. It was found that in most cases the harmonic admittance matrix has the lowest magnitude error, while the phase-angle error was lowest for the harmonic fingerprint or harmonic admittance matrix, dependent on the used voltage distortion. None of them is most accurate in general, because their errors are dependent from the observed harmonic voltages and harmonic voltages used for model derivation.

Derivation of a Norton equivalent from a field measurement is demonstrated in a case study, parallel compensated gas discharge lamps which have a very accurate Norton representation.

When multiple disturbing loads are connected to the same busbar, the summated harmonic current is usually lower than the arithmetical sum of their currents. Aggregation of harmonic sources can be characterized with diversity factors *DF* and summation coefficients α.

For variable speed drives the summation was analysed first on a computer simulation. The values of diversity factors are found to be highly dependent on the operating conditions, mostly on the rotating speeds. The values of *DF* do not monotonously decrease with the increase of frequency, contrary to the usual assumption.

The summation is also analysed on the results of seven field measurements in industrial installations. The results of three measurements in installations with VSDs confirmed the conclusions drawn from computer simulations.

The behaviour of magnitudes and phase angles in the field measurements showed that both values in almost all cases have distributions which are not close to the normal or uniform distribution. One exception was the installation with triac heaters, for which the normal distribution is a good assumption both for amplitudes and phase angles. Phase angles are covering a 90° range for harmonic orders up to the 13th in almost all cases. Above the 13th order, the range was up to 180°.

Vectorial correlations of harmonic phasors showed that there is a relatively strong correlation between the sources in many cases. Due to this, it is not correct to assume that harmonic phasors are independent variables unless this is a known fact from the nature of the process.

For all loads except for PV inverters α had a value of at least 1.1, which makes it a good value for a conservative approach. In the standards, a value of 1 is proposed. For mixed loads even 1.2 could be used. For harmonic orders higher than 9, a value of 1.4 could be used, instead of 2 which is proposed in the standards but it is too optimistic. For PV inverters, due to their dependency on the same solar irradiance, very little compensation effect occurs. Values between 1 and 1.1 were measured for all orders.

The diversity factors mostly ranged between 0.9 for $h \leq 9$ and 0.6 for orders higher than 9. Values between 0.9 and 1 are measured for PV inverters, independent on the harmonic order. A disadvantage of diversity factors is that they do not take into account the sizes of loads. When one load is dominant, higher values of *DF* should be used. A good approximation for this is limiting *DF* to *RC*, which is the share of the highest current in the arithmetical sum.

Regarding the confidence levels used, 99 % probability showed good agreement with the 95 % probability, with some exceptions. The time resolution did not show much differences (coefficients are calculated only from magnitudes), between the values obtained from 1 s and 1 h measurements, again with some exceptions.

7.1.4 Modelling of harmonic impedances

Effects of different model abstractions, load compositions, and parameter changes are analysed analytically, and on a computer model of a real distribution network. The main aim was determining the frequency of the first parallel resonance.

Lumping of LV loads on the transformer can cause significant differences in the estimated system impedance. There are several factors which influence this error: the ratio of the inductances of the upstream system and cables, the distribution of capacitive loads along the cable, and the number of parallel cables. In the example network, this representation caused a shift in the resonant frequency of about one harmonic order.

Resistive loads have only a minor effect on the frequency of the first parallel resonance. Their influence on the magnitude of the resonant impedance is high, but the worst case scenario is easily assessed with the lowest power of resistive loads.

Large directly coupled motors can have a significant influence on the first parallel resonance. However, the share of small motors in the load (e.g. residential) does not influence the resonant frequency greatly. The effect on the resonant peak is higher.

The uncertainty of LV load capacitances caused the highest effect. If this value is not known, and has to be assumed, it can lead to significant errors.

Uncertainty of the length of LV cables has a significant influence on the frequency of the first parallel resonance only in certain conditions. The error is influenced by the ratio of the inductances of the upstream system and cables, and the number of parallel cables.

The MV network representation can be of importance. The short-circuit equivalent is not sufficient if generators and PFC capacitors on the MV level are present.

7.2 Recommendations for future research

7.2.1 Standards

Even though there is considerable knowledge about the effects of harmonic voltages on equipment, it is important to further explore the reduction of equipment lifetime due to harmonics. This would help in defining the immunity levels of devices and further coordinate the international standards. Based on the additional loss of life, a procedure for derating equipment could be defined, similarly to derating of transformers due to harmonic currents.

Effects of short-duration high levels of distortion and high-frequency components should be explored further. There is not enough knowledge about these phenomena, mainly because it is difficult to obtain large amounts of measurement data.

7.2.2 Measurement methods

For the phase-angle characterization of loads, a solution needs to be found which does not aggregate the values from the time interval into a kind of average. A possible solution is to describe the time interval with the range of angles in which the phasor was located in individual data windows.

Additional short-term indices could be defined for the assessment of short-term phenomena. Methods alternative to short-term DFT can be developed further for this purpose.

7.2.3 Modelling of harmonic sources and impedances

For the modelling of harmonic sources it would be interesting to define a range of harmonic voltage magnitudes and phase angles in which loads are usually operating, based on field measurements. This would allow for better accuracy by concentrating on a range of conditions in which the source needs to be represented. Another possible benefit would be defining additional testing conditions for emission measurements, as a possible improvement in the standards for defining the impact of equipment. Also, it could be used as a starting point in the assessment of practical cases.

Regarding the summation of harmonic currents, additional measurements are needed to categorize more types of loads, e.g. household loads. This would improve the proposition for the update of summation coefficients in standards and technical recommendations, which is needed at present.

For the modelling of harmonic impedances, long-term impedance measurements would be beneficial in the further development of models. The connection between measured powers and appropriate load models could be explored in this way.

Harmonic analysis at a higher frequency range is another area which needs further research, both for modelling the disturbance sources and the network response.

Appendix 1

Considerations on the accuracy of the measurement system

The accuracy of the measurement system used in section 5.3 is primarily limited by the two types of current transducers used, which have a measurement bandwidth of 10 kHz. The first type of probes (Type 1) has a basic accuracy specified as 2 % up to 400 Hz. The second set of probes (Type 2) has a basic accuracy of 4 % up to 1 kHz. The basic accuracy is defined for a signal containing only a single frequency component, so it does not describe completely the accuracy for measuring a signal which includes several harmonic components. To give an estimate of the measurement uncertainty, we look at the magnitude differences between the measured total current of one harmonic order, and the vectorial sum of all loads for the same order. Fig A1.1 shows this difference for the 21st harmonic at location TH (triac controlled heaters), where the total current was measured with Type 2 probes and individual heaters with probes of Type 1. The difference is less than 5 % as long as the total current is higher than 100 mA.

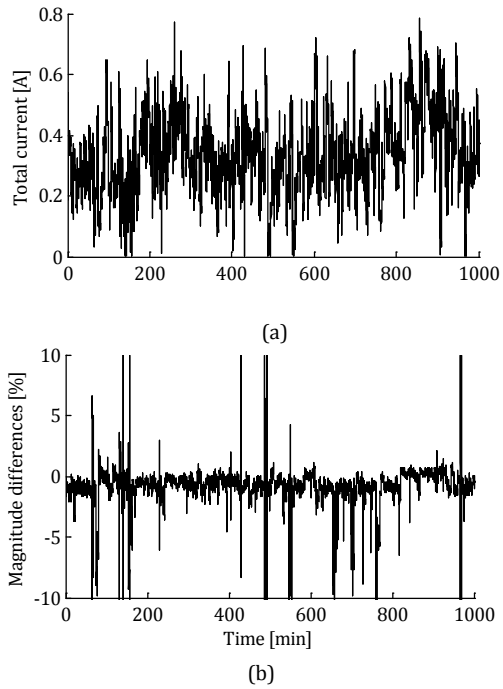

Fig A1.1 (a) Total current and (b) magnitude differences between the total current and the vectorial sum of components; location TH, 21st harmonic order

Appendix 2

Additional polar plots of harmonic currents

In addition to the results of field measurements shown in Chapter 5, polar plots of individual harmonic currents and the total current of the 7^{th} and the 11^{th} order are given in Fig A2.1 through Fig A2.14, for all seven locations.

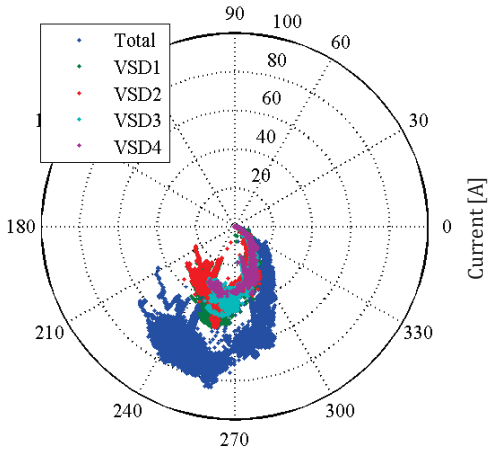

(a)

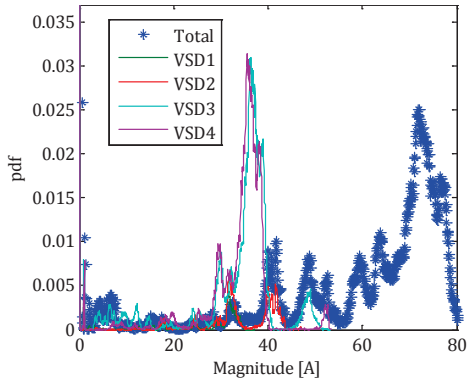

(b)

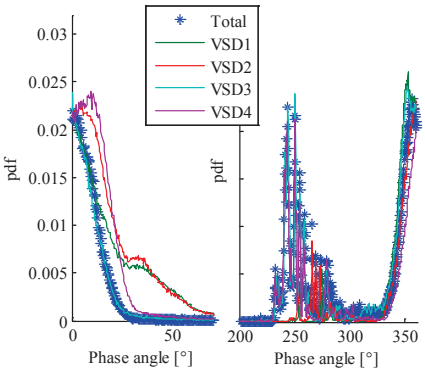

(c)

Fig A2.1 Location VSD1: (a) polar plot of currents, (b) pdf of magnitudes, (c) pdf of phase angles, 7th harmonic order

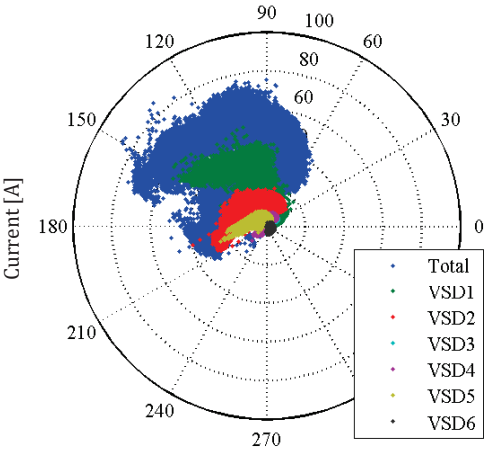

(a)

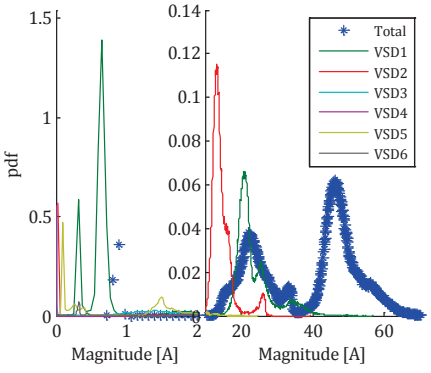

(b)

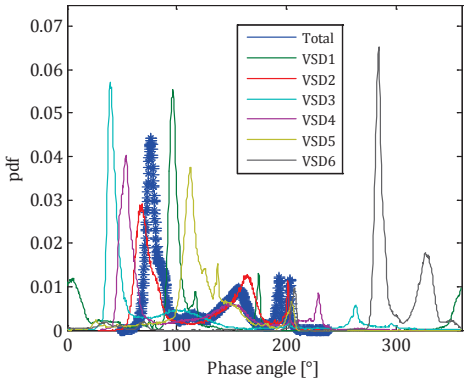

(c)

Fig A2.2 Location VSD2: (a) polar plot of currents, (b) pdf of magnitudes, (c) pdf of phase angles, 7th harmonic order

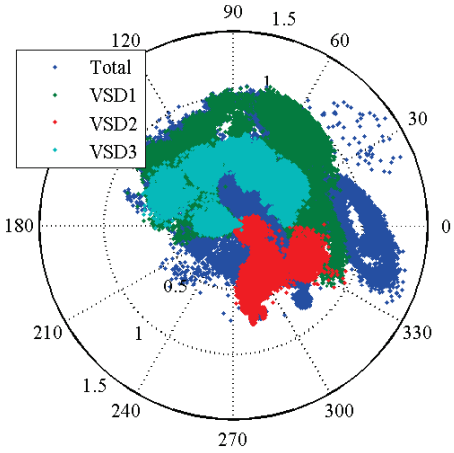

(a)

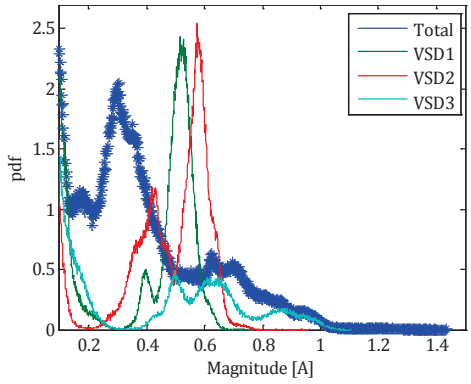

(b)

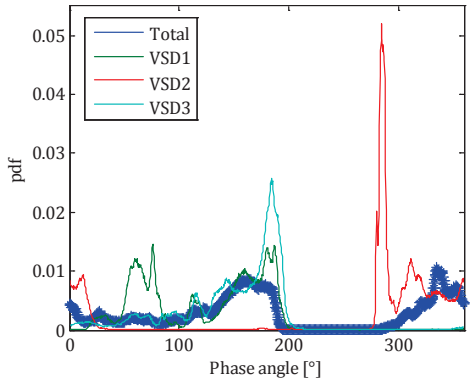

(c)

Fig A2.3 Location VSD3: (a) polar plot of currents, (b) pdf of magnitudes, (c) pdf of phase angles, 7th harmonic order

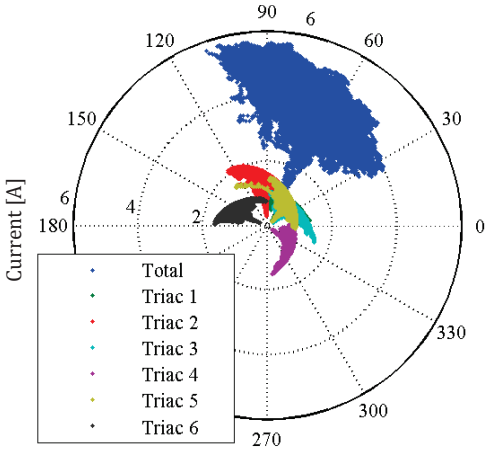

(a)

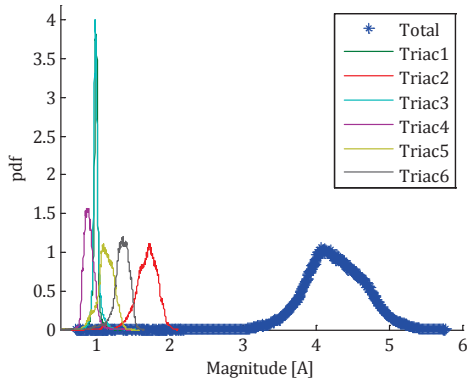

(b)

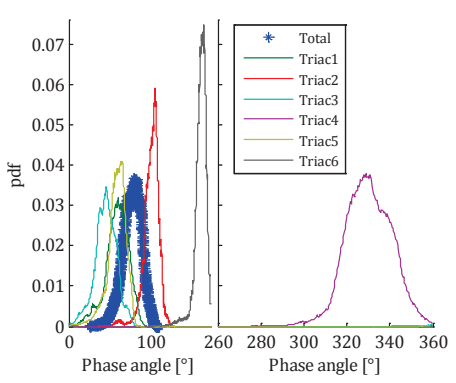

(c)

Fig A2.4 Location TH: (a) polar plot of currents, (b) pdf of magnitudes, (c) pdf of phase angles, 7th harmonic order

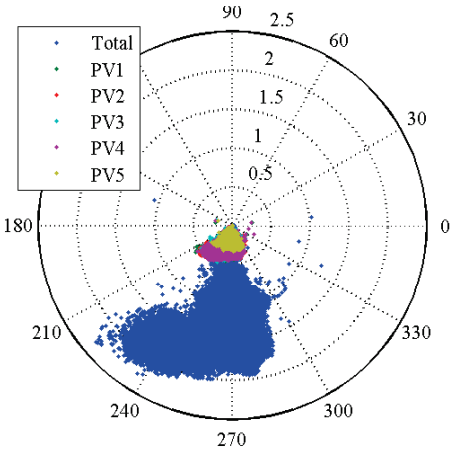

(a)

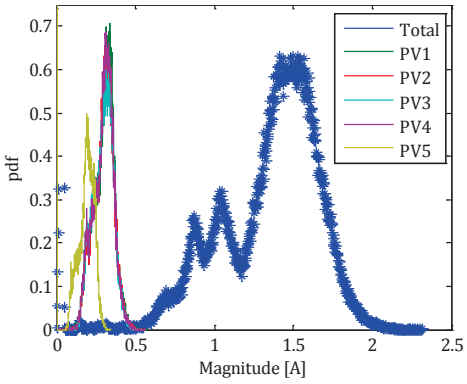

(b)

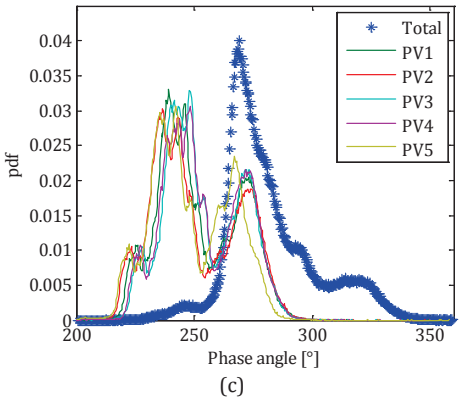

(c)

Fig A2.5 Location PV: (a) polar plot of currents, (b) pdf of magnitudes, (c) pdf of phase angles, 7th harmonic order

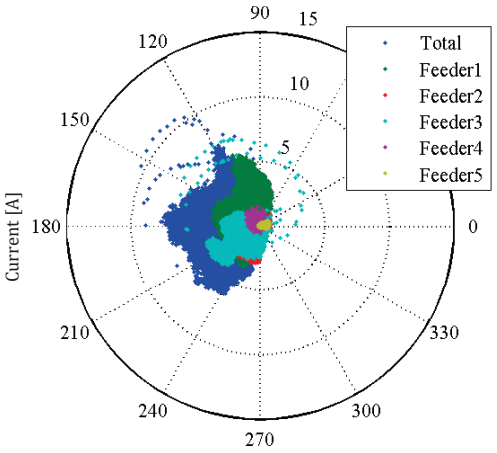

(a)

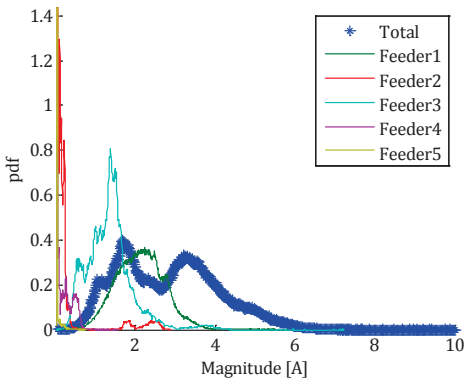

(b)

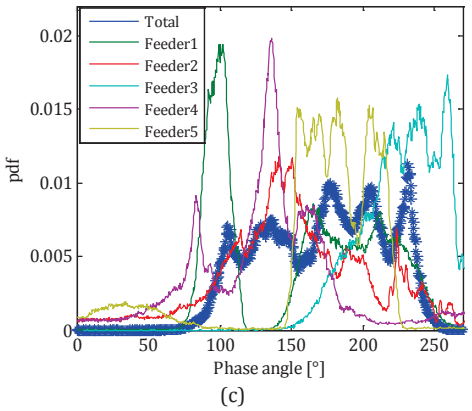

(c)

Fig A2.6 Location ML1: (a) polar plot of currents, (b) pdf of magnitudes, (c) pdf of phase angles, 7th harmonic order

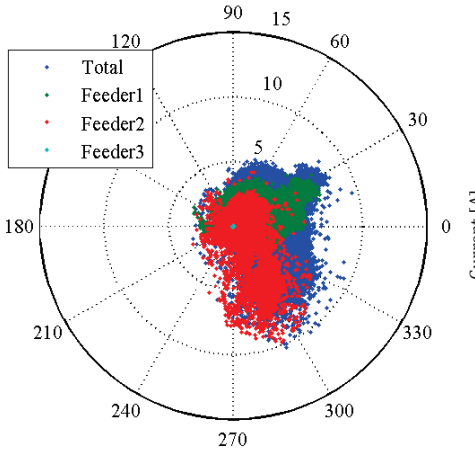

(a)

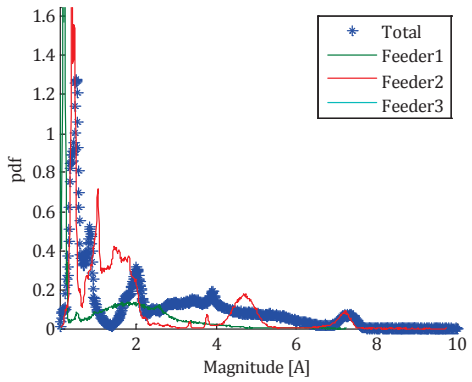

(b)

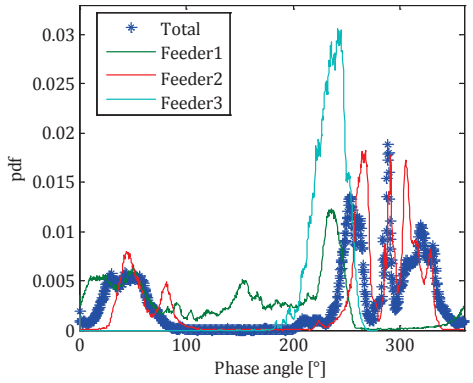

(c)

Fig A2.7 Location ML2: (a) polar plot of currents, (b) pdf of magnitudes, (c) pdf of phase angles, 7th harmonic order

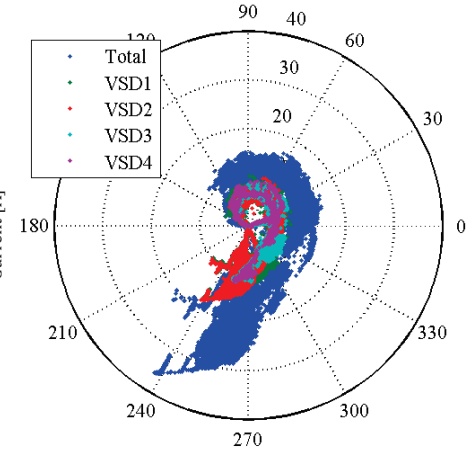

(a)

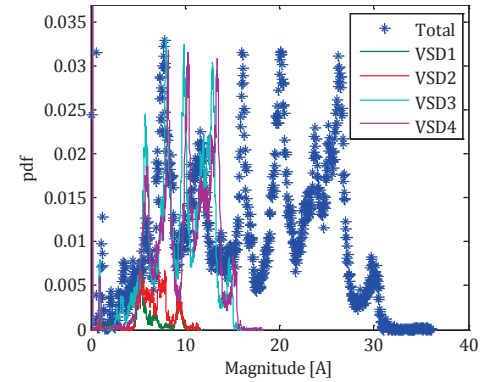

(b)

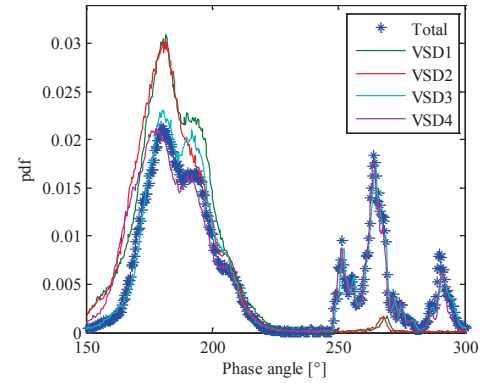

(c)

Fig A2.8 Location VSD1: (a) polar plot of currents, (b) pdf of magnitudes, (c) pdf of phase angles, 11th harmonic order

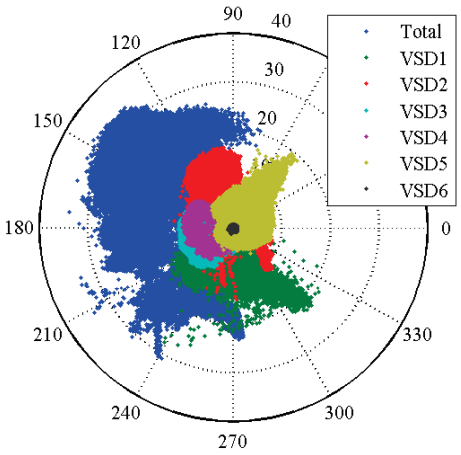

(a)

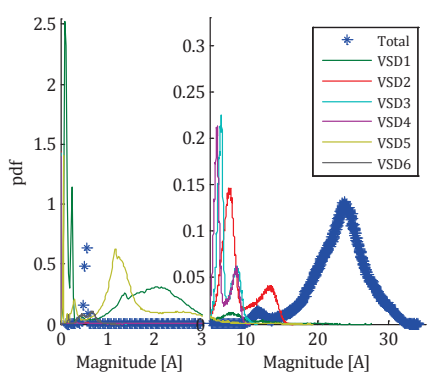

(b)

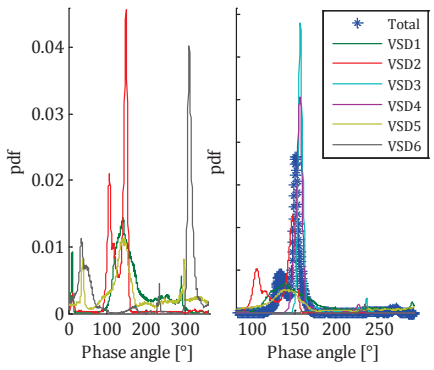

(c)

Fig A2.9 Location VSD2: (a) polar plot of currents, (b) pdf of magnitudes, (c) pdf of phase angles, 11th harmonic order

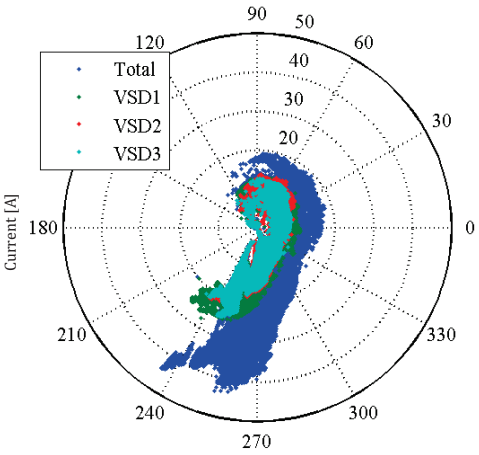

(a)

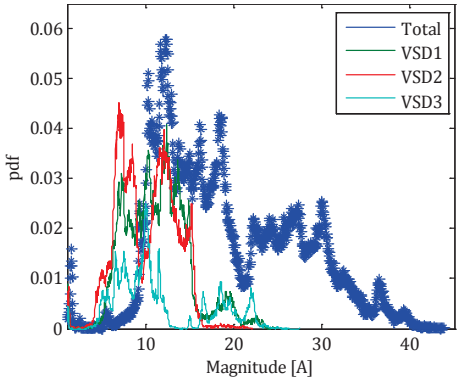

(b)

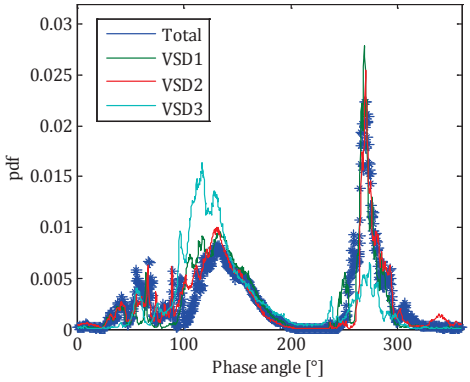

(c)

Fig A2.10 Location VSD3: (a) polar plot of currents, (b) pdf of magnitudes, (c) pdf of phase angles, 11th harmonic order

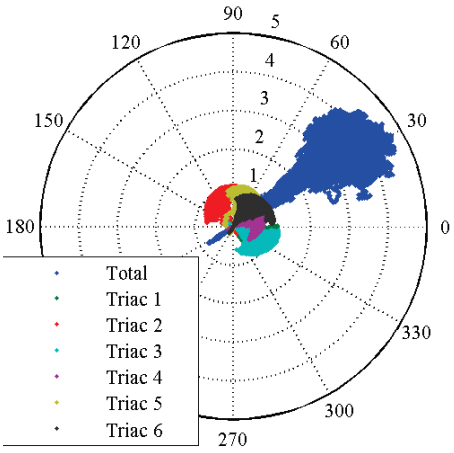

(a)

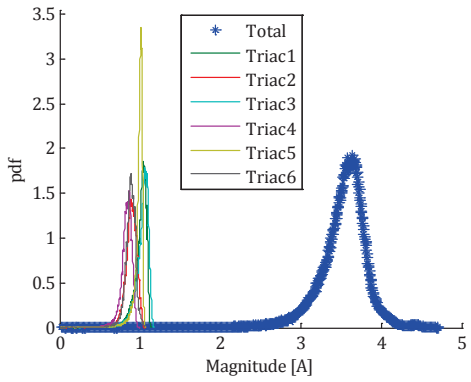

(b)

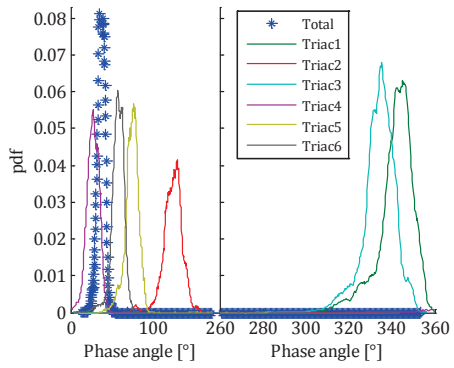

(c)

Fig A2.11 Location TH: (a) polar plot of currents, (b) pdf of magnitudes, (c) pdf of phase angles, 11th harmonic order

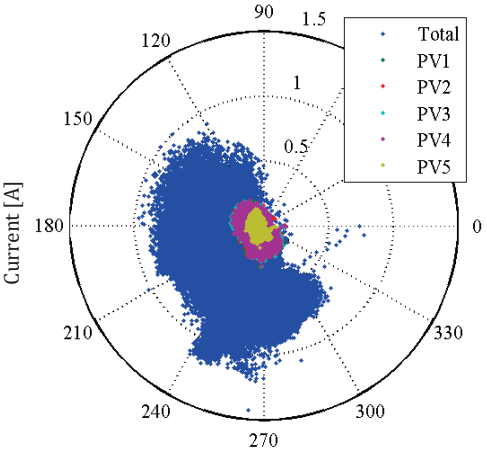

(a)

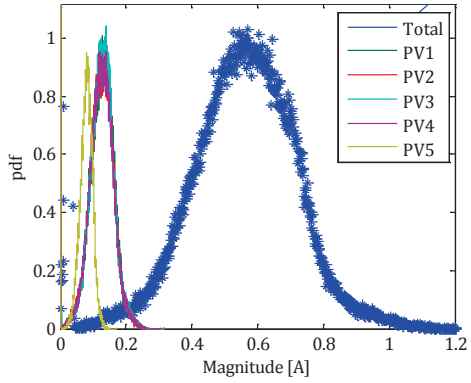

(b)

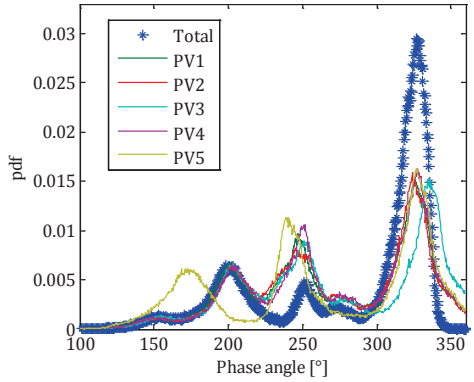

(c)

Fig A2.12 Location PV: (a) polar plot of currents, (b) pdf of magnitudes, (c) pdf of phase angles, 11th harmonic order

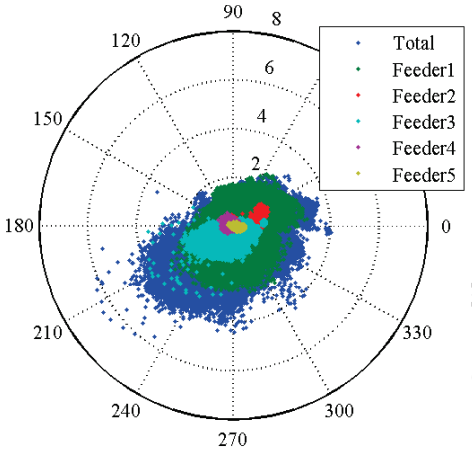

(a)

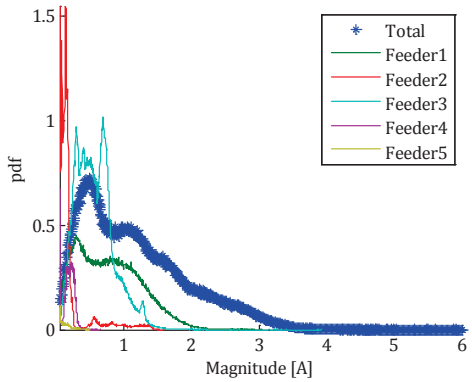

(b)

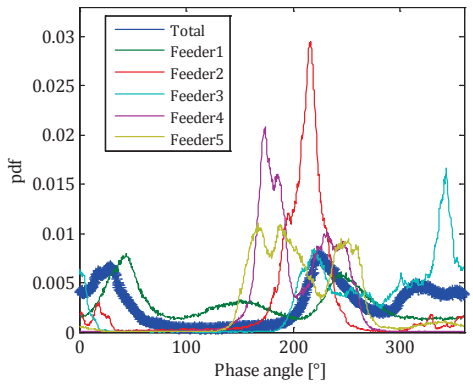

(c)

Fig A2.13 Location ML1: (a) polar plot of currents, (b) pdf of magnitudes, (c) pdf of phase angles, 11th harmonic order

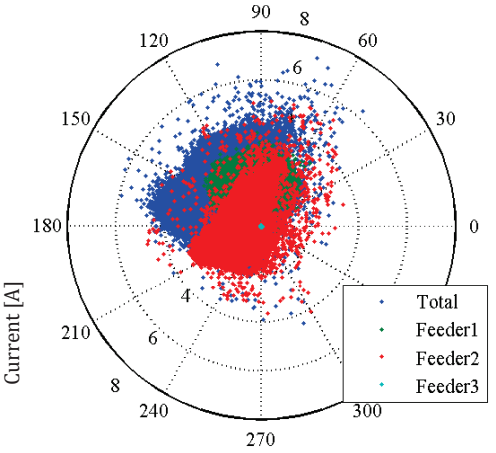

(a)

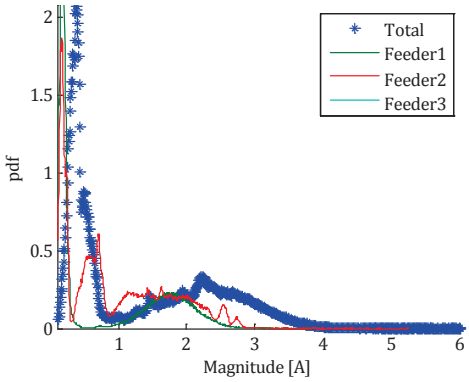

(b)

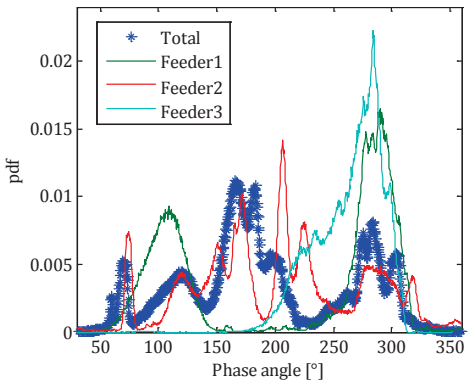

(c)

Fig A2.14 Location ML2: (a) polar plot of currents, (b) pdf of magnitudes, (c) pdf of phase angles, 11th harmonic order

Appendix 3

Vector correlation

The vector correlation method used in section 5.3.3.2 combines scaling and rotation of two vectors. First we define two arrays of complex vectors as: $\underline{z_i} = x_i + j \cdot y_i$ and $\underline{w_i} = u_i + j \cdot v_i$, with j as the imaginary unit and $i = 1, 2 \ldots N$.

The complex variance of a single array is defined as:

$$\underline{\sigma_z^2} = \frac{1}{n}\sum_{i=1}^{n}(\underline{z_i} - \underline{z_{AM}})^* \cdot (\underline{z_i} - \underline{z_{AM}}) \tag{A3.1}$$

where $\underline{\sigma_z}$ is the variance of the array $\underline{z_i}$, $\underline{z_{AM}}$ is the arithmetic mean of the array, and $\underline{z}^*$ is the complex conjugate of $\underline{z}$.

The covariance of two complex arrays is defined as:

$$\underline{\sigma_{zw}^2} = \frac{1}{n}\sum_{i=1}^{n}(\underline{z_i} - \underline{z_{AM}})^* \cdot (\underline{w_i} - \underline{w_{AM}}) \tag{A3.2}$$

If we inverse the order of the two vectors in the covariance, we get $\underline{\sigma_{zw}} = \underline{\sigma_{wz}^*}$. From the individual variances of arrays and one covariance we can define a vector correlation coefficient as:

$$\underline{\rho_{zw}} = \frac{\underline{\sigma_{zw}}}{\underline{\sigma_z} \cdot \underline{\sigma_w}} \tag{A3.3}$$

The magnitude of this complex coefficient is analogue to the Pearson's scalar correlation coefficient. This value was used in section 5.3.3.2. The real and imaginary parts of the coefficient represent measures of linear scaling and rotation, respectively.

Appendix 4

Time resolution of summation indices

In addition to the results of locations VSD1 and ML1 presented in section 5.3.7, comparisons of summation indices calculated with different time resolutions are shown in Table A4.2 through Table A4.5, for the remaining measured locations. In all cases the indices were calculated using the 95 % probability levels of currents.

Table A4.1 Influence of time resolution on diversity factors and summation coefficients, location VSD2

h	*DF1s*	*DF1m*	*DF10m*	*DF1h*	*α1s*	*α1m*	*α10m*	*α1h*
3	0.71	0.71	0.72	0.71	1.25	1.25	1.24	1.26
5	0.77	0.78	0.76	0.76	1.19	1.18	1.20	1.20
7	0.68	0.69	0.72	0.73	1.33	1.31	1.25	1.24
9	0.61	0.62	0.62	0.62	1.45	1.42	1.42	1.40
11	0.62	0.61	0.63	0.64	1.40	1.41	1.39	1.38
13	0.85	0.87	0.87	0.88	1.11	1.10	1.09	1.09
15	0.87	0.88	0.89	0.89	1.09	1.08	1.07	1.08
17	0.88	0.88	0.88	0.89	1.09	1.09	1.09	1.09
19	0.88	0.88	0.89	0.90	1.09	1.08	1.08	1.07
21	0.81	0.82	0.82	0.83	1.14	1.13	1.13	1.13
23	0.75	0.76	0.76	0.77	1.22	1.21	1.21	1.20
25	0.63	0.62	0.62	0.61	1.44	1.45	1.46	1.49
27	0.70	0.70	0.70	0.71	1.27	1.26	1.26	1.25
29	0.44	0.44	0.45	0.42	3.78	*N.D.*	*N.D.*	*N.D.*
31	0.54	0.53	0.54	0.54	2.12	2.27	2.24	2.35

Table A4.2 Influence of time resolution on diversity factors and summation coefficients, location VSD3

h	*DF1s*	*DF1m*	*DF10m*	*DF1h*	*α1s*	*α1m*	*α10m*	*α1h*
3	0.70	0.70	0.71	0.66	1.48	1.49	1.47	1.61
5	0.53	0.53	0.53	0.47	2.44	2.43	2.48	1.54
7	0.40	0.41	0.40	0.40	6.50	6.04	7.12	6.78
9	0.79	0.79	0.79	0.78	1.30	1.30	1.29	1.30
11	0.76	0.76	0.75	0.75	1.34	1.34	1.35	1.36
13	0.69	0.68	0.68	0.72	1.52	1.53	1.53	1.43
15	0.71	0.72	0.72	0.69	1.51	1.48	1.46	1.54
17	0.66	0.68	0.62	0.65	1.65	1.57	1.79	1.68
19	0.66	0.68	0.57	0.59	1.63	1.57	2.08	1.98
21	0.72	0.73	0.73	0.74	1.46	1.42	1.42	1.40
23	0.72	0.72	0.72	0.75	1.43	1.44	1.44	1.36
25	0.70	0.70	0.69	0.69	1.48	1.49	1.51	1.51
27	0.73	0.74	0.75	0.72	1.42	1.40	1.37	1.43
29	0.66	0.64	0.62	0.63	1.61	1.68	1.79	1.73
31	0.58	0.58	0.58	0.60	2.02	2.03	2.05	1.93

DF1s, *α1s* – diversity factor and summation coefficient based on 1 s time resolution, *DF1m*, *α1m* – diversity factor and summation coefficient based on 1 minute time resolution, *DF10m*, *α10m* – diversity factor and summation coefficient based on 10 minute time resolution, *DF1h*, *α1h* – diversity factor and summation coefficient based on 1 hour time resolution, *N.D.* – not defined

Table A4.3 Influence of time resolution on diversity factors and summation coefficients, location TH

h	*DF1s*	*DF1m*	*DF10m*	*DF1h*	*α1s*	*α1m*	*α10m*	*α1h*
3	0.07	0.07	0.06	0.06	-2.09	-2.07	-1.96	-1.87
5	0.81	0.81	0.80	0.80	1.14	1.14	1.14	1.14
7	0.63	0.63	0.63	0.62	1.36	1.36	1.36	1.38
9	0.17	0.16	0.15	0.14	*N.D.*	*N.D.*	*N.D.*	*N.D.*
11	0.64	0.64	0.63	0.62	1.33	1.34	1.35	1.37
13	0.26	0.25	0.25	0.23	4.96	5.08	5.51	14.25
15	0.24	0.24	0.22	0.21	7.58	8.09	27.9	*N.D.*
17	0.38	0.38	0.35	0.35	2.22	2.23	2.42	2.47
19	0.30	0.30	0.27	0.26	3.15	3.18	4.04	4.74
21	0.27	0.27	0.25	0.24	4.14	4.24	5.81	6.97

Table A4.4 Influence of time resolution on diversity factors and summation coefficients, location PV

h	*DF1s*	*DF1m*	*DF10m*	*DF1h*	*α1s*	*α1m*	*α10m*	*α1h*
3	0.72	0.73	0.75	0.77	1.26	1.25	1.22	1.19
5	0.99	0.99	1.00	1.00	1.01	1.00	1.00	1.00
7	0.98	0.99	0.99	1.00	1.01	1.01	1.01	1.00
9	0.92	0.92	0.91	0.93	1.06	1.05	1.06	1.05
11	0.96	0.97	0.97	0.96	1.03	1.02	1.02	1.02
13	0.97	0.97	0.97	1.00	1.02	1.02	1.02	1.00
15	0.86	0.86	0.84	0.83	1.10	1.10	1.13	1.13
17	0.98	0.99	0.97	0.99	1.01	1.01	1.02	1.01
19	0.92	0.90	0.90	0.88	1.05	1.07	1.07	1.09
21	0.75	0.72	0.72	0.73	1.22	1.26	1.26	1.25

Table A4.5 Influence of time resolution on diversity factors and summation coefficients, location ML2

h	*DF1s*	*DF1m*	*DF10m*	*DF1h*	*α1s*	*α1m*	*α10m*	*α1h*
3	0.85	0.83	0.83	0.84	*N.D.*	*N.D.*	*N.D.*	*N.D.*
5	0.90	0.92	0.92	0.92	1.17	1.14	1.14	1.14
7	0.74	0.68	0.67	0.70	1.83	2.40	2.42	2.24
9	0.89	0.90	0.90	0.90	1.24	1.21	1.21	1.22
11	0.69	0.69	0.70	0.69	2.12	2.11	2.03	2.09
13	0.54	0.52	0.51	0.51	10.4	19.7	23.3	29.9
15	0.85	0.84	0.84	0.84	1.30	1.31	1.32	1.31
17	0.78	0.77	0.76	0.75	1.65	1.69	1.72	1.77
19	0.88	0.89	0.90	0.90	1.27	1.23	1.20	1.20
21	0.65	0.64	0.63	0.64	2.57	2.88	3.42	3.05

DF1s, *α1s* – diversity factor and summation coefficient based on 1 s time resolution, *DF1m*, *α1m* – diversity factor and summation coefficient based on 1 minute time resolution, *DF10m*, *α10m* – diversity factor and summation coefficient based on 10 minute time resolution, *DF1h*, *α1h* – diversity factor and summation coefficient based on 1 hour time resolution, *N.D.* – not defined

Nomenclature

List of acronyms

Index	Meaning
AC	Alternating current
AIEE	American Institute of Electrical Engineers
CHP	Combined heat and power
CF	Crest factor
CFL	Compact fluorescent lamp
CIGRE	International council on large electric systems
deg.	Angle degrees
DC	Direct current
DF	Distortion factor
DFT	Discrete Fourier transformation
DWT	Discrete wavelet transformation
EMC	Electromagnetic compatibility
e.m.f.	Electromotive force
EHV	Extremely high voltage
EMI	Electromagnetic interference
EMTP	Electro-magnetic transient program
EU	European Union
FFT	Fast Fourier transformation
gen.	Generator
HD	Index of harmonic distortion, ratio of a chosen harmonic component to the fundamental
HVDC	High-voltage direct current
HV	High voltage
IEC	International Electrotechnical Commission
IEEE	Institute of Electrical and Electronics Engineers
IPC	In-plant point of coupling
LED	Light emitting diode
Loc.	Location
LV	Low voltage
ML	Mixed loads
MV	Medium voltage
ph	Phase angle
PC	Personal computer

Index	Meaning
PCC	Point of common coupling
PFC	Power factor correction
POC	Point of connection
POE	Point of evaluation
PQ	Power quality
p.u.	Per unit
PV	Photovoltaic
RMS	Root mean square
RSS	Root square sum
STFT	Short-term Fourier transformation
STDFT	Short-term discrete Fourier transformation
SWRDFT	Sliding window recursive discrete Fourier transformation
TC	Technical committee of IEC
TDD	Total demand distortion
TH	Triac controlled heater
THD	Total harmonic distortion
TIF	Telephone interference factor
TV	Television set
UPS	Uninterruptible power supply
VC	Vacuum cleaner
VSD	Variable speed drive
1ph	Single-phase
3ph	Three-phase

List of symbols

Acronym	Meaning	Unit
A_k, B_k	Orthogonal DFT coefficients of the k^{th} order	V/A
AF	Attenuation factor	-
AV	Aggregated value of voltage or current	V/A
C	Capacitance	F
$\underline{c}$	Complex Fourier coefficient in the continuous domain	V/A
$\underline{C}$	Complex Fourier coefficient in the discrete domain	V/A
CD	Device constant, exponential rate of decline of harmonic current components	
CF	Crest factor	-
CL	Compatibility level	V
CR	Constant for weighted THD for rotating machines	-
DF	Diversity factor	-
f	Frequency	Hz
$f(t)$	Time-domain signal	V/A
$f[n]$	Sampled signal	V/A
g	Function of the system	-
G	RMS of a harmonic group	V/A
GC	Global disturbance contribution	V
HVF	Harmonic voltage factor	-
h	Harmonic order	-
I	Current magnitude	A
$\underline{I}$	Complex representation of the current (phasor)	A
$[\underline{I}]$	Vector of currents	A
Im	Imaginary part of a complex number	
j	Imaginary unit of a complex number, $j^2 = -1$	-
k	Coefficient	-
L	Inductance	H
mag	Magnitude of a complex vector	-
MSE	Mean square error	A^2, $deg.^2$
N	Total number of loads or samples	-
n	Discrete representation of time, integer index of the sample	-
NDF	Normalized diversity factor	-
P	Active power	W
p	Number of pulses of a rectifier	-
pdf	Probability distribution function	-
PF	Power factor	-
Q	Reactive power	VAr
R	Resistance	Ω
RC	Ratio of the greatest component and the arithmetic sum of all components	-
Re	Real part of a complex number	
S	Apparent power	VA
SCR	Short-circuit ratio	-

Acronym	Meaning	Unit
SG	RMS of a harmonic subgroup	V/A
T	Transfer coefficient (between voltage levels)	-
t	Time	s
$[u(t)]$	Input vector	-
U	Voltage magnitude	V
$[\underline{U}]$	Vector of voltages	V
V	10/12 cycle value of voltage or current	V/A
VIF	Voltage influence factor	-
$[x(t)]$	State vector of the system	
X	Reactance	Ω
$[y(t)]$	Output vector	-
Y	Admittance	S
$[\underline{Y}]$	Matrix of admittances	S
Z	Impedance	Ω
$[\underline{Z}]$	Matrix of impedances	
α	Summation coefficient	-
β	Firing (delay) angle of a rectifier	°
δ	Partial derivative	-
φ	Phase angle of a phasor	°
Φ	Angle width of an impulse	rad
ρ	Correlation coefficient	-
ω	Angular velocity	rad/s
∞	Infinity	-

List of indices

Index	Meaning
a, b, c	Phases of the three-phase system
A, B, C	Operating regimes
AC	Alternating current
AV	Average
C	Compensation
DC	Direct current
err	Error
g	Generator
h	Harmonic order
h,i	h^{th} harmonic order of the i^{th} load
hmax,i	Maximum for the i^{th} load, h^{th} harmonic order
h,sum	h^{th} harmonic order of the sum
htot	Total harmonic component
H	Household loads
HV	High voltage
HV-MV	From high to medium voltage
i, j, k	Integer counters (e.g. number of the load, or index of a spectral component, harmonic group or subgroup, operating condition)
inv	Inverter
ii	Inter-harmonic injection
ipv	Inter-harmonic of the PV inverter
ivc	Inter-harmonic of the vacuum cleaner
I	Current
L	Maximal load
LV	Low voltage
m	Motor
max	Maximal
min	Minimal
M	Measured
MV	Medium voltage
MV&LV	Medium and Low voltage
nom	Nominal
par	Equivalent of a parallel connection
poc	Point of connection
r	Resonant
rot	Rotor
R	Weighted for rotating machines
s	Slip of an induction machine
SC	Short-circuit
sum	Total sum
sys	System equivalent
t	Total
U	Voltage
U,h	Voltage, h^{th} harmonic component

Index	Meaning
0	Excitation with a pure sinusoidal voltage
1	Fundamental component
1s	Value calculated with a 1 s time resolution
1m	Value calculated with a 1 min time resolution
10m	Value calculated with a 10 min time resolution
1h	Value calculated with a 1 h time resolution
95	Value calculated with 95 % cumulative probability levels
99	Value calculated with 99 % cumulative probability levels

List of publications

Journal publications

2013

- V. Ćuk, J.F.G. Cobben, W.L. Kling and P.F. Ribeiro, "Analysis of harmonic current summation based on field measurements," accepted for publication in *IEE Generation, Transmission and Distribution*, 2013.

- T.C.O. Carvalho, V. Ćuk, C.A. Duque, P.M. Silveira, M.A. Severo Mendes and P.F. Ribeiro, "Time-varying decomposition methods: A verification example," under review in *International Transactions on Electrical Energy Systems*, 2013.

2010

- V. Ćuk, J.F.G. Cobben, W.L. Kling, R.B. Timens and F.B.J. Leferink, "A test procedure for determining models of LV equipment," Electronics, vol. 14, no. 1, pp. 82-87, June 2010.

Conference publications

2013

- V. Ćuk, J.F.G. Cobben, P.F. Ribeiro and W.L. Kling, "Summation of harmonic currents of variable-speed induction motor drives," in Proc. *IEEE PES General Meeting*, July 2013, Vancouver, Canada.

2012

- E.C. Aprilia, V. Ćuk, J.F.G. Cobben, P.F. Ribeiro and W.L. Kling, "Modeling the frequency response of photovoltaic inverters," in Proc. *IEEE PES Innovative Smart Grid Technologies (ISGT) Europe*, October 2012, Berlin, Germany.

- T. Bantras, V. Ćuk, J.F.G. Cobben, and W.L. Kling, "Estimation and classification of power losses due to reduced power quality," in Proc. *IEEE Power & Energy Society General Meeting*, July 2012, San Diego, California.

- V. Ćuk, J.F.G. Cobben, W.L. Kling and P.F. Ribeiro, "Considerations on harmonic impedance estimation in low voltage networks," in Proc. *IEEE International Conference on Harmonics and Quality of Power (ICHQP)*, June 2012, Hong Kong, China.

- B. van Dam, V. Ćuk, J.F.G. Cobben and W.L. Kling, "A low-voltage hybrid switch for laboratory experiments," in Proc. *IEEE International Conference on Harmonics and Quality of Power (ICHQP)*, June 2012, Hong Kong, China.

- R.B. Timens, F.J.K. Buesink, V. Ćuk, J.F.G. Cobben, and F.B.J. Leferink, "Diversity and summation of large number of energy saving lighting," in Proc. *Asia-Pacific Symposium on Electromagnetic Compatibility (APEMC),* May 2012, Singapore.

2011

- V. Ćuk, P.F. Ribeiro, J.F.G. Cobben, W.L. Kling, F.R. Isleifsson, H.W. Bindner, N. Martensen, A. Samadi and L. Söder, "Considerations on the modeling of photovoltaic systems for grid impact studies," in Proc. *International Workshop on Integration of Solar Power into Power Systems*, October 2011, Aarhus Denmark.

- R.B. Timens, F.J.K. Buesink, V. Ćuk, J.F.G. Cobben, W.L. Kling and F.B.J. Leferink, "Large number of small non-linear power consumer causing power quality problems.," in Proc. *International Symposium on Electromagnetic Compatibility (EMC Europe 2011)*, September 2011, York, UK.

- R.B. Timens, F.J.K. Buesink, V. Ćuk, J.F.G. Cobben, W.L. Kling and F.B.J. Leferink, "High harmonic distortion in a new building due to a multitude of electronic equipment," in Proc. *International Symposium on Electromagnetic Compatibility (EMC 2011)*, August 2011, Long Beach, California, USA.

- V. Ćuk, J.F.G. Cobben, W.L. Kling and R.B. Timens, "Analysis of current transients caused by voltage notches," in Proc. *IEEE Power and Energy Society General Meeting 2011 (IEEE PES GM 2011)*, July 2011, Detroit USA.

- J.F.G. Cobben, V. Ćuk and W.L. Kling, "Increasing energy efficiency by improving power quality," in Proc. *WSEAS International Conference on Systems*, July 2011, Corfu, Greece.

- V. Ćuk, J.F.G. Cobben and W.L. Kling, "Inrush related problems caused by lamps with electronic drivers and their mitigation," in Proc. *WSEAS International Conference on Systems*, July 2011, Corfu, Greece.

- V. Ćuk, J.F.G. Cobben, W.L. Kling and R.B. Timens, "Analysis of harmonic current interaction in an industrial plant" in Proc. *International Conference and Exhibition on Electricity Distribution (CIRED 2011)*, June 2011, Frankfurt, Germany.

- Y. Xiang, V. Ćuk, J.F.G. Cobben, "Impact of residual harmonic current on operation of residual current devices," in Proc. *International Conference on Environment and Electrical Engineering (EEEIC 2011)*, May 2011, Rome, Italy.

2010

- V. Ćuk, J.F.G. Cobben, W.L. Kling and R.B. Timens, "An analysis of diversity factors applied to harmonic emission limits for energy saving lamps," in Proc. *IEEE International Conference on Harmonics and Quality of Power (ICHQP 2010)*, September 2010, Bergamo, Italy.

- R.B. Timens, F.J.K. Buesink, V. Ćuk, J.F.G. Cobben, W.L. Kling, M. Melenhorst and F.B.J. Leferink, "Electromagnetic interference in complex power supply networks.," in Proc. *International Symposium EMC Europe*, September 2010, Wroclaw, Poland.

- V. Ćuk, S. Bhattacharyya, J.F.G. Cobben, W.L. Kling, R.B. Timens and F.B.J. Leferink, "The effect of inrush transients on PV inverter's grid impedance measurement based on inter-harmonic injection," in Proc. *International Conference on Renewable Energies and Power Quality (ICREPQ 2010)*, March 2010, Granada, Spain.

2009

- V. Ćuk, J.F.G. Cobben, W.L. Kling, R.B. Timens and F.B.J. Leferink, "A test procedure for determining models of LV equipment," in Proc. *International Symposium on Power Electronics*, October 2009, Novi Sad, Republic of Serbia.

Acknowledgment

There are many people who deserved my appreciation, by helping me directly or indirectly to complete this work. First of all I would like to thank my first promotor prof. Wil Kling for giving me this opportunity and for all the support during the last years. Also, my deepest gratitude goes to my second promotor, prof. Sjef Cobben, for his guidance, patience, and constant encouragement during the project. Sjef, thank you for all of the technical knowledge which I got from you, and also for creating a good atmosphere which made the work both easier and enjoyable.

I would like to express my thanks to dr. Paulo Ribeiro, who also guided me during a big part of this project. Your help and enthusiasm opened up my views both regarding the topic itself and science in general. My thanks also go to prof. Frank Leferink (Universiteit Twente), dr. Jan Meyer (Technische Universität Dresden), prof. Johana Myrzik (Technische Universität Dortmund) and prof. Jan Desmet (Universiteit Gent) for their role as committee members in the defence of this thesis.

Further I would like to thank the IOP-EMVT for sponsoring this project, ir. Roelof Timens (Universiteit Twente) for the cooperation throughout the project and dr. Erik de Jong (DNV KEMA) for helping me perform laboratory experiments in the Flex Power Grid Lab.

This research involved many hours of work in the PQ lab of TU/e. I would like to thank ir. Glenn van der Wolk and ir. Eloy Maxam Martinez for their help in many experiments. Also I would like to thank all of the students with whom I had the pleasure of working with during their internship and graduation projects. Your work was an important source of inspiration for me.

I would also like to thank ir. Jerom de Haan and drs. Nelleke de Vries for correcting the Samenvatting of the thesis, and in general for teaching me Dutch. Hartstikke bedankt!

My thanks also go to many engineers and technicians from the industry which helped me perform the field measurements, in particular, companies: HyTEPS, Salzgitter Mannesmann Precision, Efteling, Nooter, KWx, Hollander Techniek, Ardagh Metal Packaging Netherlands, PPG Industries Fiber Glass, Croon Elektrotechniek and Alliander. Your input was valuable both for the measurement data and the industry view on the needed research.

To all the EES colleagues at the TU/e, thank you for the technical, but also for the social discussions during this period. It was always fun to make a break from thinking about electrons which are jumping around. Just to mention a few names, special thanks go to Chai , Totis, Sharmistha and Jerom.

Big thanks go to Jelena and Dragan, for their help in getting used to the new living space, especially in the first days when the Dutch language sounded like white noise. I would also like to thank Nikola for designing the book cover.

My endless gratitude goes to my parents and my brother Miroslav, for the motivation and support. Thank you also for teaching me the right values, which lead me to choose this pathway.

And finally, there are no words which can express my thanks to my wife Jovana. With you by my side everything is easier and not a single day is wasted.

Thank you!
Hvala!

Biography

Vladimir Ćuk was born on December 9, 1981 in Pačevo, Serbia. After finishing the secondary school in 2000 (Gymnasium Uroš Predić in Pačevo, Serbia) he studied Electrical Engineering at the University of Belgrade, Serbia. In 2005 he obtained the dipl.ing. degree within the Chair of Power Converters and Drives.

From 2006 until 2009, he was with the Electrical Measurements Department of the Electrical Engineering Institute Nikola Tesla in Belgrade.

In 2009 he joined the Electrical Energy Systems group at the Eindhoven University of Technology, as a Ph.D. candidate under the supervision of prof.ir. W.L. Kling and prof.dr.ir. J.F.G. Cobben. His main research interests are modelling and measurements of Power Quality phenomena.